Expression of an enhanced HIV broadly neutralising monoclonal antibody in plants and development of a glycoengineered *N. tabacum* host line

Melanie Grandits

St George's, University of London

2020

Supervisors:

Prof Julian Ma, Dr Pascal Drake, Dr Audrey Teh

Thesis submitted for the degree of

Doctor of Philosophy (PhD)

Declaration

I hereby declare that this document and the data obtained are my own. Any work carried out by others was clearly acknowledged.

Melanie Grandits

Abstract

HIV-1 affects about 38 million people worldwide, the majority in low income countries. Antiretroviral therapy (ART) is used to control the disease, however life-long ART is expensive, compliance is variable, it can cause severe side effects and resistance to ART is increasing. Broadly neutralising antibodies (bNAbs) offer a new perspective to pre-exposure prophylaxis (PrEP) and post-exposure therapy. However, despite their unique characteristics, several limitations hamper the therapeutic usage of bNAbs, including their cost and half-life.

To address these limitations and improve the efficacy of the bNAb 10-1074, two modifications have been investigated. Firstly, mutations (YTE/LS), that have been shown to increase the affinity to the neonatal receptor (FcRn), were introduced into the Fc-region of the antibody to extend mAb half-life. Secondly, a glycoengineered *N. benthamiana* line was used as the production host to allow human-like glycosylation, improve binding to FcγRIIIa, and potentially enhance antibody-dependent cell-mediated toxicity (ADCC). A significant negative impact on antibody yield, but no effect on affinity to gp120 or the ability to neutralise HIV-1 was observed upon introduction of the mutations into bNAb 10-1074. Enhanced affinity to FcRn was achieved with the YTE mutation, which translated functionally to increased transcytosis *in vitro*. *In vivo* studies further revealed an average 29 % reduction in blood clearance of 10-1074 YTE compared to the non-modified version. Production of a glycoengineered version of bNAb 10-1074 resulted in enhanced affinity to FcγRIIIa and an improvement in ADCC.

Finally, in anticipation of using transgenic tobacco for large scale manufacturing of HIV bNAbs for resource poor regions, inactivation of the α1,3-fucosyltransferase genes of *N. tabacum* using CRISPR/Cas9, was investigated. Five guide RNAs (gRNA) were included in a polycistronic tRNA-gRNA construct which was transformed into *N. tabacum* SR1. This resulted in a plant line at T2, with up to 65 percent reduction in fucosylation.

Table of Contents

Abstract ... III
Table of Contents ... IV
Acknowledgements ... VIII
Abbreviations ... X
List of Figures ... XVIII
List of Tables ... XXII
1 Introduction ... 1
1.1 HIV/AIDS ... 1
1.1.1 HIV genome and life cycle ... 2
1.1.2 The HIV envelope ... 5
1.1.3 Risk of transmission ... 7
1.1.4 Current treatments – Antiretroviral therapy (ART) ... 8
1.1.5 Failure of vaccination – HIV challenges ... 9
1.1.6 Broadly neutralising antibodies (bNAbs) ... 10
1.1.7 Clinical and pre-clinical trials with new generation bNAbs ... 15
1.1.8 The potential of bNAb therapy ... 18
1.1.9 Limitations of bNAbs ... 20
1.2 Fc receptors ... 20
Antibody-dependent cellular cytotoxicity and the FcγRIIIa ... 21
1.2.1 Neonatal Fc receptor (FcRn) ... 23
1.3 Expression systems for biopharmaceuticals ... 26
1.3.1 Prokaryotic expression platforms ... 26
1.3.2 Yeast expression system ... 27
1.3.3 Mammalian expression system ... 27
1.3.4 Plants as expression system ... 28
1.3.5 Comparison of downstream processing of mAb preparations between mammalian and leaf expression systems ... 31
1.4 Glycosylation ... 34
1.4.1 Impact of *N*-glycoforms on IgG functionality ... 35
1.4.2 *N*-glycosylation pathway in mammals ... 36
1.4.3 Plant *N*-glycosylation ... 37
1.4.4 The N-glycosylation pathway in plants ... 38
1.4.5 Glycan engineering in plants ... 39

1.5 CRISPR/Cas9 42
1.5.1 CRISPR in gene editing 43
1.5.2 Delivery systems 46
1.5.3 CRISPR/Cas9 in plants 47
1.6 Hypothesis and Aims 50
2 Materials and Methods 52
2.1 Production and characterisation of broadly neutralising antibodies produced in ΔXF *N. benthamiana* 52
2.1.1 Nomenclature 52
2.1.2 Cloning of antibody heavy and light chain genes into MIDAS vectors 52
2.1.3 Expression of bNAbs 53
2.1.4 Extraction and purification of bNAbs from plant leaves 54
2.1.5 Characterisation of bNAbs 55
2.2 Generation of a stable ΔF *N. tabacum* plant line 61
2.2.1 Construction of sgRNA-Cas9 vectors 61
2.2.2 Transformation of *A. tumefaciens* by electroporation 64
2.2.3 Agrobacterium transformation of *N. tabacum* plants using syringe infiltration 64
2.2.4 Plant DNA extraction 65
2.2.5 IDAA (Indel Detection Amplicon Analysis) 65
2.2.6 Stable Agrobacterium-mediated transformation of *N. tabacum* 66
2.2.7 Analysis of putative ΔF *N. tabacum* plant lines 67
2.3 Statistical Analysis 69
3 Expression and *in vitro* characterisation of variants of the anti-HIV bNAb 10-1074 70
3.1 Introduction 70
3.2 Specific objectives 71
3.3 Contributions 71
3.4 Results 72
3.4.1 Cloning of heavy and light chain into the plant expression vector pTrak.6 72
3.4.2 bNAbs 10-1074 can be expressed in ΔXF *N. benthamiana* 73
3.4.3 Yield of 10-1074 produced in ΔXF plants can be improved by addition of Tween80 76
3.4.4 10-1074 bNAbs generated in ΔXF *N. benthamiana* are fully assembled 76
3.4.5 ΔXF *N. benthamiana* yields bNAbs lacking α1,3-fucose and β1,2-xylose glycans 78
3.4.6 Plant-produced 10-1074 show high affinity to HIV-1 gp140 84
3.4.7 YTE mutation does not impact HIV-1 neutralisation 86

3.5 Discussion 89
4 Investigation of the effect of introduced modifications into bNAb 10-1074 on *in vitro* effector function and *in vivo* half-life 95
4.1 Introduction 95
4.1.1 Antibody-dependent cellular cytotoxicity (ADCC) 95
4.1.2 Half-life 96
4.2 Specific objectives 98
4.3 Contributions 98
4.4 Results 99
4.4.1 Antibody-dependent cellular cytoxicity (ADCC) 99
4.4.2 *In vitro* transcytosis and *in vivo* half life 105
4.5 Discussion 125
4.5.1 Affinity to FcγRIIIa and ADCC 125
4.5.2 FcRn affinity and transcytosis 127
4.5.3 *In vivo* half life 128
5 Generation of a stable ΔF *N. tabacum* plant line using CRISPR/Cas9 132
5.1 Introduction 132
5.2 Specific Objectives 134
5.3 Contributions 134
5.4 Results 135
5.4.1 Design and synthesis of sgRNAs 135
5.4.2 The selected sgRNAs successfully introduce indels into the fucosyltransferase gene 139
5.4.3 Stable transformation of explant using co-transformation with individual *FucT* sgRNAs results in no detectable change in fucosylation 142
5.4.4 Stable transformation of explant using tRNA-gRNA strings 145
5.4.5 T_1 transgenic plant lines show editing for at least one sgRNA 147
5.4.6 T_2 lines reveal a high number of editing events 151
5.4.7 Glycoanalysis reveals reduction in fucosylation 154
5.5 Discussion 160
5.5.1 Impact of the choice of sgRNAs and multiplexing 160
5.5.2 Impact of breeding 162
5.5.3 Impact of screening 163
5.5.4 Glycoanalysis 166
6 General discussion 168

6.1 Impact of bNAb with enhanced efficacy and their production in a plant expression system 168
6.2 Impact of a ΔF *N. tabacum* line 173
7 Conclusion and future work 174
8 Bibliography 177
9 Appendix 222
9.1 Buffers and Media 222
9.2 Primers 224
9.3 Primary and secondary antibodies 225
9.4 Alignment of retrieved fucosyltransferase mRNA sequences 226
9.5 IDAA and ICE results 229
9.6 Gels and Western Blots 234
9.6.1 SDS-PAGE with non-reduced and reduced samples 234
9.6.2 Western Blots 235
9.6.3 PNGase digest 239
9.6.4 Transcytosis and pharmacokinetics 241
9.6.5 Glycoanalysis 243

Acknowledgements

My gratitude extends to the Sir Joseph Hotung Charitable Settlement for funding this PhD project.

I would like to thank Prof Julian Ma for giving me the opportunity to do my PhD research in his exciting, wonderful group. Your friendly and fun nature created an excellent environment and made the past four years very enjoyable. I am grateful for your advice, support and encouragement. I have learned so much from you, and have grown more confident because of it.

I am grateful to Dr Audrey Teh, who has dedicated her time to supervising me and always offered her support for any problems. Your relaxed supervision and your trust in me have allowed me to develop as a scientist. I would also like to thank you for being so approachable and for taking me to various activities and outings across London.

I would like to acknowledge the Biological Research Facilities team at St George's for helping me with the *in vivo* half-life studies. I would also like to thank Prof Friedrich Altmann for allowing me to visit his group at BOKU Vienna to perform mass spectrometry and Dr Clemens Grünwald-Gruber and Daniel Maresch for their help in the laboratory.

Thanks to all my colleagues, past and present, in Julian's and Rajko's group. You've made this PhD journey absolutely fantastic. I had the best time with all of you. You make finishing my PhD a bittersweet moment. I am especially grateful to Dr Pascal Drake for his additional supervisory support, to Thais Guerra, who took great care of my plants, to Dr Matthew John Paul, who regularly helped me troubleshoot and to Dr Rajko Reljic for his help with my animal experiments.

I would also like to thank all of my friends I have met here at St George's: My bestie Andy, for joining me on incredible adventures here and around the world. Max, for challenging me and always making me laugh (even in my worst moments). Ashleigh, for always listening and for all the fun we have. J, for your kind words and our conversations. James, for always being up for anything. Jade, for

all the emotional support and laughter. Also, thanks to all my friends in Austria, who have always been there for me.

Am dankbarsten bin ich meiner Familie für deren finanzielle und liebevolle Unterstützung. Der meiste Dank gebührt meiner Mutter, Berthilde Grandits, der ich alles zu verdanken habe. Du bist mein größtes Vorbild. Ohne dich wäre das alles nicht möglich gewesen.

Abbreviations

(s)gRNA	(single) guide RNA
ΔF	fucosyltransferase deletion
ΔX	xylosyltransferase deletion
ΔXF	xylosyltransferase and fucosyltransferase deletion
A	Absorbance
A	ampere
AcCN	acetonitrile
ADA	anti-drug antibodies
ADCC	Antibody-dependent cellular cytotoxicity
ADCP	Antibody-dependent cellular phagocytosis
AIDS	Acquired Immune Deficiency Syndrome
ALC	alcobaca
API	active pharmaceutical ingredient
API	alkaline phosphatase
ART	Antiretroviral Therapy
AUC	area under the curve
av	average
BBL	berberine-bridge like
BCA	Bicinchoninic acid
b-GlcNAc	bisecting N-Acetylglucosamine
bNAb	Broadly neutralising antibody
bp	base pair
bs	binding site
BY-2	Bright-Yellow 2

Caco-2	colon carcinoma cell line
Cas	CRISPR associated protein
CCR5	C-C chemokine receptor type 5
CD4	cluster of differentiation 4
CD8	cluster of differentiation 8
CDR	complementarity determining region
CH	constant domain heavy chain
CHO	Chinese Hamster Ovary
CL	constant domain light chain
COGS	cost of goods sold
CRISPR	Clustered Regularly Interspaced Short Palindromic Repeats
crRNA	CRISPR RNA
cv	cultivar
CV	Column Volume
CXCR4	C-X-C chemokine receptor type 4
Da	Dalton
dCas9	nuclease-deficient Cas9
DDA	data-dependent acquisition
DEAE	Diethylaminoethyl
DMEM	Dulbecco's Modified Eagle's Medium
DNA	Deoxyribonucleic Acid
dpi	days post infiltration
DSB	double-strand break
DTT	Dithiothreitol
EC_{50}	Half maximal effective concentration

EIC	extracted ion chromatogram
ELISA	enzyme-linked immunosorbent assay
Env	Envelope
ER	endoplasmic reticulum
ESI	Electrospray ionisation
Fab	antigen-binding fragment
FBS	Fetal bovine serum
FcR	Fc receptor
Fc-region	fragment crystallisable region
FcRn	neonatal receptor
FP	fusogenic peptide
Fuc	Fucose
FucT	fucosyltransferase
FW	fresh weight
Gal	galactose
GalT	galactosyltransferase
GFP	green fluorescent protein
GlcNAc	N-Acetylglucosamine
GM	genetically modified
GMII	Golgi-α-mannosidase II
GMP	good manufacturing practice
GnT	N-acetylglucosaminyltransferase
gp	glycoprotein
h	hour
H_2SO_4	sulphuric acid

HBSS	Hanks' Balanced Salt Solution
HBV	hepatitis B virus
HC	heavy chain
HCl	Hydrochloric Acid
HDR	homology-directed repair
HEK	human embryonic kidney
HEPES	4-(2-hydroxyethyl)-1-piperazineethanesulfonic acid
hEPO	human erythropoietin
HIV	Human Immune Deficiency Virus
HR	heptad repeat
HRP	horseradish peroxidase
IC	immune complex
IC_{50}	half maximal inhibitory concentration
ICE	Inference of CRISPR Edits (indel percentage)
IDAA	Indel Detection Amplicon Analysis
Ig	Immunoglobulin
INDEL	insertion and/or deletion
IPTG	Isopropyl β- d-1-thiogalactopyranoside
IV	intravenous
k	kilo
KO	knockout
L	litre
LB	Luria-Bertani
LC	light chain
LC	Liquid Chromatography

LDS	lithium dodecyl sulfate
LMIC	Low middle income countries
LS	M428L/N434S
m	milli
M	molar
m	metre
mAb	monoclonal antibody
Man	Mannose
MDCK	Madin-Darby Canine Kidney
MHC	major histocompatibility complex
MIDAS	modular idempotent DNA assembly
min	minute
MPER	membrane proximal external region
mRNA	messenger Ribonucleic Acid
MS	Murashige and Skoog
MS	Mass spectrometry/spectrometer
MSN	mannosidase
MTCT	mother-to-child transmission
MW	molecular weight
n	nano
N. ben	*Nicotiana benthamiana*
N. tab	*Nicotiana tabacum*
NAb	Neutralising antibody
NeuAc	N-Acetyl-Neuraminic Acid (sialic acid)
NFAT	nuclear factor of activated T-cells

NF-κB	nuclear factor kappa-light-chain-enhancer of activated B cells
NHEJ	non-homologous end joining
NHP	non-human primate
NK cells	Natural Killer cells
NP	non-PNGase F digested
NR	non-reduced
nt	nucleotide
OD	optical density
OST	oligosaccharyl-transferase
P	PNGase F digested
PAM	protospacer adjacent motif
PBS	Phosphate-Buffered Saline
PCR	polymerase chain reaction
PDR	pleiotropic drug resistance
PDS	phytoese desaturase
PEP	post-exposure prophylaxis
PI	PAM-interacting
PK	pharmacokinetic
PrEP	pre-exposure prophylaxis
PTG	polycistronic-tRNA-gRNA
PTM	posttranslational modification
QTOF	Quadrupole time-of-flight mass spectrometry
R	reduced
RDR	RNA-dependent polymerase
REC	recognition lobe

RLU	relative light units
RNA	Ribonucleic Acid
RNAi	RNA interference
RNP	Ribonucleoprotein
rpm	rotations per minute
RSV	respiratory syncytial virus
RT	room temperature
RU	Response Unit
s	second
SD	standard deviation
SDS-PAGE	sodium dodecyl sulphate-polyacrylamide gel electrophoresis
SNP	single nucleotide polymorphism
SNR	signal-to-noise ratio
SPR	Surface Plasmon Resonance
ssRNA	single-stranded Ribonucleic Acid
ST	sialyltransferase
t1/2	half-life
Ta	annealing temperature
TALEN	transcription activator-like effector nuclease
TBS	Tris-buffered saline
TMDD	target-mediated drug disposition
tracrRNA	trans-activating RNA
tRNA	transfer Ribonucleic Acid
U	units
V	volt

V1	variable loop 1
V2	variable loop 2
V3	variable loop 3
V4	variable loop 4
V5	variable loop 5
VH	variable domain heavy chain
VL	variable domain light chain
WHO	World Health Organisation
wt	wild-type
X-Gal	5-bromo-4-chloro-3-indolyl-β-D-galactopyranoside
Xyl	xylose
XylT	xylosyltransferase
YTE	M252Y/S254T/T256E
ZNF	Zinc-finger nuclease
µ	micro

List of Figures

Figure 1-1: Estimated number of new HIV-1 infections in 2017 worldwide. 1

Figure 1-2: Genome organisation of HIV-1 and HIV-2.....2

Figure 1-3: Schematic structure of an HIV virion 4

Figure 1-4: Life cycle of HIV. 5

Figure 1-5: Side view of the Env trimer..... 7

Figure 1-6: Schematic view of the HIV Env protein..... 11

Figure 1-7: Factors that have been associated with bNAb development in HIV-1 positive patients... 14

Figure 1-8: Types of Fcγ receptors displaying their structure, function and affinity 21

Figure 1-9: Basic principle of antibody-dependent cellular cytotoxicity..... 22

Figure 1-10: IgG recycling. Serum proteins are taken up by monocytes and endothelial cells, which express the FcRn. 24

Figure 1-11: Downstream processing steps required for the GMP-compliant production of mAbs….33

Figure 1-12: Differences in complex N-glycosylation between mammals and plants. 34

Figure 1-13: N-glycosylation processing pathways in the ER and Golgi apparatus of mammals…….37

Figure 1-14: N-glycosylation processing in the ER and Golgi apparatus of plants 39

Figure 1-15: The two main glycoforms generated by plants and the key glycan structure of higher eukaryotes. 40

Figure 1-16: The mechanism of the CRISPR/Cas system as discovered in prokaryotes..... 43

Figure 1-17: Schematic depiction of genome editing mediated by CRISPR/Cas9..... 44

Figure 1-18: Crystal structure of the S. pyogenes CRISPR-Cas9 system..... 45

Figure 3-1: The Modular Idempotent DNA assembly (MIDAS) system.. 73

Figure 3-2: Western blot to verify the expression of 10-1074 LS). 75

Figure 3-3: Representative SDS PAGE with native 10-1074, 10-1074 YTE and a mAb IgG λ control... 77

Figure 3-4: Rationale of a PNGase F digest. 79

Figure 3-5: Representative SDS-PAGE analysis of the PNGase F digest 80

Figure 3-6: Representative Anti-glycan western blot with 10-1074 produced in ΔXF N. benthamiana and two positive controls. 81

Figure 3-7: Mass spectrum for 10-1074 HC ΔXF and YTE ΔXF obtained using LS-ESI-MS. 83

Figure 3-8: Workflow of measuring gp140 binding with Surface Plasmon Resonance. 84

Figure 3-9: Binding kinetics of 10-1074 to UG37 gp140 for 10-1074 HC and YTE as well as 10-1074 produced in CHO. 85

Figure 3-10: Neutralisation curves from neutralisation assays 87

Figure 3-11: Correlation of 10-1074 CHO IC50s with 10-1074 HC ΔXF IC50s 74

Figure 4-1: Strategy for determining binding kinetics of FcγRIIIa V158 to bNAbs using SPR 99

Figure 4-2: FcγRIIIa V158 binding analysis with multiple FcγRIIIa V158 concentrations using Surface Plasmon Resonance.. 100

Figure 4-3: Means with error bars (SD) of the ADCC activation assay for FcγRIIIa V-variant 103

Figure 4-4: Means with error bars (SD) of the ADCC activation assay for FcγRIIIa F-variant 104

Figure 4-5: Normalised curves of the ADCC activity assay 105

Figure 4-6: A conventional SPR strategy to measure affinity of FcRn to an antibody 106

Figure 4-7: SPR strategy to measure affinity of FcRn to an antibody using a CM5 chip coated with an anti-λ antibody. 106

Figure 4-8: SPR strategy to measure affinity of FcRn to an antibody using a CM5 chip coated with an anti-goat antibody 106

Figure 4-9: Principle of SPR workflow applied for FcRn affinity measurements. 107

Figure 4-10: SPR sensograms of single cycle kinetics for FcRn binding 108

Figure 4-11: Principle of the transcytosis assay 109

Figure 4-12: Results of representative transcytosis experiment performed with MDCK hFcRn/hβ2m cells. 109

Figure 4-13: Time course study of transcytosis of respective bNAbs through a monolayer of Caco-2 cells. 110
Figure 4-14: Serum concentration of two 10-1074 variants at 4 time points in individual mice..... 112
Figure 4-15: Serum concentration of two 10-1074 variants at 5 time points in individual mice..... 114
Figure 4-16: Serum concentration of respective 10-1074 variant at 5 time points in individual mice 115
Figure 4-17: Serum concentration of two10-1074 variants at 5 time points in individual mice 116
Figure 4-18: The impact of gender on the ratio of 10-1074 YTE left in serum at 144 h. 119
Figure 4-19: The impact of weight on the ratio of 10-1074 YTE left in serum at 144 h..... 120
Figure 4-20: The impact of initial concentration (c0) on the ratio of 10-1074 YTE left in serum at 144 h. 120
Figure 4-21: Relative IgM levels of serum diluted 100 times at 24 h and 192 and 264 h. 122
Figure 4-22: Mean and error bars (SD) of relative standardised IgM levels for all experiments..... 123
Figure 4-23: Relative IgM levels (as A450) vs c0 (µg/ml).. 124
Figure 5-1: Generation of sgRNA. 136
Figure 5-2: Representative results of PCRs to amplify the sgRNAs of choice. 137
Figure 5-3: pFGC-pcoCas9 vector..... 138
Figure 5-4: Digest of all pFGC-pcoCas9/sgRNA plasmids. 138
Figure 5-5: Percentage of peak areas for gene-editing events induced by the sgRNAs F1 and F2 141
Figure 5-6: Screening of the 20 T_0 plant line by dot-blots). 143
Figure 5-7: Anti-α(1,3) fucose ELISA for selected T_0 plant lines..... 144
Figure 5-8: Schematic illustration of the polycistronic tRNA-gRNA (PTG)/Cas9 system..... 145
Figure 5-9: Anti-α(1,3)-fucose western blot for selected T_0 lines with samples adjusted to the same concentration 146
Figure 5-10: Dot blot screening of T1 plant line 7 and 14 147

Figure 5-11: Anti-α(1,3)-fucose western blot for selected T_1 lines with samples adjusted to the same concentration 148

Figure 5-12: Results of ICE Analysis for selected T1 lines. 150

Figure 5-13: Results of ICE analysis for line B , line C and line T2 7-21 152

Figure 5-14: α-hIgG-κ western blot performed for VRC01 expressed in selected T_2 plant lines 155

Figure 5-15: Spectrum for tryptic digest of VRC01 produced in N. tabacum SR1 wild-type and the putative knockout line T2 7-21-1. 157

Figure 5-16: Spectrum for GluC digest of VRC01 produced in N. tabacum SR1 wild-type and the putative knockout line T2 7-21-1 158

Figure 5-17: Reduction in N-glycan fucosylation of VRC01 expressed in the putative knockout lines in relation to N-glycan fucosylation observed in the wild-type 159

List of Tables

Table 2-1: Nomenclature of 10-1074 variants used throughout thesis 52

Table 2-2: Accession numbers of aligned mRNA sequences of N. tabacum FucT given with label used throughout the study and the cultivar they were obtained from. 62

Table 2-3: PCR program for Phusion PCR to generate sgRNA 62

Table 2-4: PCR program for generation of amplicons for IDAA 65

Table 3-1: Crude extract yield for 10-1074 HC, YTE and LS ΔXF in mg/kg $_{\text{fresh weight}}$ 74

Table 3-2: Yield for each batch of 10-1074 HC, YTE and LS in mg/kg $_{\text{fresh weight}}$ prior to sterile-filtration 74

Table 3-3: Yield for 10-1074 HC, YTE in mg/kg $_{\text{fresh weight}}$ with addition of 0.01 % Tween80 post sterile-filtration 76

Table 3-4: Glycoform percentage in representative 10-1074 HC ΔXF and YTE ΔXF sample respectively 82

Table 3-5: IC_{50}s (ng/mL) obtained for 10-1074 HC ΔXF, YTE ΔXF neutralising various HIV-1 strains from different clades 87

Table 3-6: Neutralisation potency (IC_{50}, ng/mL) of the native 10-1074 variant produced in either ΔXF or CHO. 88

Table 4-1: Average affinity and dissociation parameters of multiple concentration FcγRIIIa V158 binding analysis obtained for of 10-1074 HC ΔXF (n=3), 10-1074 YTE ΔXF (n=3) and the 10-1074 CHO (n=1) control. 101

Table 4-2: Area under the curve given as mean for each study and as total mean. Standard deviation (SD) and sample size (n) are given next to mean. 117

Table 5-1: IDAA result for the sgRNAs F1 and F2. The height and peak area for each amplicon size (size) represent the occurrence of that particular peak. The wild-type peak is given in italics. 140

Table 5-2: Cutting efficiency of individual sgRNAs determined by IDAA. Average percentage of occurrence indel peak for each sgRNA is given. 141

Table 5-3: Primers flanking cutting sites of sgRNAs used in the tRNA-gRNA construct..... 149

Table 5-4: Parentage of T_2 putative ΔF lines..... 151

Table 5-5: Putative knockout T_2 plant lines selected for further in-depth analysis..... 153

1 Introduction

1.1 HIV/AIDS

Acquired Immune Deficiency Syndrome (AIDS) is an illness that rapidly developed into a worldwide epidemic (UNAIDS, 2019). This fatal disease was observed during the 1980s (Gottlieb *et al.*, 1981), and in 1983, the cause of the disease, the human immunodeficiency virus (HIV), was identified (Barre-Sinoussi *et al.*, 1983). HIV is mainly transmitted via unprotected sexual intercourse, contaminated needles, blood transfusions and from mother to child during pregnancy and breastfeeding (Shaw and Hunter, 2012). Nowadays, antiretroviral therapy (ART) offers HIV patients the perspective of almost normal life-expectancy and very low risk of transmission (The Antiretroviral Therapy Cohort Collaboration, 2008; Mills *et al.*, 2011). Yet, each year there are still around 2 million new infections (Figure 1-1) and a considerable, albeit declining, number of casualties (approx. 800,000 people worldwide in 2018) (UNAIDS, 2019). Considering these numbers, the high rate of spontaneous mutations of HIV, rising resistance to ART and especially the prevalence in low-income Sub-Saharan Africa, the search for a cure or effective preventative measures is as important as 40 years ago.

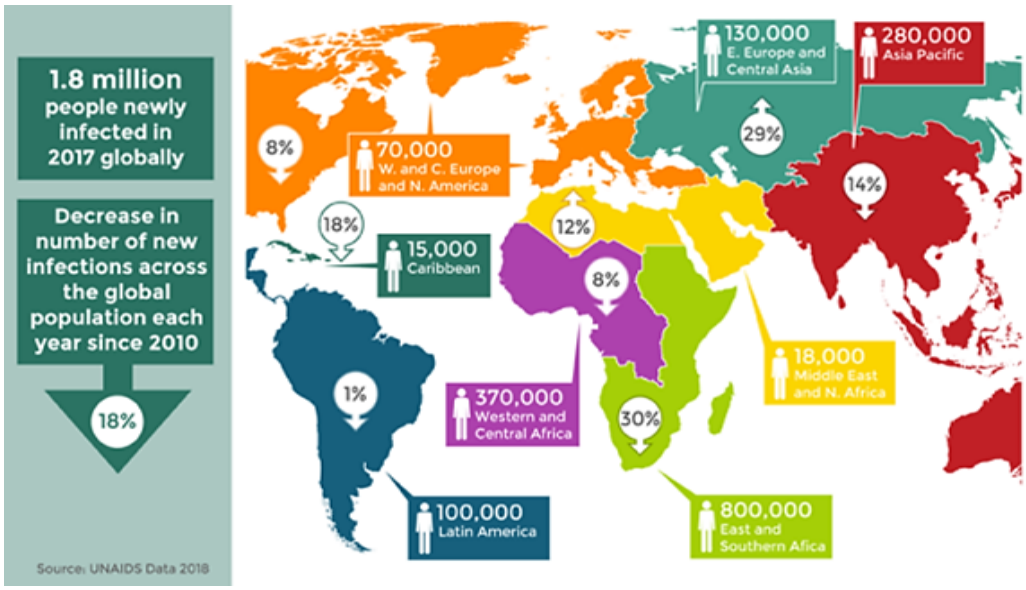

Figure 1-1: Estimated number of new HIV-1 infections in 2017 worldwide in comparison to new infections in 2010 (https://www.avert.org/global-hiv-and-aids-statistics).

1.1.1 HIV genome and life cycle

HIV is a lentivirus (Gonda *et al.*, 1985), currently classified into HIV type 1 (HIV-1) and HIV type 2 (HIV-2) on the basis of the organisation of its genome (Guyader *et al.*, 1987).

The HIV genome consists of nine genes encoding for 15 proteins with structural or regulatory functions (Frankel and Young, 1998; Watts *et al.*, 2009). It is flanked by long-terminal repeats (LTRs), which are essential for transcription and integration. The group-specific antigen (*gag*) gene encodes for the matrix protein (MA, p17), the capsid protein (p24), the nucleocapsid protein (p7), two spacer peptides (SP1 and SP2) and protein p6. The polymerase (*pol*) gene gives rise to the viral reverse transcriptase (RT), integrase (IN) and protease (PR). Transcription of the envelope gene (*env*) leads to gp160, which is cleaved into gp120 and gp41 by the viral furin protease. Two regulatory genes, namely the transcriptional transactivator (*tat*) and regulator of virion expression (*rev*) genes, are essential for viral replication. Additionally the genome contains four accessory genes, which include the viral infectivity factor (*vif*), viral protein r (*vpr*), viral protein u (*vpu*/ *vpx* in HIV-2) and negative factor (*nef*) gene. These gene products impact viral replication, budding and pathogenesis (Kräusslich *et al.*, 1995; Watts *et al.*, 2009; Checkley *et al.*, 2010; German Advisory Committee Blood (Arbeitskreis Blut), 2016).

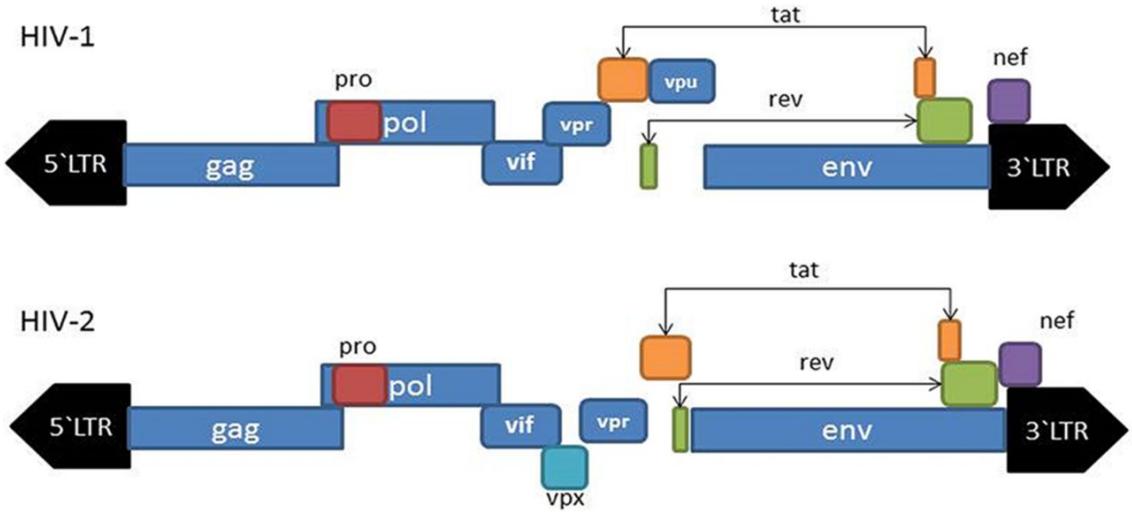

Figure 1-2: Genome organisation of HIV-1 and HIV-2. HIV-1 vpu is replaced by vpx in HIV-2.(Mahdi *et al.*, 2018)

HIV-1 is responsible for the majority of infections worldwide, whereas HIV-2 is predominantly found in Western and Central Africa and is less aggressive (De Cock *et al.*, 1993). Most of the current research mainly focuses on HIV-1 (Lorenzo-Redondo *et al.*, 2016; Tirumuru *et al.*, 2016; Kosaka *et al.*, 2017). The decryption of the structure and infection mechanism of HIV allowed for the development of targeted therapies (Hartman and Buckheit, 2012).

The HIV particle is made up of a capsid that contains 2 copies of positive sense ssRNA molecules and essential viral enzymes like reverse transcriptase and integrase (Figure 1-3). The capsid itself is surrounded by a matrix consisting of the viral protein p17, which in turn is enclosed by the viral envelope derived from the host cell. The viral envelope also includes envelope glycoprotein (gp) complexes which are necessary for attachment of the virus to the host cell (Fanales-Belasio *et al.*, 2010). Each complex consists of a trimer of gp41 to which a trimer of gp120 is non-covalently bound (Gelderblom, Ozel and Pauli, 1989). Gp120 binds to CD4, a receptor found on the cell surface of various human immune cells such as T-lymphocytes, monocytes and macrophages (Bour, Geleziunas and Wainberg, 1995; Claeys and Vermeire, 2019).

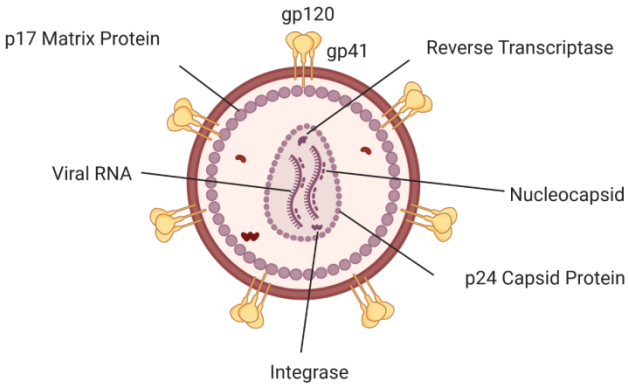

Figure 1-3: Schematic structure of an HIV virion. Two ssRNA molecules and viral enzymes like reverse transcriptase are located within the capsid. The capsid is surrounded by the matrix, which consists of protein p17. The matrix, in turn, is surrounded by the viral envelope, which is derived from the host cell. The viral envelope carries glycoprotein (gp) heterodimers, consisting of a trimer of gp41 and a trimer of gp120

Binding to CD4 triggers a change in the viral envelope complex structure, thereby exposing the binding site to the co-receptor, CCR5 (C-C chemokine receptor type 5) or CXCR4 (C-X-C chemokine receptor type 4) (Wu *et al.*, 1996). The binding of the co-receptor causes further structural changes, which are crucial for fusion of the viral and host cell membrane, which subsequently allows the virus to enter the host cell. Upon entry into the cell, the viral capsid is immediately uncoated, releasing the ssRNA which serves as template for the reverse transcriptase to synthesise viral DNA (Figure 1-4). This viral DNA is subsequently integrated into the host genome by the viral integrase (provirus) (Fanales-Belasio *et al.*, 2010). The integrated DNA may lie dormant until certain triggers, such as upregulation of NF-κB by pro-inflammatory cytokines, are present (Coiras *et al.*, 2009). After that, transcription of proviral DNA into mRNA occurs, which then migrates into the cytoplasm for the synthesis of structural precursor molecules. The HIV protease cleaves these to generate the components for a new infectious particle. Next, the capsid forms around two ssRNA molecules and the viral enzymes. Finally budding through the host membrane occurs (Fanales-Belasio *et al.*, 2010).

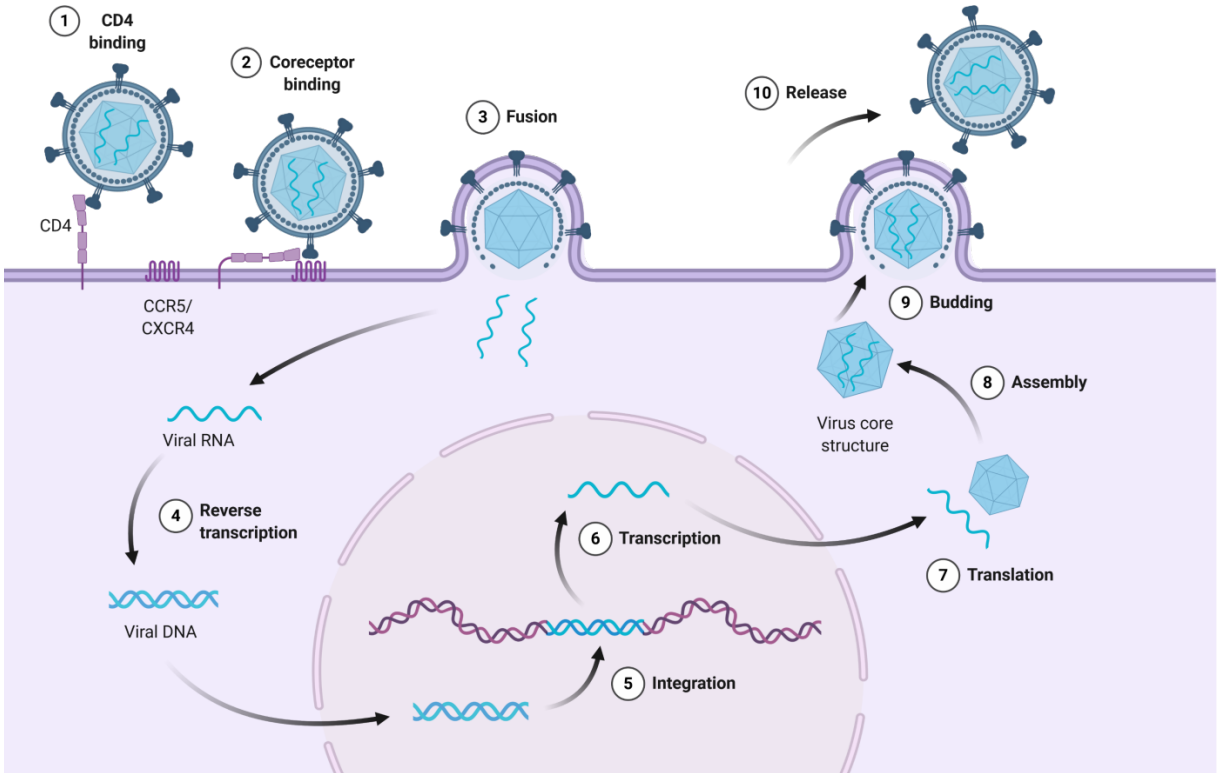

Figure 1-4: Life cycle of HIV shown. The virion binds to the CD4 and the respective chemokine receptor (CCR5/CXCR4), upon which the particle fuses with the host cell membrane and releases the viral genome into the cytoplasm. After reverse transcription, the viral DNA is integrated into the host genome in the nucleus. Proviral DNA is transcribed; the transcripts leave the nucleus, are translated and assemble, together with essential viral proteins, into the core structure. Subsequently, budding occurs which releases a new mature viral particle.

1.1.2 The HIV envelope

The elucidation of HIV-1 Env (Figure 1-5) beyond the trimeric structure of gp120-gp41 heterodimers proved challenging due to the instability of the Env protein (Ward and Wilson, 2017). Current knowledge of the HIV Env trimer therefore mainly stems from analyses of Env proteins that have been modified for stabilisation or have formed complexes with antibodies (Wyatt *et al.*, 1998; Kwong *et al.*, 2000; Huang *et al.*, 2007; Zhou *et al.*, 2007, 2010; Pancera *et al.*, 2010; Wu *et al.*, 2011; Kong *et al.*, 2013; Merk and Subramaniam, 2013; Ward and Wilson, 2017). Gp120 consists of an inner domain and outer domain which are connected by a bridging sheet (Merk and Subramaniam, 2013; Ward and Wilson, 2015). It is highly glycosylated on its surface and comprises five variable loops (V_1-V_5), which not only tolerate a high number of mutations, but are also flexible and exhibit high glycosylation levels (Merk and Subramaniam, 2013; Ward and Wilson, 2015, 2017). The variable

loops are located under and between the glycans and span out around the gp120 core, thus protecting conserved regions of the glycoprotein. The V1, V2 and V3 loops make up the trimer apex and are involved in stabilising protomer contacts, whereas the outward facing V4 and V5 loops remain unengaged (Merk and Subramaniam, 2013; Ward and Wilson, 2015, 2017). In contrast to the V1 and V2 loops, the length of V3 remains fairly constant between isolates in order to maintain essential trimer-stabilising contacts (Zolla-Pazner and Cardozo, 2010; Ward and Wilson, 2015). Furthermore, the V3 loop carries the rather conserved co-receptor binding site (Shioda, Levy and Cheng-Mayer, 1992; Sharon *et al.*, 2003; Cardozo *et al.*, 2007), explaining the positioning of the V3 loop beneath the V1 and V2 loop, which partially protects the V3 loop from neutralising antibodies. While the surface of gp120 is generally heavily glycosylated, the CD4 binding site (bs) is lacking glycans, however, accessibility is not only limited by the V1-V3 loop but also by its proximity to the interprotomer interface (Ward and Wilson, 2015). The glycans on the gp120 surface range from high mannose structures to more complex glycan types. The glycan shield, which consists of approx. 80-90 glycans, is generally perceived as a barrier for antibodies, however, broadly neutralising antibodies often recognise glycans, especially at site N332, located on the high-mannose patch of gp120 (Pejchal *et al.*, 2011; Kong *et al.*, 2013; Garces *et al.*, 2014; Sok *et al.*, 2014).

In contrast to gp120 sequences of gp41 are more conserved, as they are essential for fusion with the cell membrane (Ward and Wilson, 2015). Gp41 consists of the hydrophobic N-terminal fusogenic peptide (FP), two trimeric heptad repeats (HR), the linker region and the membrane proximal external region (MPER) (Weissenhorn *et al.*, 1997; Ward and Wilson, 2015). A trimer of the peptide N36, originating from the N-terminal heptad repeat (NHRI), forms the internal part of the gp41 core, while a trimer of C34, originating from the C-terminal heptad repeat (CHRII) forms the external shell (Chan *et al.*, 1997; Ward and Wilson, 2015).

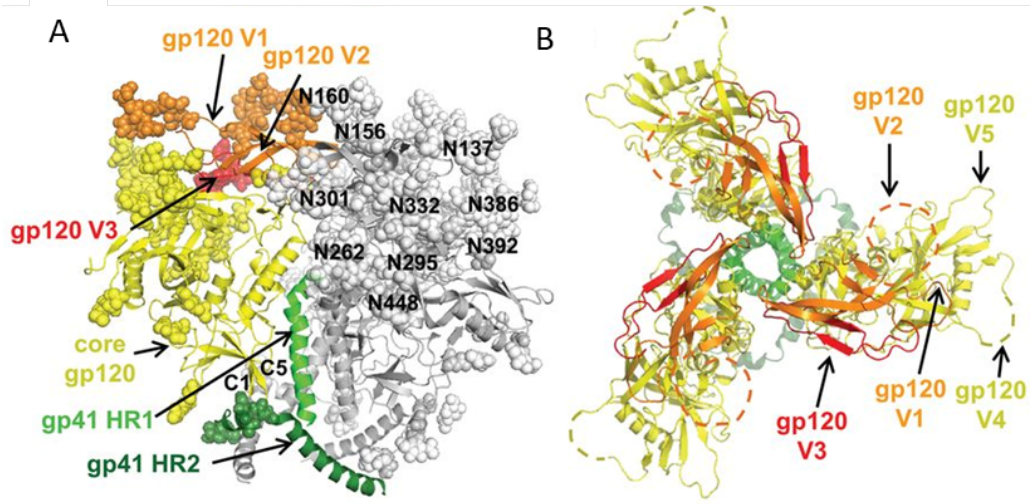

Figure 1-5: A) Side view for one protomer of the Env trimer. The gp120 core is shown in yellow, V1/V2 are shown in orange and V3 is depicted in red. The gp41 heptad repeat 1 (HR1) and heptad repeat 2(HR2) are coloured in light and dark green respectively. Glycans are shown as spheres. B) Top view of Env trimer without glycans. Variable loops are shown in yellow (V4,V5), orange (V1,V2) and red (V3) (Julien et al., 2013).

1.1.3 Risk of transmission

HIV is transmittable by various routes, most commonly blood-to-blood, mother-to-child transmission (MTCT) and through sexual intercourse. However, the risk of infection is extremely variable and dependent on the mode of exposure. The highest risk of transmission is associated with blood transfusions, with an estimated transmission rate of 92.5 percent (Patel *et al.*, 2014). This is followed by mother-to-child transmission (MTCT) with a reported rate of 15-45 percent (WHO, 2017). The risk for people who inject drugs is about 0.63 percent (Patel *et al.*, 2014). Sexual intercourse bears an increased chance of infection for the receptive partner, which is higher for anal intercourse (1.38 percent) than for vaginal intercourse (0.08 percent) (Patel *et al.*, 2014).

Despite these seemingly low probabilities, availability of antiretroviral therapy and of risk lowering contraceptives, a high number of new infections per year are caused by sexual intercourse (UNAIDS, 2019). It is hard to pinpoint what specifically causes these high numbers, but major contributing factors are extreme poverty, insufficient education on the consequences of HIV infection and unawareness of HIV status. In general, women are more likely to be aware of their HIV

status, as it is routinely tested for in case of a pregnancy, to prevent MTCT by ART intervention (DiCarlo *et al.*, 2014; Gebregziabher *et al.*, 2018; Ha *et al.*, 2019).

1.1.4 Current treatments – Antiretroviral therapy (ART)

At the present time, HIV infection is treated with antiretroviral drugs. Administration of a single antiretroviral drug proved to be inefficient, leading rapidly to the development of resistant strains (Pennings, 2013; Pau and George, 2014). Therefore, ART is now composed of a combination of drugs, each of which targets a specific step of the HIV life cycle. This combinatorial approach has proven to inhibit viral replication, in turn significantly slow down disease progression and lower the risk of transmission (Cihlar and Fordyce, 2016). Yet, treatment of HIV with ART is associated with a number of drug-specific and non-specific difficulties. A major problem -which is not specific to ART-, is to provide widespread treatment coverage. In 2018 it was estimated that only 62 percent of people living with HIV-1 globally, accessed antiretroviral therapy (UNAIDS, 2019). The percentage of HIV patients accessing treatment in individual countries is closely related to not only the economic status of the nation but also the stigma that comes with the disease. The lowest percentage of HIV-infected individuals accessing treatment was reported in the Middle East and North Africa (UNAIDS, 2019). These numbers most likely arise from the strict laws that are in place in the majority of these countries. As punishment for sex work, drug use and particularly same-sex intercourse is severe, including the death penalty, individuals are less likely to access ART (Gökengin *et al.*, 2016). This is further reflected in the Middle East and North Africa, being regions that show a rise in new infections, in contrast to the global decline since 2010 (Figure 1-1).

A major drug-related problem of ART is adherence. Currently available ART has to be taken daily, omitting a dose bears the risk of viral escape (O'Connor *et al.*, 2016) and rendering the prescribed regimen ineffective. ART is not an ideal treatment; it is not without its side-effects, which can range from less severe side effects like rashes to severe side effects like hepatitis or nephrotoxicity (Reust, 2011). Adherence is not only linked to the severity of the experienced side-

effects but also to the age and mental state of the patient. Additional factors are poverty and low infrastructure in low to middle income countries (Kim *et al.*, 2018; Mbuagbaw *et al.*, 2018; Samuel Edward *et al.*, 2018). Several measures can be taken to improve adherence, one of them being the development of long-lasting formulations, which have to be taken once a month or even less regularly (Zhang, 2018).

Last but not least, the virus frequently mutates and eventually escapes the inhibition of individual ART, thus the development of a highly drug-resistant viral strain is probable (Masenyetse, Manda and Mwambi, 2015; Cihlar and Fordyce, 2016). In fact, a report published by the WHO in 2019 revealed that in 12 out of 18 surveyed countries, pre-treatment drug resistance to two first line non-nucleoside reverse transcriptase inhibitor drugs (efavirenz, nevirapine) exceeded 10 percent. Drug resistance was more commonly seen in women than men, which may be the result of lower rates of adherence to ART. Furthermore, about 50 percent of infants (≤ 18 months) surveyed in 9 countries of Sub-Saharan Africa carried a virus resistant to efavirenz and/or nevirapine (World Health Organization (WHO), 2019). Yet, susceptibility testing to ART prior to treatment start is currently not routinely performed in LMICs, which results in some patients receiving ineffective drugs (Noguera-Julian, 2019). Follow-up appointments to ensure treatment efficiency are also scarce, thus virologic failure due to resistance often goes undetected for long periods (Gupta *et al.*, 2018), leading to increased transmission of drug-resistant virus, an increase in progression to AIDS and therefore HIV-related deaths. This further highlights the importance of the development of new treatments.

1.1.5 Failure of vaccination – HIV challenges

The most effective option to control infectious diseases is prevention by vaccination (Greenwood, 2014). Initially, it appeared relatively simple to provide a vaccine against HIV, due to its narrow tropism. Thus, the development of a recombinant vaccine comprising gp120 seemed promising (Mascola *et al.*, 1996). However, sera of healthy volunteers immunised with envelope

subunit vaccines, collected during nine different clinical phase I trials, exhibited no neutralising activity against HIV-1 primary isolates *in vitro* (Mascola *et al.*, 1996).

The vaccine trial RV144, also referred to as the 'Thai trial', utilised a prime-boost strategy combining two previously failed vaccines; ALVAC-HIV (prime) and AIDSVAX B/E (boost). 16,402 healthy volunteers from heterosexual high-risk groups were enrolled. The combination of these vaccines resulted in moderate (31.2 percent) vaccine efficacy (Rerks-Ngarm *et al.*, 2009), which remains to this date a unique result. This outcome triggered a series of vaccine trials with prime-boost approaches. One of these, the Uhambo trial (NCT02968849), used ALVAC-HIV as prime and a bivalent subtype C gp120 as boost vaccination. However, the Phase IIb/III study was discontinued in 2020, due to the vaccine being ineffective in preventing HIV infection (http://uhambo.org.za/). Two other prime-boost trials use Ad26.Mos4.HIV, a tetravalent adenovirus-based vaccine candidate, which carries mosaic HIV antigens, as the prime vaccination. The IMBOKODO trial (NCT03060629) boosts with a clade C gp140 together with Ad26.Mos4.HIV and the MOSAICO trial (NCT03964415) further includes mosaic gp140.

HIV exhibits various characteristics impeding the generation of vaccines or preventative therapeutics, such as shielding of vulnerable regions to neutralising antibodies (Wei *et al.*, 2003), rapid integration into the host genome and formation of a pool of resting cells which are not detectable by the immune system (Folks *et al.*, 1986). The poor fidelity of the reverse transcriptase (Patel and Preston, 1994) and *in vivo* recombination (Shriner *et al.*, 2004) are particularly challenging features, as they lead to continually evolving viral species, allowing the virus to escape the immune response.

1.1.6 Broadly neutralising antibodies (bNAbs)

The isolation of the first broadly neutralising antibody (bNAb) from an HIV positive patient resulted in new optimism (Klein *et al.*, 2013). Broadly neutralising antibodies (bNAbs) develop in rare

HIV positive individuals ('elite neutralisers') about one year post-infection (Doria-Rose *et al.*, 2009). They are capable of neutralising a variety of different primary strains of HIV-1 (measured in neutralisation breadth) and preventing the viral replication cycle by blocking attachment and entry into the host cell (Klasse, 2014). Yet, they are not able to completely eliminate HIV in individuals producing these bNAbs, as the virus sooner or later escapes this immune response.

The isolation and characterisation of bNAbs revealed five sites of vulnerability of the HIV envelope: the CD4 binding site of gp120, the membrane proximal external region (MPER), the V3 glycan, an epitope made up of V1/V2 and an epitope at the gp120/gp41 interface which includes the fusion peptide (Figure 1-6) (Pancera, Changela and Kwong, 2017).

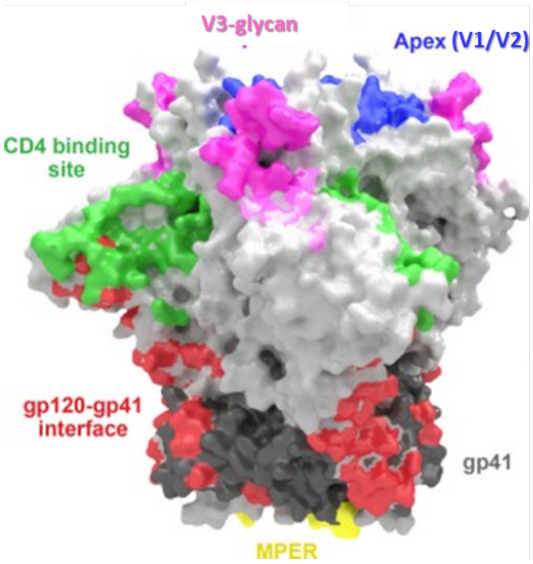

Figure 1-6: Five epitopes of broadly neutralising antibodies on the HIV-1 envelope glycoprotein. CD4 binding site (CD4bs, green), gp120/gp41 interface (red), membrane-proximal external region (MPER, yellow), variable loop 3 glycan (V3 glycan, pink) and variable loop 1 and 2 (Apex V1/V2, blue). The gp 120 and gp41 subunit are shown in light gray and dark grey, respectively. Adapted from (McCoy and Burton, 2017)

In general, the structure of bNAbs differs from 'common' antibodies e.g. by the higher occurrence of protruding loops, mostly the CDR-H3 loop, and a higher rate of somatic hypermutations (Chuang *et al.*, 2019). However, the type of structural diversions from common

antibodies is dependent on the target site of the bNAb (West *et al.*, 2014). CD4bs bNAbs are classified into two categories; CD4bs-mimetics and CDR-H3 loop dominant (West *et al.*, 2014). The V_H domain of CD4bs-mimetics engages the same position as CD4 on gp120, which mainly involves the bNAb's CDR-H2 loop. Characteristic of potent CD4bs-mimetics are a length-limited CDR-L3 loop (5 aa) and a short or glycine-rich CDR-L1 loop, to provide flexibility for avoidance of steric clashes with gp120 (Prabakaran *et al.*, 2006; Zhou *et al.*, 2010; Diskin *et al.*, 2011; West *et al.*, 2012). CDR-H3 loop dominant CD4bs bNAbs use slightly elongated CDR-H3 loops (around 20 aa) to access the CD4bs (Burton *et al.*, 1994; Liao *et al.*, 2013; Yu and Guan, 2014). While CD4bs bNAbs can be easily classified based on their mode of recognition, V1/V2 and V3-binding bNAbs are more diverse in their structural alterations. However, a common feature is the presence of long CDR-H3 loops of up to 34 amino acids, whereas the average length of CDR-H3 loops of normal mAbs is 16 amino acids (West *et al.*, 2014; Yu and Guan, 2014). Extended CDR-H3 loops with hydrophobic residues at their tip are typical for bNAbs targeting the MPER (Pinto *et al.*, 2019). Irrespective of the targeted epitope, a universal feature of anti-HIV bNAbs is a high incidence of somatic hypermutations (West *et al.*, 2014). These occur primarily in the V_H domain with up to 48 % of amino acids being mutated (Yu and Guan, 2014), thus significantly differing from common Nabs.

The exact processes leading to the development of bNAbs in contrast to NAbs are not elucidated yet. A vast number of parameters have been implicated in bNAb development (Figure 1-7), however, only the most salient will be briefly discussed here, including viral load, envelope diversity, pre-existing immunity through maternal antibodies. It is generally accepted that one of the driving factors is the constant interplay between antibody response and virus escape, though it is not clear whether virus divergence is caused by the antibody response or is the driving force (Sather *et al.*, 2012; Liao *et al.*, 2013; Moore *et al.*, 2013; Landais and Moore, 2018; Subbaraman, Schanz and Trkola, 2018). Viral escape is facilitated by glycan shifts and the virus's high rate of mutations, leading to substitutions and INDELs, therefore rendering the epitope either unrecognisable or inaccessible to strain-specific Nabs (Moore, Williamson and Morris, 2015). Viral escape triggers B

cells to undergo additional rounds of affinity maturation to yield bNAb intermediates which are able neutralise the escape variants. This in turn further drives virus diversification and the development and selection of antibody sub-lineages with higher breadth, which eventually lead to bNAbs (Landais and Moore, 2018). It is further assumed that slow virus escape is beneficial for the development of bNAbs, as an extended period of antigenic stimulation might improve the chances of antibody maturation (Anthony *et al.*, 2017; Reh *et al.*, 2018).

A characteristic that is commonly found in individuals that generate bNAbs, is a higher viral load compared to other individuals, yet bNAbs can also be found in patients with low viral loads (Landais and Moore, 2018; Subbaraman, Schanz and Trkola, 2018). Interestingly, bNAbs are more likely to develop in infants with HIV-1 (70 % of cases), which have been infected through MTCT, than in infected adults (Goo *et al.*, 2014; Muenchhoff *et al.*, 2016). It is speculated that maternal antibodies may serve as helper antibodies allowing the immune system to generate high breadth antibodies faster (Bonsignori *et al.*, 2016; Anthony *et al.*, 2017; Subbaraman, Schanz and Trkola, 2018).

Researchers anticipate that identifying the underlying mechanisms of bNAb evolution in patients, will allow for the development of an effective vaccine. However, the extent of complex processes that are likely involved in *in vivo* development of bNAbs (Figure 1-7) suggests that induction of an equivalent immune response is improbable, therefore perhaps the potential of bNAbs lies in passive immunotherapy.

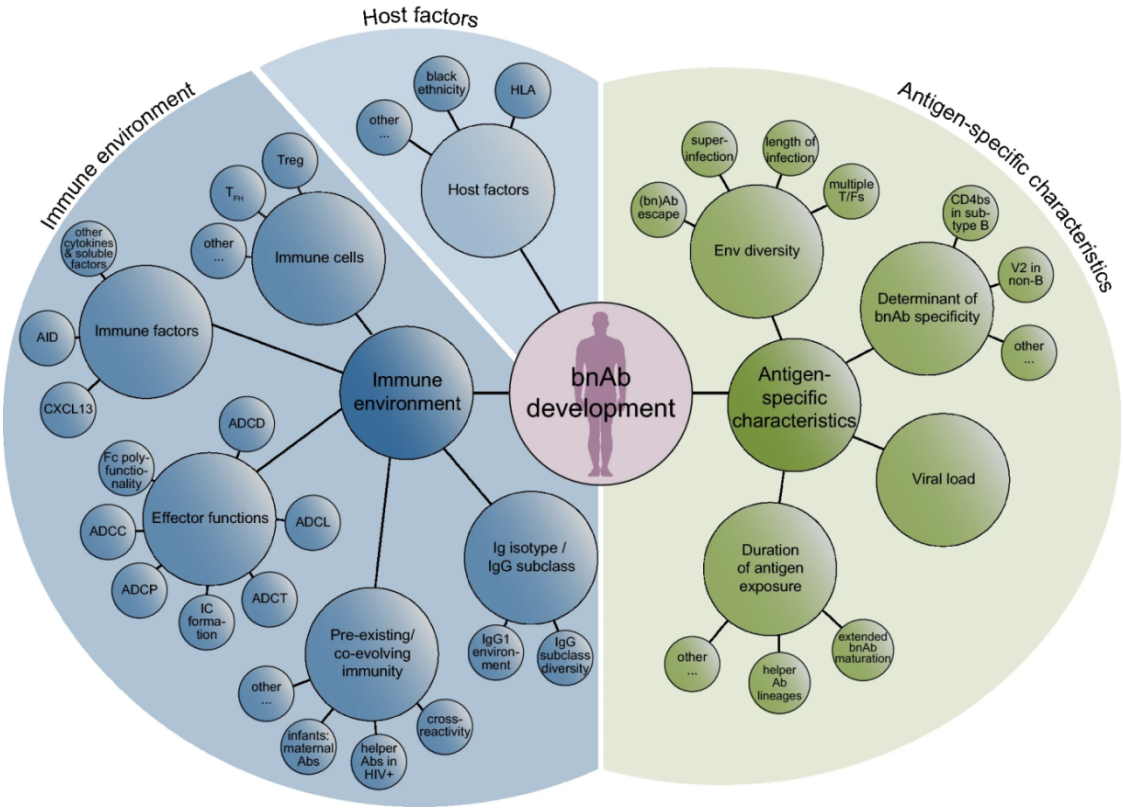

Figure 1-7: Factors that have been associated with bNAb development in HIV-1 positive patients (Subbaraman, Schanz and Trkola, 2018)

Isolation of the first bNAbs was achieved in the 1990s and include amongst others, the V3 loop binding 2G12 and the MPER-binding 4E10 antibodies (Stiegler *et al.*, 2001; Scanlan *et al.*, 2002). A number of limitations were exhibited by these first generation bNAbs, which renders them inadequate for therapeutic purposes. Firstly, their neutralisation potency is limited (Georgiev *et al.*, 2013), thus high doses (e.g. 40 mg/kg) are required. Even then they are only effective against a restricted number of HIV-1 isolates. Clinical trials demonstrated that the administered combinations (mostly 2G12, 2F5 and 4E10) were safe and well-tolerated (Armbruster *et al.*, 2004; Mehandru *et al.*, 2007; Morris *et al.*, 2014; Ma *et al.*, 2015). However, these combinations proved to be ineffective in being able to suppress viral rebound long term. One study investigated the efficacy of the three bNAbs in delaying viral rebound in 14 HIV-positive subjects, whose viral isolates were sensitive to the bNAbs at the time of recruitment. Treatment was initiated one day prior to ART cessation and a total of 13 passive immunisations were given over the course of 11 weeks. The combination showed some effect in delaying viral rebound, yet, the rebounding virus was resistant to 2G12 in 12 out of 14

subjects (Trkola *et al.*, 2005). This observation was confirmed in a similar study, with 10 HIV-positive individuals habouring viruses susceptible to all three bNAbs. In this study patients were given a total of 16 infusions over 24 weeks, which led to a slower viral rebound but 7 of the 10 patients developed 2G12 resistance (Mehandru *et al.*, 2007).

Still, studies conducted with the first generation of bNAbs revealed the potential of bNAbs to prevent and fight infection. Improved methods, e.g. single B cell sorting (X. Wu *et al.*, 2010), led to the isolation of various highly potent second-generation bNAbs, such as VRC01, 3BNC117, 10-1074 and N6, exhibiting a neutralisation breadth of up to 98 percent and increased potency (Georgiev *et al.*, 2013; Huang *et al.*, 2016). While these were primarily isolated to provide information for vaccine design (Doria-Rose *et al.*, 2009), they also paved the way for the development of effective passive immunisation therapy. Pre-clinical and clinical trials yielded promising results for a handful of the currently known antibodies, these are discussed below.

1.1.7 Clinical and pre-clinical trials with new generation bNAbs

Several trials with second generation bNAbs have been performed or are currently on-going. While numerous potent bNAbs have been isolated in recent years, the majority of research focuses on a small number and some will be introduced here with regard to their target and neutralisation breadth. VRC01 is one of the best studied second generation bNAbs (X. Wu *et al.*, 2010). It targets the CD4 binding site and has a neutralisation breadth of up to 91 percent (X. Wu *et al.*, 2010). 3BNC117, also a CD4 binding site targeting antibody, neutralises around 82 % of primary HIV-1 strains (Doria-Rose *et al.*, 2017). N6 is one of the more recently discovered bNAbs, targeting the CD4 binding site with unique potency (Huang *et al.*, 2016). This antibody exhibits a variety of traits making it especially attractive for therapeutic purposes. N6 has a neutralisation breadth of 98%, and can also neutralise 16 out of 20 strains which are resistant to VRC01. Furthermore, N6 is able to avoid steric clashes with glycans of V5, a common mode of resistance of HIV, by binding to CD4 at a slightly different angle than other VRC01 class antibodies (Huang *et al.*, 2016). A bNAb of interest

targeting the V3-loop and N332 glycan is 10-1074 (Mouquet *et al.*, 2012). This bNAb shows a neutralisation breadth of around 65 % (Doria-Rose *et al.*, 2017), and is commonly included in antibody cocktails alongside CD4bs bNAbs, to allow for targeting distinct sides on the Env protein, which essential to reduce the occurrence resistance in HIV infected individuals (Bar-On *et al.*, 2018, NCT03831945, NCT03571204, NCT03526848).

1.1.7.1 Trials investigating bNAb therapy for use in chronic HIV-1 infection

The majority of clinical trials performed with bNAbs focus on general safety and on efficacy in treating established HIV infection. Phase I clinical trials have demonstrated that VRC01, 3BNC117 and 10-1074 are well-tolerated in uninfected and infected individuals (Caskey *et al.*, 2015, 2017; Ledgerwood *et al.*, 2015). A first clinical trial testing the safety of the bNAb N6 is currently in its recruiting stage (NCT03538626).

3BNC117 delivered promising results in pre-clinical studies in non-human primates; monotherapy led to a rapid decline of viremia, which could be further improved by administration in combination with 10-1074 (Shingai *et al.*, 2013). A dose escalation study of 3BNC117 by Caskey et *al.* (2015) revealed that the pharmacokinetic profile of the bNAb differed between infected and non-infected individuals, showing a significantly reduced half-life in infected subjects ($t_{1/2}$ of 9 days vs 17 days). A single 3BNC117 IV infusion of 30 mg/kg resulted in 0.8–2.5 $\log_{10}$ reduction in viral load and significantly reduced viremia for 28 days. A decrease in sensitivity to 3BNC117 of viral isolates, after 28 days when compared to pre-treatment isolates, was observed in all individuals. However, high-level resistance was only seen in two patients. Reduction in sensitivity generally coincided with the development of viral isolates harbouring single mutations in the 3BNC117 epitope (Caskey *et al.*, 2015).

Similar observations were made for the V3 gylcan-dependent bNAb 10-1074. 10-1074 had an average half-life of 24 and 12.8 days in healthy and infected subjects, respectively. A single dose of

10 or 30 mg/kg dose of 10-1074 induced a rapid decline in viral load. Yet, upon viral rebound 10-1074 resistant strains emerged in infected individuals. 97 % of escape variants showed mutations that eliminated the *N*-linked glycan at position 332, which is essential for 10-1074 binding (Caskey *et al.*, 2017).

The development of resistance is a recurring problem in the treatment of patients with chronic infection and can presently not be prevented when administering a single bNAb, due to the high mutation rate of the virus. The focus of the majority of clinical trials shifted from administering single bNAbs to combinations of at least two bNAbs, especially a CD4bs bNAb and 10-1074, in an attempt to prevent virus escape and resistance by targeting different epitopes. A clinical phase 1b study demonstrated that a combination of 3BNC117 and 10-1074 at a dose of 30mg/kg of each bNAb was highly effective in reducing viral load. An average reduction in viral load of 2.05 $\log_{10}$ was achieved, remaining significantly reduced for 3 months. Furthermore, viral rebound was associated with the development of escape variants resistant to 10-1074, but not to 3BNC117. The authors concluded that patients were only exposed to 10-1074 at the end of therapy, due to its longer half-life, which promoted the development of resistant strains (Bar-On *et al.*, 2018). An on-going study (NCT03571204) further investigates the ability of 3BNC117 in combination with 10-1074 to control viremia in patients without ART intervention, whereas another study is evaluating the efficacy of this combination in patients with ART treatment (NCT03526848). Another trial examining combination therapy of VRC01 and 10-1074 in infected patients undergoing ART treatment interruptions (NCT03831945) was recently completed; however results have not been published to this date. Moreover, approaches to combine other agents, such as, pegylated Interferon alpha 2b, which was shown to keep viral copy levels below 50 in the absence of ART, in combination with 3BNC117 and 10-1074 are also investigated (NCT03588715).

A few studies focus on evaluating safety and efficacy of bNAbs in infants (NCT03208231, NCT03707977), as adverse reactions and pharmacokinetic profiles might differ to those in adults.

1.1.7.2 Evaluation of bNAb therapy for PrEP and PEP

A potential - less studied- application of bNAb therapy is as PrEP and PEP in adults. A major benefit of bNAbs compared to ART is that they are very well tolerated, as demonstrated in several clinical phase I trials (Caskey *et al.*, 2015, 2017; Ledgerwood *et al.*, 2015). Furthermore, the inherently longer half-life of IgGs may additionally be beneficial for the usage of bNAbs as PrEP and early PEP. For example, VRC01 has an approximate half-life of 15 days (Ledgerwood *et al.*, 2015), which may enable the usage of VRC01 for pre-exposure prophylaxis. Hence, a phase IIb efficacy study is currently underway to evaluate VRC01 for prevention of acquisition of HIV in healthy women at high risk of HIV infection in sub-Saharan Africa (ClinicalTrials.gov Identifier: NCT02568215).

BNAb treatment may improve the ability of the immune system to control the virus, in case PEP is initiated too late to prevent infection. Nishimura et *al.* (2017) demonstrated that treatment of macaques with acute infection with a single 2 week combination therapy of 3BNC117 and 10-1074, led to a delayed onset of viremia (up to 177 days post-infection) and the induction of CD8+ T-cell immunity, which ensures long-lasting virus control (Nishimura *et al.*, 2017).

1.1.8 The potential of bNAb therapy

BNAb therapy is currently being investigated as potential alternative to ART treatment, due to its longer serum half-life (15-24 days vs 0.5-100 h), better tolerability, the ability to perform cell-mediated killing and reports of inducing long-lasting virus control (Taylor *et al.*, 2007; Caskey *et al.*, 2015, 2017; Ledgerwood *et al.*, 2015; Caskey, Klein and Nussenzweig, 2016; Nishimura *et al.*, 2017; Desikan, Raja and Dixit, 2019).

While the longer half-life makes bNAbs attractive for therapy, a major disadvantage is that they have to be given intravenously by healthcare professionals while ART can be self-administered orally (Caskey, Klein and Nussenzweig, 2016). Furthermore, in recent years the development of long-

acting ART has been reported and studies revealed half-lives of more than 3 months for some long-acting drugs, like RPV, a NNRTI (Zhang, 2018). However, long-lasting ART formulations have to be injected intramuscularly, therefore losing the benefit of self-administration (Havlir and Gandhi, 2015). Furthermore, while studies suggest therapies with longer half-life are well received, especially in younger patients, others perceive it as 'loss of control' (Havlir and Gandhi, 2015). Further studies are needed to investigate the acceptability and feasibility of long-acting therapies. These studies are especially important in LMICs in which stigma impacts adherence to conventional ART, but patients are often lacking the funds for travelling to a doctor or clinic regularly.

BNabs seem to be generally better tolerated than ART and might be especially attractive for patients that suffer from serious side-effects of the treatment. BNAbs may also be preferred for long-term treatment as long-term ART is linked to e.g. nephrotoxicity and hepatitis (Grobben, Stuart and van Gils, 2019).

A major advantage of bNAbs compared to ART is their ability to kill virus-infected cells and potentially reduce latent reservoirs (Caskey, Klein and Nussenzweig, 2016; Grobben, Stuart and van Gils, 2019). Several studies have demonstrated that cell-mediated killing of HIV-infected cells triggered by bNAb therapy are contributing to the bNAbs protective potential (Hessell *et al.*, 2007, 2009; Bournazos *et al.*, 2014; Grobben, Stuart and van Gils, 2019). Lastly, bNAbs may induce long-lasting virus control during early stages of infection, even after cessation of therapy (Nishimura *et al.*, 2017; Desikan, Raja and Dixit, 2019).

Whether bNAbs will be administered as sole therapy or in conjunction with ART, may depend not only on the outcome of on-going clinical trials but also on patient acceptance and the treatment target, that is, use as PrEP/PEP or for treatment of chronic infection.

1.1.9 Limitations of bNAbs

In spite of the unique abilities of current bNAbs, there are still considerable limitations to overcome. First of all, no currently isolated bNAb is able to neutralise all prevailing variations of the virus (Kwong, Mascola and Nabel, 2013), plus the high mutation rate of the virus enables HIV to escape the conferred immunity quickly. For that reason, a combination of various antibodies has to be administered in order to ensure effective immunisation (Klein *et al.*, 2013). Secondly, half-life of these antibodies - even though longer in comparison to ART (Caskey, Klein and Nussenzweig, 2016)- is an issue, as dosing frequency is dependent on the half-life of the bNAb. Thus bNAbs with shorter half-lives require more frequent dosing (Desikan, Raja and Dixit, 2019). Furthermore, extended half-life is desirable for pre-exposure prophylaxis (Caskey, Klein and Nussenzweig, 2016). Thirdly, the manufacturing of antibodies is expensive (Caskey, Klein and Nussenzweig, 2016), making these treatments accessible only to developed countries, thus unaffordable to the majority of patients. Hence, a major focus of passive immunisation HIV research currently lies on improving binding to receptors and stability as well as producing them economically (Ko *et al.*, 2014; Teh *et al.*, 2014; Ma *et al.*, 2015; Gaudinski *et al.*, 2018; NCT04250636, NCT03254277).

1.2 Fc receptors

Fc receptors (FcR) are proteins located on the surface of effector cells (Fridman, 1991), such as macrophages and natural killer (NK) cells. Upon the formation of an antibody-antigen complex, the Fc receptor binds to the Fc region of the antibody, thereby initiating various processes, particularly the destruction of pathogens (Wieland and Ahmed, 2019). In humans, a variety of antibody-class specific Fc receptors exist (Fridman, 1991) and are classified according to the type of immunoglobulin they bind. There are 2 functional types of Fc receptors known for IgGs: those that induce cell activation and others that do not (Daëron, 1997). 'Activatory' receptors include FcγRI, FcγRIIa, FcγRIIc, FcγRIIIa, and FcγRIIIb which induce effector functions, such as antibody-dependent cellular cytotoxicity (ADCC) and antibody dependent cellular phagocytosis (ADCP). The second class

is composed of the inhibitory FcγRIIb as well as the neonatal Fc receptor (FcRn), which is involved in homeostasis and transcytosis of IgGs (Nimmerjahn and Ravetch, 2008)(see Figure 1-8).

Name	FcγRI CD64	FcγRIIa CD32a	FcγRIIb C32b	FcγRIIc CD32c	FcγRIIIa CD16a	FcγRIIIb CD16b
Structure	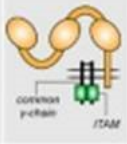					
Function	Activating	Activating	Inhibitory	Activating	Activating	Activating
Affinity	High	Low	Low	Low	Low	Low

Figure 1-8: Types of Fcγ receptors displaying their structure, function and affinity. Adapted from (Vogelpoel *et al.*, 2015)

Research with regard to bNAbs mostly focuses on the neonatal Fc receptor (see 1.2.1), due to its role in IgG salvage, and on FcγRIIIa, as the main receptor for antibody-dependent cellular cytotoxicity (ADCC) induction. As this mechanism might be beneficial for the control of viremia and clearing of HIV reservoirs, the affinity of binding to the FcγRIIIa is also taken into account during bNAb improvement (Parsons, Chung and Kent, 2018; Grobben, Stuart and van Gils, 2019).

Antibody-dependent cellular cytotoxicity and the FcγRIIIa

Antibody-dependent cellular cytotoxicity (ADCC) is an immune-defence mechanism through which target cells decorated by antibody, are lysed by effector cells (Gómez Román, Murray and Weiner, 2013). IgG-dependent ADCC can be mediated by three types of receptors, the FcγRI, FcγRII and FcγRIIIa (Wallace, Howell and Fanger, 1994; Horner *et al.*, 2007; Tudor and Bomsel, 2011), however, the latter is regarded as the main receptor, due to high expression levels on Natural Killer (NK) cells (Sanseviero, 2019). The FcγRIIIa is expressed by NK cells, macrophages, monocytes and γδ-T cells (Wallace, Howell and Fanger, 1994; Gómez Román, Murray and Weiner, 2013). Killing of target cells has been suggested to occur through three pathways; perforin-granzyme cell death, FAS-ligand and oxidative burst (ROI/ROS) (Gómez Román, Murray and Weiner, 2013). The perforin-granzyme cell death pathway is best described (Figure 1-9). Upon FcγRIIIa crosslinking, signalling

pathways trigger various intracellular changes and the release of cytotoxic granules containing granzyme B and perforin, which form macromolecular complexes. An interaction of granzyme B with mannose-6-phosphate receptors expressed on the surface of the target cells leads to endocytosis of the macromolecular complex. Granzyme B is further involved in apoptosis by activating caspases directly or indirectly to induce DNA fragmentation, whereas perforin leads to cell lysis and death (Gómez Román, Murray and Weiner, 2013).

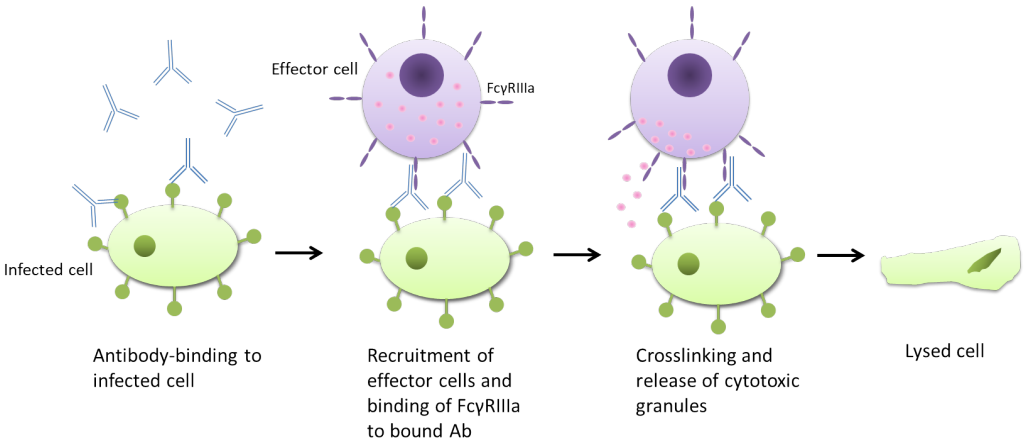

Figure 1-9: Basic principle of antibody-dependent cellular cytotoxicity. Upon binding of specific antibodies to antigens on the surface of an infected cell, effector cells are recruited and binding via FcγRIIIa to the antibodies in the immune complex occurs. After crosslinking, which induces intracellular pathways, cytotoxic granules are released. These lead to cell death of the infected cell by lysis and DNA fragmentation.

In general high affinity of the immunoglobulin Fc-region to FcγRIIIa is associated with increased ADCC (Dall'Ozzo *et al.*, 2004). In humans this affinity is currently known to be determined by two factors; the polymorphism of the FcγRIIIa and the structure of the *N*-glycan in the Fc-region of the antibody. Several polymorphisms have been identified in humans; however, the best studied and currently most important one is the V158F polymorphism, which is caused by a single nucleotide polymorphism (SNP) (Mahaweni *et al.*, 2018). Individuals homo- or heterozygous for valine (V/V or V/F) at position 158 exhibited higher levels of NK-cell mediated ADCC compared to individuals homozygous for phenylalanine (F/F) at position 158 (Wu *et al.*, 1997; Congy-Jolivet *et al.*, 2008;

Hogarth and Pietersz, 2012; Dekkers *et al.*, 2017). This stems from FcγRIIIa V158s 3-5-fold higher affinity to IgG1 or IgG3 (Wu *et al.*, 1997; Congy-Jolivet *et al.*, 2008; Dekkers *et al.*, 2017). Cancer patients with the V polymorphism were shown to have improved outcomes compared to patients who were homozygous for the F-variant (Hogarth and Pietersz, 2012). It is of importance to take these differences into account to adjust treatment plans accordingly; however, direct modifications of the receptor to improve therapy outcomes are not yet possible.

The second factor influencing the affinity of FcγRIIIa to IgG is the *N*-glycan in the Fc-region of the antibody. Studies have shown that core fucosylation of the *N*-glycan decreases the affinity of FcγRIIIa to IgG when compared to afucosylated IgGs (Ferrara *et al.*, 2011)(see 1.4.1). This knowledge allows for the adjustment of ADCC (Li *et al.*, 2017), by using an expression system modified to generate afucosylated mAbs (Stelter *et al.*, 2020).

1.2.1 Neonatal Fc receptor (FcRn)

The neonatal receptor differs from other Fc-receptors structurally and by not being directly involved in immune-regulatory functions. FcRn is a heterodimer consisting of an α-chain and β2-microglobulin, structurally resembling the major histocompatibility class I (MHC I) family (Burmeister *et al.*, 1994). However, in contrast to MHC I, it has a non-functional peptide-binding groove (Burmeister *et al.*, 1994) and is therefore not involved in the presentation of antigenic peptides to T-cells.

The neonatal Fc receptor (FcRn) was first discovered in rats for being responsible for mother-to-pup transmission of maternal antibodies (Brambell, 1967; Simister and Rees, 1985). The FcRn serves the same purpose in humans along with other roles, most importantly transcytosis and recycling of IgGs and albumin (Petkova *et al.*, 2006). This is the reason for the comparatively long half-life (21 days) of IgG antibodies compared to other immunoglobulins like IgA (max. 9 days) (Morell *et al.*, 1973; Petkova *et al.*, 2006). Recycling of IgG takes place within the acidic environment

of endothelial cells (Roopenian and Akilesh, 2007). The FcRn interaction is strongly pH-dependent; binding occurs at pH 6.0 and release at 7.4. This pH-dependency comes from the histidine residues at the C_H2 and C_H3 interface, where binding occurs (Raghavan *et al.*, 1995). Figure 1-10 shows the IgG salvage process, which starts with endocytosis of IgG along with other serum proteins. In the acidic conditions of the endosome (pH 6.0), only IgGs and albumin bind to the FcRn. They are then sorted and transported back to the cell surface, where they are released into the serum at physiological pH. Unbound proteins will be degraded in the lysosome (Bern *et al.*, 2015).

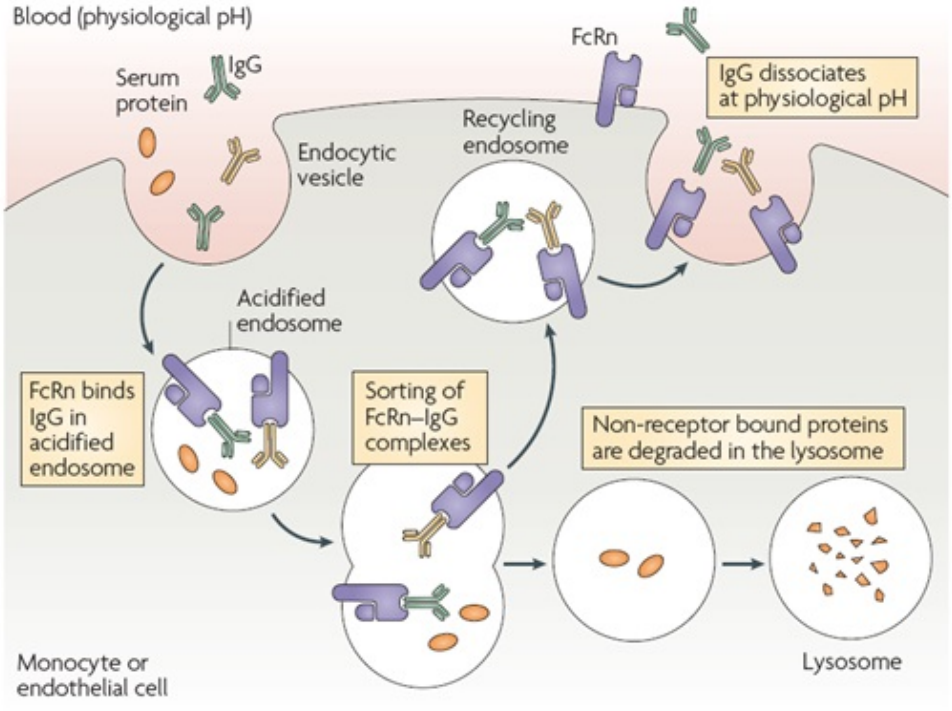

Figure 1-10: IgG recycling. Serum proteins are taken up by monocytes and endothelial cells, which express the FcRn. The FcRn binds to IgG in an acidified (pH 6) endosome. Non-bound proteins are degraded in the lysosome, while IgG is recycled back into the serum (pH 7.4), thereby extending its serum half-life (Roopenian and Akilesh, 2007).

1.2.1.1 Presence of FcRn in other tissues

Aside from endothelial cells, expression of the neonatal receptor can be found in epithelia and cells of hematopoietic origin.

FcRn expression in the epithelium was confirmed in the placenta, liver, intestines and kidney, however only the first three will be discussed in more detail.

In the placenta the FcRn is found in syncytiotrophoblasts, which are in direct contact with the maternal blood circulation, and in the fetal endothelium (Leach *et al.*, 1996; Simister *et al.*, 1996; Latvala *et al.*, 2017). Transport of immunoglobulins across the placenta is limited to IgG (Malek, Sager and Schneider, 1994; Malek *et al.*, 1995; Firan *et al.*, 2001). This transport is independent of IgG glycosylation (Einarsdottir *et al.*, 2013), but dependent on the affinity of the Fc-region of the IgG to FcRn, as revealed by a study that showed that an IgG engineered to have a higher affinity to FcRn was transported through the placenta more efficiently (Vaccaro *et al.*, 2006). Interestingly, not only IgG but also IgG-immune complexes (IgG-ICs) seem to be transported through the placenta to the fetus (Malek, Sager and Schneider, 1998; May *et al.*, 2009), indicating the involvement of the FcRn, however this role is not yet fully understood.

The liver is one of the major sites of FcRn expression (Fan and Neubert, 2016; Fan *et al.*, 2016) and has been shown to be involved in FcRn-mediated IgG recycling (Eigenmann *et al.*, 2017). Yet, a major function of the neonatal receptor in cells of the liver seems to be the efficient transport of albumin into the circulation (Pyzik *et al.*, 2017), as hepatocytes are the sole producer of albumin (Feldmann *et al.*, 1972).

In the intestine the neonatal receptor is expressed at the mucosal surfaces in the small and large intestine (Pyzik *et al.*, 2019). In the presence of FcRn, circulating monomeric IgG can be transported to the intestinal lumen (Yoshida *et al.*, 2004). This transport is bidirectional, therefore monomeric IgG and IgG ICs can be transcytosed from the lumen back into the lamina propria, part of the mucosa, allowing for the delivery of luminal antigens as IgG ICs to dendritic cells and regulation of immune responses (Yoshida *et al.*, 2004, 2006; Pyzik *et al.*, 2019). The presence of FcRn in the intestines is of great interest, since it might allow for oral delivery of mAbs and therapeutic fusion molecules.

FcRn is expressed by macrophages, dendritic cells, monocytes, neutrophils and B lymphocytes (Zhu *et al.*, 2001; Vidarsson *et al.*, 2006; Pyzik *et al.*, 2019). The hematopoietic

compartment was shown to be of importance for IgG homeostasis (Pyzik *et al.*, 2017), however, it is not yet known whether this is performed by all of the above mentioned cells or by a particular cell type. Several studies suggest that the presence of FcRn in these cells is necessary for a potent immune response by facilitating antigen presentation of peptides originating from IgG immune complexes (Pyzik *et al.*, 2019). However, the exact mechanism has not been revealed yet.

The function in the endothelium and other tissues highlights that the Fc-FcRn interaction is a crucial target to modulate the therapeutic properties of mAbs or Fc-fusion molecules and plays an important role in the pharmacokinetics and pharmacodynamics of antibodies. Several mutations in the Fc-region of mAbs, such as YTE (M252Y/S254T/T256E) (Acqua *et al.*, 2002) and LS (M428L/N434S) (Zalevsky *et al.*, 2010), have been identified. These are able to enhance the binding affinity to FcRn and allow for e.g. prolonged *in vivo* half-life of mAbs (see 3.1) (Acqua *et al.*, 2002; Zalevsky *et al.*, 2010).

1.3 Expression systems for biopharmaceuticals

A range of expression platforms are available for the production of biopharmaceuticals, which include prokaryotic and eukaryotic systems. While each platform comes with advantages and disadvantages, the choice of the expression platform is primarily dependent on the characteristics of the product, e.g. the requirement of posttranslational modifications (PTMs) for being functional.

1.3.1 Prokaryotic expression platforms

Bacteria are an attractive expression system due to low cost, rapid growth and good yields. *Escherichia coli* is prevalently used, owing to being well-studied and its easily manipulable genome. A number of biopharmaceuticals, such as interferons, tumour necrosis factor and interleukins, are currently produced using *E. coli* as production host (Ferrer-Miralles *et al.*, 2009; Owczarek, Gerszberg and Hnatuszko-Konka, 2019). However, due to the lack of intracellular compartmentalisation of prokaryotes, no PTMs are performed, which are necessary for e.g. folding processes, stability and

glycosylation, therefore restricting the usage of this system to a limited number of therapeutic proteins (Ferrer-Miralles *et al.*, 2009; Owczarek, Gerszberg and Hnatuszko-Konka, 2019).

1.3.2 Yeast expression system

Yeasts are able to generate a high yield of protein which is directly secreted into the medium, facilitating purification (Nielsen, 2013; Owczarek, Gerszberg and Hnatuszko-Konka, 2019). Similar to bacteria, rapid proliferation allows for cultivation to high cell densities in bioreactors, with the additional benefit of being capable of PTMs, enabling the production of more complex therapeutic proteins than bacterial expression platforms (Ferrer-Miralles *et al.*, 2009; Owczarek, Gerszberg and Hnatuszko-Konka, 2019). However, the glycosylation pattern is markedly different from the one seen in higher eukaryotic cells, severely impacting the authenticity of generated therapeutic glycoproteins, such as mAbs (Wildt and Gerngross, 2005; Nielsen, 2013; Owczarek, Gerszberg and Hnatuszko-Konka, 2019). The potential of yeasts as a cheap expression platform resulted in the development of glycoengineered yeast strains, which are able to perform human-like glycosylation (Nielsen, 2013; Owczarek, Gerszberg and Hnatuszko-Konka, 2019). Yet, yeasts are prone to undergo conformational stress, which can lead to the generation of partially or completely inactive proteins (Ferrer-Miralles *et al.*, 2009).

1.3.3 Mammalian expression system

The majority of therapeutic proteins, such as mAbs, enzymes, hormones etc., are currently produced using mammalian cell fermentation platforms, as this system is well-established and is able to provide products with human-like glycosylation (Ghaderi *et al.*, 2012). Chinese Hamster Ovary (CHO) cells and mouse myeloma cells, both capable of generating vast amounts of complex proteins with (more or less) appropriate glycosylation, are primarily utilised (Nissim and Chernajovsky, 2008; Dumont *et al.*, 2016; Owczarek, Gerszberg and Hnatuszko-Konka, 2019). Then again, mammalian production platforms exhibit several limitations, such as high expenses.

Mammalian cells require complex growth medium and are prone to infections, for example through animal viruses and prions (Houdebine, 2009; Dumont *et al.*, 2016). This not only results in the need of facilities providing sterility but also quality analyses to verify the absence of pathogens. Furthermore, upscaling of the production process post-construction of the facility is not possible; therefore, a new facility is necessary to meet increased demand of a product. Another major disadvantage of CHO cells, production host to around 70% of all therapeutic recombinant proteins on the market, is their genetic instability. This is caused by a number of factors such as chromosome rearrangement and silencing, leading to an unpredictable decline in productivity and potentially impacting product quality (Dahodwala and Lee, 2019).

1.3.4 Plants as expression system

The use of plants as host for the production of therapeutic proteins potentially overcomes several of the limitations of the aforementioned production systems. Plants are able to perform complex mammalian-like glycosylation and provide a high product quality and safety, as they are not susceptible to animal pathogens (Hiatt and Pauly, 2006; Łojewska *et al.*, 2016). Furthermore, this system has the potential of low-cost production of therapeutic proteins, as neither specialized facilities nor highly trained personnel are needed for the cultivation of plants (Pogue *et al.*, 2010). Scale-up can be achieved by simply expanding production acreage (Fischer and Emans, 2000; Sabalza, Christou and Capell, 2014). Most importantly this approach might not only facilitate therapies at a lower price in the future but also allows manufacturing therapeutics for rare diseases, as the initial capital investment required is much lower (Murad *et al.*, 2020).

Plant expression platforms may be especially attractive for LMICs, as the majority of pharmaceutical manufacturing sites are located in high income countries (Grilo and Mantalaris, 2019). As pharmaceutical companies are for-profit corporations, development and production of therapeutics is focused on diseases of high-income countries, often overlookingthe needs of LMICs (Surur *et al.*, 2020). While the production of drugs for neglected diseases is not only hindered by the

location and investment cost of manufacturing sites, but also by the capital required for according research (Surur *et al.*, 2020), plant-expression platforms have received attention in several LMICs (Murad *et al.*, 2020). This is not only due to lower initial investment but also because they allow for local sourcing of culture media (soil and fertiliser), instead of being dependent on the import of cell culture media from abroad (Murad *et al.*, 2020).

Antibody expression in plants has been established for almost 30 years (Hiatt, Cafferkey and Bowdish, 1989; De Muynck, Navarre and Boutry, 2010). Nowadays, transient expression platforms are more widely used for antibody production than transgenic platforms, due to their rapidity, while still providing high yields (De Muynck, Navarre and Boutry, 2010). Transient expression is performed via syringe or vacuum infiltration of leaves and is mediated by *Agrobacterium tumefaciens* or a viral vector (e.g. tobacco mosaic virus) without integration of the transgene into the plant genome (De Muynck, Navarre and Boutry, 2010; Q. Chen *et al.*, 2013). The development of transgenic plants is a longer process, as stable transformation requires regeneration of leaf discs or protoplasts to full plants. However, for the production of antibodies in resource-poor areas, transgenic plants would further reduce the costs and complexity of production, as only seeds of the plant carrying the gene are required (Q. Chen *et al.*, 2013; Teh *et al.*, 2014).

In 2012 the FDA approved the first plant-produced biologic; ELELYSO (taliglucerase alfa), an enzyme produced in Carrot cells to treat Gaucher's disease (Mor, 2015). During the Ebola crisis in 2014 the mAb cocktail ZMapp, produced in *N. benthamiana*, was one of several experimental drugs approved for emergency treatment (Qiu *et al.*, 2014; Wong and Kobinger, 2015). However, up to this date no mAb produced in plants has entered the market. A major impediment was the lack of a defined GMP-compliant manufacturing process, which is also required to gain regulatory approval for clinical trials (Ma *et al.*, 2015). This has been addressed in the EU-funded project Pharma-Planta; a GMP-compliant production process was developed and additionally a first-in-human phase I clinical trial of a plant-produced mAb was performed. Intravaginal delivery of the plant-produced

anti-HIV bNAb 2G12 was shown to be safe and well-tolerated (Ma *et al.*, 2015). This study paved the way for other plant-produced mAb to be investigated in clinical trials and to eventually enter the market.

Secondly, companies and countries are hesitant to invest in an emerging manufacturing platform considering that an established platform is already available (Murad *et al.*, 2020). Furthermore, for years, plant expression platforms were not able to compete with mammalian, mainly CHO, cell production systems, especially due to low yields and the lack of an optimised downstream process for plant-produced biologics(Buyel, 2019). Significant advances have been made in the past few years (Zischewski, Sack and Fischer, 2016; Buyel, 2019; Diamos *et al.*, 2020), yet, further development with regard to yield improvement and optimisation of downstream processes may be needed for the platform to be able to reach its full potential (Schillberg *et al.*, 2019).

A techno-economic analysis has estimated that in order to compete with an equivalent CHO cell production platform, a minimal yield of 0.4 g/kg FW at a production capacity of 300 kg/year and downstream recovery of 65 % for transient leaf expression systems is necessary. With a yield of 1 g/kg FW the cost of goods sold (COGS) were calculated to be $121/g mAb with depreciation, which in 2015 translated to a 50 % reduction compared to the CHO produced mAb (Nandi *et al.*, 2016). For transgenic leaf expression with greenhouse cultivation a COGS of $98/g with a yield of 1 g/kg FW were calculated and initial investment costs were estimated to be 25 % of that for a cell culture manufacturing site(Wilken and Nikolov, 2012).

Yields of the required magnitude have been achieved and even been exceeded with 1.2-2 g/kg FW for some mAbs after optimisation of the expression vector and production conditions (Zischewski, Sack and Fischer, 2016; Diamos *et al.*, 2020). However, achieving competitive yields for any plant-produced mAb after initial characterisation generally requires yield studies and a robust downstream processing procedure (Schillberg *et al.*, 2019; Diamos *et al.*, 2020).

1.3.5 Comparison of downstream processing of mAb preparations between mammalian and leaf expression systems

While plant expression platforms simplify upstream processing compared to cell-based expression, downstream processing requires additional steps in case of leaf expression systems (Figure 1-11). A standard commercial downstream process for mammalian-produced mAbs starts with the removal of cells and cell debris using centrifugation, followed by depth-filtration for clarification of the mAb-containing supernatant. The main purification step is performed using Protein A affinity chromatography, which, due to its selectivity for antibodies, achieves high purity in a single chromatography step (>95%). This is followed by a holding step at low pH for virus inactivation. For further reduction of host cell proteins, aggregates, host cell DNA and leaked protein A. Most commonly cation-ion exchange chromatography is followed by an anion chromatography step, however, other systems can be employed depending on the product and impurities. For safety purposes these steps are followed by viral filtration as mammalian cells are prone to infection with animal viruses. Finally, a buffer exchange to the formulation buffer is achieved using ultra- and diafiltration and sterile filtration is performed prior to filling (Shukla *et al.*, 2007).

Downstream processing of mAbs produced in leaf material follows a similar set up, but a number of additional steps are required to extract the mAbs from the leaves. The process described here is based on the procedure developed for obtaining regulatory approval for a clinical phase I trial with the plant-produced anti-HIV bNAb 2G12 (Ma *et al.*, 2015). Leaf harvest was performed manually, followed by a machine-based washing step with water to remove particles. Weighing of total biomass and correct amounts of extraction buffer were added automatically before shredding was performed. Clarification was achieved by bag-filtration, with subsequent depth-filtration. Protein A chromatography was used as main purification step and any remaining impurities, as well as leached protein A, were reduced using by a hydroxyapatite chromatography step. Next, viral

filtration was performed, despite not necessarily being needed as plants are generally not infected by animal viruses, however, at this stage this was needed to satisfy regulatory policy. For buffer exchange ultra- and diafiltration was employed and the product sterilised by 0.2 µm filtration (Ma *et al.*,2015).

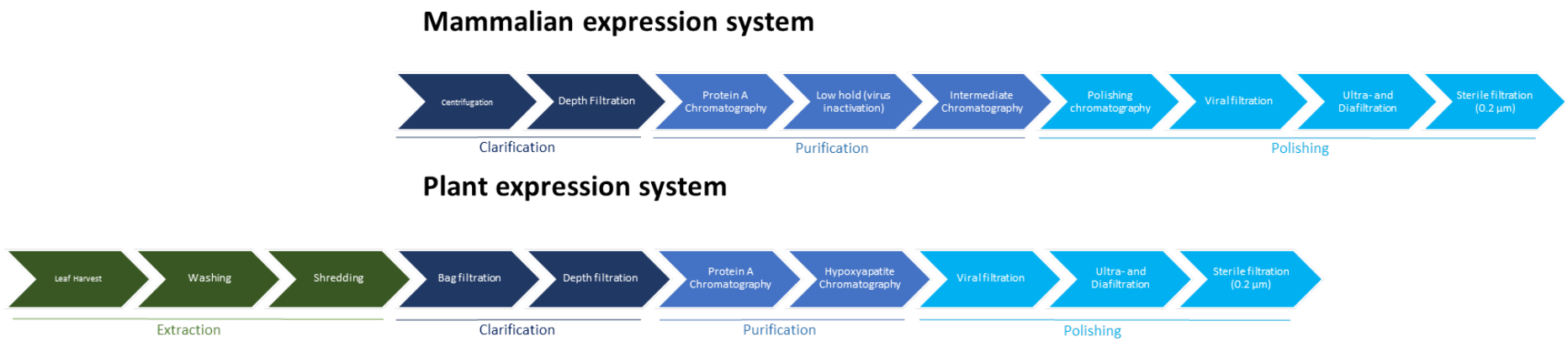

Figure 1-11: Schematic comparison of downstream processing steps required for the GMP-compliant production of mAbs.

1.4 Glycosylation

In general, glycosylation is essential to ensure correct folding and functionality of glycoproteins for highest efficacy. *N*-glycosylation of IgG antibodies occurs consistently at asparagine 297 (Asn297) of each heavy chain. Glycosylation at Asn297 is extremely important for Fc receptor binding and the induction of effector functions. Upon complete removal of the Fc-glycan, almost complete loss of Fc receptor binding was observed (Lu *et al.*, 2015; Subedi and Barb, 2015), as the conformation of aglycosylated IgGs may hinder Fcγ receptor binding.

About 20 percent of antibodies show additional *N*-glycosylation sites within the Fab (Vidarsson, Dekkers and Rispens, 2014), however, Fc receptor binding is unaffected by the Fab-glycan. IgGs with complex N-glycosylation commonly carry a biantennary glycan. The glycan core (GnGn) is made up of 2 N-Acetylglucosamine (GlcNAc) moieties, followed by a mannose moiety, to which 2 mannose (Man) antennae are attached. To each mannose antenna an additional GlcNAc is attached. Additional sugars can be added to this core structure (see Figure 1-12 A). Modifications include the addition of a α1,6-fucose (Fuc) to the first GlcNAc, galactose (Gal) to each antennary GlcNAc and sialic acid (NeuAc) to each galactose moiety. Furthermore, a bisecting GlcNAc (b-GlcNAc) can be attached to the core mannose (Stanley P, Taniguchi N, 2017) (Figure 1-12 A).

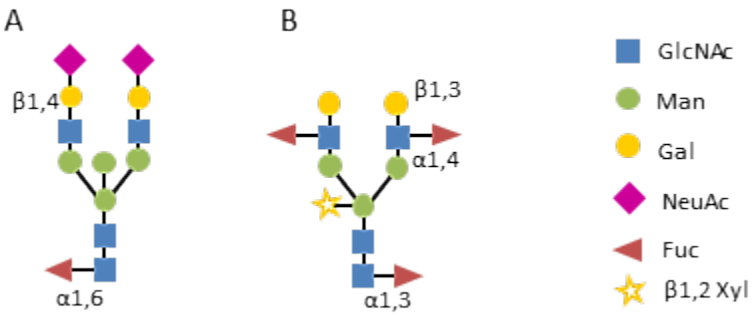

Figure 1-12: Differences in complex N-glycosylation between mammals (A) and plants (B). The core structure is identical consisting of two N-Acetylglucosamine and three Mannose moieties. Both types show fucosylation, however, they differ in the type of linkage; α1,3/α1,4 in plants versus α1,6 in mammals. Mammalian glycosylation involves the attachment of sialic acid (NeuAc), which cannot be performed by plants. Furthermore, xylose is a sugar that can be found in plant glycans but not in the glycans of mammals.

1.4.1 Impact of *N*-glycoforms on IgG functionality

While the ability of IgG to bind to FcγRs is dependent on the presence of the *N*-glycan in the Fc region (Lu *et al.*, 2015; Subedi and Barb, 2015), affinity to FcγRs is influenced by variations in glycoforms. Altered antibody functionality can be detected upon addition or removal of the variably added sugar moieties at Asn297 in the Fc region. Hypergalactosylation seems to promote ADCC by enhancing binding to the FcγRIIIa (Thomann *et al.*, 2016). Furthermore, galactosylation in absence of sialylation leads to enhanced C1q binding and consequently in significantly increased complement-dependent cytotoxicity (Quast *et al.*, 2015; Peschke *et al.*, 2017). *N*-glycans with terminating sialic acid moieties have shown to exhibit anti-inflammatory effects (Kaneko, Nimmerjahn and Ravetch, 2006), the underlying mechanism, however, is heavily debated. A commonly proposed mechanism is increased conformational flexibility of the Fc region promoted by sialylation, which is thought to allow binding to DC-SIGN (dendritic cell-specific intercellular adhesion molecule-3-grabbing non-integrin), a type C-lectin on dendritic cells, which results in the release of regulatory cytokines. These cause upregulation of FcγRIIb on effector macrophages, thus reducing inflammation (Anthony and Ravetch, 2010; Pincetic *et al.*, 2014). However, this interaction is controversial and some studies have demonstrated that no binding of IgG to DC-SIGN occurs, regardless of sialylation (Temming *et al.*, 2019).

The glycan modification with the highest impact on IgG function seems to be afucosylation of the core GlcNAc, leading to an up to 100 fold increase in antibody affinity to the FcγRIIIa receptor and thus to a significant increase in ADCC activity (Ferrara *et al.*, 2011). This effect was reported to stem from direct interactions of the afucosylated IgG Fc-glycan with the *N*-linked glycan (Asn162) of the FcγRIII family leading to stabilising contacts, which were lacking when using fucosylated IgGs (Ferrara *et al.*, 2011). However, another study suggested that no glycan-glycan interactions occur, but IgG fucosylation displaces the FcγRIII N162-glycan, therefore reducing the proximity of the receptor to the IgG when compared to an afucosylated IgG (Falconer *et al.*, 2018). While the

underlying mechanisms of the effects of different glycoforms on FcγR binding have not been fully elucidated yet, it has been accepted that controlled and well-defined glycosylation is of importance to ensure maximum efficacy of mAb therapeutics (Spearman, Dionne and Butler, 2011).

1.4.2 *N*-glycosylation pathway in mammals

The *N*-glycosylation pathway across all kingdoms follows the same central *N*-glycan processing pathway in the endoplasmic reticulum (ER) but differs in the processing in the Golgi apparatus (Chung *et al.*, 2017). The highest similarity in *N*-glycan structure and processing can be found between mammals and plants. The first step of the central *N*-glycosylation pathway of proteins is the transfer of Glc3Man9GlcNAc2 oligosaccharide from dolichol pyrophosphate to an asparagine residue, which is part of the correct sequence Asn-X-Ser/Thr (X cannot be proline) (Helenius and Aebi, 2001; Pattison and Amtmann, 2009; Chung *et al.*, 2017). This step occurs in the ER and is catalysed by the oligosaccharyl-transferase (OST) complex. The initial processing steps also occur in the ER, where the *N*-glycan is trimmed to give rise to Man9GlcNAc2 (Helenius and Aebi, 2001; Pattison and Amtmann, 2009), which is further processed by ER α-Man (MNS III) to create Man8GlcNAc2.

In the Golgi of mammalian cells (Figure 1-14) the removal of three mannidose residues by α1,2-mannosidase I (GMI) generates Man5GlcNAc2 (Hossler, Khattak and Li, 2009; Liebminger *et al.*, 2009). Next, N-acetylglucosaminyltransferase I (GnTI) transfers one GlcNAc residue to the α1,3-linked Man to produce GlcNAcMan5-GlcNAc2 (von Schaewen *et al.*, 1993; Strasser *et al.*, 1999; Hossler, Khattak and Li, 2009; Chung *et al.*, 2017), which is followed by the cleavage of two Man residues catalysed by Golgi-α-mannosidase II (GMII). The subsequent transfer of a GlcNAc residue to the α1,6-linked Man by β1,2-N-acetylglucosaminyltransferase II (GnTII), which yields the GnGn glycan core common to both mammalian and plant N-glycan (Hossler, Khattak and Li, 2009; Strasser, 2016; Chung *et al.*, 2017).

Subsequently, a number of glycosyltransferases give rise to a multitude of different *N*-glycoforms in mammalian cells. GlcNAc-transferases III-V (GnTIII-IV) are responsible for bisected (GNTIII) and tri-or tetra-antennary glycans (GNTIV-V). These glycan structures can be further modified by α1,6-fucosyltransferase (α1,6 FucT), β1,4-galactosyltransferase (β1,4 -GalT), α2,3-sialyltransferase (α2,3 ST) and α2,6-sialyltransferase (α2,6 ST) (Hossler, Khattak and Li, 2009). The final *N*-glycan composition is dependent on several factors such as expression levels of the various glycosyltransferases and accessibility of the glycosylation site (Hossler, Khattak and Li, 2009).

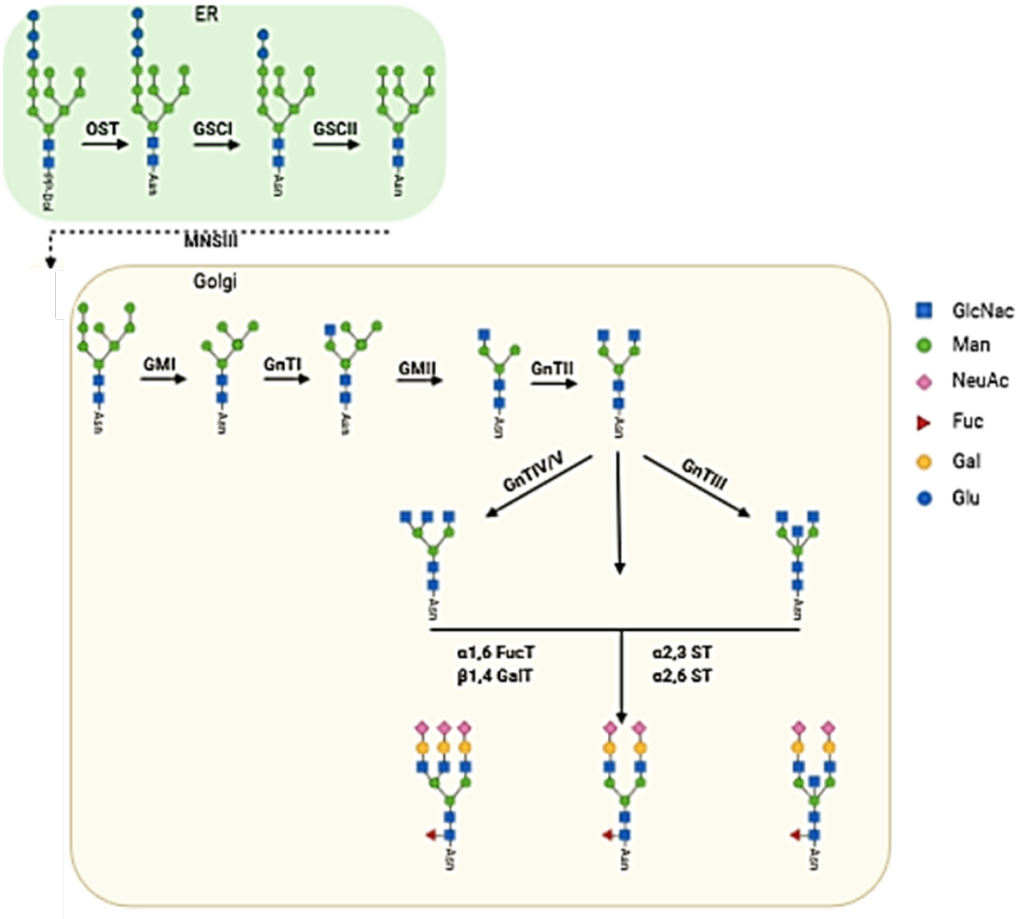

Figure 1-13: Overview of common N-glycosylation processing pathways in the ER and Golgi apparatus of mammals. The final complex N-glycoforms displayed represent only a small number of possible glycoforms.

1.4.3 Plant *N*-glycosylation

Plants perform complex glycosylation of proteins. Indeed, the glycan core is identical in plant and mammalian-produced glycoproteins, but the glycans diverge beyond this point (Figure 1-12).

Plants attach a β(1,2)-xylose to the β-mannose of the glycan core, a sugar absent in mammalian *N*-glycans. Furthermore, a α(1,3)-fucose is added instead of a α(1,6)-fucose to the core GlcNAc in plants (Figure 1-12 B). Additionally, plants lack the machinery to perform galactosylation and sialylation (Cabanes-Macheteau *et al.*, 1999). Sialylation is only observed in about 10 percent of serum antibodies, so it may not be critical, but it might be desirable for some glycoproteins for human use (Stadlmann *et al.*, 2008). While hypergalactosylation can enhance ADCC activity (Thomann *et al.*, 2016), this can also be achieved by the removal of the core fucose (Ferrara *et al.*, 2011). In order to use plant-produced antibodies for therapeutic purposes, afucosylation and the removal of xylose are favourable to prevent the unlikely event of an immunogenic reaction (Bardor *et al.*, 2003; Bencúrová *et al.*, 2004). Moreover, afucosylation leads to improved ADCC activity as discussed previously.

Several technologies allow the engineering of plant-glycans via silencing or knock-out of targeted glycosyltransferases. A ΔXF *Nicotiana benthamiana* plant line was generated using RNAi technology (Strasser *et al.*, 2008). A similar ΔXF *Nicotiana tabacum* plant line is not yet available, but would be important, as stable expression of antibodies in *N. tabacum* may be a more feasible strategy for low-income countries (Garabagi, McLean and Hall, 2012; Murad *et al.*, 2020).

1.4.4 The N-glycosylation pathway in plants

The *N*-glycosylation pathway in plants is identical to the mammalian *N*-glycosylation pathway up to the removal of two Man residues by Golgi-α-mannosidase II (GMII) in the Golgi. This is followed by the transfer of a GlcNAc residue to the α1,6-linked Man by β1,2-N-acetylglucosaminyltransferase II (GnTII), and the attachment of β1,2-Xyl and α1,3-Fuc (Strasser, 2016). Alternatively, the GlcNAcMan5-GlcNAc2 substrate can be modified with β1,2-xylosyltransferase (XYLT) or by core α1,3-fucosyltransferase prior to GNTII (Bencúr *et al.*, 2005) , however, it is assumed that β1,2-Xyl is commonly attached prior to α1,3-Fuc. The last step in N-glycan processing, which is rarely observed, is the attachment of Gal to terminal GlcNAc residues and

the transfer of α1,4-Fuc to the terminal GlcNAc residues catalysed by α1,4-fucosyltransferase (Strasser *et al.*, 2007; Strasser, 2016).

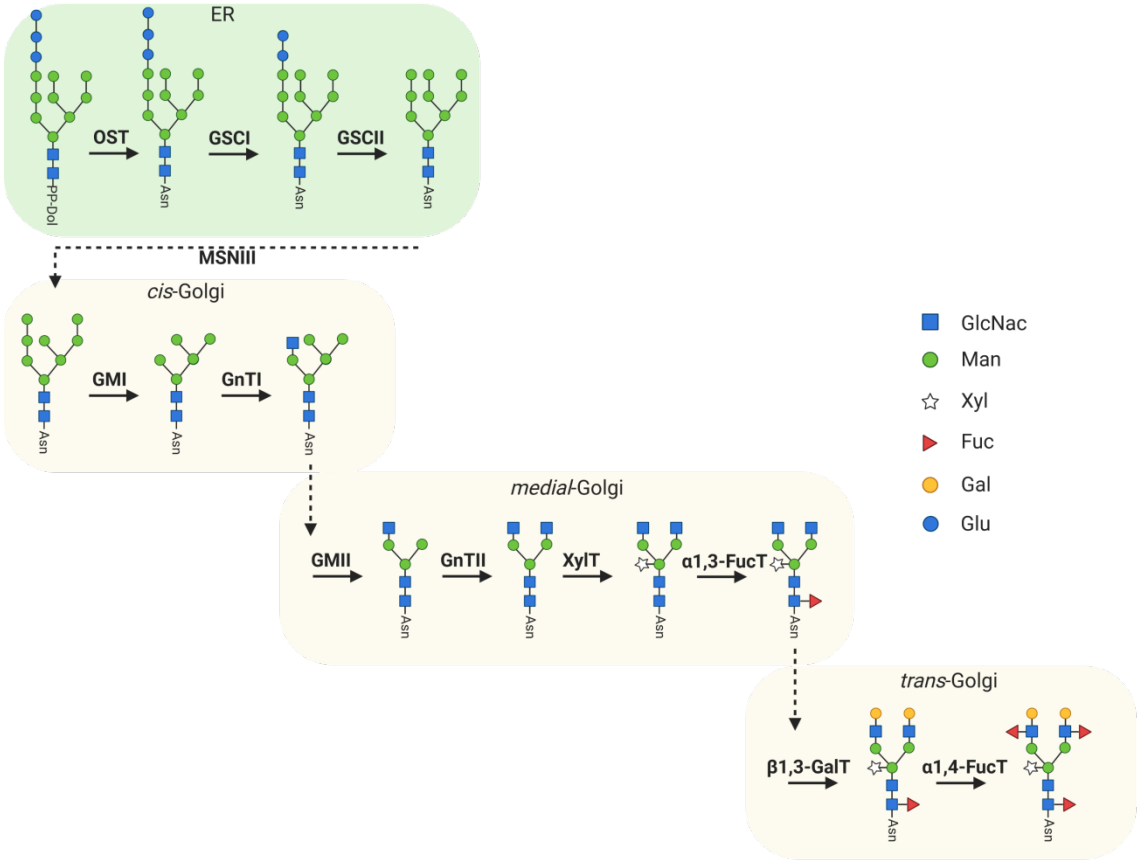

Figure 1-14: N-glycosylation processing in the ER and Golgi apparatus of plants. The most commonly observed pathway, with GnTII preceding XylT and α1,3 FucT activity, is shown.

1.4.5 Glycan engineering in plants

While mammalian cells have the advantage of producing human-like glycoproteins, they tend to generate hundreds of glycoforms (Montero-Morales and Steinkellner, 2018). This heterogeneity complicates providing a product with consistent, predictable efficacy (Ren *et al.*, 2020). In contrast, plants display a limited number of *N*-glycans, with GnGnXF accounting for more than 60 percent and MMXF for 20-40 percent of all observed glycoforms (Figure 1-15)(Montero-Morales and Steinkellner, 2018). Even though plants are not naturally equipped with the tools to perform human-like glycosylation, this homogeneity makes them not only attractive for the

production of glycoproteins, but also facilitates genetic glycoengineering (Schoberer and Strasser, 2018).

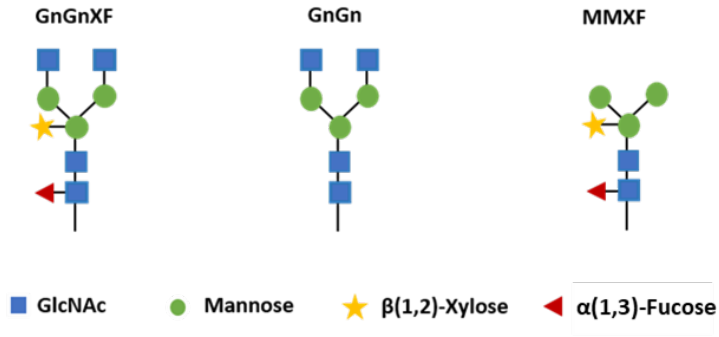

Figure 1-15: The two main glycoforms GnGnXF (left) and MMXF (right) generated by plants and the key glycan structure of higher eukaryotes GnGn (middle).

The first step to engineering plants that yield complex human *N*-glycans, is a plant line devoid of α1,3-fucose and β1,2-xylose in order to obtain mainly GnGn, which is the key glycan structure found in higher eukaryotes (Strasser, Altmann and Steinkellner, 2014; Montero-Morales and Steinkellner, 2018). This requires inactivation of the genes encoding α1,3-fucosyl- and β1,2-xylosyltransferases (ΔXF), which was achieved in a variety of plants with traditional knockout techniques, gene editing or gene silencing using RNA interference (RNAi) and will be further discussed here for *Nicotiana benthamiana* and *Nicotiana tabacum*. For the development of a ΔXF *N. benthamiana* plant line, several strategies were applied; however, the best results were obtained using RNAi and CRISPR/Cas9, respectively. The first ΔXF *N. benthamiana* line was engineered in 2008 using RNAi (Strasser *et al.*, 2008) and has since been widely used in the Plant Molecular Farming community for the production of glycoproteins, like mAbs (Lai *et al.*, 2014; Teh *et al.*, 2014; Hurtado *et al.*, 2020; Stelter *et al.*, 2020). This plant line was generated by first silencing *XylT* and *FucT* separately, which was accomplished by transforming wild-type *N. benthamiana* with constructs encoding for *XylT* or *FucT* RNAi, respectively. Subsequently, the best ΔX and ΔF line, which exhibited no or significantly reduced presence of the residues in immunoblots, were crossed to obtain a ΔXF

plant line. Several plants of the T_1 progeny seemed to lack *FucT* or *XylT* activity and one line was selected for further breeding to T_4 generation. All tested plants of this progeny exposed no detectable *XylT* and *FucT* activity on immunoblots. The full *N*-glycan composition was investigated using mass spectrometry, which revealed the lack of β1,2-xylose and a significant reduction of α1,3-fucose (Strasser *et al.*, 2008). Over 10 years later, a complete XF *N. benthamiana* knockout line was generated with the help of CRISPR/Cas9 (Jansing *et al.*, 2019). While a polycistronic tRNA-gRNA (PTG) approach, with three sgRNAs targeting *XylT* and four targeting *FucT,* was used to inactivate the two glycosyltransferase genes, Jansing *et al.* (2019) followed the same overall strategy of initially creating ΔX and ΔF lines, which were then crossed to establish the ΔXF line. The transformation of wild-type *N. benthamiana* with either PTG construct, led to a complete lack of *XylT* or *FucT* activity in the T_2 generation, which was confirmed by mass spectrometry. Crossing of the respective best lines resulted in a plant line devoid of *XylT* activity at T_1, whereas complete elimination of *FucT* activity required further breeding to T_2 (Jansing *et al.*, 2019).

In *Nicotiana tabacum*, ΔXF knockouts have only been reported for *Nicotiana tabacum* L. cv Bright Yellow 2 (BY-2) suspension cells, however by two individual groups (Hanania *et al.*, 2017; Mercx *et al.*, 2017). In both cases CRISPR/Cas9 was applied, though their approaches differed slightly. Mercx *et al.* (2017) opted for a PTG approach, with a total of nine sgRNAs in the same construct - three specific to *XylT* and six to *FucT*. Several putative knockout lines were obtained after a single round of transformation, with two lines showing no xylose or α1,3-fucose residues on immunoblots. Their absence was further confirmed by mass spectrometry. In contrast, Hanania *et al.* (2017) designed a construct with each sgRNA being under control of a separate U6 promoter and only used one sgRNA for *XylT* and four for *FucT*. Similarly, a ΔXF cell line, confirmed by mass spectrometry, was acquired after a single round of transformation.

These ΔXF plant lines can be further modified to produce human glycan structures by recombinant expression of human glycosyltransferases, which has been demonstrated using ΔXF *N.*

benthamiana. For example, the production of human erythropoietin (hEPO) with bisected (GnGnbi) *N*-glycans, commonly found in mammalians, was accomplished by the expression of modified versions of three human glycosyltransferases in ΔXF *N. benthamiana* (Castilho *et al.*, 2011). The same research group managed to produce a sialylated version of the anti-HIV bNAb 2G12 *in planta* (Castilho *et al.*, 2010). Achieving sialylation is especially complicated, as plants not only lack sialyltransferase (ST), but also the machinery to produce the precusor CMP-N-acetylneuraminic acid (CMP- Neu5Ac) and a transporter that efficiently delivers the precursor to the Golgi apparatus. However, Castilho *et al.* (2010) obtained sialylation *in planta* by the expression of six mammalian genes, that code for the missing proteins. While the ability to generate glycoproteins with a complex human *N*-glycan profile is beneficial, it is not always necessary in order to obtain a highly efficient product.

1.5 CRISPR/Cas9

The original CRISPR/Cas (Clustered Regularly Interspaced Short Palindromic Repeats, CRISPR associated proteins) system (Jansen *et al.*, 2002) was discovered in prokaryotes acting as an adaptive immune system (Horvath and Barrangou, 2010; Makarova *et al.*, 2011). Currently, there are 2 classes and 6 types of CRISPR systems known (Rojo *et al.*, 2018), but type II is most commonly used for gene editing purposes (Sander and Joung, 2014; Rojo *et al.*, 2018) and will be described in detail here.

A CRISPR locus consists of short direct repeats combined with spacer sequences. The short direct repeats are identical in length and sequence; the spacers, which are derived from previous exposures to foreign DNA, vary in sequence even though they are similar in size. At the beginning of each CRISPR locus, a highly conserved AT-rich leader sequence can be found, which is followed then by the direct repeats-spacer sequences.

The defence response can be classified into three stages: acquisition, biogenesis and interference (Figure 1-16). During acquisition, new viral or foreign plasmid DNA is captured and

inserted as a new spacer sequence in-between repeat by Cas1 and Cas2. The spacer sequence is selected based on the recognition of protospacer adjacent motifs (PAM), short nucleotide sequences, which cannot be found in the DNA of the host. During biogenesis (stage 2, Figure 1-16), the CRISPR locus is transcribed into pre-crRNA, which hybridises with small RNA molecules that are complementary to the palindromic repeats, the trans-activating RNA (tracrRNA). This allows RNase III to cleave the precursor crRNA into mature crRNA, which in turn forms a complex with Cas9. During interference (stage 3, Figure 1-16), the crRNA guides the Cas9 to its complementary sequence in the intruding DNA and Cas9 cleaves the target DNA three base pairs away from the PAM, thus inducing double strand breaks (DSB) (Sander and Joung, 2014; Westra, Buckling and Fineran, 2014; Rath *et al.*, 2015; Marraffini, 2016).

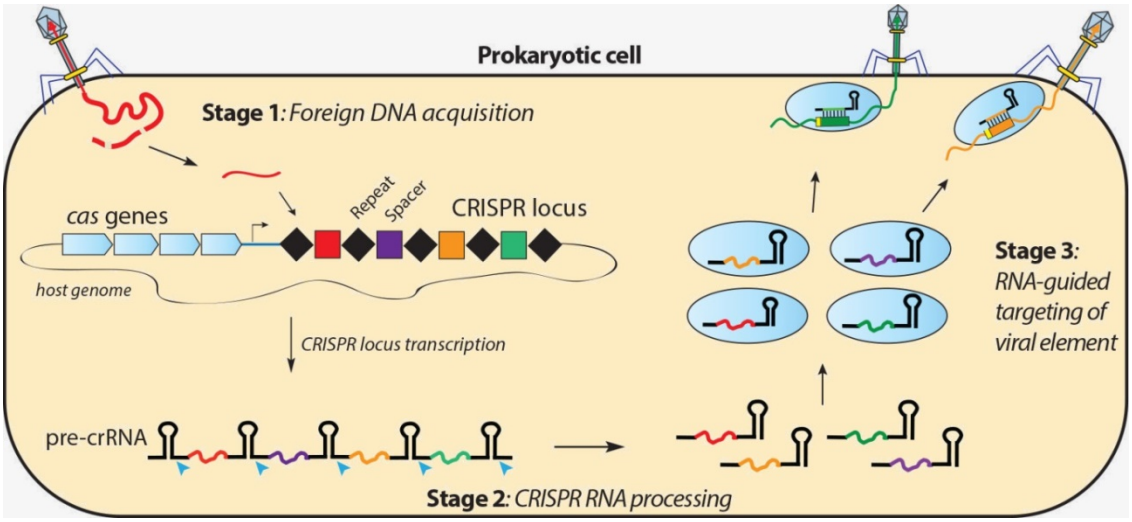

Figure 1-16: The mechanism of the CRISPR/Cas system as discovered in prokaryotes. Stage 1 shows the acquisition of foreign DNA, which is inserted as spacer sequence into the CRISPR locus. Stage 2 represents biogenesis, therefore transcription of the CRISPR locus into pre-cRNA and RNA processing to release mature crRNA. Stage 3 displays interference, during which the crRNA leads the Cas9 complex to the intruding DNA and leads to cleavage induced by Cas9. (http://doudnalab.org/research_areas/crispr-systems/)

1.5.1 CRISPR in gene editing

To simplify the system for genome editing purposes, the crRNA and tracrRNA were combined to form a single guide RNA (sgRNA) (Jinek *et al.*, 2014b). Gene editing is simplified using CRISPR/Cas9 as the only requirement is a 20 nt RNA sequence upstream of the respective PAM, which in the most prominent system, Cas9 from *Streptococcus pyogenes* (SpCas9), is NGG. The

sgRNA then guides the Cas9 to the target sequence, where Cas9 induces a double strand break (DSB), which can be repaired either by non-homologous end joining (NHEJ) or homology-directed repair (HDR) (Figure 1-17). In NHEJ, the DSB is repaired by the endogenous repair machinery, which is error-prone and often results in indels (insertions and/or deletions). This is used to induce frameshift mutations, which will result in gene knockouts, as the gene cannot be translated correctly. The second type of repair is the HDR, during which a repair template with homology arms can be supplied to repair the DSB (Ran *et al.*, 2013). This results in highly specific replacements, however the efficiency of this pathway is comparatively low (Chu *et al.*, 2015).

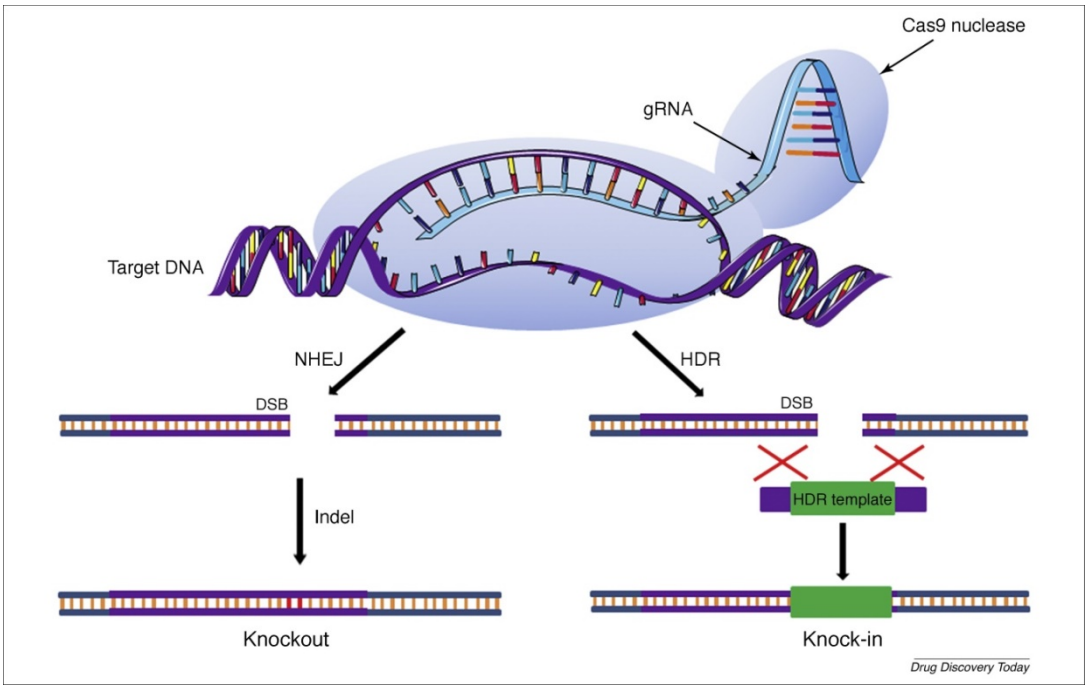

Figure 1-17: Schematic depiction of genome editing mediated by CRISPR/Cas9 and subsequent host-directed DNA repair mechanisms. The Cas9 endonuclease, which is guided by the desired guide RNA (gRNA), cuts the double-strand and induces a double strand break (DSB). In vivo DNA repair occurs via non-homologous end joining (NHEJ) or homology-directed repair (HDR), respectively.(Liu, Saber and Haisma, 2019)

Cas9 is a multidomain protein (Jinek *et al.*, 2014a) (Figure 1-18). HNH and RuvC are nuclease domains making up the nuclease lobe, which is bridged to the recognition lobe (RECI-III) via the arginine-rich bridge helix. The C-terminal and PAM interacting (PI) domain are responsible for initiating binding to the target DNA (Palermo *et al.*, 2016; Jiang and Doudna, 2017) .

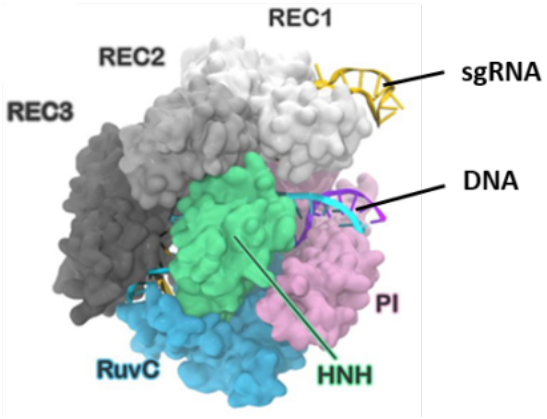

Figure 1-18: Crystal structure of the S. pyogenes CRISPR-Cas9 system The guide RNA (yellow), the target DNA (cyan) and non-target DNA (violet) strands are shown.(5) The two endonuclease domains, HNH and RuvC, are shown in green and cyan, respectively. The PAM-interacting (PI) domain is shown in pink and the three recognition domains (REC1-3) are shown in different shades of grey (Palermo *et al.*, 2019).

The native Cas9 was further modified to use the CRISPR system for different applications. By exchanging an aspartate for an alanine (D10A) in the RuvC domain, a Cas9 nickase was created. The Cas9 nickase will only nick DNA, leading to single-strand breaks that are preferentially repaired by HDR (Ramirez *et al.*, 2012). Another variant of Cas9 is a nuclease-deficient Cas9 (dCas9), which was generated by mutations in both nuclease domains, RuvC (D10A) and HNH (H840A), that inactivate cleavage activity but do not impact DNA binding (Sander and Joung, 2014). The nuclease-deficient Cas9 (dCas9) can be used for transcriptional regulation. Repression is achieved by dCas9 itself through steric hindrance or by coupling it with a repressor. For transcription activation, an activator is fused to dCas9 (Shalem, Sanjana and Zhang, 2015). Furthermore, it can be used to visualise specific DNA sequences by fusing dCas9 with GFP (B. Chen *et al.*, 2013).

While SpCas9 is most commonly applied as an effector nuclease , other Cas9 endonucleases, such as from *Staphylococcus aureus* (SaCas9) (Ran *et al.*, 2015) and *Neisseria meningitidis* (NmCas9) (Zhang *et al.*, 2013), have been isolated. These primarily differ in their respective PAM sequence, allowing for targeting sites that lack the NGG motive. Furthermore, endonucleases of different types, such as the smaller type V Cas12a (previously Cpf1) (Zetsche *et al.*, 2015), have been discovered. Cas12a recognises AT-rich PAM sites and induces a DSB with staggered ends (Rojo *et al.*,

2018). This continuous identification and modification of Cas endonucleases further facilitates genome engineering by enabling scientists to employ the system best fit for their target.

Major advantages of the CRISPR system compared to zinc-finger nucleases (ZFNs) and transcription-activator like effector nucleases (TALENs) are its simplicity, versatility and the cost (Bortesi and Fischer, 2015). Protein engineering steps are redundant. Cas9 endonucleases are active as a monomer; therefore, a double-strand break can be induced without the need of a guide RNA on the opposite DNA strand. Both simplify the genome engineering process, testing of the efficiency of the designed gRNA and also reduce cost. Furthermore, CRISPR is able to edit methylated DNA (Hsu *et al.*, 2013) and can be easily used in a multiplexing system (Li *et al.*, 2013), which allows targeting several genes at the same time, by simply designing and introducing several sgRNAs simultaneously. These advantages make CRISPR/Cas9 the preferred genome editing tool.

1.5.2 Delivery systems

Currently,a variety of systems for the delivery of the sgRNA and Cas9 into mammalian cells exist. The four main systems are viral delivery, delivery via DNA, RNA or Cas9/gRNA ribonucleoprotein (RNP) systems (Kelton *et al.*, 2016).

An established method is delivery via plasmid (DNA delivery), as all that is needed is a plasmid that expresses Cas9 and the respective sgRNA can easily be cloned into the multiple cloning site. Advantages of this system include the modularity and no size restriction of the cargo. However, plasmids always bear the risk of integration of exogenous DNA into the host genome. Moreover, generating and screening plasmids can be comparatively time-consuming.

These problems can be tackled by using RNA or RNP delivery systems. In the case of RNA delivery, Cas9 and sgRNA are delivered as mRNA into the cell, thus circumventing the problem of possibly incorporating exogenous DNA into the host genome and furthermore saving time by by-

passing the transcription process. Both of the advantages also apply to RNP delivery, but this system also allows for controlled ratios of Cas9 to sgRNA, thereby decreasing off-target.

These systems can be also applied to plants where RNA or RNP can be delivered into protoplasts (Woo *et al.*, 2015; Lowder, Malzahn and Qi, 2016). The protoplasts need to be regenerated to whole plants later on and that can sometimes prove to be rather challenging. For DNA delivery, agroinfiltration is used (Lowder, Malzahn and Qi, 2016), but it has the same downsides as discussed for mammalian cells.

1.5.3 CRISPR/Cas9 in plants

The immense potential of the CRISPR/Cas system for crop improvement has been recognised; hence it was adapted for application in plants. Initially, proof-of concept studies for CRISPR/Cas9 with predominantly NHEJ were performed in a variety of crop plants (Jaganathan *et al.*, 2018). As these studies exhibited promising results, CRISPR has now been used for a multitude of targeted knockouts in monocots and dicots. Here only a few studies are presented to highlight the potential and versatility of CRISPR/Cas9 in plant genome editing, but the system has also been used in a variety of other monocotyledons including wheat and dicocotyledons like soybean, cotton, potato (Jaganathan *et al.*, 2018), which are not discussed here.

Extensive studies have been performed using *Oryza sativa* (rice), due to its importance as a major crop plant and having a genome that can be easily manipulated. In rice, genes that are regulators of abiotic and biotic stress responses were commonly targeted. For example, Zhou *et al.* (2015) developed rice mutants with enhanced resistance to bacterial blight, caused by *Xanthomonas oryzae pv. oryzae*. This was achieved by knocking out the promoter for OsSWEET13 (Zhou *et al.*, 2015), a disease susceptibility gene, which is essential for infection. In *Zea mays* (maize), another monocot, genes responsible for phytic acid synthesis were disrupted using CRISPR/Cas9 (Liang *et al.*,

2014), as phytic acid is thought to be anti-nutritional, but constitutes about 70 percent of the maize seed.

First attempts to utilise CRISPR/Cas9 in dicotyledons were performed in *Arabidopsis thaliana,* as its small genome and diploidy render it an ideal model organism. An important study that focused less on functional disruption of genes but more on monitoring the specificity, heritability and efficiency of CRISPR/Cas-induced mutations over several generations in *A. thaliana* allowed for better understanding of the impact of breeding with regard to CRISPR. It revealed that the majority of induced mutations were 1 bp insertions or short deletions and showed mutation rates of 58-79 % in T_1 to T_3 generations. Homozygous mutants were first observed in T_2 and were passed on to the next generation without new mutations. Furthermore, no off-target effects were observed (Feng *et al.*, 2014). These observations are essential for the generation of new plant lines using the CRISPR/Cas system. Although most researchers make use of the simpler NHEJ DNA repair pathway, HDR offers the unique possibility of exchanging genes, which might be advantageous when disruption of genes is incapable of providing the desired trait. For example, the shelf-life of *Solanum lycopersicum L.* (tomato) was prolonged by exchanging the dominant ALC (Alcobaca) gene with the recessive alcobaca (alc) gene, using a HDR-mediated CRISPR approach (Q. H. Yu *et al.*, 2017). This further highlights the versatility and potential of CRISPR as tool for crop improvement.

1.5.3.1 CRISPR/Cas 9 applications in the genus Nicotiana

Compared to other crop plants, only a limited amount of CRISPR usage in plants of the genus *Nicotiana* has been reported. Yet, both, *N. tabacum* and *N. benthamiana*, are key plant species used in plant molecular farming, therefore genome engineering using CRISPR/Cas9 to generate plant lines with favourable characteristics has been performed by a few groups.

In contrast to *N. tabacum* an annotated genome of *N. benthamiana* (Bombarely *et al.*, 2012) has been available for a few years, facilitating the design of efficient sgRNAs. Initial studies

performed in *N. benthamiana* targeted the phytoese desaturase (*PDS*) gene (Li *et al.*, 2013; Nekrasov *et al.*, 2013), as disruption of *PDS* impairs carotenoid and chlorophyll synthesis which leads to albino leaves, thus simplifying identification of edited plants. Contrary to *A. thaliana*, substantial, rather than single-nucleotide, deletions and insertions were observed for *N. benthamiana* (Li *et al.*, 2013), however, the source of these differences has not been identified so far. Recently, a complete CRISPR-mediated knockout of α(1,3)- fucosyltransferase (*FucT*) and β(1,2)-xylosyltransferase (*XylT*) in *N. benthamiana* was reported (Jansing *et al.*, 2019). This KO plant line might be superior for the production of glycoproteins to the currently used RNAi ΔXF plant line, as silencing of the transferase genes is incomplete. A major limitation of plant molecular farming is low yields, partly caused by the plant's RNA-silencing mechanism, which degrades transgene-derived mRNAs. By disrupting the RNA-dependent RNA polymerase (RDR6) gene, a key component of the RNA-silencing mechanism, enhanced expression of a recombinant protein was achieved in *N. benthamiana*. Additionally, this mutation resulted in abnormal flower growth and sterility (Matsuo and Atsumi, 2019), a characteristic that might be favourable for open-field cultivation.

Despite the unavailability of a fully annotated *N. tabacum* genome, Gao et *al.* (2015) were able to demonstrate that CRISPR/Cas9 is highly efficient in inducing mutations in *N. tabacum* by targeting the *NtPDS* (phytoene desaturase) and *NtPDR6 (*pleiotropic drug resistance type transporter) genes. The mutation rate was above 80 percent for each gene (Gao *et al.*, 2015). Furthermore, Hanania et *al.* (2017) and Mercx et *al.* (2017) were able to knock out the β(1,2)-xylosyltransferase (*XylT*) and α(1,3)-fucosyltransferase (*FucT*) genes in BY2 suspension cells using CRISPR/Cas9 (Hanania *et al.*, 2017; Mercx *et al.*, 2017). Only recently, a nicotine-free *N. tabacum* plant-line was created using a single gRNA targeting six berberine-bridge like enzyme (BBL) genes (Schachtsiek and Stehle, 2019). However, up to this date, no knockout of *XylT* and *FucT* in *N. tabacum* plants via CRISPR/Cas9 has been reported.

1.6 Hypothesis and Aims

The main hypothesis of this thesis is the ability of plant expression systems to produce fully functional anti-HIV bNAbs, which have been modified to exhibit enhanced *in vivo* half-life and superior ADCC activity. Testing this hypothesis is of interest as plant expression systems provide many benefits, which mammalian cell culture systems lack (see 1.3.4), especially regarding facilitation of local production of therapeutics for treating diseases with a high incidence rate in LMICs. Furthermore, this thesis is trying to investigate whether effects of half-life extending mutations, as reported in literature, are exclusive to mAbs produced in mammalian cells. The hypothesis was tested using the V3-glycan dependent bNAb 10-1074. 10-1074 was chosen with the future development of an anti-HIV bNAb cocktail in mind, due to showing promising results in combination with CD4bs bNAbs, by targeting two different epitopes on the HIV Env glycoprotein.

The aim of this thesis is the characterisation of the native and modified version of the bNAb 10-1074, which have been produced in a *Nicotiana* plant expression system. The results serve as basis for the decision which version of the bNAb will be further developed to eventually be included in an anti-HIV antibody cocktail. An additional objective is the development of a stable ΔF *N. tabacum* plant line, to contribute to the advancement of the plant expression technology platform in anticipation of using transgenic tobacco for large scale mAb manufacturing in LMICS.

The specific objectives are:

Producing bNAb 10-1074 with enhanced efficacy in a plant expression system and its characterisation, which involves:

1. Cloning and transient expression of the 10-1074 versions of interest using ΔXF *N. benthamiana*
2. Characterisation the expressed 10-1074 variants with regard to their yield and glycosylation

3. Determination of binding kinetics (to gp120, FcRn, FcγRIIIa), neutralisation breadth and potency, ADCC and *in vivo* half-life
4. Identify the 10-1074 variant with the best overall properties to evntually be included in an anti-HIV bNAb cocktail

Using the CRISPR/Cas9 system to produce a stable glycoengineered fucosyltransferase deficient (ΔF) *N. tabacum* plant line, which involves:

1. Design, synthesise and test sgRNAs targeting the *N. tabacum* fucosyltransferase genes
2. Select 4-5 sgRNAs with the highest cutting efficiency and using them for the knock-out of the fucosyltransferase genes
3. Analyse putative ΔF plants with regard to their glycosylation profile and identify plants which will be further bred
4. Expression of selected bNAbs, purification and glyco-analysis

2 Materials and Methods

All recipes for buffers, details of antibodies and primers can be found in the appendix.

2.1 Production and characterisation of broadly neutralising antibodies produced in ΔXF *N. benthamiana*

2.1.1 Nomenclature

Throughout this thesis the nomenclature of the bNAb variants has been simplified, as shown in Table 2-1. The same approach of labelling was used for other modified antibodies that have been mentioned as part of the introduction and discussion.

10-1074 variants generated using ΔXF *N. benthamiana* as expression host are frequently labelled additionally with ΔXF.

Table 2-1: Nomenclature of 10-1074 variants used throughout thesis

Simplified name	Description
10-1074 HC	bNAb 10-1074 in its native form (unmodified Fc-region), generated in glycoengineered ΔXF *N. benthamiana*
10-1074 YTE	bNAb 10-1074 modified with a YTE mutation in the Fc-region, generated in glycoengineered ΔXF *N. benthamiana*
10-1074 LS	bNAb 10-1074 modified with a LS mutation in the Fc-region, generated in glycoengineered ΔXF *N. benthamiana*
10-1074 CHO	bNAb 10-1074 in its native form (unmodified Fc-region), generated in CHO cells*

*This monoclonal antibody was obtained from CFAR and kindly supplied by the Nussenzweig laboratory. The antibody was supplied in a buffered solution containing sodium phosphate, potassium phosphate, potassium chloride, sodium chloride, and polysorbate 80.

2.1.2 Cloning of antibody heavy and light chain genes into MIDAS vectors

Sequences for mAb 10-1074 were obtained from Mouquet *et al.* 2012 and the light and heavy chain variable regions (V_L and V_H) were synthesized by GeneArt (ThermoFisher Scientific, USA) and cloned into vectors upstream of sequences for constant regions of human IgG heavy chain (C_H)

or human IgG lambda chain. The full-length heavy and light chain genes were then amplified and cloned into the MIDAS entry vectors pWhite and pBlue (Teh *et al.,* in preparation) respectively.

The pWhite vector containing the heavy chain was assembled with the destination vector pTRAk.6 using the same amount of p.TRAk.6 and pWhite (50-200 ng), 1 µl of BsaI (10000 U/ml, New England Biolabs, USA), 1 µL T4 DNA ligase (400000 U/ml, New England Biolabs, USA), 2 µL of 10x T4 DNA ligase buffer (New England Biolabs, USA) and water to 20 µL. The reaction was performed for 50 cycles at 37 °C for 2 min, followed by 16 °C for 5 min, with a final step at 37 °C for 5 min. The vector was then transformed into DH5α cells as described in 2.2.1.3 and 50 µL were streaked onto plates containing IPTG (Isopropyl-β-D-thiogalactopyranoside) and X-Gal (5-Brom-4-chlor-3-indoxyl-β-D-galactopyranoside) for blue-white screening. Colonies were picked and analysed by restriction digest with NcoI (10000 U/ml, New England Biolabs, USA) and XbaI (20000 U/ml, New England Biolabs, USA). Positive plasmids were used for the second cloning step in which pBlue containing the light chain was assembled with HC:pTRAk.6 following the same protocol but using BsmBI (10000 U/ml, New England Biolabs, USA) instead of BsaI. Plasmids that showed the correct restriction profile (NcoI and XbaI) were sent for sequencing (Genewiz, UK) with appropriate primers to confirm the expected sequences. pTRAk.6 containing the heavy and light chain genes was transformed into *Agrobacterium tumefaciens* GV3101/PMPRK as described in section 2.1.2.

2.1.3 Expression of bNAbs

2.1.3.1 Agrobacterium transformation of *N. benthamiana* plants using syringe infiltration

Syringe infiltration of *N. benthamiana* was performed as per 2.2.3 with a few modifications. The pellet was re-suspended in infiltration buffer until an OD_{600} of 1 was obtained. ΔXF *N. benthamiana* (Strasser *et al.*, 2008) leaves were infiltrated and harvested 6 days post-infiltration (dpi).

2.1.3.2 Agrobacterium transformation of *N. benthamiana* plants using vacuum infiltration

For each construct, a 10mL pre-culture of transformed *A. tumefaciens* was grown. After 24 hours, the pre-culture was transferred into 200 mL of LB with antibiotics and incubated at 28 °C overnight with shaking (220 rpm). The OD_{600} of the culture was measured. The culture was centrifuged at 7354 g (Beckman Coulter) for 15 min at 15 °C. The supernatant was discarded and the pellet was re-suspended in infiltration buffer to an OD_{600} of 0.2. 0.5 mL of 200 µM acetosyringone were added per litre and the suspension was left at room temperature for 2 hours.

ΔXF *Nicotiana benthamiana* plants were immersed into the infiltration solution in a vacuum chamber, a vacuum (150 mbar) was applied for 3 minutes and quickly released. The plants were then left at 26 °C for 6 days until the leaves were harvested.

2.1.4 Extraction and purification of bNAbs from plant leaves

Antibodies were extracted from the leaves in 3 volumes (w/v) of PBS pH 7.4 using a blender (Waring). The extract was passed through miracloth and centrifuged (Beckman Coulter) at 15008 g for 50 min at 4 °C. The supernatant was poured through miracloth again and filtered through a 0.22 micron (Millex-GP, Merck Millipore, USA) syringe disc filter.

The crude extract was purified using a column packed with Protein A-Agarose Fast Flow (Sigma Aldrich, USA). Washing steps were performed using 10 CV (column volume) binding buffer (Sodium phosphate pH 7.0) and elution was performed using 0.1 M Glycine-HCl (pH 2.7). The eluate was neutralised using 1 M Tris-HCl (pH 9.0) and protein concentration was measured using Nanodrop 2000 at A_{280}. Protein containing fractions were transferred into a Slide-A-Lyzer Dialysis Cassette (3500 MWCO) and dialysis was performed in 4 L of 1 x PBS (pH 7.4) overnight at 4 °C. The next day the sample was re-dialysed in another 4 L of PBS for an hour. The sample was aspirated from the cassette and centrifuged at 2987 g and 4 °C for 10 min. An Amicon Ultra – 15 Centrifugal filter was used to concentrate the sample approximately 10-fold.

2.1.5 Characterisation of bNAbs

2.1.5.1 SDS PAGE

For SDS PAGE an appropriate volume of the sample was mixed with NuPAGE LDS sample buffer (4x, Novex, Invitrogen, USA) and heated for 10 min at 95 °C. For reducing conditions, 10% (v/v) β-mercaptoethanol (Sigma Aldrich, USA) was added to the solution prior to heat denaturation. Electrophoresis was run using NuPAGE 4-12% or 10% Bis-Tris gels (Novex, Invitrogen, USA) with 1% MOPS buffer (Novex, Invitrogen, USA) with running conditions of 100 V for 10 min and 150 V (100 V for PNGase digest samples) for 1 h 20 min. Gels were stained with Instant Blue (Expedeon, UK).

2.1.5.2 Western Blot

For Western Blot analysis, SDS PAGE with 50 ng of protein was performed as described in 2.2.4.1 but without staining. Instead, the separated proteins were blotted onto a nitrocellulose membrane (Amersham, GE Healthcare, UK) by semi-dry transfer using a Hoefer T-70 blotting unit. The transfer was performed at 20 mA per gel for 1 h 20 min. Blocking of the membrane was performed for 45 min with 5% (w/v) non-fat dried milk powder (Marvel) in TBST (1% (v/v) TBS + 0.1 % (v/v) Tween 20). The respective primary antibody at the correct dilution (Appendix) was added and incubated for another hour. When needed, a secondary antibody was added diluted in blocking buffer and incubated for one hour (Appendix). Membranes were washed 5x with TBST between each step. The blot was developed using Pierce ECL Plus Western Blotting detection system following the protocol.

2.1.5.3 PNGase F digest

Digestion was carried out following the manufacturer's instructions (New England Biolabs, PNGase F). The digested and non-digested glycoproteins were then separated via SDS-PAGE using a NuPAGE 10% Bis-Tris gel (Novex, Invitrogen, USA).

2.1.5.4 HIV Neutralisation assay

HIV-1 pseudoviruses were used for neutralisation assays. For pseudovirus production HEK 293T cells (ATCC) were pre-grown in high-glucose DMEM supplemented with L-glutamine (Sigma Aldrich, USA), 10% Fetal bovine serum (FBS) and Penicillin (100 U/mL) - Streptomycin (0.1 mg/mL) (Sigma Aldrich, USA). 24 h pre-transfection, 2mL of 10^5 cells/mL were seeded onto a 6 well plate and incubated at 37 °C and 5% CO_2. Cells were transfected using FuGENE HD (Promega, USA) following the protocol. A 3:1 FuGENE to DNA ratio with 1500 ng of ΔEnv and 500 ng of the respective Env plasmid (CFAR, USA) was used. Transfected cells were incubated for 48 h (37 °C, 5% CO_2). Pseudovirus was harvested by filtering the supernatant through a 0.45 µm syringe filter. Aliquots were immediately frozen at -80 °C.

Viruses were titrated using 96 well clear flat-bottom plates. A 1:1 dilution row in duplicates was prepared in DMEM, starting with an initial 1:5 dilution. 100 µL of a 10^5 cells/ml TZM-bl (CFAR, USA) cell suspension (with DEAE dextran) were added to 100 µL of virus and plates were incubated for 48 h (37 °C, 5% CO_2). After incubation, the supernatant was removed, cells were washed with 100 µL PBS prior to adding 100 µL of lysis buffer (Promega, USA). The plate was kept at -80 °C overnight to ensure complete virus inactivation. After thawing, 50 µL of the supernatant were mixed with 50 µL of Bright-Glo luciferase substrate (Promega Luciferase Assay System, USA) in a black flat bottom 96 well plate. Luminescence was measured using a GloMax plate reader (96 Microplate Luminometer, Promega, USA). The amount of virus required for luminescence readouts of 20 times the negative control (cells only) was calculated and used for neutralization assays.

For neutralisation assays bNAbs were diluted to 20 µg/mL and a 3-fold serial dilution in triplicate was performed in flat-bottom 96 well plates, with a final volume of 50 µL per well. 50 µL of pseudovirus were added to each well, with exception to the cells only control. After 1 h incubation, 100 µL of a 10^5 cells/ml TZM-bl – DEAE dextran cell suspension were added and plates were

incubated for 48 h (37 °C, 5% CO_2). Lysis and luminescence measurement were performed as described for virus titration.

2.1.5.5 Surface Plasmon Resonance

Surface Plasmon Resonance (SPR) was used to determine bNAb concentrations, gp140 binding and FcγRIIIa V158 binding. Protein A (Sigma Aldrich, USA) was immobilised on a CM5 chip (GE Healthcare, UK) by amine coupling, aiming at an RU of 5000. All measurements were performed using Biacore X100 instrument (GE Healthcare, UK) with HBS-EP+ (GE Healthcare, UK) as running buffer and 10 mM glycine-HCl (pH 1.5, pH 2.1 for FcRn) as regeneration solution.

The antibody concentration was determined using the standard curve from a monoclonal IgG1 λ (Sigma Aldrich, USA) with concentrations of 1000, 500, 250, 125, 62.5, 31.25 and 15.625 ng/mL. Each bNAb was diluted to be in the range of the standard curve based on A_{280} measurements. To determine the actual concentration, a sample was flowed over the chip for 180s and the signal was compared to the standard curve using the built-in BIAevaluation software. The chip was regenerated before the next sample was applied.

To determine the binding kinetics of gp140 and FcγRIIIa V158 with the bNAbs, a scouting step was performed before the kinetics measurement. Each bNAb was diluted 1:1000 (if necessary dilutions were adjusted accordingly) and was flowed over the chip for 30 s (t_{scout}). The obtained RU was used to calculate the contact time for each antibody to reach a R_{max} of 50.

$$R_{max} = \frac{MW_{analyte}}{MW_{ligand}} * R_L * S$$

MW…molecular weight (Da)

R_L…level of immobilised/captured ligand (RU)

S…stoichiometric ratio

$$t_{contact} = \frac{RU_{obtained}}{t_{scout}} * R_L$$

BNAb capture during the actual measurement was carried out with a flow rate of 20 µL/min. Only one flow cell of the chip (Fc2) was used for bNAb capture while the other flow cell (Fc1) was used as a baseline reference. The analyte (gp140 or FcγRIIIa V158) was flowed simultaneously to both flow cell.

After capturing of the respective bNAb, UG37 gp140 (CFAR, USA) was applied at a concentration of 80 µg/ml and a flow rate of 40 µL/min. A contact time of 135 s and a dissociation time of 3600 s were used. A kinetic curve was fitted and the kinetic parameters were determined using the built-in software.

For FcγRIIIa V158, multiple FcγRIIIa V158 (FcγRIIIa, R&D Systems, USA) concentrations (1, 0.5, 0.25, 0.125 and 0.0625 µM) were applied to determine the binding kinetics of FcγRIIIa V158 to each bNAb. A contact time of 40 s and a flow rate of 50 µL/min were used. A kinetic curve and kinetic parameters were determined as above.

Binding kinetics to hFcRn were determined by coating flow cell 2 of a CM5 chip with 10-1074 HC and 10-1074 YTE (RU 10000) respectively. Flow cell 1 was coated with BSA (RU 10000) serving as reference cell during measurements. A range of concentrations (75,100,150,200,250 nM) of rhFcRn (R&D Systems, USA) were flowed over both flow cells at a rate of 30 µL/min and a contact time of 60 s. Fitting of kinetic curves and obtaining kinetic parameters was performed by using the built-in software.

2.1.5.6 Transcytosis assay

For evaluating the transcytosis profile for each bNAb, $0.75*10^6$ MDCK hFcRn/hβ_2m or MDCK hβ_2m (control) cells were seeded onto transwells (CoStar, Corning Incorporated, USA) in 0.5 mL of DMEM with HEPES (Sigma Aldrich, USA). 1 mL of the same medium was put into each lower well and plates were incubated at 37 °C, 5% CO_2. After 48 h the medium was exchanged for fresh medium and incubated overnight. About 32 h later the medium of upper and lower was aspirated, wells were

washed with DPBS (Sigma, USA) and DMEM with HEPES lacking FBS and antibiotics was added. At 96 h, medium was aspirated and cells were washed with HBSS pH 7.4 (Gibco). 1 mL of HBSS pH 6 was added to each lower well and 0.25 ml of HBSS 7.4 to each upper well. Equilibration was performed for 20 min in a 37 °C incubator. 10, 5 or 2.5 µg of respective bNAbs were added in duplicates to the apical side (pH 6) of the cell monolayers and incubated. Basolateral supernatant was collected after 2 h. To determine the amount of transcytosed IgG an anti-hIgG ELISA was performed.

2.1.5.7 α-hIgG ELISA

An α-hIgG ELISA was used to determine transcytosis. The same assay was also used to determine the concentration of bNAb in serum (*in vivo* half-life studies). 96 flat-bottom immunosorbent plates were coated with an α-hIgG γ-chain antibody (The Binding Site, UK), diluted 1 in 200 in PBS pH 7.4 and incubated overnight at 4 °C. Wells were blocked with 5% non-fat dry milk (w/v) in PBS with 0.1% (v/v) Tween 20 and incubated for 1 h at 37 °C. Duplicates were performed for each sample.

For transcytosis, basolateral supernatants were applied neat. IgG λ (Sigma Aldrich, USA) was used as standard with an initial concentration of 0.25 µg/mL. A 3-fold dilution row was performed using blocking buffer as diluent. Plates were incubated overnight at 4 °C, contents flicked out and washed with water containing 0.1% Tween 20. Anti-IgG λ-HRP (Sigma Aldrich, USA) (1 in 1000) in blocking buffer was applied and incubated for 1 h at 37 °C. Plates were washed and remaining liquid removed from wells. 50 µL of TMB (Invitrogen, USA) were added to each well 50 µL of 2M H_2SO_4 were used to stop the reaction. A_{450} was measured using a Tecan Sunrise plate reader.

For half-life studies, serum samples were applied as 1:50 (Bleed 1) or 1:15 (all remaining bleeds) dilution. All other steps were performed as described for transcytosis.

The limit of detection (LOD) for this assay was determined to be $5*10^{-5}$ µg/ml and the limit of quantification (LOQ) $1.5*10^{-4}$ µg/ml.

2.1.5.8 ADCC activation assay

To determine the ability of the bNAbs to activate ADCC, an ADCC Reporter Assay (Promega, USA) for the V and F-variant was used. bNAbs were diluted to 12 µg/mL and a 3-fold dilution series was performed in sterile white flat bottom 96 well plates. An antibody-only, gp140 only, cells only and substrate only control was performed on each plate. An equal volume of gp140 was added to each well and plates were incubated for 1 h at 37 (5% CO_2). ADCC effector cells were thawed, added to 3.6 mL of ADCC assay medium and an equal volume of cells was added to each well. Plates were incubated for 6 h, left at room temperature for 20 min before adding Bio-Glo Luciferase Substrate (Promega, USA). After 5 min luminescence was measured using a GloMax. Changes in ADCC activation were expressed as fold of induction.

2.1.5.9 *In vivo* half-life studies

For *in vivo* half-life studies 7-9 week old hFcRn transgenic mice (B6.Cg-*Fcgrt*^{tm1Dcr} Tg(CAG-FCGRT)276Dcr/DcrJ, Jackson Laboratory, USA) were used. Mice were weighed two days prior to IV injection. BNAbs were injected intravenously via the tail vein at a dose of 2mg/kg. PBS was injected as negative control. Blood samples of 50 µL were taken from the tail or saphenous vein on days 1, 4, 6, 8. Mice were sacrificed on Day 11 and a final blood sample by cardiac puncture was taken.

Blood samples were processed immediately. To enhance clotting, samples were incubated for 1 h at 37 °C and then transferred to 4 °C overnight. Samples were centrifuged (Heraeus fresco 17, Thermo Scientific) at 6200 g for 20 min to separate the serum from red blood cells. Serum was transferred into a new tube and frozen at -20 °C. Analysis of bNAb present in serum was performed by an α-hIgG ELISA (2.1.5.7).

2.1.5.10 Murine IgM anti-human IgG ELISA

A murine IgM anti-human IgG ELISA was used to determine immunogenicity of the bNAbs *in vivo*. 96 flat-bottom well immunosorbent plates were coated with 5 µg/mL human IgG1 λ (Sigma Aldrich, USA) in PBS 7.4 and incubated overnight at 4 °C. All blocking and washing steps were performed as described in 2.1.5.7. Serum was applied in a 1 in 100 dilution in duplicates and further diluted 1:1 using blocking buffer. Plates were incubated overnight at 4 °C. After washing, an anti-murine IgM antibody (1 in 1000) in blocking buffer was applied and plates were incubated for 1 h at 37 °C. For detection 100 µL of SIGMA*FAST*™ OPD (Sigma Aldrich, USA) were added to each well. A_{492} was measured using a Tecan Sunrise plate reader.

2.2 Generation of a stable ΔF *N. tabacum* plant line

2.2.1 Construction of sgRNA-Cas9 vectors

2.2.1.1 Design of sgRNAs

5 mRNA sequences of *FucT* were found and retrieved from Genbank (Table 2-2) using *N. benthamiana* equivalents as templates. The sequences were aligned using Clustal Omega (http://www.clustal.org/omega/) and protospacer elements were designed using the criteria $GN_{20}GG$ (beginning with 'G' for U6 promoters) and confirmed using the online tool CRISPR-P (Lei *et al.*, 2014). sgRNAs were designed to cut within the fucosyltransferase (*FucT*) gene of *N. tabacum* c.v. SR1. Twelve different protospacer elements were chosen (Appendix). All protospacer elements target regions around the first 1000bp of the fucosyltransferase gene. Specific primers with the respective 20 bp sequence and a short overlap sequence to pUC119-gRNA (Addgene ID 52255; (Li *et al.*, 2013)) were designed and used to construct each sgRNA (Appendix).

Table 2-2: Accession numbers of aligned mRNA sequences of N. tabacum FucT given with label used throughout the study and the cultivar they were obtained from.

Accession number	Label	Cultivar
NM_001324945.1	*FucT* 1	TN90
XM_016585847.1	*FucT* 3	
XM_016657530.1	*FucT* 4	
XM_016620229.1	*FucT* 5	
AB498916.1	*FucT* 2	Bright Yellow

2.2.1.2 Phusion PCR for sgRNA construction

To construct the sgRNA DNA, a two-step Phusion PCR was carried out (Li *et al.*, 2013). In the first step, two separate PCRs using a combination of a universal (forward/reverse) with a specific (reverse/forward) primer were performed. The vector pUC119-gRNA (Addgene ID 52255; J. F. Li et al. 2013) was used as template. For the second step, 50 ng of the purified PCR products from step 1 were combined in a 1:1 ratio and used as templates. The full-length sgRNA was amplified using both universal primers. A 1% agarose gel to verify the presence of the expected band was run after each PCR step. PCR products were purified using QIAquick PCR purification Kit (QIAGEN, Germany).

Table 2-3: PCR program for Phusion PCR to generate sgRNA

Step	Cycles	First step	Second step
Initial Denaturation		98 °C, 30 s	
Denaturation	30	98 °C, 10 s	
Annealing		50 °C, 20 s	53 °C, 20 s
Extension		72 °C, 60 s	
Final extension		72 °C, 10 min	

2.2.1.3 Cloning of sgRNAs

The vector pFGC-pcoCas9 (Addgene ID 52256; Li et al., 2013) and the purified PCR products were digested with SbfI (10000 U/ml, New England Biolabs, USA) or AscI (10000 U/ml, New England Biolabs, USA) and PacI (10000 U/ml, New England Biolabs, USA) with CutSmart buffer (New England Biolabs, USA). The successful digest of the vector and inserts was verified using agarose gel electrophoresis. The ends of the digested vector were dephosphorylated by adding 1 µL of Antarctic phosphatase (5000 U/ml, New England Biolabs, USA) and 3.3 µl of Antarctic phosphatase reaction buffer (10 x, New England Biolabs, USA) to the reaction. Incubation was carried out for 30 min at 37 °C, followed by an inactivation step for 25 min at 80 °C.

100 ng of the digested vector were combined with 150 ng of sgRNA insert, 2 µL of T4 ligation buffer (10 x with 10 mM ATP, New England Biolabs, USA), 1.5 µL of T4 ligase (400000 U/ml, New England Biolabs, USA) and the volume was adjusted with dH_2O to 20 µL. Samples were incubated for 2 hours at 16 °C.

Chemically competent DH5α cells (Invitrogen, USA) were transformed according to the manufacturer's instructions. After heat shock, 450 µL of SOC medium (Invitrogen, USA) were added and regeneration was performed at 37 °C and 225 rpm. After one hour, 50 µL of the suspension were spread onto LB plates with appropriate antibiotics and incubated at 37 °C overnight.

Selected colonies were grown overnight at 37 °C and 225 rpm in LB with appropriate antibiotics. A mini-prep was performed using QIAprep Spin Miniprep Kit (QIAGEN, Germany) following the manufacturer's protocol. DNA was eluted using 40 µL of EB buffer (QIAGEN, Germany) and a diagnostic digest with appropriate restriction enzymes was performed. Selected DNA samples were sequenced (Genewiz, UK) using primers flanking the region of interest.

2.2.1.4 Cloning of tRNA-gRNA constructs

A DNA string containing the 5 chosen sgRNAs separated by a tRNA sequence was synthesised by GeneArt (ThermoFisher Scientific, USA). The string was cloned into the pCR-BluntII-TOPO vector (ThermoFisher Scientific, USA) following the manufacture's protocol. Colonies were screened for successful integration of the string via PCR with M13 f and rev primers. The U6 promoter was cloned into pUC119 and strings were cloned into pUC119-U6 using GoldenGate Assembly with BsaI (parameters as in 2.1.2). Positive colonies were screened for complete assembly using M13 f and rev primers. The plasmid was digested with AscI and PacI and the insert cloned into pFGC-pcoCas9 as described in 2.2.1.3.

2.2.2 Transformation of *A. tumefaciens* by electroporation

Electrocompetent *A. tumefaciens* GV3101/PMP (RK) cells were thawed on ice and 15 µL were mixed with 1 µL of plasmid and incubated on ice for 5 min. An electric pulse (1.8 kV and 25 Ω, Gene Pulser II BIO-RAD, USA) was applied. The sample was immediately pipetted into 1 mL of YM broth and allowed to regenerate for 2 h at 28 °C and 220 rpm. 50 µL of the suspension were streaked onto YM plates containing the selective marker and incubated for 2 days at 28 °C.

2.2.3 Agrobacterium transformation of *N. tabacum* plants using syringe infiltration

For each gene construct, 10 mL of LB with appropriate antibiotics were inoculated with *A. tumefaciens* carrying the desired plasmid and grown overnight at 28 °C and 220 rpm. After incubation, the OD_{600} was measured with a spectrophotometer (Jenway Genova) and the suspension was then centrifuged for 10 min at 4667 g rpm at RT. The pellet was re-suspended in the calculated amount of infiltration buffer (10mM MES, 10mM $MgCl_2$, pH5.6) to obtain an OD_{600} of 0.5. The suspension was infiltrated into the abaxial surface of wild-type *N. tabacum* leaves. The plants were kept in a temperature regulated room and leaves were harvested 2 days post infiltration (dpi).

2.2.4 Plant DNA extraction

DNA extraction was performed after freezing harvested leaves using liquid nitrogen, by mechanically disrupting using a pestle and mortar and then using the DNeasy Plant Mini Kit (QIAGEN, Germany) as per the manufacturer's instructions.

2.2.5 IDAA (Indel Detection Amplicon Analysis)

IDAA was performed as described by Yang et al. (2015). Briefly, DNA extracted from leaves infiltrated with different pFGC-pcoCas9-sgRNA, as well as non-infiltrated wild-type controls, was used as template. Gene-specific primers flanking 100-250bp regions of the fucosyltransferase gene targeted by the designated sgRNAs were used (Appendix). The gene-specific forward primers were designed with 5' sequences that overlap with an additional third 6-FAM forward primer (Appendix). The 6-FAM primer had a 5' 6-FAM tag and 3' sequence overlap with the gene-specific primers. After addition of nuclease-free distilled water and 2 µL of DNA, the following final concentrations were obtained: 1x Q5 Reaction buffer (New England Biolabs, USA), 0.24 mM dNTPs (New England Biolabs, USA) , 0.5 µM 6-FAM primer, 0.1 µM forward primer, 1 µM reverse primer, 0.04 U/µL Q5 High-Fidelity DNA Polymerase (New England Biolabs, USA). The reaction was carried out in Mastercycler Nexus Gradient with the program given in Table 2-4.

Table 2-4: PCR program for generation of amplicons for IDAA

Cycle number	Denaturation	Annealing	Extension
1	95 °C, 5 min		
2-16	95 °C, 30 s	72 -58 °C touchdown -1°C /cycle, 30 s	72 °C, 30 s
17-40	95 °C, 30 s	T_a of primer pair	72 °C, 30 s
41			72 °C, 20 min

The products obtained from IDAA PCR were purified using QIAquick PCR purification Kit (QIAGEN, Germany) and DNA concentration was measured using Nanodrop 2000 (ThermoFisher Scientific, UK). The samples (15 µL a 50 ng/µL) were sent to Eurofins Genomics for fragment length analysis.

2.2.6 Stable Agrobacterium-mediated transformation of *N. tabacum*

N. tabacum SR1 seeds were sterilised using 70% Ethanol with 0.01% Tween 20, followed by a wash with absolute Ethanol. Sterilised seeds were germinated on MS Agar under constant light at 22 °C. Plantlets were transferred onto MS Agar in sterile glass jars and cultured under the same conditions. Leaf discs were obtained from 4-6-week-old plants grown *in vitro* and incubated in 10 mL *Agrobacterium tumefaciens* suspension (prepared as described in 2.2.3) containing 200 µM acetosyringone for 20 min at RT. For removal of excess bacterial suspension, inoculated leaf discs were transferred to sterile Whatman filter paper. Leaf discs were co-cultivated on shoot regeneration medium (without antibiotics) for 48 h. Explants were then transferred onto shoot regeneration medium containing 200 µg/mL timentin (Melford). Leaf discs were transferred onto fresh shoot regeneration medium with timentin every two weeks until shoots appeared. Each shoot was transferred into a separate glass jar and grown on MS Agar with timentin for another 3-4 weeks. Plantlets with roots were transplanted onto soil and grown at 28 °C under a light cycle (16h on/8h off).

2.2.6.1 Establishing the T_1 and T_2 generation

For obtaining theT_1 generation, flowering plants of T_0 were self-crossed. Seeds were collected, sterilised as described in 2.2.6 and germinated on MS Agar containing 3 µg/mL PESTANAL (Glufosinate-ammonium) as selection. Single plantlets were transferred onto fresh selection medium and grown for 2 weeks before transplanting them onto soil.

To generate the T_2 generation, selected lines from T_1 were cross and self-fertilised. Seeds were germinated on soil without selection and transplanted after 2 weeks. For all lines, analysis was performed using leaves of about 4-week old plants.

2.2.7 Analysis of putative ΔF *N. tabacum* plant lines

2.2.7.1 Analysis on protein expression level

2.2.7.1.1 Anti-fucose dot-blot

Proteins were extracted from two leaf discs in 300 µL PBS (pH 7.4) by disrupting the cell membrane using beads and a mill (Retsch MM400). Samples were centrifuged (VWR MIcroStar 17R) at 16200 g and 4 °C for 15 min. The crude extract was transferred into a new tube and used for further analysis.

2 µL of each sample, a positive (ΔXF *Nicotiana benthamiana*) and negative (*Nicotiana tabacum* wild-type) control were pipetted onto a nitrocellulose membrane (Amersham, GE Healthcare, UK). After letting the membrane completely dry, the membrane was blocked, primary and secondary antibody applied as described in 2.1.5.2.

2.2.7.1.2 Anti-fucose western blot with standardised total protein concentration

Total protein concentration of each crude extract sample was determined using Pierce BCA Protein Assay Kit (ThermoFisher Scientific, USA) following the microplate protocol. Absorbance was measured at 562nm using a Tecan (Infinte F200 Pro) plate reader. Total protein concentration was calculated using the standard curve.

Samples were prepared in NuPAGE LDS sample buffer to contain the same amount of total protein and heated for 10 min at 95 °C. 5 µg or 500 ng were loaded onto a NuPAGE 4-12% Bis-Tris gel for SDS-PAGE or western blot respectively. SDS PAGE and western blot were performed as described in 2.1.5.1 and 2.1.5.2.

2.2.7.2 Genetic analysis

DNA for genetic screening of putative knockout plants was extracted using *REDExtract*-N-Amp Tissue PCR Kit (Sigma Aldrich, USA) following the manufacture's protocol.

For amplification of regions of interest, the same primers as for IDAA were used together with Phusion High-Fidelity Polymerase (New England Biolabs, USA). PCR was performed according to manufacturer's instructions using the program described in 2.2.1.2 with a 60 s annealing step at the T_a of the respective primer pairs. A 1% agarose gel was run to verify the presence of the expected band. PCR products were purified using QIAquick PCR purification Kit (QIAGEN, Germany) and sent for sequencing (Genewiz, UK). The obtained sequencing chromatograms were analysed using ICE Analysis (Synthego) to determine the ICE (indel percentage) and KO (knockout) score of each putative knockout line.

2.2.7.3 Glycoanalysis by Liquid Chromatography Mass Spectrometry (LC-MS)

Prior to loading the samples onto the column, samples were S-alkylated and digested in solution as follows:

An equal volume of 15 mM DTT dissolved in 8M Urea buffer (in 100 mM ammonium bicarbonate buffer) was added to the antibody samples and the mixture incubated at 56 °C with shaking. After 45 min, 1/3 of total final volume of 55 mM iodoacetamide (dissolved in 100 mM ammonium bicarbonate buffer) was added to the reduced samples and incubated at RT for 30 min in darkness. Four volumes of ice-cold acetone were added and samples were kept at -20 °C for an hour. The suspension was centrifuged at 13000 rpm for 5 min, the supernatant discarded and the pellet dried using a speed-vac. The dried pellet was then dissolved in 20 µL of 100 mM ammonium bicarbonate buffer and 5 µl of trypsin were added. The digest was incubated overnight at 37 °C.

For the GluC digest, 4 µL of GluC were added to the previously trypsin digested samples and incubated overnight at 37 °C.

Digested samples were loaded onto a C18 column (BioBasic-18, 150 x 0.32 mm, 5 µm, Thermo Scientific) with 80 mM ammonium formiate buffer as aqueous solvent. Elution was performed at a flow rate of 6 µL/min and by applying a gradient from 5% to 40% B (B: 80% ACCN) in 25 min, followed by a 5 min gradient from 40% to 95% B to facilitate the elution of large peptides. A QTOF MS (Bruker maxis 4G) with a standard ESI source in positive ionisation), DDA (data-dependent acquisition) mode was used for detection. MS scans between 150-2200 Da were recorded and the three highest peaks selected for fragmentation. Calibration of the instrument was performed using ESI calibration mixture (Agilent).

For manual glycopeptide annotation of obtained MS spectra DataAnalysis 4.0 (Bruker) was used. For quantification of the various glycoforms, peak areas of EICs of the first four isotopic peaks were added up, using Quant Analysis (Bruker) as software.

2.3 Statistical Analysis

Statistical data analysis was performed using GraphPad Prism version 8.0.2. Appropriate statistical tests were chosen for each individual experiment. The applied statistical method is indicated in the figure legends of the respective analysed data.

3 Expression and *in vitro* characterisation of variants of the anti-HIV bNAb 10-1074

3.1 Introduction

This chapter focuses on the expression and *in vitro* characterisation (yield, glycosylation, neutralisation potency) of the broadly neutralising antibody 10-1074 with and without YTE or LS mutations in the Fc-region, using *Nicotiana benthamiana* ΔXF as the expression platform.

The neonatal receptor (FcRn) is responsible for the comparatively long half-life of IgG (approx.21 days) in humans, by selectively binding to IgG and rescuing it from degradation (Petkova *et al.*, 2006). Shields et al. (2001) performed an extensive study to determine the most important amino acid residues in the IgG Fc region for effective binding to the neonatal receptor (FcRn), by alanine scanning of the C_H2 and C_H3 domains. This study revealed not only that I253, S254, H435 and Y436 are essential for binding to the FcRn but also that the mutation of specific residues rendered better binding variants (Shields *et al.*, 2001). Introduction of random mutations at and close to these key residues resulted in the discovery of Fc variants with higher affinity to the FcRn at pH 6.0. Two variants performed especially well – those with YTE (M252Y/S254T/T256E) (Acqua *et al.*, 2002) and LS (M428L/N434S) (Zalevsky *et al.*, 2010) mutations. The introduction of the YTE mutation into the Fc region of a humanized anti-respiratory syncytial virus (RSV) monoclonal antibody (MEDI-524) resulted in a 10-fold increase in binding to both cynomolgus monkey and human FcRn at pH 6.0, and a 4-fold increase in serum half-life in cynomolgus monkeys (Acqua *et al.*, 2002). On the other hand, the LS mutation resulted in an 11-fold improvement of binding to hFcRn and a 3 fold increase in serum half-life in cynomolgus monkeys of bevacizumab (cancer drug) (Zalevsky *et al.*, 2010). Furthermore, Ko et al. (2014) showed that VRC01 with LS mutation has a 3-fold longer serum half-life than non-mutated VRC01 in macaques (Ko *et al.*, 2014). A clinical phase I trial with VRC01LS in healthy adults revealed that serum half-life was extended by more than 4-fold (Gaudinski *et al.*, 2018). Anti-HIV bNAbs with half-life extending mutations are currently investigated in several phase I clinical trials (e.g. NCT04250636, NCT03254277) to determine safety and pharmacokinetics. To this

date, no mAb with half-life extending mutations has entered the market, however, it can be expected that this will change in the foreseeable future.

3.2 Specific objectives

- Engineer and clone bNAb 10-1074 light chain, heavy chain and YTE and LS mutants of the heavy chain
- determine the expression level of all 10-1074 variants in ΔXF *N. benthamiana*
- purification of the generated antibodies
- establish the purity and quality of the expressed antibodies
- glycoanalysis of generated bNAbs
- determine any impact of the expression system or half-life modifying mutations on antigen binding, neutralisation breadth and potency

3.3 Contributions

- Site-directed mutagenesis to introduce the YTE and LS mutation into the pDONR was performed by Dr Audrey Teh
- Cloning of the 10-1074 variable region into non-mutated pDONR and mutated pDONR and cloning of these into the MIDAS system was performed by Dr Audrey Teh, however re-cloning of 10-1074 LS was performed by me
- Glycoanalysis by mass spectrometry of 10-1074 HC and 10-1074 YTE was performed by Dr Clemens Grünwald-Gruber at BOKU Vienna

3.4 Results

3.4.1 Cloning of heavy and light chain into the plant expression vector pTrak.6

The genes for broadly neutralising antibody (bNAb) 10-1074 in its native form, as well as in two variations, carrying either the heavy chain mutation YTE (M252Y/S254T/T256E)(Acqua *et al.*, 2002) or LS (M428L/N434S)(Zalevsky *et al.*, 2010) were cloned. The three versions differed only in the heavy chain sequence and were named HC, YTE and LS accordingly (cloning of 10-1074 HC and YTE was performed by Dr Audrey The). To introduce the YTE or LS mutation into pDONR carrying the constant region of the heavy chain, site-directed mutagenesis was applied. The MIDAS (Modular Idempotent DNA assembly) system (Figure 3-1) was used to express the bNAb light and heavy chains in one construct. The heavy (V_H) and the light variable region (V_L) were first synthesised and cloned into the scaffold vector pDONR containing the human IgG γ with or without modification (for the heavy chains) or IgG λ (for 10-1074) constant regions. The complete heavy chain was cloned into separate pWhite vectors while the light chain was cloned into pBlue. Blue-white screening was used as initial indicator of successful cloning and was further confirmed by restriction enzyme digestion.

From all the clones that showed the correct restriction profile, one for each gene was chosen to assemble the respective heavy chain and light chain into pTrak.6. To that end, pWhite was digested with BsaI and the heavy chain gene was cloned into pTrak.6, yielding HC:pTrak.6 using Golden Gate Assembly (Engler, Kandzia and Marillonnet, 2008). Successful cloning was again verified by restriction digest with NcoI and XbaI. Next, the light chain was cloned into HC:pTrak.6 using BsmBI and Golden Gate cloning . Clones that showed the correct restriction profile were sequenced with appropriate primers to confirm the expected sequences (not shown).

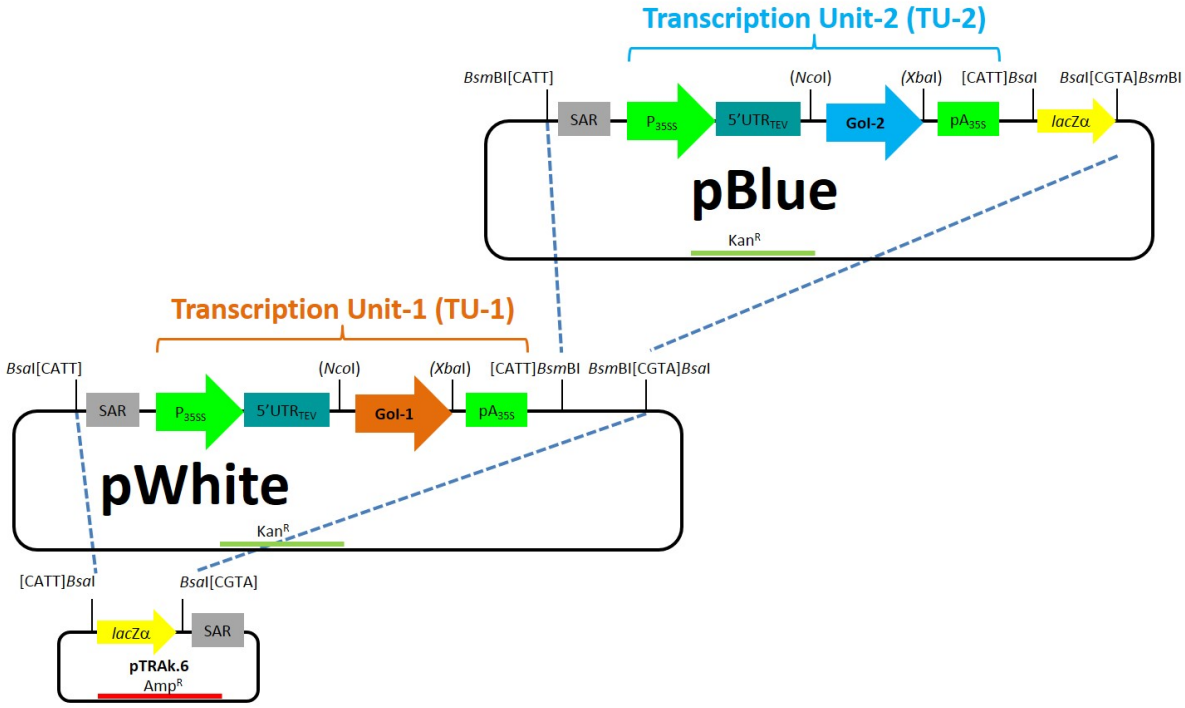

Figure 3-1: The Modular Idempotent DNA assembly (MIDAS) system. The genes of interest are initially cloned into pWhite or pBlue respectively, to form transcription unit 1 and 2. pWhite (GOI-1 = Heavy chain) and pTrak.6 are digested with BsaI. The transcription unit of pWhite (TU-1) replaces the lacZ gene of pTrak.6, thus positive transformants are white (HC:pTrak.6) in the presence of XGal and IPTG. In the second step pBlue (GOI-2 = Light chain) and HC:pTrak.6 are digested with BsmBI and the transcription unit of pBlue (TU-2) is cloned into HC:pTrak.6 after the TU-1. pBlue carries a lacZ gene, thus positive transformants are blue in the presence of XGal and IPTG.

3.4.2 bNAbs 10-1074 can be expressed in ΔXF *N. benthamiana*

The three plasmids 10-1074 HCLC:pTrak.6, YTELC:pTrak.6 and LSLC:pTrak.6 were transformed into *Agrobacterium tumefaciens* strain GV3101/PMPRK.

After confirming correct expression by syringe infiltrating 2-3 leaves in ΔXF *N. benthamiana*, a batch of antibodies were produced by vacuum infiltrating 20-25 ΔXF *N. benthamiana* plants and harvesting the leaves 6 days post infiltration (dpi). The antibodies were extracted from the leaves, by homogenising leaves with PBS (pH 7.4) and the clarified plant extract was purified using a Protein A column. IgG-containing fractions were dialysed into PBS and concentrated.

Crude extract yields for each 10-1074 variant were determined using an anti-IgG ELISA with technical duplicates (Table 3-1). Frozen crude extract samples from batch 1 to 3 were used for 10-

1074 YTE and from batch 1 and 2 for 10-1074 HC. For LS no frozen crude extract samples were available, therefore, additional batches of 10-1074 LS were produced by infiltrating three plants per batch and extracting 6 dpi. The expression levels of 10-1074 LS are about 15 times lower than the expression levels of both 10-1074 HC and 10-1074 YTE.

Table 3-1: Crude extract yield for 10-1074 HC, YTE and LS ΔXF in mg/kg $_{\text{fresh weight}}$

	Yield [mg/kg$_{\text{fresh weight}}$]		
Batch	**10-1074 HC ΔXF**	**10-1074 YTE ΔXF**	**10-1074 LS ΔXF**
1	47.79	74.33	3.24
2	40.26	26.74	3.02
3	not determined	42.06	3.24
av ± SD	**44.03 ± 5.32**	**47.71 ± 24.29**	**3.16 ± 0.13**

Post-purification yields for 10-1074 (given in Table 3-2) from three independent batches were calculated using the fresh weight of extracted leaves, the volume and concentration (measured with BIAcore) obtained after purification prior to sterile filtration. A limitation of this approach is that the resulting concentration may include not only fully assembled antibodies but also Fc fragments.

Table 3-2: Yield for each batch of 10-1074 HC, YTE and LS in mg/kg $_{\textit{fresh weight}}$ prior to sterile-filtration

	Yield [mg/kg$_{\text{fresh weight}}$]		
Batch	**10-1074 HC ΔXF**	**10-1074 YTE ΔXF**	**10-1074 LS ΔXF**
1	11.40	7.89	Not detected
2	17.65	14.48	Not detected
3	10.75	5.22	Not detected
av ± SD	**13.3 ± 3.1**	**9.2 ±3.9**	Not detected

The purification steps further reduced the yield of 10-1074 LS to almost undetectable concentrations. Even after re-cloning twice and expressing the re-cloned constructs in ΔXF *N. benthamiana,* only minimal yields could be achieved after purification. Anti-gamma (HC) western blot analysis of the crude extract, flow-through and specific elution fractions confirmed expression of the heavy chain, which can be seen in the elution fractions (Figure 3-2). To confirm that the light chain was also expressed, an additional anti-lambda western blot was performed, which verified its presence.

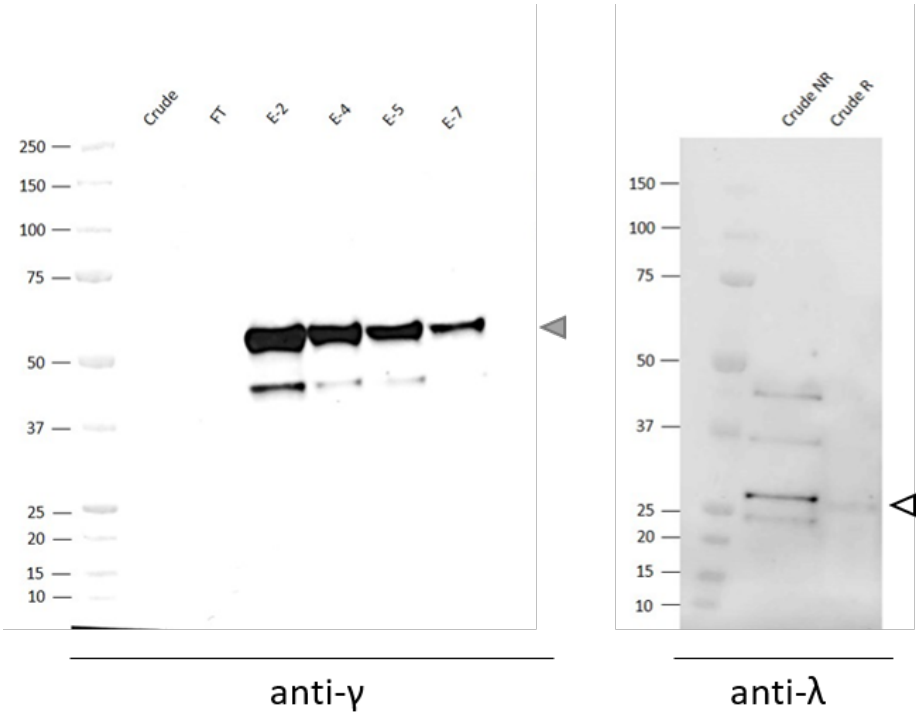

Figure 3-2: Western blot to verify the expression of 10-1074 LS. The anti-γ chain western blot with reduced samples confirmed the presence of 10-1074 LS (grey triangle) in the four displayed elution fractions (E). The anti-λ western blot of the crude extract in non-reduced (NR) and reduced (R) condition verifies the presence of the light chain (white triangle).

An aim of this project is to identify the best version of each bNAb to include in an affordable antibody cocktail, the LS variation of 10-1074 was excluded.

3.4.3 Yield of 10-1074 produced in ΔXF plants can be improved by addition of Tween80

Intravenous administration of bNAbs requires sterility of the product. Sterile filtration (0.45 µm filter) of 10-1074 YTE obtained from the first three batches resulted in significant loss of product, however, the loss of product when filtering 10-1074 HC was considerably less (not shown). This suggests that the YTE mutation might increase aggregation compared to the native bNAb. To counteract aggregation, 0.01% Tween80 was added to the extraction buffer (PBS pH 7.4), after elution from the affinity column and during concentration steps. Addition of Tween80 not only reduced the loss of product during the final filter sterilisation step to only 2%, but also resulted in an improvement in yield (Table 3-3).

Table 3-3: Yield for 10-1074 HC, YTE in mg/kg $_{fresh\ weight}$ with addition of 0.01 % Tween80 post sterile-filtration

	Yield [mg/kg$_{\text{fresh weight}}$]	
Batch	**10-1074 HC ΔXF**	**10-1074 YTE ΔXF**
4	57.8	12.8
5	36.2	12.5
av ± SD	**47.0 ± 10.8**	**12.6 ± 0.15**

While the addition of Tween80 improved the post-purification yield of 10-1074 HC by 3.5 times, the yield of 10-1074 YTE was merely stabilised.

3.4.4 10-1074 bNAbs generated in ΔXF *N. benthamiana* are fully assembled

The quality and integrity of each batch of 10-1074 antibodies were characterised by SDS-PAGE and western blot. In both cases, concentrations obtained from A280 nm measurements were used to calculate the amount loaded onto the gel. SDS-PAGE was performed with 1 µg of non-reduced and reduced samples in order to determine the purity of the obtained product and to identify possible degradation events. Figure 3-3 A shows a representative SDS PAGE. All of the non-

reduced (NR) samples display a band just above 150 kDa, which is the expected size for the fully assembled antibodies. Both, the plant produced antibodies, and the control (IgG1 λ) show bands below 150 kDa. These are commonly seen in antibody expressing plants (Hehle *et al.*, 2015)and have been shown to be degradation products. The reduced samples (R) clearly show the heavy chain slightly above 50 kDa. A band at about 40 kDa could be observed for the native (HC) and modified (YTE) 10-1074, but not for the control. This suggests a plant-based degradation event; however, the majority of the heavy chain seems to be intact. The bands at 25 kDa match the expected size of the light chain for 10-1074. Interestingly, the light chain of the monoclonal antibody control is slightly above 25 kDa, which could be a result of light chain glycosylation.

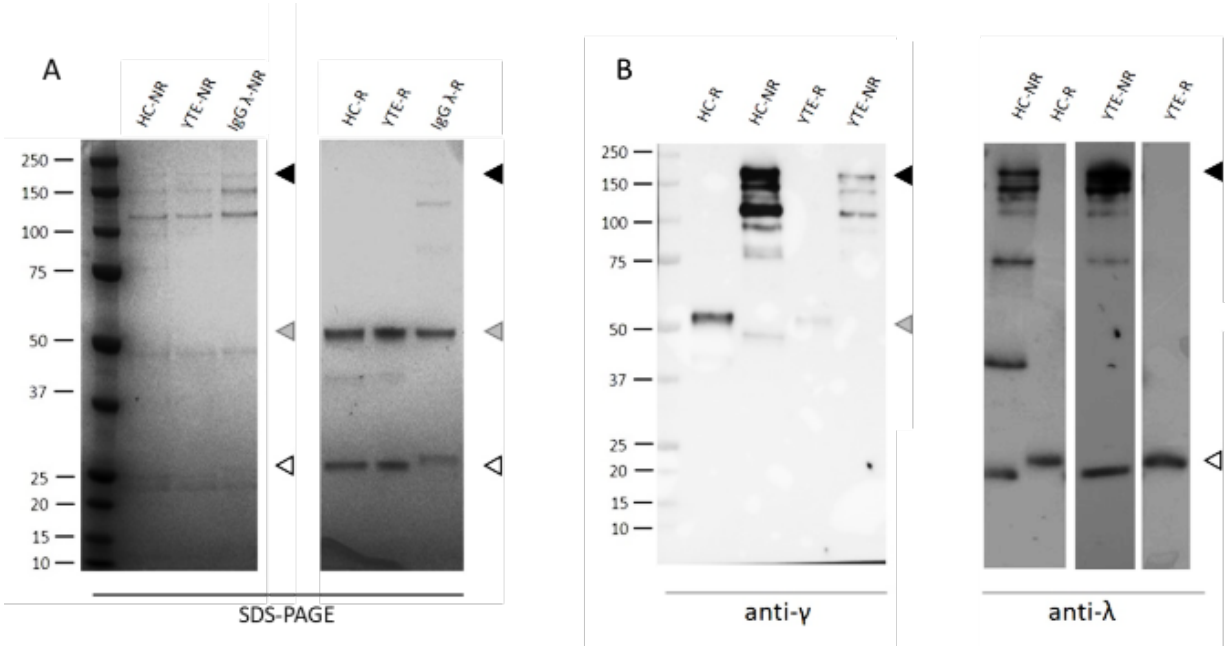

Figure 3-3: A) Representative SDS PAGE with native 10-1074 (HC), 10-1074 YTE (YTE) and a mAb IgG λ control. The fully assembled antibody is indicated by a black triangle. The reduced (R) samples show the single γ-heavy and λ-light chains. The heavy chain is indicated by a grey triangle. The light chain is indicated by a white triangle. B) Representative western blot to verify the integrity of the produced antibodies. The anti-γ western blot to visualise the heavy chain. Fully assembled antibodies are indicated by a black triangle. Heavy chains are marked with a grey triangle. Anti-λ western blot visualises the light chain. Fully assembled antibodies are indicated by a black triangle. Light chains are marked with a white triangle.

To verify the identity of the bands, western blots with anti-γ (against human IgG heavy chain) and anti-λ (against human IgG light chain) antisera were performed. A non-reduced and reduced sample of 50 ng of each antibody were run simultaneously. Representative western blots

are shown in Figure 3-3 B. In the anti-γ western blot (Figure 3-3 B, left), the band above 150 kDa in the non-reduced samples verifies that fully assembled antibody is present in the purified sample. For reduced samples, a band slightly above 50 kDa is visible, which is consistent with the size of a single IgG heavy chain. In the anti-λ western blot (Figure 3-3 B, right), the non-reduced samples clearly exhibit the same major band at 150 kDa, again validating the presence of a fully assembled antibody. The band for a single λ- light chain can be observed at 25 kDa for reduced samples. These western blots confirm that the bands seen on SDS PAGE (Figure 3-3 A) do not come from impurities but can solely be attributed to the generated antibodies and possible degradation products. No additional chromatography steps were employed to reduce the level of degradation products, as the occurrence of fully assembled antibody to degradation products is similar between the native and modified variant. The level of fully assembled antibody was considered sufficient for subsequent characterisation.

3.4.5 ΔXF *N. benthamiana* yields bNAbs lacking α1,3-fucose and β1,2-xylose glycans

In order to generate antibodies lacking α1,3-fucose and β1,2-xylose glycans a ΔXF *N. benthamiana* plant line was used. The fucosyl- and xylosyltransferase genes were silenced by RNAi in the ΔXF plant line (Strasser *et al.*, 2008) used to produce the presented bNAbs. To confirm the absence of these two plant-related sugars, a PNGase F digest (see Figure 3-4) followed by an SDS PAGE and an anti-lectin western blot were performed. Furthermore, a representative sample of 10-1074 HC and YTE was sent for MS glycoanalysis, to obtain information about the distribution of glycoforms.

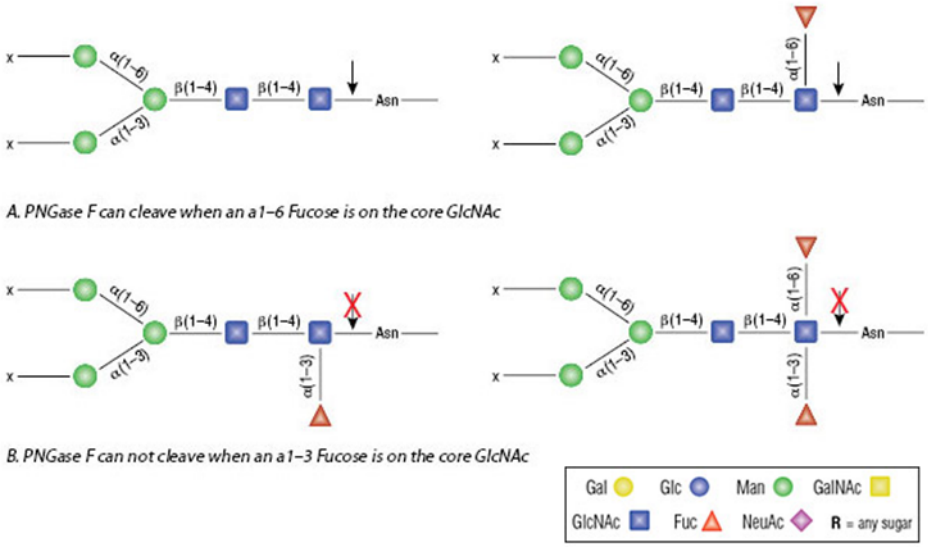

Figure 3-4: Rationale of a PNGase F digest. PNGase F cleaves the bond between the asparagine and the first core GlcNAc, as long as there is no α1,3 fucose on it.An α1,6-fucose stills allows digestion. Therefore, a shift in band size of the heavy chain compared to the non-digested antibodies should be observed on a SDS-PAGE in case of afucosylated antibodies.

Figure 3-5 shows a representative PNGase F digest followed by SDS PAGE. A clear size shift (black triangle) for the digested (P) heavy chain compared to the non-digested (NP) control can be observed for all the samples, including the IgG control. This verifies that the heavy chains are glycosylated and suggests α1,3-fucose is absent on the core GlcNAc. There was no shift in the light chain due to lack of glycosylation sites.

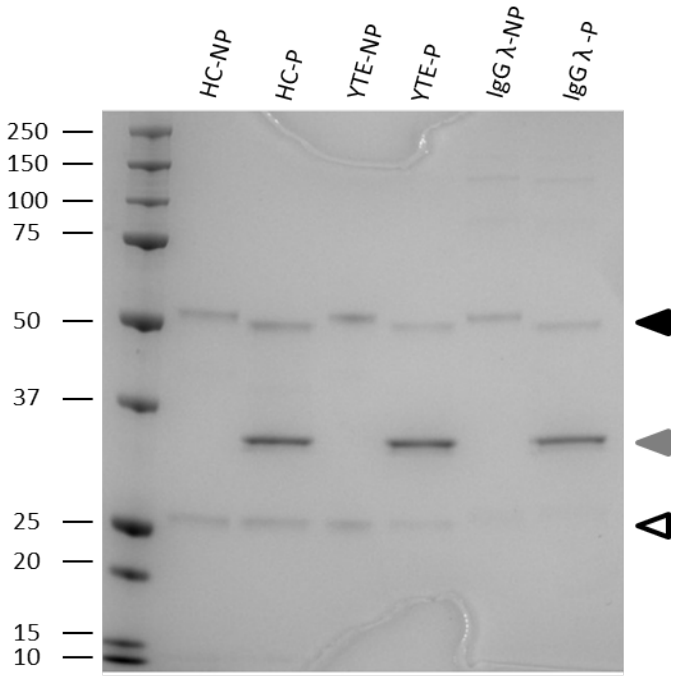

Figure 3-5: Representative SDS-PAGE analysis of the PNGase F digest (P) with non-digested control (NP). mAb IgG λ served as positive control. Band size shift in the heavy chains is marked with a black triangle. PNgase is indicated by a grey and the light chain by a white triangle.

To further validate that neither fucose nor xylose is present in the plant-generated antibodies, a western blot was performed, using an anti-lectin antibody that binds to xylose and/or fucose on plant glycoproteins (Figure 3-6).

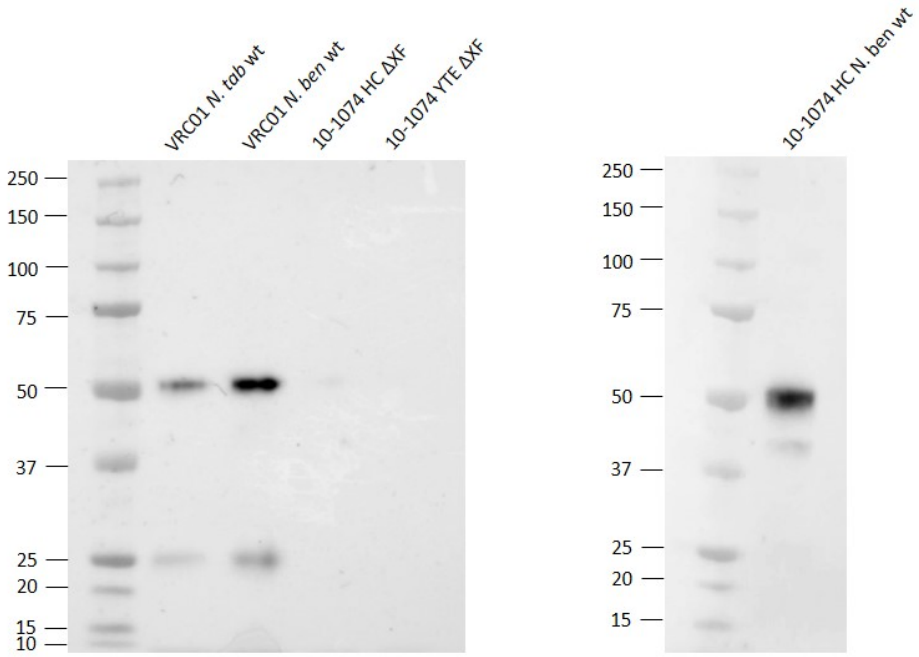

Figure 3-6: Representative Anti-glycan western blot with 10-1074 produced in ΔXF N. benthamiana and two positive controls; VRC01 produced in wild-type N. tabacum (N. tab wt) and N. benthamiana (N. ben wt) (left). Anti-glycan western blot with 10-1074 produced in wild-type N. benthamiana.

bNAb VRC01 produced in wild-type *N. tabacum* (*N. tab* wt) and wild-type *N. benthamiana* (*N. ben* wt) were used as positive controls. Additionally, a western blot with 10-1074 expressed in wild-type *N. benthamiana* was performed demonstrating 10-1074 HC glycosylation. Both positive controls show clear bands at 50 kDa (heavy chain) and 25 kDa (light chain), as VRC01 is an antibody that has glycosylation sites in both the heavy and light chain. This confirms that neither xylose nor fucose was present in those samples. It has to be noted that for 10-1074 HC, a faint band at 50 kDa is visible, which could also be observed (for both, HC or YTE) in the other batches. The most likely explanation is that RNAi is not 100 percent efficient, thus low-level expression of either glycosyltransferase is still possible.

Glycoform percentage was determined using LC-ESI-MS (incl. analysis performed by Clemens Grünwald-Gruber at BOKU, Vienna) (Table 3-4). For quantification peak areas of the first four isotopic peaks of extracted ion chromatograms (EICs) were added up using Quant Analysis (Bruker) as software. MS analysis shows that although the majority of the respective bNAb is afucosylated (GnGn: 78-82%), 1-2 % of GnGnF glycoform is present (Table 3-4). This is consistent with the results of the lectin western blot and low-level expression of α1,3-fucosyltransferase in the used ΔXF *N. benthamiana* plant line. Furthermore, the analysis reveals that up to 15 % of the respective bNAb is aglycosylated.

Table 3-4: Glycoform percentage in representative 10-1074 HC ΔXF and YTE ΔXF sample respectively

	10-1074_HC ΔXF	**10-1074_YTE ΔXF**
not glyc	15.42	11.63
Man5		
Man7		
Man8		
Man9		
GnM	4.75	4.89
GnGn	78.49	81.75
GnGnF	1.34	1.73

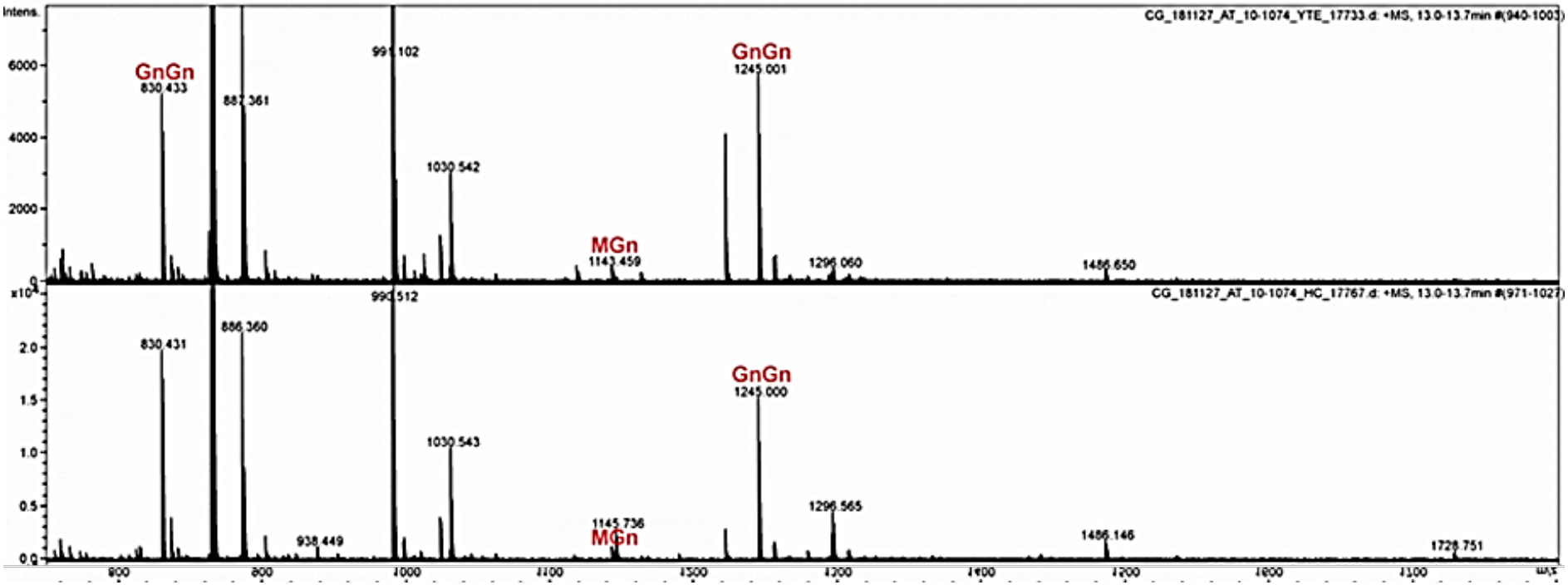

Figure 3-7: Mass spectrum for 10-1074 HC ΔXF (bottom) and YTE ΔXF (top) obtained using LS-ESI-MS.

3.4.6 Plant-produced 10-1074 show high affinity to HIV-1 gp140

High binding affinity to the HIV-1 envelope glycoprotein is essential for any HIV neutralising antibody. Gp140 (which contains the external domains of HIV-1, i.e. gp120 and gp41 ectodomain) was used for analysis. Binding of the antibodies to UG37 gp140 was determined using Surface Plasmon Resonance (SPR) with the strategy shown in Figure 3-8. UG37 gp140 is a recombinant uncleaved and truncated homotrimeric version of the Env glycoprotein isolated from a clade A patient (CFAR, Bowles *et al.*, 2014). Despite mainly adapting aberrant and non-native like conformations, most epitopes are intact and it is commonly used *in vitro* to mimic the Env glycoprotein.

Figure 3-8: Workflow of measuring gp140 binding with Surface Plasmon Resonance.

Protein A was immobilised on a CM5 chip and the antibody was reversibly bound to protein A on the chip surface. The analyte gp140 was flowed over the chip and captured. The chip was then washed with the working buffer until a dissociation of 10% or more had occurred. Afterwards, the chip was regenerated with glycine pH 1.5.

The binding of 10-1074 HC ΔXF and 10-1074 YTE ΔXF to gp140 is shown in Figure 3-9. A CHO produced native 10-1074 antibody was included as 'gold standard' control throughout the thesis. The affinity of all variants to gp140 is high and comparable, as highlighted by the obtained K_D values, which are in a low nanomolar range (Figure 3-9). These low values mainly result from the very low dissociation constants. This result confirms that the YTE mutation of the 10-1074 heavy chain has no impact on the antibody binding to its cognate antigen.

A

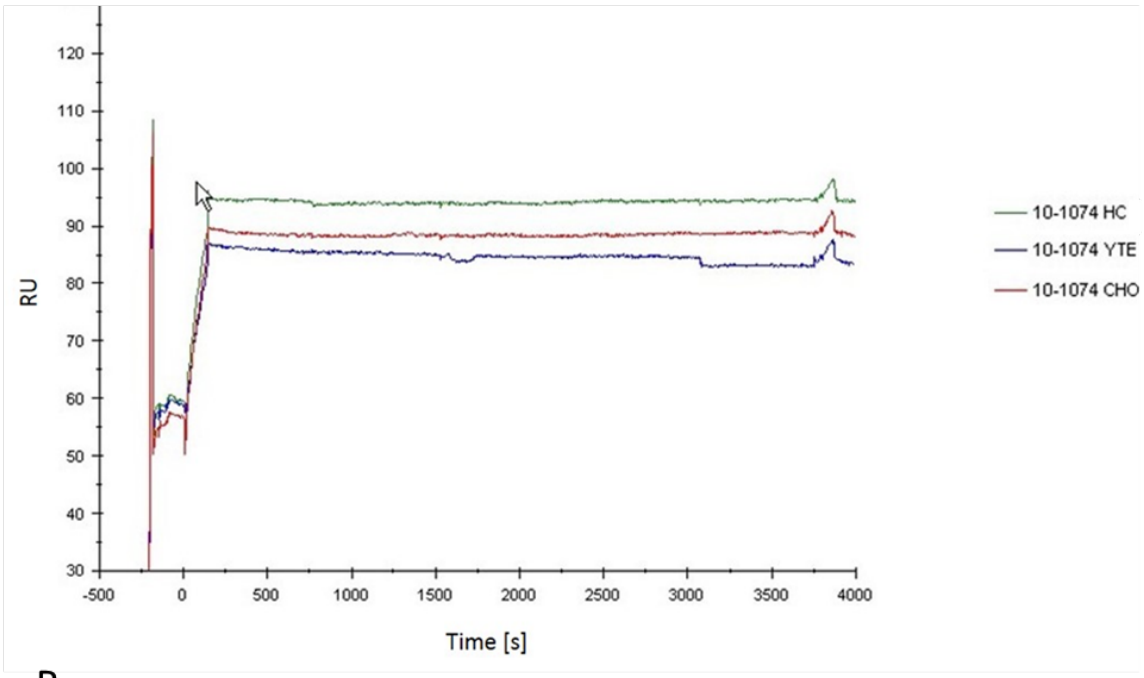

B

Sample	K_D [M]	k_a [1/Ms]	k_d [1/s]
10-1074 HC	$1.87*10^{-9} \pm 7.71*10^{-10}$	$1.18*10^{4} \pm 3.52*10^{3}$	$2.04*10^{-5} \pm 3.95*10^{-6}$
10-1074 YTE	$2.22*10^{-9} \pm 2.86*10^{-9}$	$1.39*10^{4} \pm 5.35*10^{3}$	$2.19*10^{-5} \pm 2.44*10^{-5}$
10-1074 CHO	$8.24*10^{-10}$	$1.43*10^{4}$	$1.18*10^{-5}$

Figure 3-9: A) Representative binding kinetics of 10-1074 to UG37 gp140 of 10-1074 HC and YTE as well as 10-1074 produced in CHO. B) Affinity and dissociation parameters of gp140 binding analysis obtained for three batches of each antibody (average with standard deviation).

3.4.7 YTE mutation does not impact HIV-1 neutralisation

The ability to neutralise a variety of primary HIV-1 strains is the most important quality of bNAbs when considered for application as pre- or post-exposure treatment. In order to test the bNAbs with regard to their neutralisation capacity, TZM-bl cells which express CD4, CCR5 and CXCR4 and carry a luciferase gene under the HIV Tat promoter were used. The rationale behind the assay is that upon infection with HIV, the TZM-bl cells are induced to express luciferase. Cell lysis releases the luciferase which catalyses the decarboxylation of luciferin (substrate) in the presence of $MgCl_2$, resulting in the release of energy in the form of light. Hence, the more cells are infected, the more luciferase will be expressed, and thus the emitted light will be stronger. As neutralising antibodies obstruct HIV binding to the host cells, a reduction in light emission should be observed when neutralisation takes place.

In each assay, a background (cells only) and a positive control (virus+cells with no antibody) were performed. To determine whether the general neutralisation breadth profile remains intact when expressing 10-1074 in ΔXF *N. benthamiana,* HIV-1 strains resistant and susceptible to 10-1074 were used. Neutralisation of HIV BaL.26 was performed with CHO produced 10-1074 alongside the bNAbs of interest and the obtained IC_{50}s are directly comparable (Figure 3-10). Results given in Table 3-5 verify that YTE does not impact the neutralisation potential of 10-1074, as IC_{50}s for the native (HC) and the YTE variant are similar. However, as IC_{50}s of the 10-1074 ΔXF variants deviated from values given in literature, 10-1074 CHO was directly compared to the ΔXF variants for all six tested susceptible strains. This direct comparison (see Table 3-6, Figure 3-11) revealed almost identical IC_{50}s for plant and mammalian-produced 10-1074, with exception of strain QH0692_42.

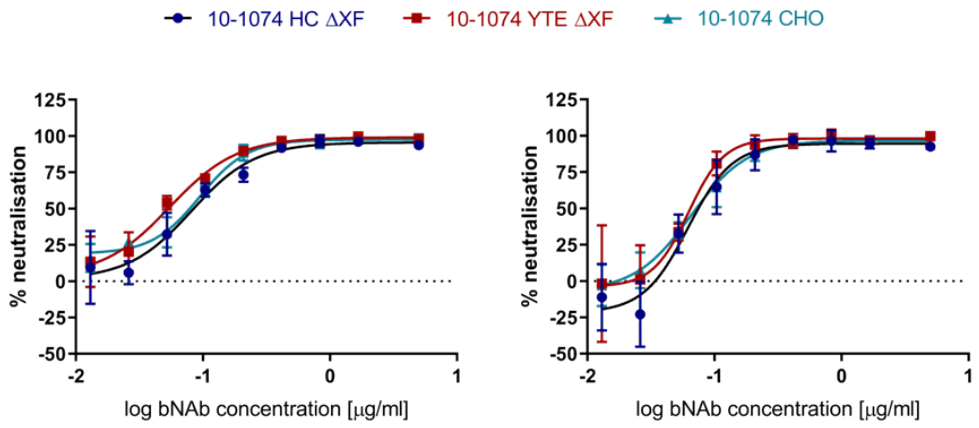

		IC50 (ng/mL)		
HIV Pseudovirus	Clade	HC ΔXF	YTE ΔXF	CHO
BaL.26	C	93±15	74±15	81±10

Figure 3-10: Neutralisation curves from neutralisation assays with BaL.26 (left) and CAAN5342 (right) pseudovirus for 10-1074 HC ΔXF, YTE ΔXF and CHO are shown. Error bars for data points with minimal SDs are not visible as they lie within the range of the data symbols size. IC_{50}s for BaL.26 neutralisation of all three 10-1074 variants are given in ng/mL.

Table 3-5: IC_{50}s (ng/mL) obtained for 10-1074 HC ΔXF, YTE ΔXF neutralising various HIV-1 strains from different clades

		IC_{50} (ng/mL)	
HIV Pseudovirus	Clade	HC ΔXF	YTE ΔXF
CAAN5342	B	61	62
SC422-661.8	B	277	224
ZM109F.PB4	C	>20000	>20000
pX1632	G	>20000	>20000
pCNE55	CRF01_AE	>20000	>20000
QH0692_42	B	469	373
REJO4541_67	B	>20000	>20000
6535	B	88	56
AC10.0	B	129	121
ZM135M.PL10a	C	333	386
CAP45_G3	C	>20000	>20000
ZM53M.PB12	C	>20000	>20000

Table 3-6: Neutralisation potency (IC_{50}, ng/mL) of the native 10-1074 variant produced in either ΔXF or CHO.

		IC_{50} (ng/mL)	
HIV Pseudovirus	**Clade**	**HC ΔXF**	**CHO**
CAAN5342	B	61	65
SC422-661.8	B	277	239
QH0692_42	B	967	536
6535	B	88	77
AC10.0	B	244	244
ZM135M.PL10a	C	652	675

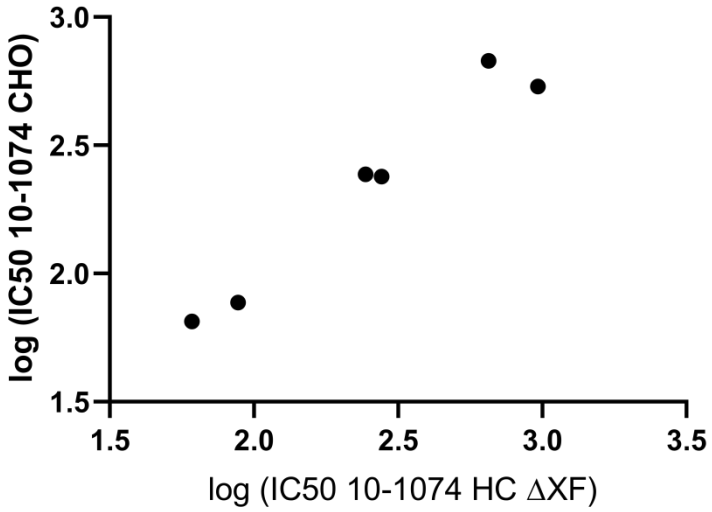

Figure 3-11: Correlation of 10-1074 CHO IC50s (ng/μL) with 10-1074 HC ΔXF IC50s (ng/μL). Spearman correlation analysis calculated an r value of 0.89 ($p<0.05$).

3.5 Discussion

bNAb therapy comes at a high expense, resulting in an imbalance between demand and affordability in low income countries. Ideally, production of the bNAbs would occur locally, simplifying the supply chain. However, most countries with high prevalence of HIV-1 lack the capital to invest in mammalian-cell production sites, which is highlighted by the fact that about 93% of mAb production sites are located in either Europe or the USA (Grilo and Mantalaris, 2019). Plants as an expression system offer an attractive alternative, as initial investment for upstream processes would be greatly reduced compared to mammalian-cell expression systems (Nandi *et al.*, 2016). Stably expressing plant lines would limit upstream facilities to greenhouses with appropriate lighting and watering systems. Furthermore, cultivation of plants does not require highly specialised personnel (Pogue *et al.*, 2010). Successful expression of several bNAbs has been demonstrated in *N. benthamiana* (transiently) or *N. tabacum* (stably) with yields up to 0.4 g/kg (Teh *et al.*, 2014; Rosenberg *et al.*, 2015). Currently there are no published yields of 10-1074 neither in plants nor mammalian expression systems.

Of the three 10-1074 variants, only two, could be expressed in ΔXF *N.benthamiana* at sufficient levels for initial studies. The LS variant, however, was excluded from further analysis, due to low crude extract yields (3.16 mg/kg). Purification further yielded inadequate amounts of bNAb, which were insufficient for analysis. A pre-purification yield of around 30 mg/kg is acceptable for production of a mAb used in clinical trials (Ma *et al.*, 2015). However, crude extract yields need to be significantly higher in order to be economically favourable to mammalian-cell expression systems. Nandi *et al.* (2016) calculated a 50 percent reduction per gram in cost of goods sold (COGS) based on a yield of 1 g/kg fresh weight (FW) compared to an equivalent CHO production facility (250 kg/year), but also showed that the minimal yield to obtain a competitive COGS is 0.4 g/kg FW at a production capacity of 300 kg/year. Despite reported yields of up to 2 g/kg FW of mAbs generated in plants (Zischewski, Sack and Fischer, 2016) , expression of unmodified HIV bNAbs has only resulted in the 'minimum' yield for economically competitive production (Teh *et al.*, 2014; Rosenberg *et al.*, 2015).

While the average crude extract yields of 10-1074 HC and 10-1074 YTE were similar with 44.03 and 47.71 mg/$kg_{fresh\ weight}$, product loss for 10-1074 YTE was around 80% (average final yield of 9.2 mg/ $kg_{fresh\ weight}$) compared to 70% loss for 10-1074 HC (average final yield of 13.3 mg/ $kg_{fresh\ weight}$). These variances in purification efficiency of almost identical bNAbs cannot be explained yet, but have also been observed for two other HIV-1 bNAbs, VRC01 and 3BNC117, upon introduction of mutation into the Fc region (personal communication Dr Audrey Teh). Unfortunately, yields and purification efficiency of antibodies with half-life extending mutations compared to the unmodified antibody produced in mammalian expression systems have not been reported. This data would be of great value in order to establish whether yield losses are specific to the mutations or the plant production system. However, a proper comparison of yields and recovery of the two different production systems and the three 10-1074 variants was out of the scope of this project.

One explanation for the differences in yield recovery would be increased aggregation potential of modified antibodies, resulting in higher losses during filtration prior to protein A chromatography and during dialysis. This hypothesis arose from the observation that a few months of storage caused an unacceptable loss of 10-1074 YTE during sterile filtration, whereas loss of the native version was less (not shown). It was further supported by studies looking into stability of antibodies with mutations in the Fc-region. An accelerated stability study of a model mAb (Motavizumab), revealed a significant decrease in monomer content of the YTE and LS variants compared to the native antibody over the course of 30 days (Booth *et al.*, 2018). Furthermore, Edgeworth et al. (2015) showed that Fc-modifying mutations frequently lead to a decrease in thermodynamic stability compared to the native mAb. The introduction of YTE into several mAbs led in average to an 11% reduction in thermal stability compared to their native counterpart and also lowered the energy barrier needed to induce unfolding (Edgeworth *et al.*, 2015). Partial or complete unfolding of antibodies results in higher irreversible aggregation (Vermeer and Norde, 2000), which is undesirable for therapeutic mAbs. Aggregation not only leads to loss in recovery but more importantly mAb aggregates are more likely to induce immunogenicity (anti-drug antibodies)

compared to monomers (Uchino *et al.*, 2017). Therefore, it is crucial to minimise aggregation during extraction and in mAb formulations.

In commercial products, surfactants, especially Tween 20 or 80, are used to stabilise antibodies and decrease aggregation (Kerwin, 2008) and was also used in the formulation of the CHO produced 10-1074 standard obtained from CFAR. The use of Tween80 during the extraction and purification process of 10-1074 led to stabilisation of 10-1074 YTE final yield with an average of 12.6 mg/ $kg_{fresh\ weight}$ and a 3-4 fold increase in 10-1074 HC final yield with an average of 47.0 mg/ $kg_{fresh\ weight}$, suggesting that a significant amount of native antibody can be lost during purification due to aggregation. However, the addition of Tween80 did not balance out recovery differences between the native and modified bNAb, but made them more prominent, which could be interpreted as an indication that factors other than aggregation might play a role in poor YTE yields. It has to be noted though, that polysorbates seem to primarily stabilise the Fab region of mAbs (Singh *et al.*, 2017), explaining the lack of the expected yield compensation with regard to 10-1074 YTE. In general, even after addition of Tween80, post-purification yields are low when compared to reported yields (100-400 mg/kg)(Teh *et al.*, 2014; Rosenberg *et al.*, 2015) of other bNAbs produced transiently in *Nicotiana benthamiana*. Yet, expression of different antibodies can greatly vary (Garber and Demarest, 2007). The obtained yield for either 10-1074 variant cannot be compared to 10-1074 yields acquired from mammalian or other expression systems, which are not published. Garber et al. (2007) showed that stability variations between mAbs of the same subclass can be attributed to the variable domain, thus low Fab stability can lead to expression problems. This partly elucidates yield fluctuations between antibodies with identical constant but different variable regions.

Improved crude extract yields are important to achieve the goal of low cost therapeutics; yet, the significance of optimised downstream processes to minimise the loss of product during purification is often overlooked. In order to obtain regulatory approval for clinical trials and pave the way for future marketing of plant-produced mAbs, Ma *et al.* (2015) developed a GMP-compliant

manufacturing process, which included a detailed optimised downstream process. Commercial and research downstream processing of mAbs differs greatly, as quality standards of commercial products are higher, therefore additional chromatography and filtration steps are used when compared to purification in a research laboratory. Furthermore, upscaling of some methods applied on a laboratory production scale (e.g. centrifugation) is not easily attainable. Centrifugation was replaced by filtration to remove plant debris and an additional filtration step as well as pH adjustment was included before affinity chromatography with Protein A. A second chromatography step and several post-chromatography filtration steps were introduced to ensure the highest product quality. Importantly, the generated model bNAb 2G12 was tested not only with regard of the final product quality (e.g. API activity, purity, nicotine content) but also with regards to the stability of the product. It revealed that the product remained stable and active despite storage, thawing and re-freezing (Ma *et al.*, 2015). This study not only paved the way for commercialisation of plant-produced mAbs, but also gives indications on optimisation of downstream processes in research laboratories in order to reduce yield losses.

Western blots of 10-1074 HC and YTE confirmed that both variants are fully assembled albeit with a number of degradation events, which are commonly seen in mAbs expressed in tobacco plants (Hehle *et al.*, 2015). 10-1074 CHO was not available when the three batches of bNAbs were produced; therefore an IgG1 λ control was used on the SDS PAGE and western blots. The inclusion of 10-1074 CHO would have been informative, as a comparison of the degree of degradation could have been performed and would have allowed for better comparison of neutralisation and affinity data.

One of the major impediments of achieving higher yields *in planta* seems to be degradation. Degradation through proteases leads to a multitude of incompletely assembled antibodies, which not only affects the yield, but also the quality of the product. A common misconception is that these degradation processes occur after extraction of the mAb from the leaves, which resulted in addition

of expensive protease inhibitors to the plant extract. These proteases show no significant activity *ex planta* at a pH above 5, thus the majority of degradation processes negatively affecting the yield take place *in planta* (Hehle *et al.*, 2011). As plants produce hundreds of endogenous proteases (van der Hoorn, 2008) , inactivation of all proteases is hardly feasible. Hehle *et al.* (2015) revealed that the cleavage sites of mAbs generated in *N. tabacum* are located in close proximity to interdomain regions. These sites could possibly be modified in order to increase yield. However, extensive mutation studies would be necessary, as even minimal manipulation of the amino acid sequence of an antibody can lead to changes in stability, folding and *in vivo* activity (S. J. Wu *et al.*, 2010; Edgeworth *et al.*, 2015; Nichols *et al.*, 2015).

Glycoanalysis by mass spectrometry revealed that up to 15% of the respective 10-1074 variation are aglycosylated, which would result in a small size shift on a western blot compared to the fully glycosylated version. Detailed information of an antibody's glycosylation pattern is helpful for several reasons. First of all, mAbs with human-like glycans are more likely to be accepted by regulatory agencies than mAbs with plant-like glycans. Secondly, glycosylation can interfere with Fc receptor binding, thus negatively impact the induction of Fc mediated effector functions (Lu *et al.*, 2015; Subedi and Barb, 2015; Stelter *et al.*, 2020). Lastly, N-glycosylation of antibodies influences their stability, conformation and aggregation potential (Kiyoshi *et al.*, 2017). Aglycosylated antibodies are more prone to heat aggregation and exhibit an increased tendency to chemical denaturation.

Neutralising antibodies hamper the attachment of the virion to a host cell by blocking sites on the viral envelope which are essential for binding to the host cell receptor (Reading and Dimmock, 2007). Upon changing the expression system or introducing mutations into the Fc region, it is necessary to verify that these changes do not negatively affect neutralisation potential, even though neither are likely to alter the specificity of the Fab region. However, in recent years it has become evident that the two independent functional domains, the variable and constant region,

influence each other's functions. For instance, half-life is partly dependent on the variable region despite not being directly involved in initial binding to the FcRn (Igawa *et al.*, 2010; Schoch *et al.*, 2015; Jensen *et al.*, 2017). Moreover, antigen specificity appears to be partly associated with the constant region, as class switching with an unmodified variable region led to variations in antigen affinity (Cooper *et al.*, 1994; Tudor and Bomsel, 2011). Therefore antigen specificity and neutralisation potential have to be re-validated upon introduction of any mutation into the Fc region. SPR analysis showed that neither the expression system nor the changes in the Fc region negatively impact antigen binding. The obtained K_D for all three variants (10-1074 HC, YTE and CHO) is similar and lies expected low nanomolar range (Teh *et al.*, 2014). Obtained IC_{50}s from the performed neutralisation assays further corroborate that plant-produced variants are not inferior in neutralisation potential when directly compared to its mammalian counterpart (Yoon *et al.*, 2015). Although for BaL.26, Mouquet et al. (2012) reported an IC_{50} of 33 ng/ml, other studies (Yoon *et al.*, 2015) showed an IC_{50} of 4 ng/ml. These results illustrate lab-to-lab variation in the assay, a factor that was addressed here by side-to-side comparison of plant and CHO expressed 10-1074.

As expected, the introduction of the YTE mutation did not affect 10-1074's neutralisation potential. These results allow for more in-depth analysis to compare the bNAb variants with regard to effector functions, binding to the neonatal receptor and its impact on *in vivo* half-life.

4 Investigation of the effect of introduced modifications into bNAb 10-1074 on *in vitro* effector function and *in vivo* half-life

4.1 Introduction

This chapter investigates the effects the change in expression system and the introduced YTE mutation have on antibody-dependent cellular cytotoxicity (ADCC) mediated by the bNAb 10-1074, and on its *in vitro* transcytosis by FcRn expressing cells and *in vivo* half-life.

The role of antibodies is diverse; functions include neutralisation, activation of the complement system and opsonisation. Since the ability to neutralise a vast variety of HIV-1 primary isolates is the key function of bNAbs, research has primarily focused on neutralisation. Yet, their efficacy seems to not solely rely upon neutralisation potential but is also dependent on FcγR functions.

4.1.1 Antibody-dependent cellular cytotoxicity (ADCC)

Treating macaques with a modified version of the bNAb b12, carrying mutations that eliminated FcγR induced functions, resulted in more rapid infection when compared to the non-modified bNAb (Hessell *et al.*, 2009). Likewise, HIV-1 infected humanised NRG-mice treated with combination therapy of either wild-type or FcγR enhanced affinity bNAbs displayed a reduced viral load, when compared to a combination of the same bNAbs with FcγR abolishing mutations (Bournazos *et al.*, 2014). One of the effector functions thought to be especially important is antibody-dependent cellular cytotoxicity (ADCC). BNAbs can efficiently prevent infection (of uninfected cells) by binding to and neutralising cell-free virions. But infection of cells can often be caused by cell-to-cell transmission without exposure to the extracellular environment (Schiffner, Sattentau and Duncan, 2013). However, ADCC competent bNAbs might be able to prevent cell-associated transmission by targeting Env infected cells, recruiting effector cells such as NK cells to kill the infected cell. This mechanism might be advantageous as the efficacy of the bNAb is not reliant

on its ability to enter the viral synapse (Lee and Kent, 2018). It has been shown that some bNAbs, including 10-1074, lead to apoptosis of HIV-infected cells *in vitro* (Bruel *et al.*, 2016).

As ADCC could play a crucial part in inhibition of infection, bNAbs engineered to exhibit higher affinity to FcγRIIIa, resulting in elevated ADCC, might prove beneficial. Several mutations leading to increased ADCC have been identified, however, the introduction of a multitude of mutations into the Fc-region might not be always favourable, as modifications have the tendency to destabilise antibodies (Edgeworth *et al.*, 2015). Besides mutations, changes in glycosylation are also able to improve binding to FcγRIIIa. Several studies have shown that the removal of fucose (independent of the position of the glycosidic linkage) from the core glycan significantly enhance binding to FcγRIIIa (Shields *et al.*, 2002; Okazaki *et al.*, 2004; Ferrara *et al.*, 2011; Luo *et al.*, 2017). This can be achieved in plant expression platforms using ΔXF plants, also serving to provide antibodies with more human-like glycosylation (Strasser *et al.*, 2008).

4.1.2 Half-life

10-1074 has an average half-life of 24 days in uninfected individuals, consistent with human IgG (21 days,(Petkova *et al.*, 2006)), reducing to 12.8 in infected individuals, determined by (Caskey *et al.*, 2017) using dosing regimens of 3 mg/kg, 10 mg/kg and 30 mg/kg, respectively. Despite exhibiting a comparatively long half-life to other bNAbs (e.g. $VRC01_{t1/2healthy}$= 15 days (Ledgerwood *et al.*, 2015)), it is too short to feasibly replace ART with bNAb therapy. Currently bNAbs have to be given intravenously by health care professionals, whereas ART can be conveniently self-administered. The short half-life of bNAbs is a significant drawback, especially in remote areas, where hospital visits come with high costs and long journeys. Furthermore, the shorter the half-life the more doses per year would be necessary, thus cost of therapy increases. Monoclonal antibody therapies are inherently expensive (average annual cost: $96,731) (Hernandez *et al.*, 2018), therefore it is crucial to greatly improve half-life in order to make bNAb therapy more attractive and lower the burden on recipients.

A major player in determining half-life of IgG is the neonatal receptor (FcRn), which rescues IgG from being degraded in the lysosome (Petkova *et al.*, 2006). As discussed in 3.1 ,studies have shown that increased affinity at pH 6 of antibodies to FcRn leads to improvement in half-life, which can be achieved by introducing e.g. an YTE (Acqua *et al.*, 2002) or LS (Zalevsky *et al.*, 2010) modification into the Fc-region of the target antibody. These modifications resulted in a 3-4 fold improvement in half-life of the studied mAbs in NHPs in initial studies and have been used subsequently to achieve prolonged half-life of various IgGs *in vivo* (Acqua *et al.*, 2002; Zalevsky *et al.*, 2010; Gaudinski *et al.*, 2018; Gautam *et al.*, 2018).

Introduction of the YTE mutation into an anti-HBV (E6F6) antibody resulted in 1.5 fold increased half-life in mice and 2.5 fold increase in cynomolgus monkeys (Kang *et al.*, 2018). Motavizumab, an anti-RSV mAb not only showed prolonged half-life in NHPs (Acqua *et al.*, 2002), but also in humans between 2-4 fold longer half-life (up to 100 days) (Robbie *et al.*, 2013). A LS-modified version of the bNAb VRC01 showed a 4-fold increase in half-life in humans when compared to the native VRC01 (Gaudinski *et al.*, 2018). A plant-produced version of the bNAb PGT121 modified with YTE resulted in a variable half-life extension (0-10 x), which depended on the level of anti-drug antibody formation (Rosenberg *et al.*, 2019).

Most research focuses on the improvement of half-life through increasing affinity to the neonatal receptor, yet, increased affinity might also be beneficial for other reasons. For example, a higher affinity to the neonatal receptor could have implications for transport of the respective maternal IgG through the placenta to the foetus. HIV-1 can be transmitted from mother to child during pregnancy, delivery and breastfeeding (Newell, 1998). The highest risk of mother-to-child-transmission (MTCT) is during the last few weeks of pregnancy (Teasdale, Marais and Abrams, 2011). The risk of MTCT without treatment is about 15-45% and decreases to below 5% when viral suppression with ART is achieved (WHO, 2017). However, there remains some controversy regarding the safety of ART treatment during pregnancy or even before conception. Meta-analysis from a

number of studies with ART during pregnancy showed that preterm delivery or low birthweight was more commonly seen in women treated with specific combinations of ART (Siemieniuk *et al.*, 2017) and receiving treatment (Snijdewind *et al.*, 2018). Furthermore, if ART is started late during pregnancy, it is often too late to fully suppress viral replication (Gill *et al.*, 2016) increasing the risk of MTCT. BNAbs with increased affinity to the neonatal receptor might therefore represent a superior treatment to prevent MTCT, especially when treatment initiation in pregnant HIV-positive women is started late.

4.2 Specific objectives

Determination of the interaction of the 10-1074 variants and specific Fc receptors to investigate potentially enhanced immune effector funtions and bNAb half-life.

- determine the differences in kinetic parameters of the three 10-1074 variants to FcγRIIIa
- investigate the impact of afucosylation and the YTE mutation of 10-1074 on ADCC
- determine the effect of the YTE mutation on 10-1074's binding affinity to the neonatal receptor
- investigate the *in vitro* transcytosis potential of the three 10-1074 variants
- determine the effect of the YTE mutation on *in vivo* half-life of 10-1074

4.3 Contributions

- ADCC activity assay (n=1) was performed by Francesc Cunyat Viaplana (Albajuna)
- Transcytosis assay with Caco-2 cells was performed by Elliot Higgins at King's College London. The subsequent ELISA was performed by me.
- Dosing and blood collection of transgenic mice for half-life studies was performed by the Biological Research Facilities Team. Processing and analysis of samples was performed by me.

4.4 Results

4.4.1 Antibody-dependent cellular cytoxicity (ADCC)

4.4.1.1 10-1074 produced in ΔXF *N. benthamiana* show higher affinity to FcγRIIIa V158 than 10-1074 produced in CHO

Binding of the native (HC) and the YTE variant (YTE) of 10-1074 to different concentrations of FcγRIIIa V158 was determined using SPR following the workflow given in Figure 4-1. 10-1074 produced in CHO was included as a standard. Both the HC and the YTE versions of the antibody produced in ΔXF plants (3.4.2) exhibit efficient binding to FcγRIIIa V158. On the other hand, the CHO produced 10-1074 shows less affinity to FcγRIIIa V158 (Table 4-1, Figure 4-2)). Compared to 10-1074 CHO, 10-1074 produced in ΔXF plants displayed an approximately 5-fold improvement in K_D. It has to be noted that the stark difference in dissociation (k_d) observed in the sensorgrams between the plant and mammalian produced 10-1074 was not reflected in the calculated parameters, which most likely resulted from the suboptimal fit of the model.

Figure 4-1: Strategy for determining binding kinetics of FcγRIIIa V158 to bNAbs using SPR. A CM5 chip (orange) with immobilised protein A (red) was used to capture the respective bNAB (green). FcγRIIIa V158 (blue) was flowed over the chip in various concentrations, followed by a wash with running buffer (dissociation). To remove the captured bNAb, glycine was flowed over the chip (regeneration step)

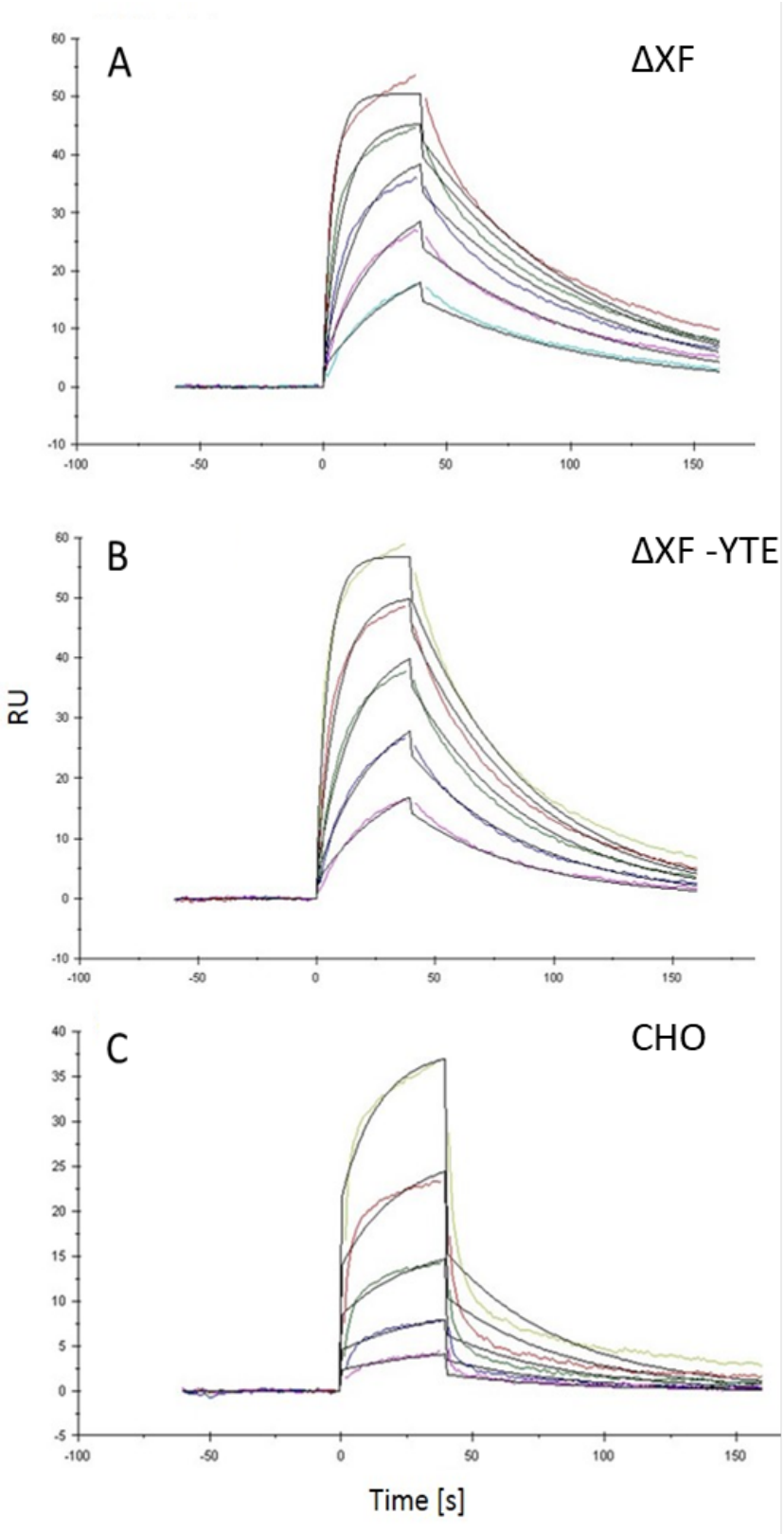

Figure 4-2: FcγRIIIa V158 binding analysis with multiple FcγRIIIa V158 concentrations using Surface Plasmon Resonance. A representative result for 10-1074 HC ΔXF (A) and 10-1074 YTE ΔXF (B) plus the CHO produced 10-1074 (C) as comparison is displayed.

Table 4-1: Average affinity and dissociation parameters of multiple concentration FcγRIIIa V158 binding analysis obtained for of 10-1074 HC ΔXF (n=3), 10-1074 YTE ΔXF (n=3) and the 10-1074 CHO (n=1) control.

Sample	K_D [M]	k_a [1/Ms]	k_d [1/s]
10-1074 HC ΔXF	$8.89*10^{-8} \pm 2.2*10^{-8}$	$1.88*10^{5} \pm 2.65*10^{4}$	0.016 ± 0.0032
10-1074 YTE ΔXF	$9.79*10^{-8} \pm 3.3*10^{-8}$	$1.89*10^{5} \pm 3.69*10^{4}$	0.018 ± 0.0032
10-1074 CHO	$4.628*10^{-7}$	$4.80*10^{4}$	0.022

4.4.1.2 Removal of α1,3-Fucose results in higher ADCC activation, YTE shows an inhibitory effect

To determine the effect of improved binding to FcγRIIIa V158 on ADCC, an *in vitro* ADCC activation assay was performed. This assay uses a modified Jurkat cell line, which stably expresses FcγRIIIa and NFAT (Nuclear factor of activated T-cells)-induced luciferase. Upon binding of the immune complex to the FcγRIIIa on the effector cell, the NFAT-pathway is triggered and luciferase is expressed. Thus, the luminescence signal directly correlates with ADCC activation (Promega).

To circumvent difficulties related to the usage of HIV-1 infected cells, recombinant gp140 trimer was used as antigen. However, this approach represents a steady-state system, which is limited by its inability to mimic the impact of continuous infection of cells and dynamic processes of exposing Env on target cells. While the results only display the ability of the bNAb variants to activate the ADCC pathway under ideal conditions, they provide a first indication of their cytotoxicity-inducing potential.

The assay was performed under the same conditions for the V- and F-variant of FcγRIIIa respectively. Fold of induction was calculated according to the following formula:

$$Fold\ of\ Induction = \frac{RLU\ (induced - substrate\ only)}{RLU\ (gp140\ only - substrate\ only)}$$

Three independent repeats with technical duplicates for FcγRIIIa V158 and FcγRIIIa F158, respectively, were carried out. At a bNAb concentration of 10 µg/ml only one measurement FcγRIIIa V158 with technical duplicates was performed. Measurements of 10-1074 HC at the highest

concentration used in the respective assay (10 µg/ml or 4 µg/ml) without gp140 (no gp140) were used as negative control.

Figure 4-3 displays ADCC activation with FcγRIIIa V158. Statisically significant differences in ADCC activation between different antibodies can only be observed for bNAb concentrations of 4 µg/ml and above. Improved activation was exhibited by the two ΔXF variants when compared to 10-1074 CHO. This concurs with the results of CD16a binding analysis and the scientific consensus that fucose reduces ADCC (Shields *et al.*, 2002; Okazaki *et al.*, 2004; Ferrara *et al.*, 2011). Surprisingly, the effect of afucosylation was less significant for 10-0174 YTE than 10-1074 HC at higher concentrations, even though the binding kinetics to FcγRIIIa V158 were similar. This suggests that either the discrepancies are not evident due to the fit of the model, or the YTE variant binds equally well, but exhibits an inhibitory effect on ADCC.

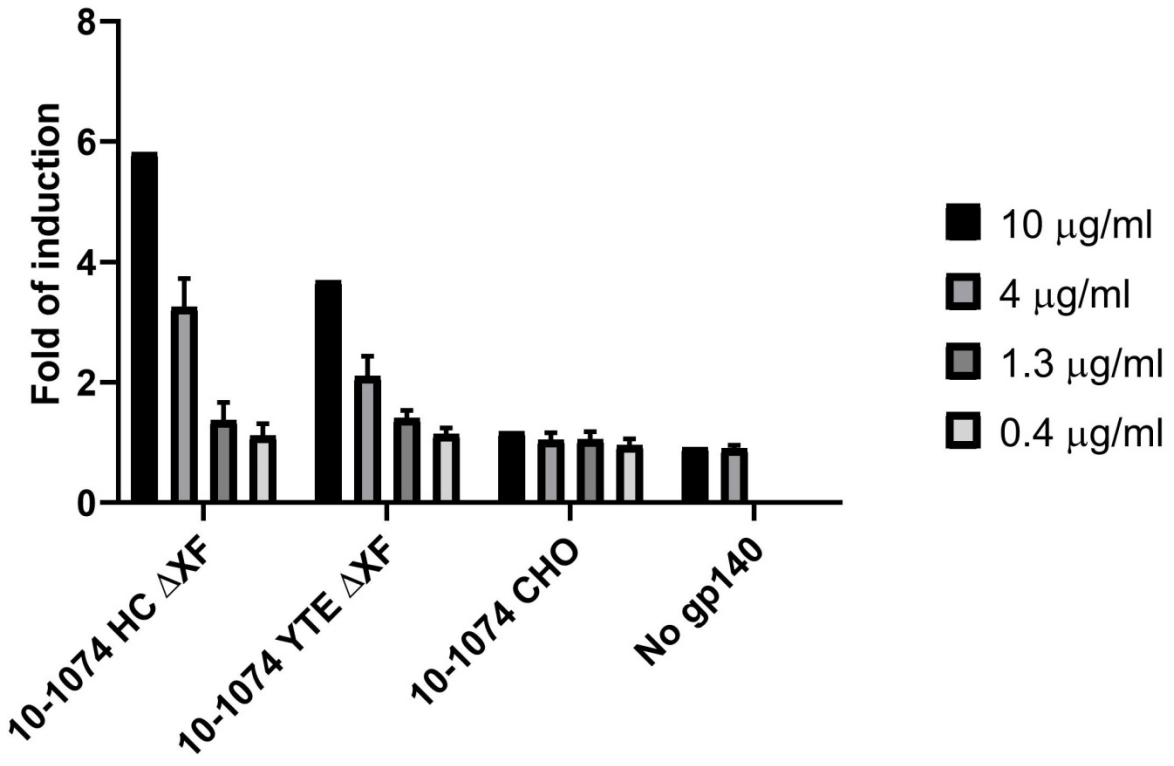

	10 μg/ml	4 μg/ml	1.3 μg/ml	0.4 μg/ml
10-1074 HC ΔXF vs. 10-1074 YTE ΔXF	****	****	ns	ns
10-1074 HC ΔXF vs. 10-1074 CHO	****	****	ns	ns
10-1074 HC ΔXF vs. No gp140	****	****	ND	ND
10-1074 YTE ΔXF vs. 10-1074 CHO	****	***	ns	ns
10-1074 YTE ΔXF vs. No gp140	****	***	ND	ND
10-1074 CHO vs. No gp140	ns	ns	ND	ND

Figure 4-3: Means with error bars (SD) of the ADCC activation assay for FcγRIIIa V-variant (biological repeats: n=3, n=1 for 10 μg/ml)). 10-1074 HC ΔXF at 10 or 4 μg/ml without gp140 (no gp140) was used as negative control. Statistical significance was determined using a Two-Way ANOVA with Tukey's multiple comparison test. P-values are denoted by asterisk; p≤0.05 (*), p ≤0.01 (**), p≤0.001 (***) and p≤0.0001.

The differences in ADCC activation between the variants were less obvious for FcγRIIIa F158 (Figure 4-4). Statistically significant changes in activation were only detectable at antibody concentrations of 12 μg/ml. This, however, was to be expected due to the lower affinity of FcγRIIIa F158.

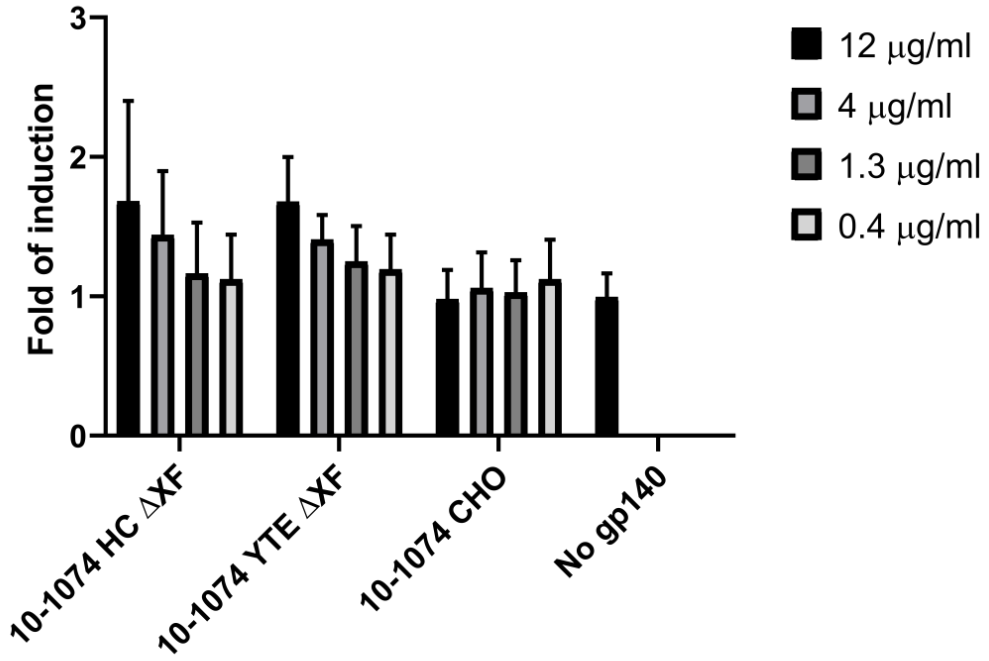

	12 µg/ml	4 µg/ml	1.3 µg/ml	0.4 µg/ml
10-1074 HC ΔXF vs. 10-1074 YTE ΔXF	ns	ns	ns	ns
10-1074 HC ΔXF vs. 10-1074 CHO	**	ns	ns	ns
10-1074 HC ΔXF vs. No gp140	**	ND	ND	ND
10-1074 YTE ΔXF vs. 10-1074 CHO	**	ns	ns	ns
10-1074 YTE ΔXF vs. No gp140	**	ND	ND	ND
10-1074 CHO vs. No gp140	ns	ND	ND	ND

Figure 4-4: Means with error bars (SD) of the ADCC activation assay for FcγRIIIa F-variant (biological repeats n=3). 10-1074 HC ΔXF at 12 µg/ml without gp140 (no gp140) was used as negative control. Statistical significance was determined using a Two-Way ANOVA with Tukey's multiple comparison test. P-values are denoted by asterisk; p≤0.05 (*), p ≤0.01 (**), p≤0.001 (***) and p≤0.0001.

4.4.1.3 ADCC activity assay does not support ADCC activation data

To further investigate the effect of afucosylation of 10-1074 on ADCC activity, an ADCC activity assay (10:1 effector to target ratio) was performed by Francesc Cunyat Viaplana (Albajuna). The assay uses NKR24 cells (CD4+,CCR5+) as target cells, which carry a luciferase gene under the HIV TAT promoter. N6 cells, a human NK cell line KHYG-1 stably expressing the V158 variant of human FcγRIIIa , serve as effector cells. Effective crosslinking of effector cells with immune complexes, followed by ADCC leads to a reduction of luciferase-expressing cells. ADCC activity is therefore inversely proportional to luminescence.10-1074 HC ΔXF, 10-1074 YTE ΔXF and 10-1074 CHO were tested alongside another bNAb 3BNC117 and its variants, and are shown together in Figure 4-5 as no

individual graph was provided for 10-1074. The ADCC activity assay (n=1) did not support the results of the ADCC activation assay, as the 10-1074 HC ΔXF variant has a similar EC50 (µg/ml) as 10-1074 CHO, whereas the EC50 of 10-1074 YTE is almost 6 times lower. This assay not only contradicts the ADCC activation and SPR data but also previous observations with other bNAbs and numerous studies.

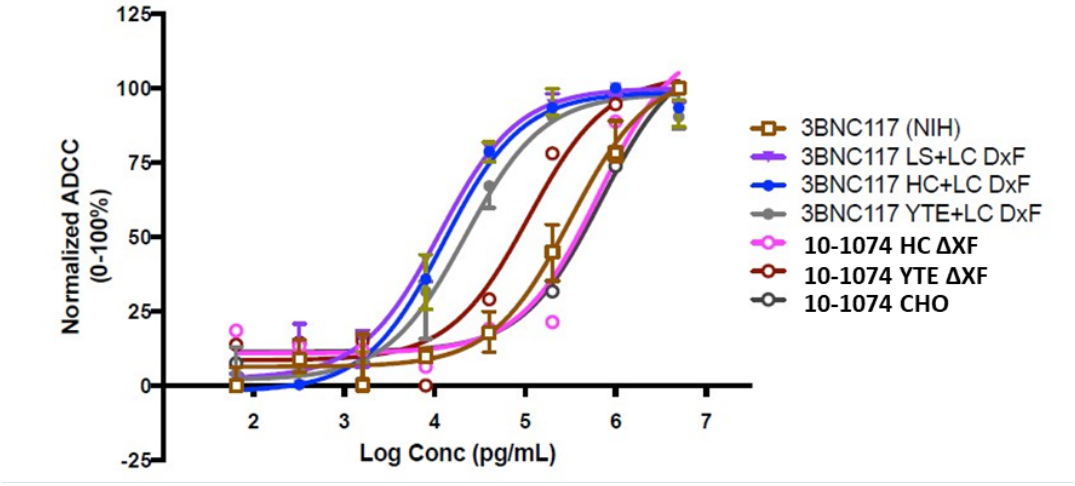

	10-1074 HC ΔXF	10-1074 YTE ΔXF	10-1074 CHO
EC50 (µg/ml)	0.65	0.11	0.69

Figure 4-5: Normalised curves of the ADCC activity assay (n=1). The EC50 (µg/ml) for each variant alongside are given in the table.

4.4.2 *In vitro* transcytosis and *in vivo* half life

4.4.2.1 YTE mutation leads to enhanced affinity to the neonatal receptor

Binding to the neonatal receptor allows IgG to be recycled when endocytosed, instead of being degraded, therefore resulting in longer half-life of IgG compared to other immunoglobulins. Prior to determining whether the introduction of the YTE mutation into 10-1074 results in enhanced *in vitro* transcytosis and *in vivo* half-life, the binding kinetics of hFcRn to 10-1074 HC and YTE ΔXF at pH 6 were evaluated using SPR.

Figure 4-6: A conventional SPR strategy to measure affinity of FcRn to an antibody. A CM5 chip (orange) with immobilised anti-Fab fragment (blue) is used to capture the bNAb (green). The analyte hFcRn (blue) is flowed over the chip, followed by a wash with the running buffer (dissociation). The captured antibody is removed from the chip using glycine (regeneration)

A conventional strategy is to coat a CM5 chip with an anti-Fab fragment (Human Fab Capture Kit, GE Healthcare), capture the respective antibody and flow an hFcRn at a range of concentrations over the chip (Figure 4-6). Regeneration is performed using glycine-HCl at pH 2.1. However, this strategy failed for 10-1074 as the antibody could not be captured by the anti-Fab fragment at a pH of 6.

Figure 4-7: SPR strategy to measure affinity of FcRn to an antibody using a CM5 chip (orange) coated with an anti-λ antibody (blue). After capturing the bNAb (green), the analyte hFcRn (blue) is flowed over the chip, followed by a wash with the running buffer (dissociation). The captured antibody is removed from the chip using various methods.

To maintain the same overall strategy, a CM5 chip was coated with an anti-lambda antibody (Figure 4-7). Binding of the bNAbs to this antibody at pH 6 was confirmed via ELISA (results not shown). Despite being able to capture the bNAb, this method could not be applied, as the chip could not be fully recovered after each run, thus some bNAb would stay bound to the anti-lambda antibody, regardless of the regeneration method used (low pH, high salt etc.). Harsher regeneration methods like 5M NaOH could not be used without damaging the anti-lambda antibody.

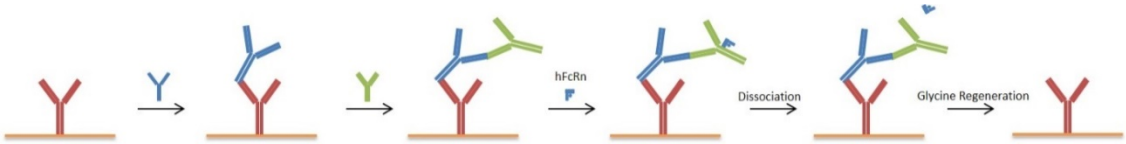

Figure 4-8: SPR strategy to measure affinity of FcRn to an antibody using a CM5 chip (orange) coated with an anti-goat antibody (red). The anti-lambda antibody (blue) was captured, followed by a second capturing step of the respective bNAb

(green). Lastly, hFcRn is flowed over the chip (blue), followed by a wash with the running buffer (dissociation). The captured antibody is removed from the chip using glycine.

As this strategy suggested that the affinity of 10-1074 to the anti-lambda antibody was too high to disrupt binding with low pH or high salt, an anti-goat antibody was used to coat the chip, capture the anti-lambda antibody, then capture the respective bNAb and finally flow FcRn over the chip (Figure 4-8). However, again complete regeneration with glycine failed

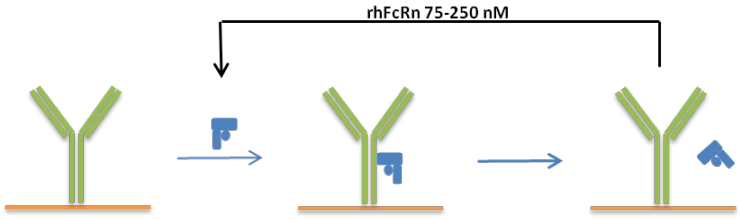

Figure 4-9: Principle of SPR workflow applied for FcRn affinity measurements. A CM5 chip (orange) with the respective immobilised bNAb (green) was used. The analyte hFcRn (blue) was flowed over the chip, followed by a wash with running buffer. No regeneration was performed.

Since all other approaches failed, CM5 chips were coated with the respective bNAb and a single cycle kinetic program was chosen to determine the binding kinetics of five different concentrations of rhFcRn to the bNAb (Figure 4-9). No regeneration was performed, as the captured bNAb is likely to be damaged in course of regeneration. This strategy was successful, showing that at all concentrations of FcRn, 10-1074 HC has a lower affinity to the neonatal receptor than 10-1074 YTE. This was not reflected in the obtained kinetic parameters (not given), due to issues with modelling of the data. The evaluation software interpreted the long stretches of constant signal for 10-1074 HC between FcRn concentrations as undissociated sample, thus resulting in a very low k_d, and therefore a lower K_D of 10-1074 HC to FcRn than for YTE (see Figure 4-10). However, the trend of enhanced affinity of 10-1074 YTE compared to 10-1074 HC can be easily observed in the obtained sensorgrams.

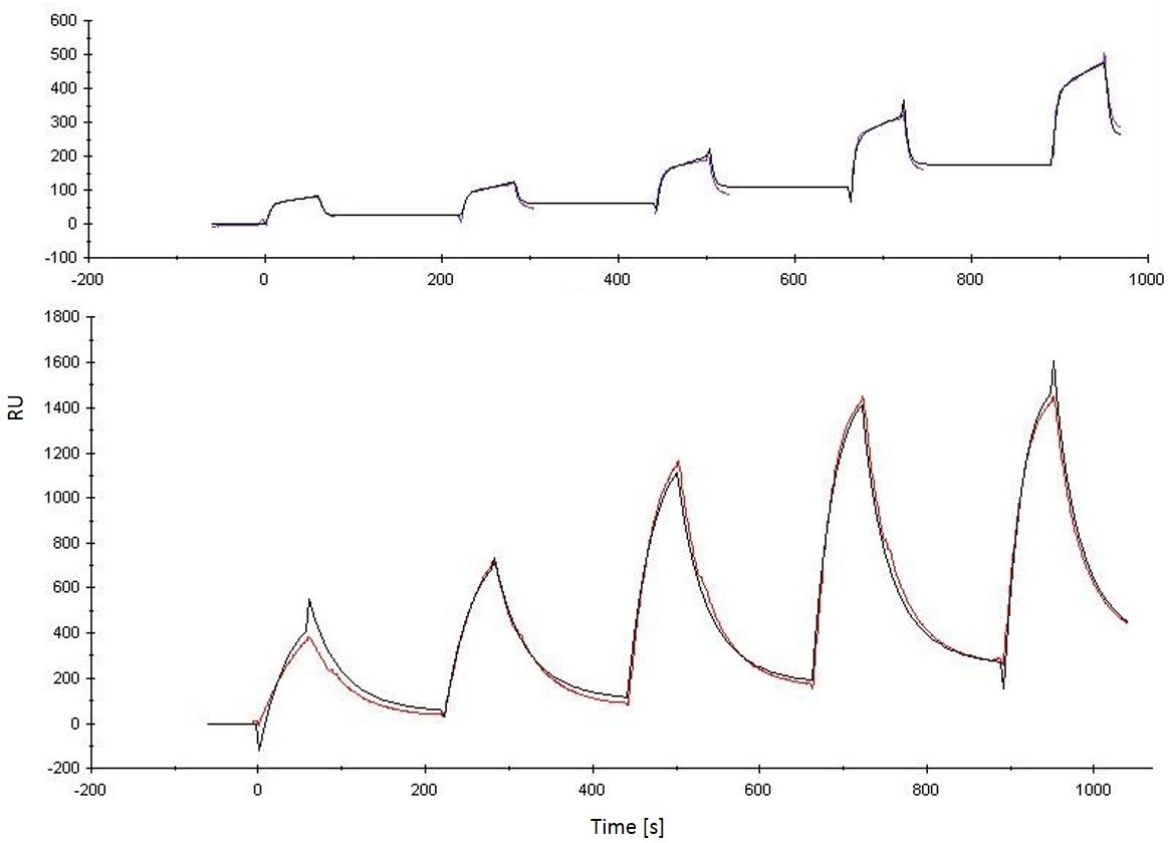

Figure 4-10: SPR sensorgrams of single cycle kinetics for FcRn binding with five hFcRn concentrations. The top sensorgram displays the kinetics of hFcRn to 10-1074 HC, while the bottom sensorgram shows the same for 10-1074 YTE.

4.4.2.2 mAb 10-1074 YTE shows increased transcytosis in an *in vitro* model

Enhanced affinity to the neonatal receptor could improve transcytosis from the apical to the basolateral side of a cell. Transcytosis capacity not only gives an indication of binding to FcRn, but also gives a first glimpse on the efficiency of transport through the placenta in order to provide protection to an unborn child.

A monolayer of transgenic MDCK hFcRn/hβ_2m was grown on transwells, MDCK hβ_2m cells served as control. BNAbs were added to the lower well containing HBSS pH6, representing the apical side of a cell. The upper well (basolateral side) contained HBSS pH 7.4. The underlying principle of this assay is that after endocytosis of the bNAb on the apical side, FcRn binds to it and transports it through the monolayer onto the basolateral side, releasing the bNAb at pH 7.4 (Figure 4-11). Therefore, the higher the affinity to the neonatal receptor, the more bNAb is transcytosed in a

specific amount of time. The basolateral supernatant is then used in an anti-hIgG ELISA, to determine the transcytosed amount of bNAb.

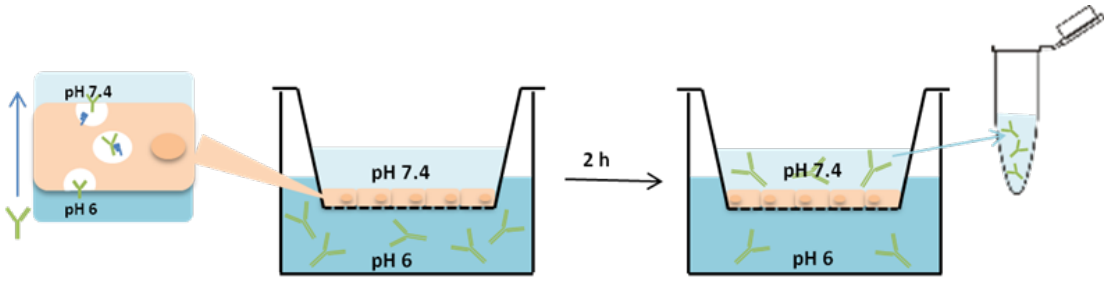

Figure 4-11: Principle of the transcytosis assay. The apical side is filled with HBSS pH 6 and the respective bNAb at a defined concentration. A pre-cultured monolayer of hFcRn expressing cells on transwells separates the upper (basolateral) and lower (apical) well. On the basolateral side HBSS pH7.4 leads to the release of IgG transported across the monolayer by hFcRn and the level can be determined via ELISA.

A significantly higher amount of 10-1074 YTE is transcytosed compared to 10-1074 HC at all bNAb input levels (µg) (Figure 4-12).

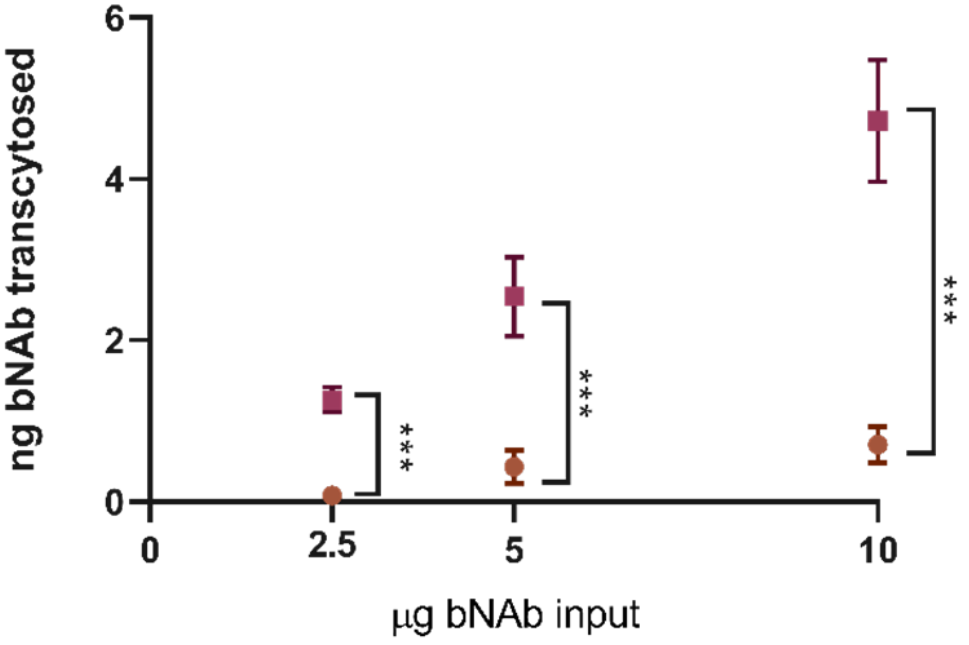

Figure 4-12: Results of representative transcytosis experiment performed with MDCK hFcRn/hβ2m cells is displayed. Means with error bars (SD) for 10-1074 HC ΔXF and 10-1074 YTE ΔXF (n=4) are shown. Statistical significance was determined using a multiple t-test (Holm-Sidak method). P-values are denoted by asterisk; p≤0.05 (*), p ≤0.01 (**), p≤0.001 (***) and p≤0.0001.

The same trend was observed in repetitions of the assay (Appendix) and 10-1074 CHO exhibited similar transcytosis to 10-1074 HC ΔXF (Appendix). While the trend was consistent, the transcytosed amount for each assay differed, which can arise from cell-to-cell variations.

To verify this effect in cells that naturally express hFcRn, a similar transcytosis assay with Caco-2 cells was performed (Elliot Higgins, King's College London), following the same overall strategy. For this assay samples accounting for 1/3 of total basolateral volume were taken every 30 minutes for 2 hours and replaced by an equal volume of fresh HBSS 7.4. The basolateral samples were then used in an α-IgG ELISA to determine the amount of bNAb transcytosed and total amount of transcytosed bNAb was calculated by taking the removal of 1/3 of basolateral sample at each time point into account.

The results show superior transport of 10-1074 YTE through the monolayer (Figure 4-13), supporting the results obtained from the transgenic MDCK transcytosis assay.

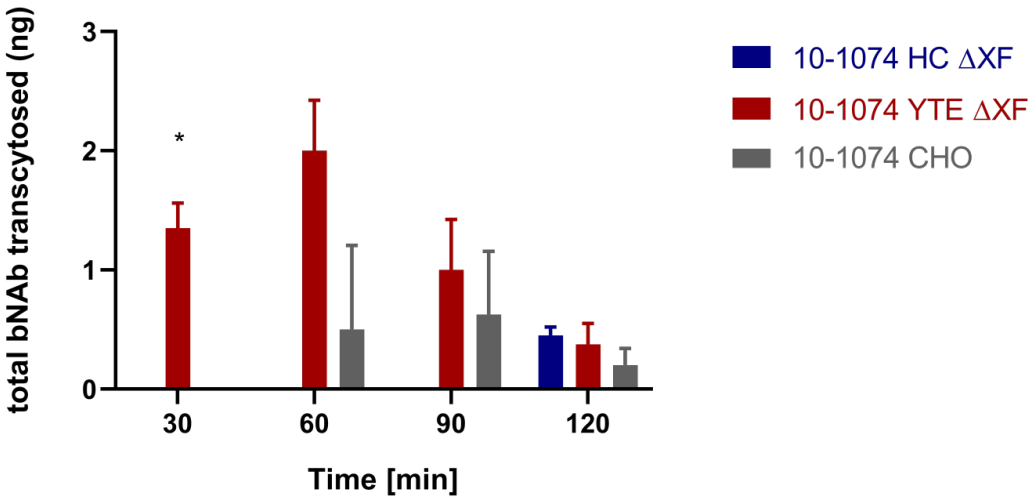

Figure 4-13: Time course study of transcytosis of respective bNAbs through a monolayer of Caco-2 cells. Means (n=2) and error bars (SD) are shown. Statistical significance was determined using a multiple t-test (Holm-Sidak method). P-values are denoted by asterisk; p≤0.05 (*), p ≤0.01 (**), p≤0.001 (***) and p≤0.0001.

4.4.2.3 *In vivo* half-life of 10-1074 is prolonged by YTE mutation

To determine the effect of the YTE mutation on the *in vivo* half-life of 10-1074 compared to the native 10-1074 (HC), half-life studies using transgenic hFcRn mice were performed. To this end mice of 7-9 weeks of age were injected with 2 mg/kg of the respective bNAb via the tail vein. As a control, PBS was injected into one mouse per study. The animal license did not allow for same day intravenous (IV) injection and blood sampling, hence the first post-injection sample was taken after 24 hours. Further samples were taken on day 4 (96h), 6 (144h), with a final sample at day 8 (192 h) for the first study. For all other studies an additional sample on day 11 (264 h), as final sample, was taken (performed by the Biological Research Facilities Team). The obtained serum was used in an α-hIgG ELISA to determine the level of bNAb for each sampling time point. In rare cases, no blood could be obtained from an individual for a specific time point, resulting in a missing data point.

For the first study, 3 mice per bNAb group were used. It has to be noted that while a defined dose of 2 mg/kg was administered, the actual dose might differ between mice, due to the difficult nature of tail vein injections. Therefore, the determined bNAb level at 24 h was considered to be c_0.

The results of this study revealed that 10-1074 HC (Figure 4-14 A) and 10-1074 YTE (Figure 4-14 B) exhibit different pharmacokinetic profiles. 10-1074 HC follows the characteristic linear profile with a first order elimination rate. All mice show less than half of c_0 at 96 hours. For subject 9035 and 9032 bNAb serum levels show an increase at 144 h compared to 96 h.

In contrast to the native version (HC), 10-1074 YTE follows a nonlinear or mixed pharmacokinetic profile, which can be observed for some drugs in case of target-mediated drug disposition (TMDD) (Peletier and Gabrielsson, 2012). Initially, there is a slow elimination phase up to 144 hours, followed by a rapid elimination phase which results in serum levels close to zero at 192 h for all subjects. Half of c_0 was reached between 144 and 192 h.

A simple method of determining half-life ($t_{1/2}$) is to extend a straight line from $y=c_0/2$ until it intercepts the respective curve. Using this approach an average for each variant with $t_{1/2\ 10\text{-}1074\ HC}$=71.33 ± 13.32 h and $t_{1/2\ 10\text{-}1074\ YTE}$= 157.00 ± 7.55 h was calculated, suggesting an improvement in $t_{1/2}$ by 2.2 times by the introduction of the YTE mutation. However, as the variants follow different profiles, direct comparison of these half-lives is insufficient to conclude an improvement in serum persistence.

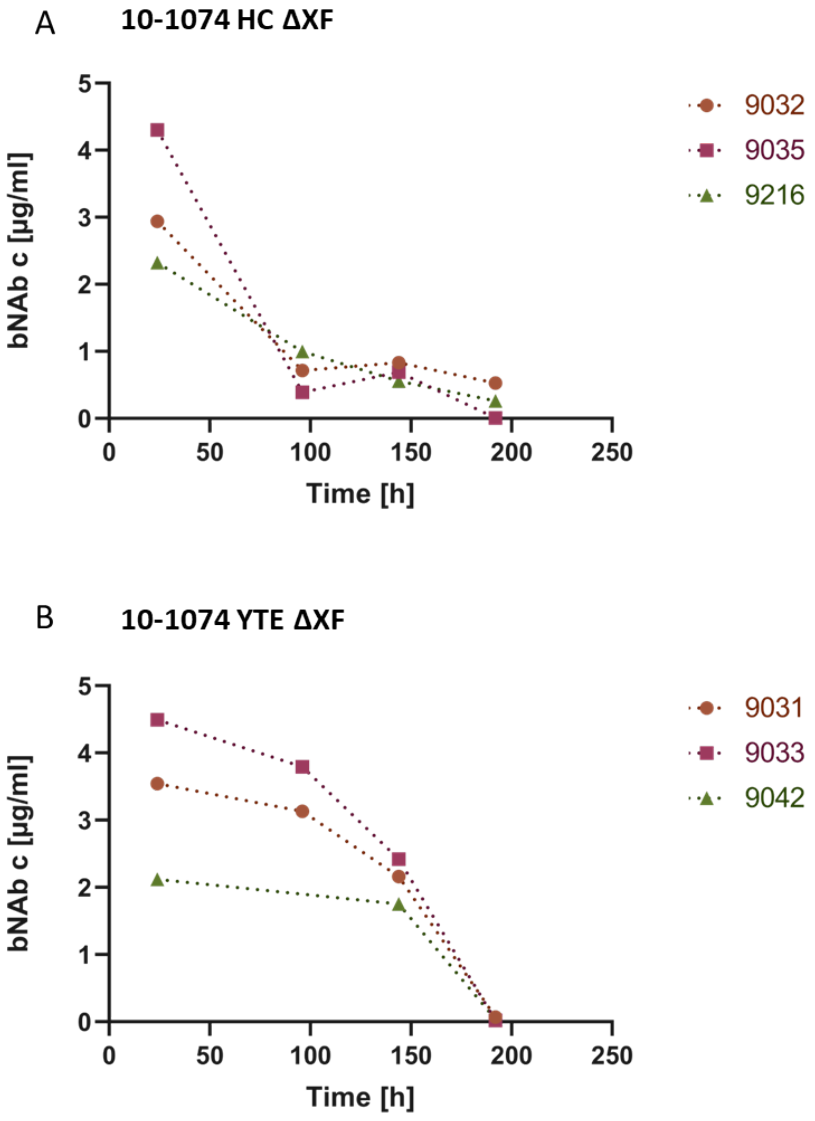

Figure 4-14: Serum concentration of two 10-1074 variants at 4 time points in individual mice A) Levels of 10-1074 HC in serum of 3 individual transgenic hFcRn mice. B) Levels of 10-1074 YTE in serum of 3 individual transgenic hFcRn mice.

To verify the trends observed in the first study, another study was performed. 5 mice were used for 10-1074 HC and 4 for 10-1074 YTE. However, one mouse (9453) was excluded from the 10-1074 HC pharmacokinetic calculation, as it demonstrated outlier results with a very different profile. Data including mouse 9453 are given in the appendix. With the exception of subject 9453, 10-1074 HC presented the same pharmacokinetic profile as in study 1 (Figure 4-15 A). However, the trend for 10-1074 YTE (Figure 4-15 B) appeared to differ from study 1. The profile up to 96 h is identical, however, the bNAb serum level drops below detection level after 144 h, whereas in study 1 60-80 percent of c_0 were still detectable. The obtained average half-life from the curve was $t_{1/2\ 10\text{-}1074\ HC}$=102.00 ± 16.25 h and $t_{1/2\ 10\text{-}1074\ YTE}$= 114.25 ± 4.79 h, which represents only a 1.12 times improvement. Due to the observed differences of 10-1074 elimination from the blood in study 1 and 2, a third experiment was performed.

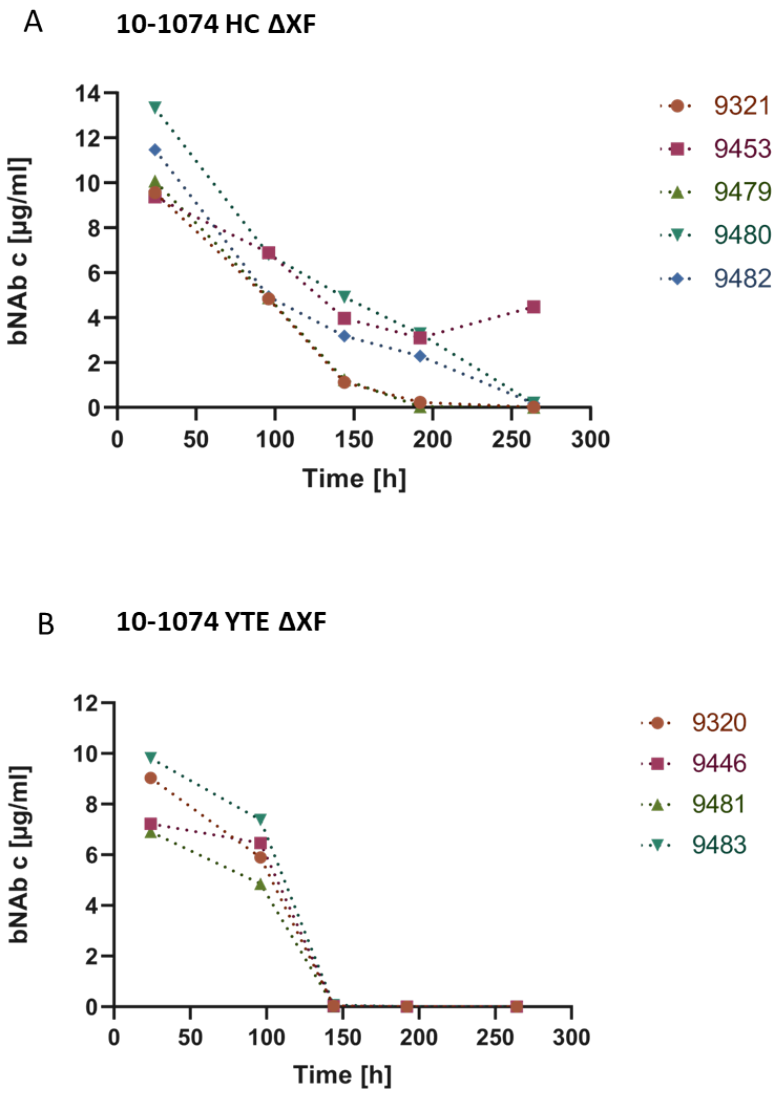

Figure 4-15: Serum concentration of two 10-1074 variants at 5 time points in individual mice A) Levels of 10-1074 HC in serum of 4 individual transgenic hFcRn mice. B) Levels of 10-1074 YTE in serum of 4 individual transgenic hFcRn mice.

For the third study 4 mice for the 10-1074 HC group and 5 for the 10-1074 YTE group were used. The trend of 10-1074 HC remains consistent (Figure 4-16 A). For 10-1074 YTE (Figure 4-16 B) the profile of 2 mice is consistent with the profile observed in study 1 and the rest with the profile of study 2 suggesting that other factors, such as e.g. experiment-related variables and/or murine immune response, might influence this trend. Estimated half-lives are $t_{1/2\ 10\text{-}1074\ HC}$=118.00 ± 7.66 h and $t_{1/2\ 10\text{-}1074\ YTE}$= 146.80 ± 32.21 h, suggesting a 1.24-fold enhancement in half-life.

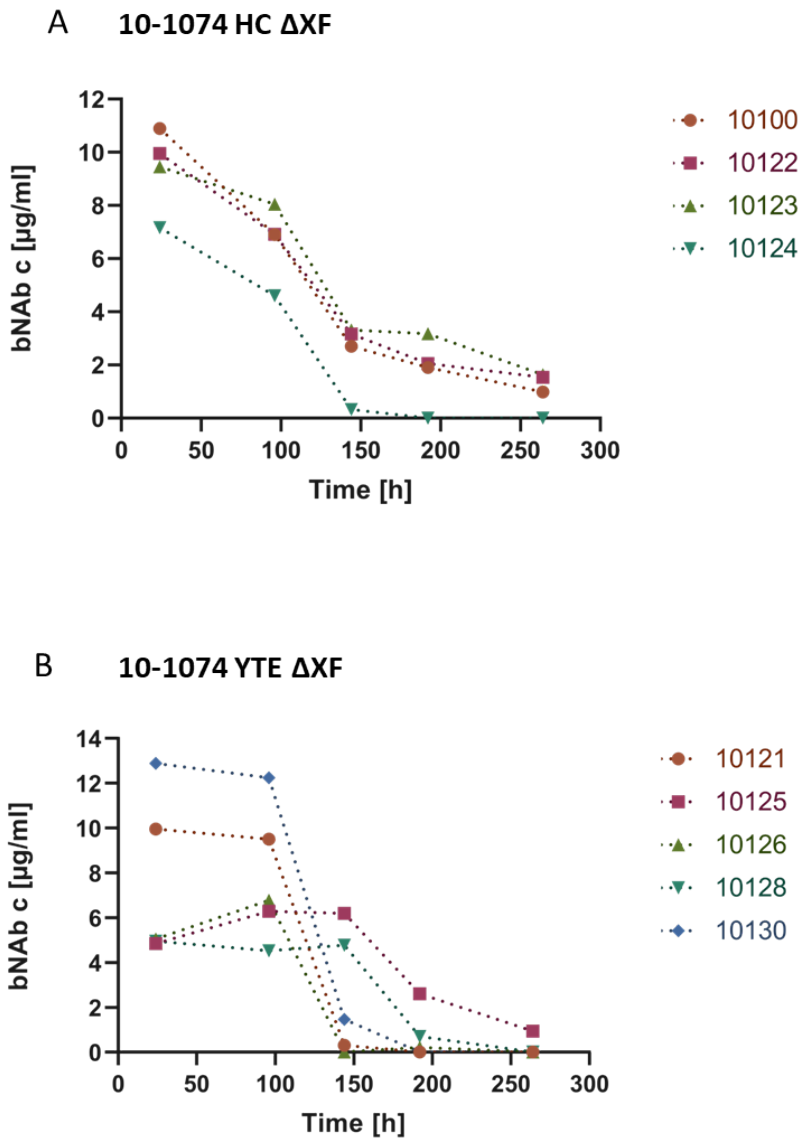

Figure 4-16: Serum concentration of respective 10-1074 variant at 5 time points in individual mice A) Levels of 10-1074 HC in serum of 4 individual transgenic hFcRn mice. B) Levels of 10-1074 YTE in serum of 5 individual transgenic hFcRn mice.

A final *in vivo* half-life study comparing the plant-produced 10-1074 HC with its CHO-produced counterpart (10-1074 CHO) was performed to evaluate the impact of change in production system on the half-life. Only two mice were assigned to the 10-1074 HC group, as consistent data was available from previous experiments. 3 mice were used for the 10-1074 CHO group. Figure 4-17 A shows the expected first order elimination for 10-1074 HC. 10-1074 CHO (Figure 4-17 B) shows a similar trend in the first 144 hours of the experiment. While mouse 737 continues following a linear pharmacokinetic profile, the other two show a rise in hIgG serum levels at 192 h, with a drop at 264

h for subject 724 but not for 728. Small increases in serum level between two time points might be attributable to recycling processes. Estimated half-lives are $t_{1/2\ 10\text{-}1074\ HC}$= 78.00 ± 2.83 h and $t_{1/2\ 10\text{-}1074\ YTE}$= 100.67 ± 21.57 h, suggesting that 10-1074 CHO has a 1.29-fold longer half-life than 10-1074 HC. It has to be noted that in case of mouse 728 the half-life estimation is particularly flawed and might stem from technical issues. However, due to the minimal blood sample size the analysis could not be repeated.

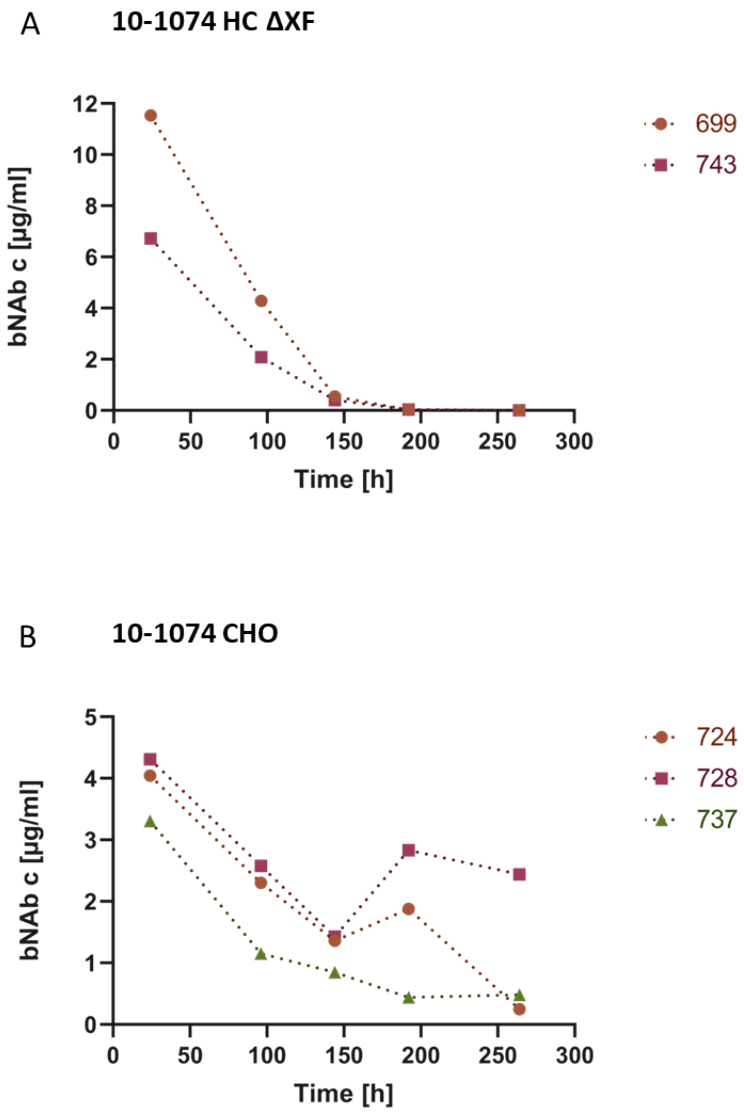

Figure 4-17: Serum concentration of two 10-1074 variants at 5 time points in individual mice. A) Levels of 10-1074 HC in serum of 2 individual transgenic hFcRn mice. B) Levels of 10-1074 CHO in serum of 3 individual transgenic hFcRn mice.

4.4.2.4 Area under the curve and clearance

Due to the differences in pharmacokinetic profile, the estimated half-lives are unreliable. In this case, the area under the curve (AUC) of the elimination curves (4.4.2.3) is a more reliable parameter to compare. The AUC is inversely proportional to clearance (L/min), thus the higher the AUC the lower the clearance, meaning that the drug resides longer in the circulation. Direct comparison of the AUC using time-concentration curves is possible if the administration of the total intended dose can be guaranteed. However, in the presented *in vivo* studies, the variability in dosing by IV tail vein injections does not allow the calculation of the AUC using the concentration as y-value, since a high c_0 would automatically lead to a greater AUC compared to the curve at a lower c_0. Therefore, each individual c_0 was assumed to be 1 (=100 % bNAb) and the amount of bNAb present at each time point calculated relative to c_0.

$$Ratio\ present\ at\ t_x = \frac{c_x}{c_0}$$

Table 4-2: Area under the curve given as mean for each study and as total mean. Standard deviation (SD) and sample size (n) are given next to mean.

Study	**10-1074 HC**			**10-1074 YTE**			**10-1074 CHO**		
	Mean	**SD**	**n**	**Mean**	**SD**	**n**	**Mean**	**SD**	**n**
1	**64.5**	13.8	3	**120.4**	8.7	3			
2	**82.9**	26.9	4	**81.2**	6.9	4			
3	**104.4**	22.3	4	**134.4**	49.0	5			
4	**59.2**	2.1	2				**115.5**	32.6	3
total	***81.6***	*26.7*	*13*	***113.2***	*38.6*	*12*	***115.5***	*32.6*	*3*

The results of the AUC calculations are shown in Table 4-2 as mean for each study and as total mean. The AUC of 10-1074 YTE is 1.87 times higher than 10-1074 HC in study 1. However, for study 2 10-1074 HC shows a similar AUC (1.02x AUC 10-1074 YTE), which stems from the sudden drop in 10-1074 YTE in the blood at 144 h. Yet, the AUC of 10-1074 YTE is 1.29 times higher than the AUC of 10-1074 HC in study 3 and the total AUC of YTE is 1.39 times higher than the one of 10-1074

HC. Overall, this indicates that the introduction of the YTE mutation into the Fc-region of 10-1074 leads to slower clearance and in turn longer half-life of the bNAb.

The highest total mean of AUC was obtained for 10-1074 CHO, which might be interpreted as being superior to the plant-generated versions of 10-1074. However, due to the small sample size used in a single study this conclusion needs to be confirmed. From the data above, it is obvious that great fluctuations in AUC can be observed between individual studies.

4.4.2.5 Differences in YTE elimination profile correlate with initial concentration

Considering that similar elimination profiles of 10-1074 YTE were detected in all mice up to 96 h post-injection, which then significantly differed after 144 h, it was speculated that other experiment-related factors must influence elimination of 10-1074 YTE, which was therefore investigated. All the following analyses were only performed for 10-1074 YTE as no considerable pharmacokinetic differences between mice and/or individual experiments were seen for 10-1074 HC and 10-1074 CHO. Thus the statements in this section solely refer to data of 10-1074 YTE.

First, the role of gender with regard to the ratio of 10-1074 YTE left in the serum at 144 h was investigated (Figure 4-18). An almost equal amount of female (n=6) to male (n=5) subjects was used for the *in vivo* half-life studies. The gender of subject 9446 was not stated in the pre-study report and was therefore excluded from this analysis. The analysis revealed that the level of serum bNAb at 144h seems to be independent of the gender of the subject (Figure 4-18).

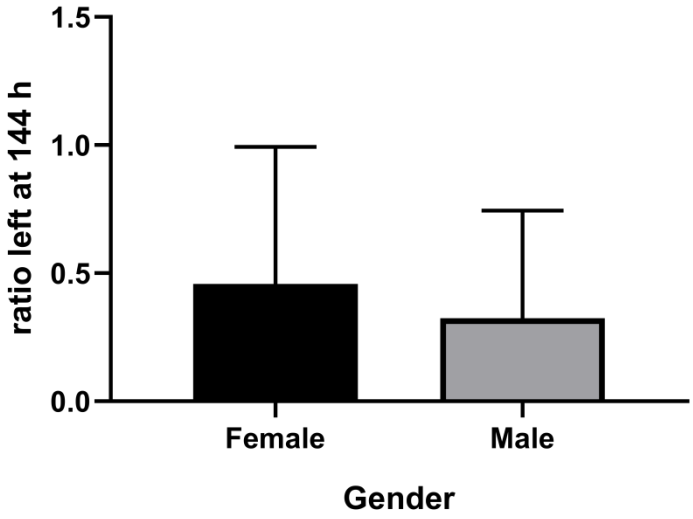

Figure 4-18: The impact of gender on the ratio of 10-1074 YTE left in serum at 144 h. Means with error bars (SD) are shown. Six female and five male mice were included in the analysis. No statistically significant difference ($p > 0.05$) was observed (Mann-Whitney Test).

Next the impact of the weight of the subjects on the pharmacokinetics of 10-1074 YTE at 144 h was examined (Figure 4-19). The analysis depicted no correlation between weight and the bNAb serum level at 144 h.

Due to lack of information about the age of each individual, the effect of age on the discrepancies at 144h could not be studied. However, as the weight of young mice generally correlates with their age, it can be assumed that there is no correlation between age of the subjects and remaining bNAb serum levels.

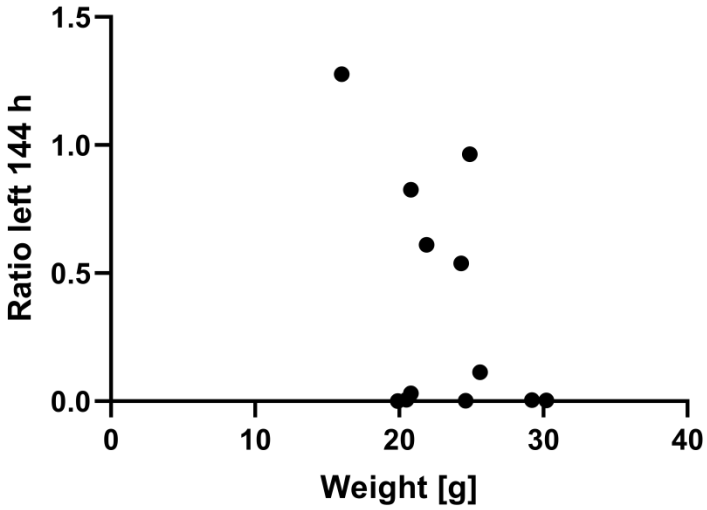

Figure 4-19: The impact of weight on the ratio of 10-1074 YTE left in serum at 144 h (n=12). No correlation between weight of the subject and bNAb level could be observed (Spearman test, p>0.05, r= -0.4698).

Lastly, the impact of the initial serum concentration c_0 was investigated (Figure 4-20). The results indicate that the initial serum level of 10-1074 YTE influences the elimination from the blood, even though the correlation seem to be not statistically significant. A c_0 below 5 µg/ml resulted in all cases in lower clearance and therefore high levels of bNAb present after 144 h, whereas a c_0 greater than 5 µg/ml resulted in almost complete elimination of the bNAb after 144 h.

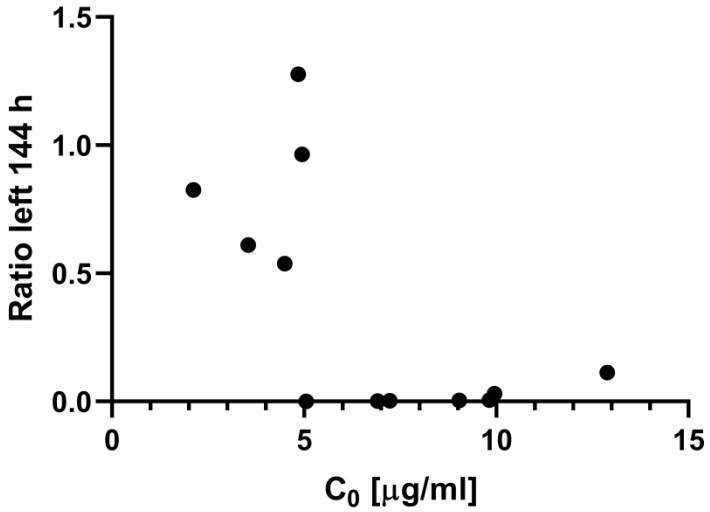

Figure 4-20: The impact of initial concentration (c0) on the ratio of 10-1074 YTE left in serum at 144 h (n=12). Not statistically significant (Spearman test, p>0.05, r= -0.5035).

4.4.2.6 Anti-drug-antibodies (ADA)

The development of neutralising anti-drug antibodies (ADA) can lead to sudden and rapid clearance of drugs, especially mAbs (Lobo, Hansen and Balthasar, 2004). As all 10-1074 variants are human antibodies, immunogenicity might occur when tested in mice. A sudden drop in 10-1074 YTE levels was observed after 144 h; thus it was assumed that any immune response would be mediated by IgM. Consequently, an anti-murine IgM ELISA with the serum samples was performed. In all cases, IgM levels are shown for serum at a dilution of 1:100 after the background was subtracted. In the following paragraph, any mention of IgM refers to murine IgM against hIgG-λ.

To determine whether the administration of the 10-1074 variants might induce an immune response the relative level of IgM (given as A450) at 24 h was compared to the level of the final sample (192 or 264 hours). No standardisation between plates was performed, therefore only changes in IgM levels of the respective subject at the start and end of the study can be evaluated. Figure 4-21 displays the results for murine IgM development against hIgG λ for each mouse. No PBS control serum sample was included for study 1, as the sample for 24 h was depleted (Figure 4-21 A). With the exception of experiment 4, samples of all individuals injected with a variant of 10-1074 display an increase of specific murine IgM over the course of the study, whereas no change in IgM levels was observed for subjects that were administered PBS. This indicates some level of immunogenicity of the human IgG variants in mice.

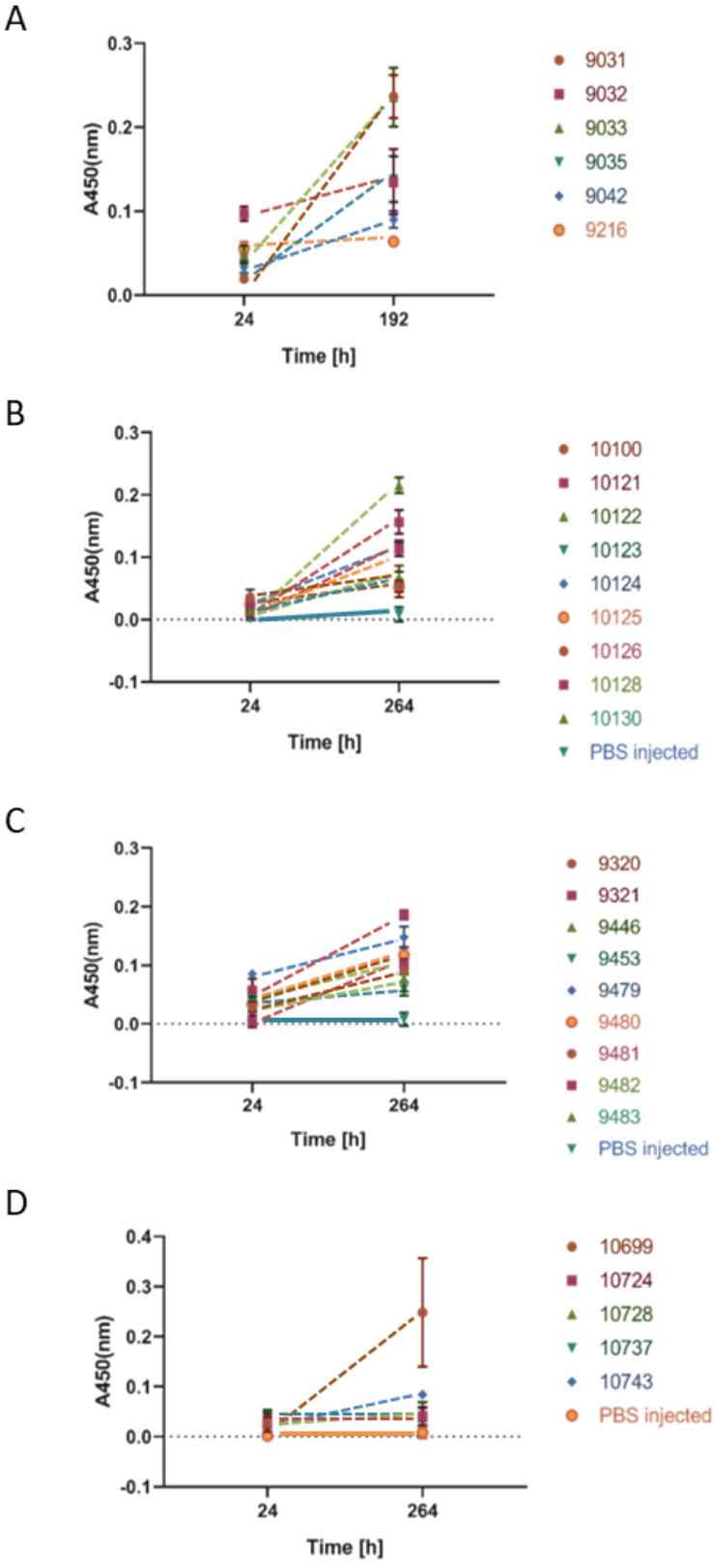

Figure 4-21: Relative IgM levels of serum diluted 1:100 at 24 h and 192 and 264 h respectively. PBS control is shown as solid line. A) Changes in IgM levels during experiment 1. B) Changes in IgM levels during experiment 2. C) Changes in IgM levels during experiment 3.D) Changes in IgM levels during experiment 4.

Subsequently, the impact of the 10-1074 variant on IgM levels was investigated. To this end, another α-IgM ELISA was performed using the final bleed sample (264 h) of 10128 as calibration sample, thus the colorimetric reaction was not stopped until 10128 reached a defined value. This allowed for comparison of relative IgM levels (A492) across different plates. Figure 4-22 shows the average serum IgM levels of the final bleed for all experiments grouped into 10-1074 HC, 10-1074 YTE and 10-1074 CHO. No significant correlation between the administered 10-1074 variant and IgM levels can be observed.

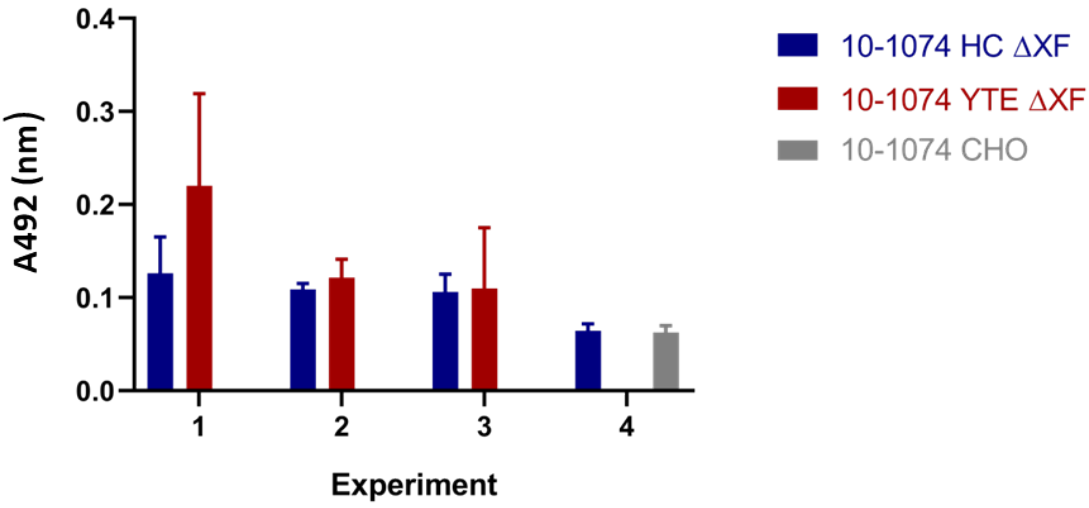

Figure 4-22: Mean and error bars (SD) of relative standardised IgM levels (serum dilution 1:100) for all experiments of 10-1074 HC (blue), 10-1074 YTE (red) and 10-1074 CHO (gray) respectively. Mann-Whitney test shows that IgM levels of each experiment are not statistically significant (p≥0.05) between 10-1074 variants.

As the analyses of experiment-related variables revealed a correlation between serum levels at 144 h and the initial serum concentration (c_0) of 10-1074 YTE, IgM levels were plotted against serum levels of 10-1074 YTE at 144 h. The final bleed of study 1 occurred 72 hours prior to that of study 2 and 3, hence data of study 1 was plotted separately (Figure 4-23 A) as IgM levels might naturally vary at different time points. In general, the analysis does not support the hypothesis that a higher c_0 results in increased immunogenicity and thus faster clearance. Though IgM levels of all other time points would be valuable information, this investigation could not be performed as only

limited blood volumes can be obtained from mice. In the majority of cases no serum was left after performing α-hIgG ELISAs to determine the *in vivo* half-life of the 10-1074 variants.

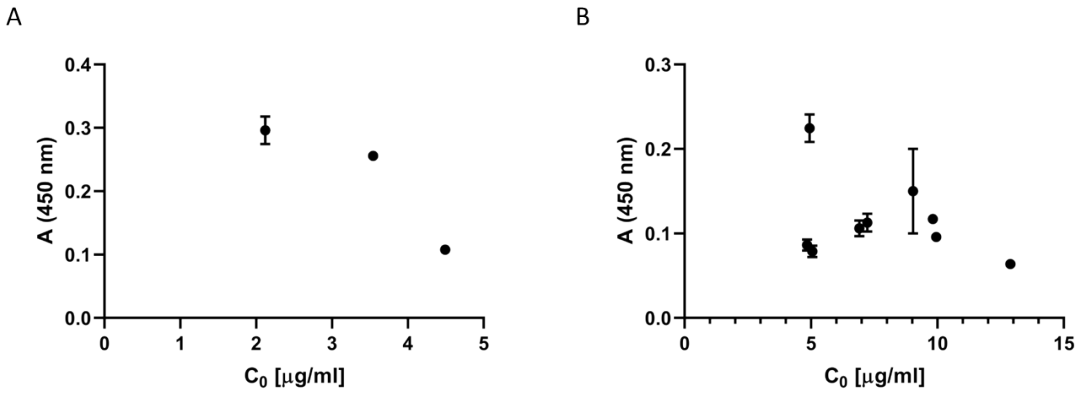

Figure 4-23: Relative IgM levels (as A450) vs c0 (µg/ml) at a serum dilution of 1:100. A) Plot for experiment 1 with IgM levels at 192 h B) Plot for experiment 2 and 3 with IgM levels at 264 h.

4.5 Discussion

The comparison of the three 10-1074 variants, namely 10-1074 HC ΔXF, 10-1074 YTE ΔXF and 10-1074 CHO revealed that the plant-produced variants (ΔXF) are likely to enhance *in vivo* ADCC and that the introduction of the YTE mutation resulted in improved *in vitro* transcytosis and reduced *in vivo* clearance.

4.5.1 Affinity to FcγRIIIa and ADCC

Afucosylation of mAbs has shown to result in an up to 100-fold increase in antibody affinity to the FcγRIIIa receptor (Ferrara *et al.*, 2011) and in turn in a significant increase in ADCC activity (Pereira *et al.*, 2018). The removal of α (1,3)-fucose from the *N*-glycan of 10-1074 also led to an improvement in affinity to FcγRIIIa V158, however, only by 5-fold. This discrepancy to the data presented by Ferrara et al. (2011) may partly stem from a limited model fit for the kinetics of the two plant-produced 10-1074 versions. However, even a perfectly fitted kinetic model would not result in a 100-fold improvement.

Affinities to receptors differ between IgGs specific for various antigens (see 3.5) and a recent study has shown that the Fab-region participates in the interaction of IgG1 with FcγRIIIa (Yogo *et al.*, 2019). Therefore the variable region might also influence the magnitude of affinity improvement by afucosylation. This is supported by studies that revealed a 10-fold affinity improvement of afucosylated Rituximab (Okazaki *et al.*, 2004) but only a 3.2 fold improvement of the affinity of Pertuzumab (Luo *et al.*, 2017) compared to their fucosylated counterpart.

The capturing methods for the respective SPR measurements differed. An anti-Fab antibody was used to capture IgG by Ferrara *et al.* (2011), whereas in this project protein A was used to capture IgG via the Fc-region. While capturing an IgG with protein A by its Fc-region may result in steric hindrance of other ligands, it is improbable in the case of FcγRIIIa which binds to the CH2

domain close to the hinge region (Vidarsson, Dekkers and Rispens, 2014), whereas protein A binds between the CH2 and CH3 domain (Wines *et al.*, 2000).

The ADCC activation assay exhibited the expected result of increased ADCC of the plant-produced afucosylated 10-1074 variants compared to the fucosylated CHO produced 10-1074 variant. While similar observations were made in several studies (Shields *et al.*, 2002; Okazaki *et al.*, 2004; Luo *et al.*, 2017), direct comparisons cannot be made, as different assays were used. Differences in ADCC activation were more pronounced when using effector cells expressing the V158 polymorphism than when expressing the F158 polymorphism. This is in accordance with previous research that highlights the lower affinity of the FcγRIIIa F158 allotype (Koene *et al.*, 1997) which in turn results in lower ADCC, therefore possibly higher bNAb concentrations would be needed for clear differences to be observable. However, as SPR measurements were not performed with the F158 allotype for all three 10-1074 variants, it is not clear whether the lowered ADCC activation improvement by removal of the core fucose only stems from less enhancement of affinity to the receptor.

The ADCC activation assay not only revealed the impact of afucosylation on ADCC but also indicated that the introduction of the YTE mutation might negatively impact ADCC. While this was not confirmed by the subsequently performed ADCC activity assay, this phenomenon has been reported in previous studies. MEDI-522 YTE showed a 2-fold reduction in affinity to FcγRIIIa when tested with the F158 allotype compared to the native MEDI-522 (Etaracizumab). ADCC assays further revealed a reduction in cytotoxicity from around 30 percent (MEDI-522) to 10 percent (MEDI-522 YTE) (Dall'Acqua, Kiener and Wu, 2006). Similarly, the YTE version of Rituximab showed lower affinity to both allotypes, which further resulted in a reduction of ADCC from 40 to 30 percent and 25 to 20 percent for the V158 and F158 allotype respectively. In contrast to the aforementioned studies, only a reduction by 0.3-fold in affinity of 10-1074 YTE to FcγRIIIa V158 compared to 10-1074 HC was observed by SPR.

As already mentioned, the ADCC activity assay failed to support the observations made in the ADCC activation assays. Not only did it suggest that the YTE mutation improves ADCC but also showed no difference between the fucosylated (CHO) and afucosylated (HC ΔXF) version of 10-1074. This result, however, was from a single experiment. Different storage times of the used 10-1074 variants might have influenced the result, as prolonged storage can lead to increased aggregation due to partial or complete unfolding of the mAb (Bansal, Dash and Rathore, 2020; Wälchli *et al.*, 2020). As the outcome of the ADCC activity assay not only contradicts the results obtained in other assays but also common observations made in literature, this result needs to be confirmed using freshly produced 10-1074 variants.

4.5.2 FcRn affinity and transcytosis

For antibodies carrying the YTE mutation a 10-fold affinity improvement to FcRn at pH 6 and no impact on dissociation at pH 7.4 was reported (Dall'Acqua, Kiener and Wu, 2006). While the SPR spectra clearly demonstrated a higher affinity of 10-1074 YTE to FcRn, the degree of enhancement could not be determined due to modelling issues that arose from the limitations of the chosen SPR assay strategy. No alternative strategies were successful, including the often utilised commercially available anti-Fab capture kit. It is probable that some of these strategies failed due to the machine being limited to only one running buffer, therefore all steps, including antibody capturing, had to be performed at pH 6. A similar approach to the one utilised in this study, was applied to determine the binding kinetics of FcRn to various Fc mutants, including YTE. Chips were coated with the respective IgG-Fc mutant, however, the setup allowed for more than one running buffer (Acqua *et al.*, 2002). Despite the lack of kinetic parameters that can be directly compared, it is obvious that 10-1074 YTE has favourable binding characteristics compared to 10-1074 HC.

This was further supported by the transcytosis assays, which showed that more bNAb is transported across a monolayer of cells expressing FcRn when carrying the YTE mutation. *In vitro*

transcytosis assays have proven to be a good indicator of *in vivo* clearance for antibodies that were engineered to modulate binding to the neonatal receptor (Jaramillo *et al.*, 2017).

4.5.3 *In vivo* half life

The *in vivo* half-life studies revealed an up to 46 percent reduction in clearance of 10-1074 when modified with the YTE mutation, which is consistent with the *in vitro* data. The average reduction in clearance of 29 percent of 10-1074 when modified with YTE, is in accordance with data from other studies that investigated half-life extension in the Tg276 hFcRn mouse model (Kang *et al.*, 2018; Valente *et al.*, 2020). In general, half-lives of the same mAbs in Tg276 hFcRn transgenic mice are up to 4.5 times shorter than in NHPs (Valente *et al.*, 2020). Yet, pharmacokinetic data obtained from hFcRn mice has proven to correlate with pharmacokinetics observed in NHPs and humans, thus is reliable in predicting favourable pharmacokinetic profiles (Tam *et al.*, 2013; Avery *et al.*, 2016). The magnitude of changes in pharmacokinetic parameters, however, might differ between species and is generally less pronounced in Tg276 mice when compared to NHPs, often showing more than a 2-fold difference (Ko *et al.*, 2014; Borrok *et al.*, 2015; Kang *et al.*, 2018).

Considerable differences in clearance profiles of 10-1074 YTE were detected between experiments and/or individual mice. Correlation analysis revealed that mice with an initial plasma concentration below 5 µg/ml of 10-1074 YTE retained the bNAb for longer, whereas initial concentrations higher than 5 µg/ml resulted in accelerated clearance after 96 h. While dose-dependent elimination is well-documented, no reports of this specific trend could be found. Rapid drops in mAb levels are normally observed when ADA occurs. A study by Rosenberg *et al.* (2019) revealed that the normally non-Immunogenic bNAb PGT121 led to ADA when modified with the YTE mutation. This development led to sudden rapid clearance between day 7 and 14 (Rosenberg *et al.*, 2019), as observed in the performed half-life studies. According to the IgM data, only 3 out of 12 mice injected with 10-1074 YTE showed statistically significantly higher IgM levels (analysis not shown) than mice injected with 10-1074 HC. Furthermore, higher IgM levels do not correlate with

higher c_0. This suggests that immunogenicity does not increase with higher doses. Indeed, studies have shown that ADA is more likely to occur at lower doses and lower serum concentrations, than when mAbs are given in excess (Chaigne and Watier, 2015). Another possible explanation for rapid clearance at a higher initial concentration is the saturation of the neonatal receptor, thus instead of being recycled, unbound antibody will be degraded, which would lead to a sudden decrease in bNAb (Jin and Balthasar, 2005). However, in this scenario some residual level of bNAb is expected, as the bNAbs that are bound to the receptor and lead to saturation, would be released back into the serum. This hypothesis is further refuted by half-life experiments in the same hFcRn mice which were performed with antibody doses of up to 10 mg/kg (Proetzel and Roopenian, 2014). Yet, it is unknown if and how the expression level of hFcRn in these specific transgenic mice changes with age and breeding. Data on the expression levels in all different organs showed highest expression in the liver of these transgenic hFcRn mice (Li and Balthasar, 2018). While a comparison of expression levels in the liver of ten mice after 3 rounds of breeding was attempted using flow cytometry and western blots (data not shown), the results were inconclusive and would have been insufficient to provide accurate insights. In order to reliably quantify and monitor expression, analysis using several organs of a significant number of mice per generation would have been necessary, which was unfeasible in the scope of this project.

The observed pharmacokinetic profile for the bNAb modified with YTE seems to be rather unique. Most studies showed a first-order elimination profile for any mAb with YTE mutation (Dall'Acqua, Kiener and Wu, 2006; Robbie *et al.*, 2013; Ko *et al.*, 2014; Borrok *et al.*, 2015; Griffin *et al.*, 2016; X. Q. Yu *et al.*, 2017; Domachowske *et al.*, 2018; Rosenberg *et al.*, 2019), however, the majority of those studies were performed in either NHPs or human subjects. Yet, motavizumab-YTE displayed a similar elimination trend to 10-1074 YTE in 3 out of 4 cynomolgus monkeys, while showing a linear profile in transgenic mice (Borrok *et al.*, 2015). Even though the authors neither further investigated nor discussed this trend, it corroborates the here presented mixed elimination profile.

While a mixed elimination profile is typical for target-mediated drug disposition (TMDD), TMDD cannot explain the trend observed for 10-1074 YTE. TMDD results in dose-dependent changes in the PK profile, which are commonly seen for drugs, such as mAbs, that bind their target antigen at high-affinity (Ovacik and Lin, 2018). The characteristic mixed profile stems from an initial linear elimination rate during target-saturation where clearance is mainly mediated by the FcRn. At lower mAb concentrations, a nonlinear elimination rate can be observed, as clearance is partially caused by receptor-mediated endocytosis triggered through mAbs antigen-specific interactions (Ryman and Meibohm, 2017; Ovacik and Lin, 2018). Since the experiments were performed in uninfected mice, receptor-mediated endocytosis could not have taken place.

The performed *in vivo* half-life studies not only revealed enhanced half-life and reduced clearance for 10-1074 YTE, but also exposed the more favourable pharmacokinetic profile of 10-1074 CHO compared to 10-1074 HC. These two native bNAbs only differ in the expression system used for their production, thus both the Fc- and Fab-region are identical, which is further supported by the presented *in vitro* data, which showed comparable antigen-binding and neutralisation potency (3.4.6, 3.4.7) and nearly identical transcytosis profiles in MDCK hFcRn/hβ_2m cells. This indicates that factors besides FcRn-binding are involved in serum half-life. As the main difference between 10-1074 HC and 10-1074 CHO is the production host, discrepancies in either quality or glycosylation of the bNAb are the most plausible explanation for the detected pharmacokinetic differences. 10-1074 CHO was not expressed in-house but was obtained from CFAR (Dr. Michel C. Nussenzweig) and was produced for a clinical trial; hence this bNAb will be of higher purity and quality than 10-1074 HC. Furthermore, plant-produced bNAbs tend to show a higher amount of degradation products than their mammalian counterparts (Hehle *et al.*, 2011, 2015; Donini *et al.*, 2015). These degradation products not only contribute to the measured concentration of the bNAb, but are likely to be eliminated faster than fully assembled antibodies. Secondly, the presence of sialic acid on the N-glycan has shown to result in longer half-life compared to desialylated mAbs (Bas *et al.*, 2019). As plants do not perform sialylation naturally, it is probable that the lack of this glycan

moiety leads to faster clearance compared to 10-1074 CHO, however, further experiments are necessary to confirm this hypothesis.

The data presented here and in chapter 3 demonstrated that ΔXF *N. benthamiana* is able to produce a modified version of the bNAb 10-1074 with the potential of enhanced ADCC, transcytosis and *in vivo* half-life, without negatively impacting its high neutralisation potency.

5 Generation of a stable ΔF *N. tabacum* plant line using CRISPR/Cas9

5.1 Introduction

This chapter focuses on the generation of a stable α1,3-fucosyltransferase deficient (ΔF) *N. tabacum* cv. Petit Havana SR1 plant line, which requires the knockout of α1,3-fucosyltransferase (*FucT*) genes. Currently, the most efficient and straightforward way to achieve a complete knockout is by gene-editing using CRISPR/Cas9. In this project, the most common system, wild-type Cas9 from *S. pyogenes* with non-homologous end joining (NHEJ) was used.

The need for plant-lines expressing proteins which are lacking non-human like glycans, namely α(1,3) fucose and β(1,2) xylose, was recognised when plant-molecular farming started to be established as an alternative to mammalian expression systems (Buyel, 2019). At that time, CRISPR/Cas9 was not developed. Therefore, other techniques were employed to achieve this goal. In *Arabidopsis thaliana* the *FucT* and *XylT* genes were knocked out using T-DNA insertion – inserting foreign DNA into those genes to disrupt their function (Strasser *et al.*, 2004). In *Physcomitrella patens*, a moss, *FucT* and *XylT* genes were knocked out using homologous recombination. This technique is not normally applied in plants due to the low frequency of this event; however, uniquely moss shows a high rate of homologous recombination (Kamisugi *et al.*, 2006). Genes were - similarly to the T-DNA approach- disrupted by replacing small fragments of the gene with a selection cassette (Koprivova *et al.*, 2004). In the case of *N. benthamiana*, transcription activator-like effector nucleases (TALENs) were employed to achieve disruption of the *FucT* and *XylT* genes. However, while this strategy resulted in a complete knockout of *XylT*, for *FucT* it only led to a reduction in overall fucosylation, (Li *et al.*, 2016).

As gene knockouts often require laborious rounds of transformation and screening, other approaches to impair the function of the transferase genes, such as silencing using RNA interference (RNAi) (Fire *et al.*, 1998), were used. In contrast to a traditional knockout, this approach can be

utilised transiently, as demonstrated by Biolex Therapeutics. Co-expression of their target mAb with a single RNAi construct targeting the *XylT* and *FucT* gene in *Lemna minor*, a small aquatic plant, resulted in a product lacking α(1,3) fucose and β(1,2) xylose (Cox *et al.*, 2006). Yet, RNAi was more commonly used to create transgenic plant lines with substantial *FucT* and *XylT* knockdown. An important example is the widely used ΔXF *N. benthamiana* plant line, which was generated by transforming wild-type *N. benthamiana* with either a *XylT*-RNAi or *FucT*-RNAi construct, followed by crossing the best *XylT*-RNAi and *FucT*-RNAi line to obtain the ΔXF line (Strasser *et al.*, 2008). This strategy was also applied to achieve products lacking xylose and fucose produced in tobacco BY-2 cells, using a binary RNAi construct targeting both, *XylT* and *FucT* (Yin *et al.*, 2011). However, RNAi does not guarantee complete inactivation of the targeted gene products, as observed in *Medicago sativa* (alfalfa) for *FucT* and *XylT*, which translated only in a reduction of fucosylation (86%) and xylosylation (80%) (Sourrouille *et al.*, 2008). Furthermore, our own observations showed varying levels of residual fucosylation and xylosylation on glycoproteins generated in the aforementioned ΔXF *N. benthamiana* line (Strasser *et al.*, 2008) . Although gene-silencing via RNAi was successful in almost completely eliminating α(1,3) fucose and β(1,2) xylose from therapeutic proteins expressed in some of these plant lines, the system does not provide the same consistency as a knockout line.

While interference with the function of these two transferase genes would appear to be potentially disruptive, none of the above mentioned studies have reported alterations in phenotype, plant development, growth and protein secretion, regardless of the approach used to achieve a deletion or knockdown. This suggests that neither α1,3-fucosyltranferase nor β1,2 xylosyltransferase, which both act on proteins to perform *N*-glycosylation (Bencúr *et al.*, 2005; Soto, Urbanowicz and Hahn, 2019), are essential for plant growth and development, which raises questions about the function of fucosylation and xylosylation of proteins. Little is known about the role of *N*-glycosylation in plants, especially about the function of individual glycan moieties. In contrast to the previously mentioned knockout studies, lack of α(1,3) fucose on the *N*-glycan of rice (*Oryza sativa*) resulted in morphological and developmental changes, such as decreased shoot

growth, root elongation and delayed flowering time (Harmoko *et al.*, 2016). Furthermore, a recent study showed that *A. thaliana* plant lines deficient in active α(1,3)-fucosyltransferase exhibited increased susceptibility to pathogens (Zhang *et al.*, 2019). This negative effect on plant-immunity may not have been detected for the aforementioned knockout or knock-down lines, due to being cultured in controlled environments. This finding could lead to implications for ΔF or ΔXF plants, which are intended for large scale cultivation, as significant crop-loss could occur by reduced resistance to plant-pathogens. Then again, the extent of weakened immunity to pathogens might vary between different plants and should be determined after the establishment a ΔF or ΔXF line, if intended for open-field applications.

5.2 Specific Objectives

- Design of suitable sgRNAs for *FucT* knockout in *N. tabacum*
- Synthesis and cloning of the designed sgRNAs
- Testing of cutting efficiency of the designed sgRNAs
- Selection of suitable sgRNAs to generate a transgenic ΔF *N. tabacum* SR1 line
- Stable transformation of *N. tabacum* SR1 with sgRNA/Cas9 constructs via ex-plant
- Breeding and analysis of putative knockout lines

5.3 Contributions

- Retrieving of FucT mRNA sequences and design of sgRNAs was performed by Dr Audrey Teh. All the following PCR steps and cloning steps were performed by me.
- The tRNA-gRNA construct was cloned into pCR-BluntII-TOPO by Dr Audrey Teh. All the subsequent steps were performed by me.

5.4 Results

5.4.1 Design and synthesis of sgRNAs

All available mRNA sequences of the *N. tabacum FucT* gene were retrieved from GenBank and aligned using Clustal Omega. None of the retrieved mRNA sequences were obtained from *N. tabacum* cultivar SR1. Additionally, gene walking was performed to determine intron sites, in order to avoid designing sgRNAs that span an intron (Appendix). This is imperative as a gene knockout by CRISPR/Cas9 using NHEJ is based on the introduction of indels into coding regions to induce gene disrupting frameshift mutations.. Four of the mRNA sequences were obtained from *N. tabacum* cultivar TN90 (XM_016657530.1; XM_016620229.1; NM_001324945.1; XM_016585847.1) and one from cultivar Bright Yellow (AB498916.1) (see 2.2.1.1). Two (*FucT* 4 and 5) of the five retrieved sequences significantly differed from the other three sequences and lack 45 and 54 bp at the beginning of the gene, respectively. As the impact of these missing base pairs on the functionality of the protein is not known, these two sequences were considered to potentially represent a pseudogene. The aligned sequences were scanned for the protospacer-adjacent motive (PAM) specific to *S. pyogenes* Cas9 (NGG) (performed by Dr Audrey Teh). Twelve 20 nucleotide (nt) sequences upstream of a PAM starting with the base 'G' (for U6 promoter; first bases can also be changed to 'G' if necessary) were chosen to be used as single guide RNAs (sgRNAs; see Appendix for all sgRNA sequences and their corresponding regions in the *FucT* gene). Most of the designed sgRNAs recognise either the gene or the pseudogene, only one sgRNA could be designed recognising both (F6, Appendix). To generate the sgRNAs, the approach shown in Figure 5-1 was utilised. In the first round of PCR, pUC119-gRNA served as template. Two PCRs were performed. Primer R1 and Primer F2 both have the respective 20 nt sequence and an pUC119-gRNA overlap. The universal primer F1 and primer R2 carry the desired restriction sites and an overlap to pUC119-gRNA. By combining F1 with R1 and F2 with R2, two products containing a restriction site and the 20 nt sequence were amplified. In the second round, the purified product 1 and 2 were used as template

and only the universal primers were used for amplification, yielding the full-length sgRNA with the U6 promoter and restriction sites for cloning.

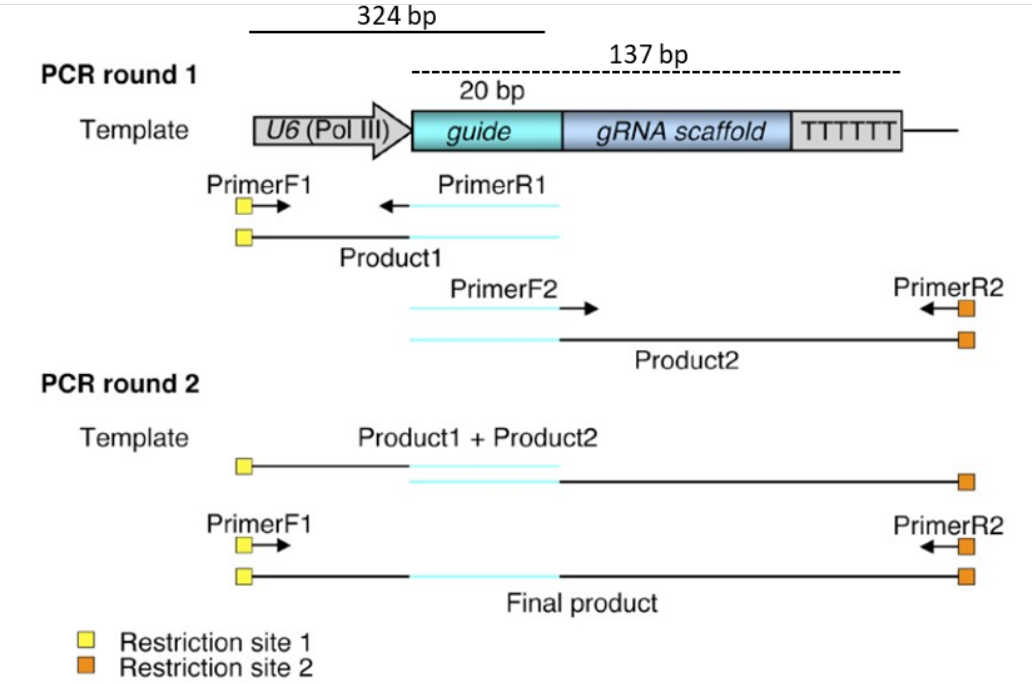

Figure 5-1: Generation of sgRNA. During the first round of PCR, the custom sgRNA 20 nt sequence was introduced via PrimerR1 and PrimerF2. The restriction sites for cloning were contained in PrimerF1 and PrimerR2. During 2nd round of PCR, the complete sgRNA together with the U6 promoter and the restriction sites was amplified (Adapted from Li et al. 2013).

Figure 5-2 displays a representative result. The results of the first round of PCR can be seen in Panel A in Figure 5-2. Product 2 (Fxf) is shorter than product 1 (Fxr). Both PCRs yielded strong, clear bands which were purified and used to generate the full-length sgRNA (Panel B, Figure 5-2). The second round of PCR produced the desired amplicons of the expected size around 400 bp.

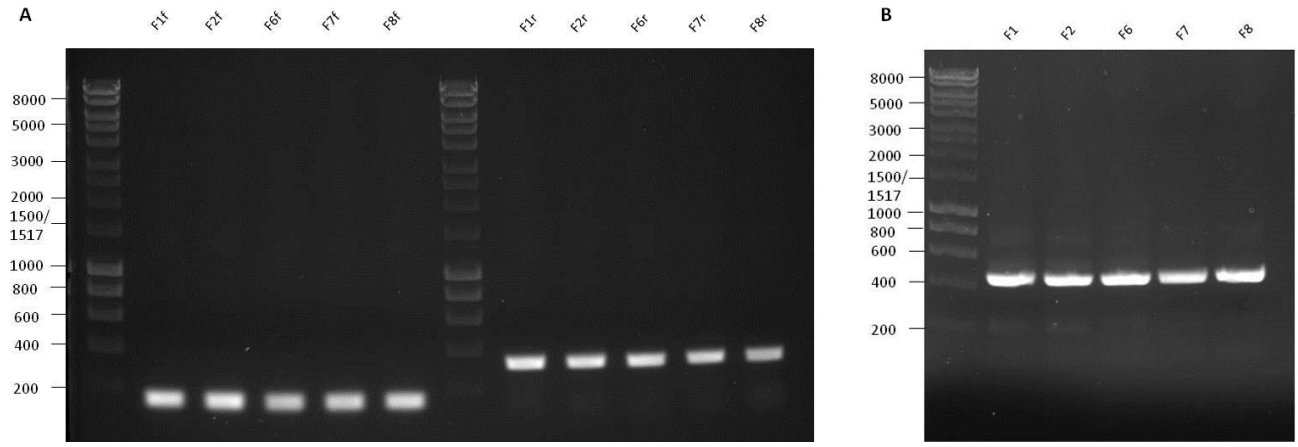

Figure 5-2: Representative results of PCRs to amplify the sgRNAs of choice. A) First round of PCR. A strong band for product 2 (F1f, F2f, F6f, F7f, F8f) was visible below 200 bp. Product 1 (F1r, F2r, F6r, F7r, F8r) was longer. The band can be observed slightly below 400 bp. B) Final sgRNA product. The bands of the full-length product (F1, F2, F6, F7, F8) can be detected slightly above 400 bp.

The final product was cloned into the pFGC- pcoCas9 vector (Figure 5-3)(Li *et al.*, 2013) via the restriction sites introduced by PCR. The plasmid was proliferated in *E. coli*, extracted and analysed by restriction digest with XhoI and XmaI (Figure 5-4 A). F1, F2, F7 and F8 were cloned into the vector using SbfI and PacI, thus the band of the insert can be observed slightly below 600 bp. All other sgRNAs were cloned into the vector using AscI and PacI show bands at 600 bp. F1 shows a second band around 1000 bp, however, in a digest with SbfI and PacI no additional band was observed (Figure 5-4 B). DNA of clones exhibiting the correct restriction profile was sent for sequencing to verify the presence of the correct 20 nt sequence. Confirmed pFGC-pcoCas9/sgRNA plasmids were transformed into *A. tumefaciens* GV3101/PMP.

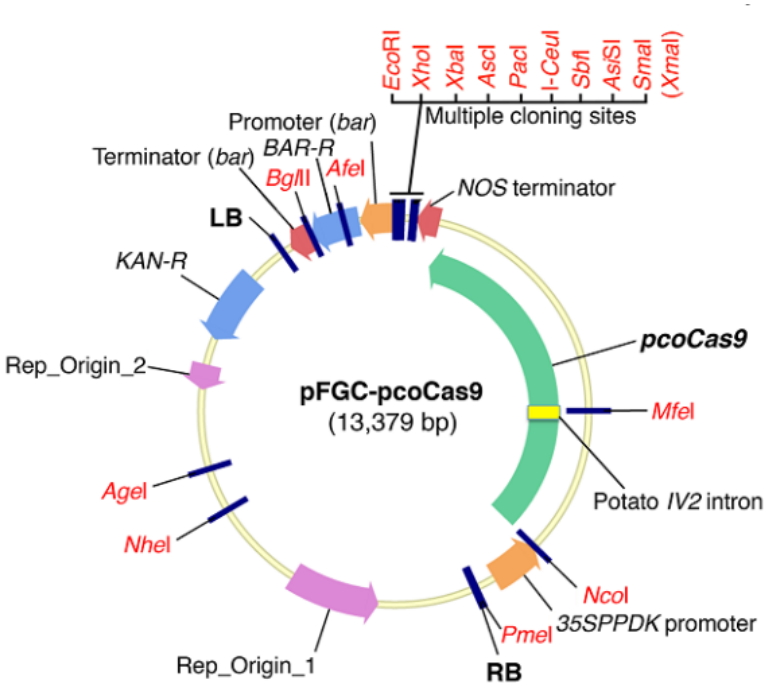

Figure 5-3: pFGC-pcoCas9 vector (Addgene number ID 52256). Plasmid carrying a plant-codon optimised Cas9 (pcoCas9) under a 35S promoter. sgRNA was cloned into the multiple cloning site using the desired restriction sites. The U6 promoter was cloned into the multiple cloning site together with the sgRNA. The plasmid carries a kanamycin resistance gene as selective marker. ((Li *et al.*, 2013)

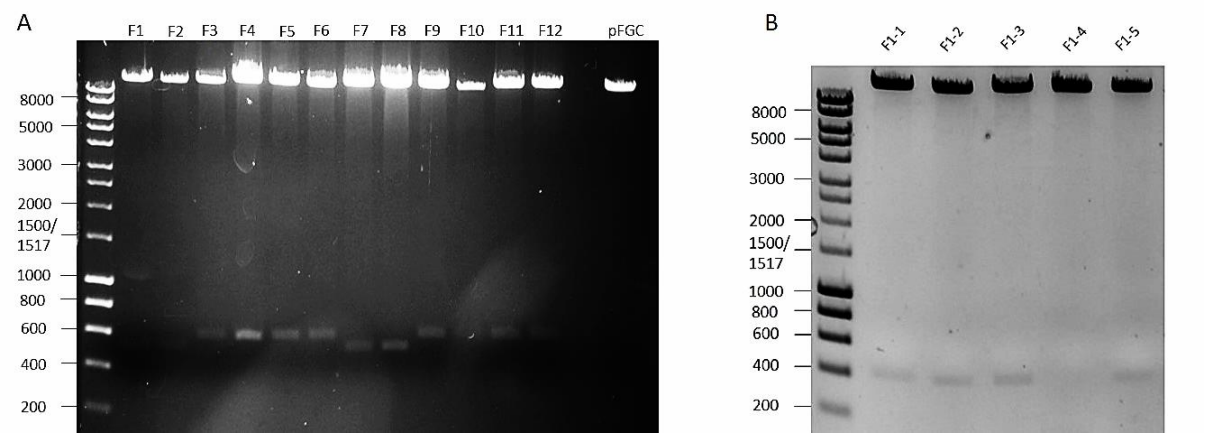

Figure 5-4: A) Digest of all pFGC-pcoCas9/sgRNA plasmids with XhoI and XmaI. The vector without insert (labelled pFGC) was used as control. B) Digest of all F1 transformants with SbfI and PacI.

5.4.2 The selected sgRNAs successfully introduce indels into the fucosyltransferase gene

The cutting efficiency of Cas9 is dependent on the respective sgRNA (Moreno-Mateos *et al.*, 2015), thus each sgRNA was tested individually with regard to its efficacy in introducing indels into the *FucT* gene. Leaves of wild-type *N. tabacum* cv. SR1 were syringe-infiltrated with *A. tumefaciens* harbouring the respective sgRNA construct. Two leaves were infiltrated per sgRNA, serving as biological duplicates. Two days post infiltration, the leaves were harvested and DNA from each leaf was extracted separately. Additionally, the DNA of non-infiltrated wild-type leaves was extracted as control. The occurrence of indel events was analysed via Indel Detection by Amplicon Analysis (IDAA) (Yang *et al.*, 2015), a capillary gel electrophoresis technique (performed by Eurofins Genomics, Ebersberg, Germany). The sgRNA targeted site of the gene was amplified in a tri-primer PCR, in which the extracted DNA served as template. Primers flanking the region of interest (cutting site) were used, together with a FamF primer, carrying a 6-Fam at its 5'end. Possible products are the wild-type (wt) amplicon, as well as amplicons that carry an insertion or deletion. Each primer set was also used to amplify the same region of non-edited wild-type *N. tabacum*, which served as control.

The results were analysed by comparing the potentially gene-edited DNA with the wild-type DNA. The amplicon size of the wild-type peak can be determined using the alignment and by knowing where the respective primers bind. Upon identification of the wild-type peak, peaks with amplicon sizes slightly above or below the wild-type amplicon size indicate an insertion or deletion event.

Table 5-1 displays the result for two sgRNAs, F1 and F2, each performed in biological duplicates (Fx-1, Fx-2). The sequences recognised by F1 and F2 are both located between the FucT1 primer pair. The expected amplicon size for the wild-type peak (in italics) was 226 bp (including the Fam extension). The peak is present in all the samples including the wild-type (WT 1), however, peaks with sizes of 231 and 240 bp are also present for the gene-edited samples, indicating that an insertion event has taken place.

Table 5-1: IDAA result for the sgRNAs F1 and F2. The height and peak area for each amplicon size (size) represent the occurrence of that particular peak. The wild-type peak is given in italics.

Sample	Size	Height	Peak Area	Size	Height	Peak Area	Size	Height	Peak Area
F1-1	*226.51*	*1512*	*16555*	231.01	432	4004	240.21	3879	46668
F1-2	*226.24*	*4934*	*83660*	231.11	467	4475	240.2	3428	45397
F2-1	*226.14*	*4893*	*79119*	230.85	7513	110709	240.24	7493	98190
F2-2	*226.6*	*4344*	*82009*	231.05	1355	13121	240.21	8895	157021
WT 1	*226.27*	*2366*	*19862*						

To calculate the editing efficiency of the sgRNAs it was assumed that the sum of the peak areas of the wild-type peak and the indel peaks represents 100 percent. For each of the individual peaks the percentage of peak area (thus presence in the genome) was calculated.

$$\%\ of\ presence\ in\ genome = \frac{Area\ of\ Peak}{\sum wt + indel\ peaks} * 100$$

Figure 5-5 shows that the sgRNAs F1 and F2 led to an edit rate of almost 80 percent. However, the biological duplicates of F1 differ in their mutation rate (80 % to 40 %). In Table 5-2 the cutting efficiency of the individual sgRNAs is given as average of the biological duplicates for the percentage of the wild-type (WT) peak and indel peaks present in the genome. For sgRNAs with target regions amplified by either the FucTa or FucT4 primer, the predicted wild-type peak could not be found in the results, suggesting possible differences in the *FucT* sequence of the SR1 plant line used compared to the sequences used to design the sgRNAs. Therefore, the peak closest to the predicted wild-type peak, that was present in all samples, was used for determining the editing efficiency of these sgRNAs.

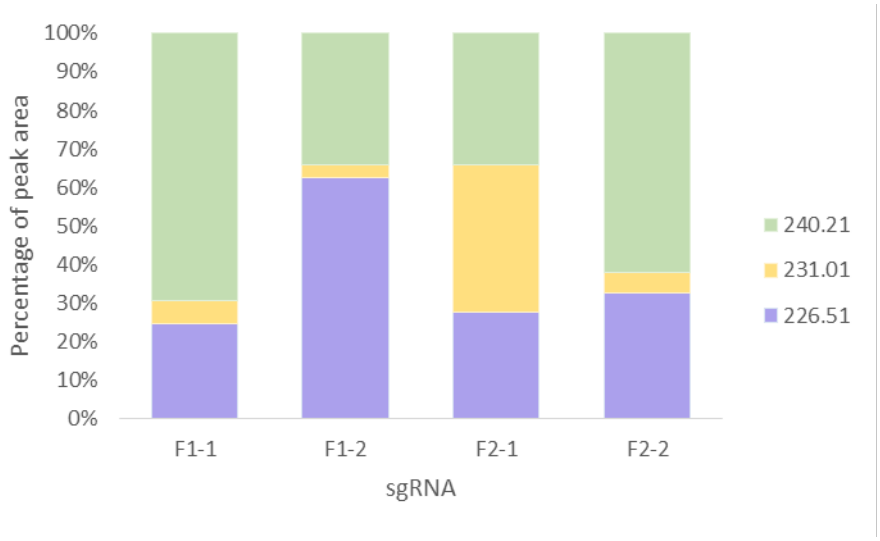

Figure 5-5: Percentage of peak areas for gene-editing events induced by the sgRNAs F1 and F2. Fx-1 and Fx-2 represent the biological duplicates of the sgRNAs. The wild-type peak (226 bp) is given in blue, the insertion peaks are given in yellow (231 bp) and green (240 bp)

Table 5-2: Cutting efficiency of individual sgRNAs determined by IDAA. Average percentage of occurrence indel peak for each sgRNA is given.

sgRNA	% Indel
F1	57.5
F2	77
F3	22
F4	20
F5	100
F6	80
F7	64
F8	9
F10	70
F11	78.5
F12	20

Based on high cutting efficiencies F5, F6 and F7, were chosen for the first stable transformation. F10 showed slightly higher cutting efficiency than F7, however, F7 recognises a sequence in the first exon and was therefore given priority over F10. Additionally F1 was chosen for the co-transformation approach, as it cuts at the very beginning of the *FucT* gene and would maximise the chance of functional disruption.

5.4.3 Stable transformation of explant using co-transformation with individual *FucT* sgRNAs results in no detectable change in fucosylation

To perform the co-transformation of *N. tabacum* SR1 with the four *FucT* sgRNAs, individual *A. tumefaciens* GV3101/PMP cultures carrying either the F1, F5, F6 or F7 sgRNA, were grown separately overnight. Sterile leaf discs of *N. tabacum* SR1 were incubated in an equal mixture of the four sgRNA *A. tumefaciens* cultures. After 48 hours of co-cultivation, leaf discs were transferred onto regeneration medium with selection until shoots formed. Individual shoots were transferred into individual jars with MS Agar and grown until roots developed. The plantlets were then further cultivated in soil and analysed after a few weeks of growth. In total 20 regenerated plants were obtained.

Screening of transgenic plants was performed using an anti-α(1,3) fucose antibody for dot blotting and ELISA. Total soluble protein was extracted from two leaf discs per plant. The crude extract was used for further analyses and compared to fucosylation detection in *N. tabacum* wild-type and *N. benthamiana* ΔXF plants. For the dot-blot, 2 µL of each protein extract were pipetted onto a nitrocellulose membrane and, after drying, the membrane was blocked and incubated with primary and secondary antibody. The results of the dot-blot suggest a reduction in fucosylation in a few transgenic plants, namely 6,7,8,14 and 16 (Figure 5-6). Plant line 15 showed a signal comparable to that of the ΔXF control; however, Ponceau S staining revealed a lower amount of total protein present for plant line 15 on the membrane than for all other samples, therefore this low signal most likely resulted from the lack of total protein. All other samples showed a comparable or elevated protein level to the wild-type control.

Figure 5-6: Screening of the 20 T_0 plant line by dot-blots. Fucosylation in the crude extract was detected using an anti-α(1,3) fucose antibody (upper blot) and presence of total proteins was confirmed by Ponceau S stain (bottom blot).

Dot blots are relatively insensitive (Villafañez, Gottifredi and Soria, 2019), so to further analyse potential changes in fucosylation levels induced by CRISPR/Cas9, three lines with apparent reduced fucosylation and two lines with apparent enhanced fucosylation were assayed in an anti-α(1,3) fucose ELISA. The total protein content of selected samples was determined using BCA assay. To perform the anti-α(1,3) fucose ELISA wells were coated with the crude plant extracts at seven different dilutions. Anti-α(1,3) fucose antiserum was used as primary antibody and an anti-rabbit-HRP as secondary antibody (Figure 5-7). The results revealed the expected reduction for the ΔXF plant line. In contrast, no change in fucosylation, neither increase nor decrease, compared to the wild-type control could be detected for any of the selected transgenic lines.

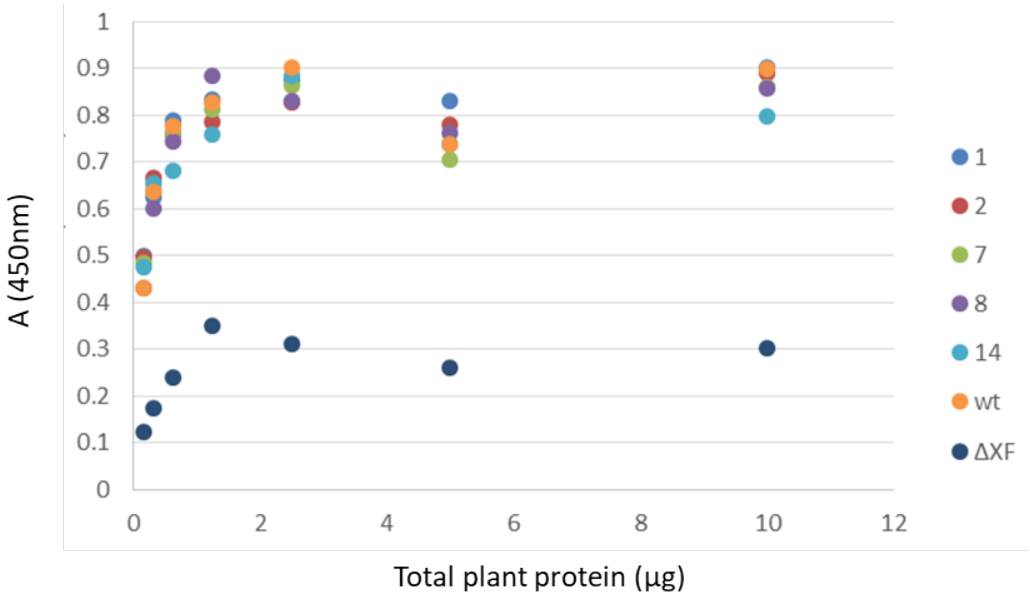

Figure 5-7: Anti-α(1,3) fucose ELISA for selected T_0 plant lines resulting from co-transformation with four sgRNAs. Wells were coated with seven different amounts of total protein extract of the selected T_0 plant lines.

5.4.4 Stable transformation of explant using tRNA-gRNA strings

To increase the likelihood of four sgRNAs entering the same cell, a polycistronic tRNA-gRNA approach was utilised (Xie, Minkenberg and Yang, 2015). In this system the individual sgRNA sequences are separated by a tRNA sequence. The primary transcript is then processed and RNase P and RNase Z remove the tRNA, releasing the individual sgRNAs (Figure 5-8). For this approach five sgRNAs, namely F2, F5, F6, F7 and F11, were chosen. SgRNA F2 replaced sgRNA F1 which was initially chosen due to cutting at the very beginning of the *FucT* gene, however, the cutting site of sgRNA F2 is similarly relatively close to the start of the gene and F2 displayed better cutting efficiency than F1. Furthermore, F11 was added to obtain an equal number of sgRNAs specific for the gene and putative pseudogene.

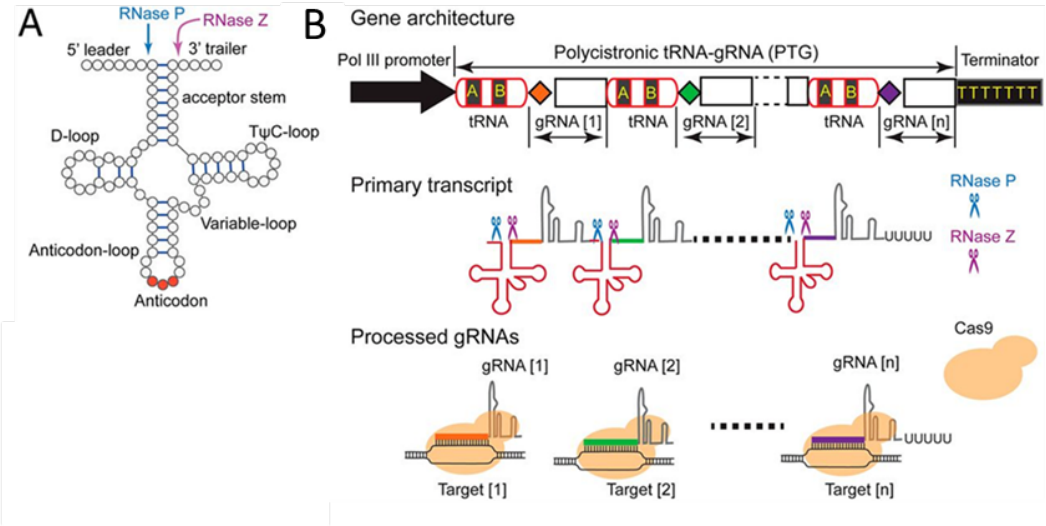

Figure 5-8:.(A) RNase P and RNase Z cleave the eukaryotic pre-tRNA at specific sites. (B) Schematic illustration of the polycistronic tRNA-gRNA (PTG)/Cas9 system for targeting multiple sites at the same time. The synthetic PTG *consists of tRNA-gRNA elements arranged in tandem, with each sgRNA containing a target-specific spacer (depicted as differently coloured diamonds) and conserved gRNA scaffold (rectangle). Endogenous RNase P and RNase Z (scissors) cleave the primary PTG transcript to release mature sgRNAs and tRNA (shown as cloverleaf structure). The mature sgRNAs direct Cas9 to their specific targets. Adapted from* Xie, Minkenberg and Yang, 2015

The tRNA-gRNA string was synthesised (GeneArt) and cloned into pCR-BluntII-TOPO vector (performed by Dr Audrey Teh), as PCR based approaches to clone the string into the destination vector were unsuccessful, due to the repetitiveness of the string sequence. The U6 promoter was

cloned into the pFGC-pcoCas9 vector and strings cloned into pFGC-pcoCas9-U6 using GoldenGate assembly with BsaI. Transformants were sequenced to confirm the presence of the complete string. The plasmid was then transformed into *A. tumefaciens* GV3101/PMP.

Stable transformation and regeneration of transgenic plants was performed as described in 5.4.3. To select for plant cells with the integrated cassette, 3 µg/ml glyphosate (PESTANAL) were added to the regeneration medium. In total the transformation yielded 14 viable transgenic plants. To screen for possible knockouts the previous strategy of screening for the presence of α(1,3) fucose was chosen. Samples were adjusted to the same concentration and an anti-α(1,3) fucose western blot was performed. The initial western blot (Figure 5-9) suggested complete knockouts for line tgF7, 13 and 14, as no bands could be observed for these three transgenic lines, whereas a signal could be detected for the negative (*N. tabacum* wild-type) but not for the positive control (*N. benthamiana* ΔXF). However, upon re-extraction of proteins and repetition of the analysis, bands could be observed for the three putative knockout lines (see Appendix). Nevertheless those lines were chosen for further breeding as they still exhibited a reduction in fucosylation compared to the wild-type control.

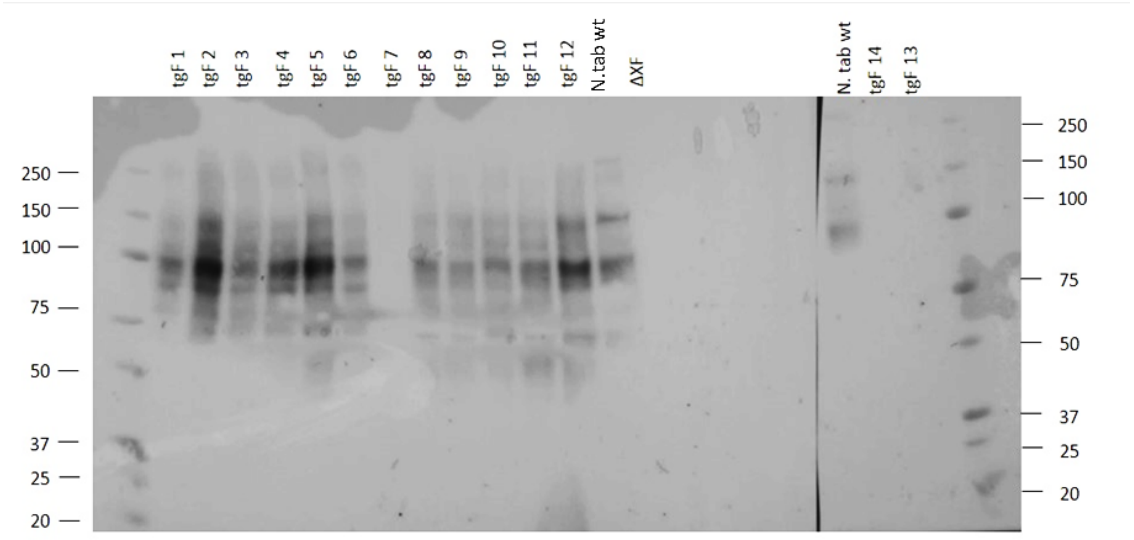

Figure 5-9: Anti-α(1,3)-fucose western blot for selected T_0 lines with samples adjusted to the same concentration

5.4.5 T_1 transgenic plant lines show editing for at least one sgRNA

To generate the T_1 transgenic plant lines, T_0 lines tgF 7, 13 and 14 were self-crossed, seeds collected and sterilised. Single seeds were placed onto MS medium containing 3 µg/ml PESTANAL as selection marker. For tgF 7 and 14 the majority of seeds germinated and grew into plantlets. In case of tgF 13, only one out of 20 seeds developed into a plantlet, suggesting that the rest was not carrying the expression cassette. Plantlets were transferred to soil and grown until mature enough for analysis.

Initial screening was performed by dot-blot with an anti-α(1,3) fucose antibody (Figure 5-10). The dot blots revealed a few plant lines that seemed to have reduced or completely absent fucosylation. The membranes were also stained with Ponceau S prior to blocking to confirm protein binding. Missing numbers in the dot-blots are from seeds that failed to develop into a plantlet.

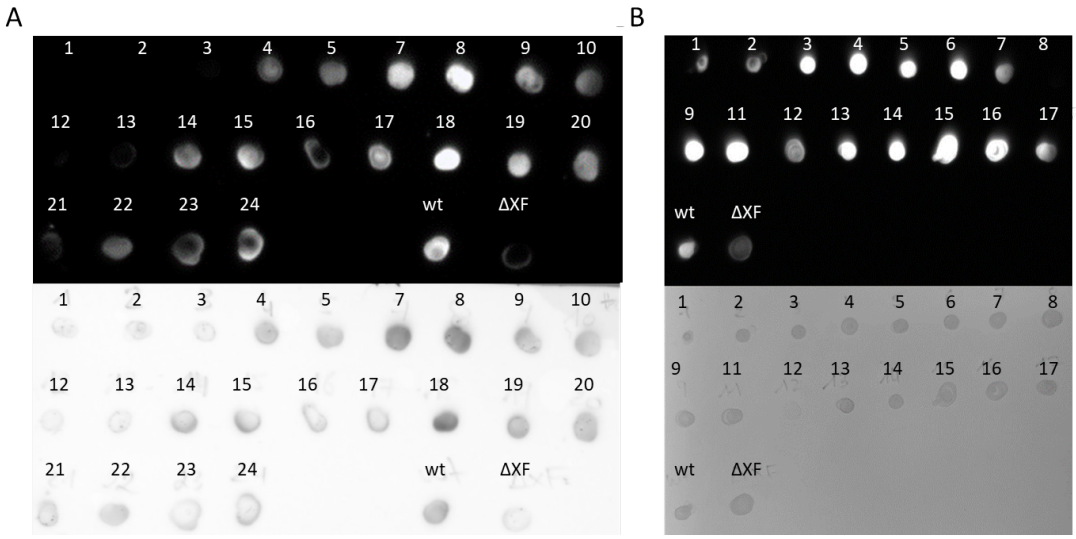

Figure 5-10: Dot blot screening of T1 plant line 7 (A) and 14 (B) using crude extract and anti-α(1,3)-fucose antibody. Upper blot shows immunoblot, lower blot shows protein present on the membrane visualised with Ponceau S stain.

To obtain a better idea of the degree of fucosylation reduction, protein samples from selected plant lines were adjusted to the same concentration and a western blot and SDS-PAGE were performed. The SDS-PAGE (Figure 5-11 B) demonstrates equal loading of total protein for each

sample onto the western blot. However, the results obtained by western blot analysis (Figure 5-11 A) do not match the results of the dot blot. This is most obvious when comparing results for T_1 14-8, which shows no signal on the dot-blot and similar protein concentrations to the rest of the samples. However, a stronger signal for T_1 14-8 than for the wild-type control was obtained for the western blot. Having observed variability when repeating screens with the anti-α(1,3) fucose antiserum, the specificity of the antibody was questioned. No cross-reactivity with either xylose or other plant extract components was stated as part of the description of the antibody, whereasa published dot-blot (www.agrisera.com) shows absence of a signal for Fetuin (Fuc-,Xyl-), but a signal can be seen for Mur1-2 (Fuc-,Xyl+).

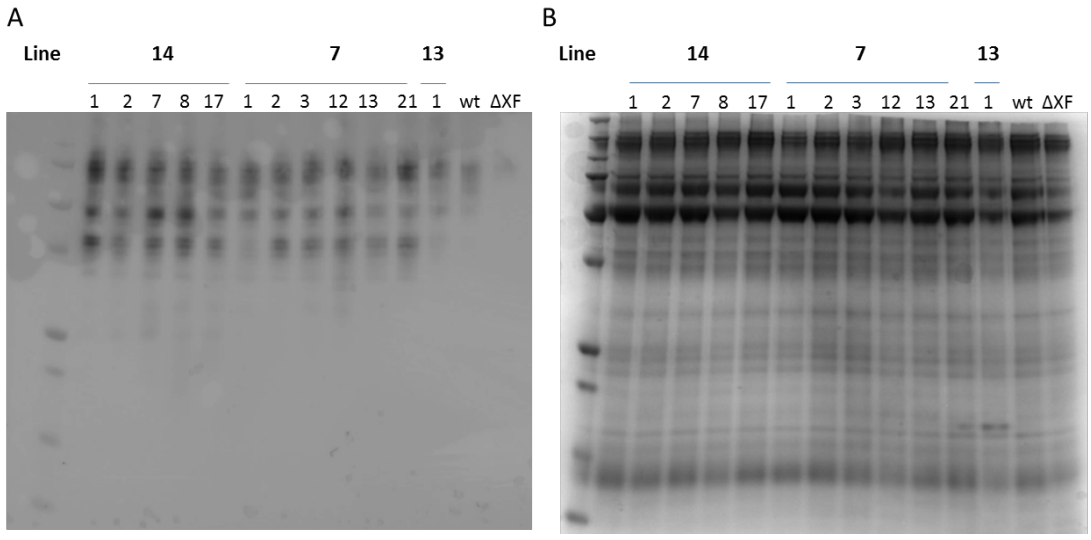

Figure 5-11: Anti-α(1,3)-fucose western blot for selected T_1 lines with samples adjusted to the same concentration (A). SDS-PAGE stained with Coomassie Brilliant Blue to confirm samples loaded onto the western blot were of comparable concentrations (B).

Therefore a genetic approach was used for further screening of putative knockout lines. The previously selected T_1 plant lines were re-analysed using Synthego's ICE (Inference of CRISPR Edits) Analysis tool, which is based on comparing sequences of amplification products of the wild-type to putative knockouts and assigning those two different scores; an ICE score and a KO score. The ICE score gives the percentage of indels present in the putative knockout compared to the wild-type and the KO (knockout) score indicates how many of these would most likely result in a knockout. Thus, if

a plant lines has an ICE score of 95%, but all indels are three base pairs or a multiple of three, the KO score would be 0.

For ICE analysis, DNA from the plant lines of interest was extracted using REDExtract-N-Amp™ (Sigma Aldrich) and amplified using Phusion Polymerase and primers flanking the regions of the putative cutting sites (Table 5-3).

Table 5-3: Primers flanking cutting sites of sgRNAs used in the tRNA-gRNA construct

Primer	sgRNA
FucTa	F7
FucT1	F2
FucT3	F5
FucT4	F6 and F11

Altogether, 4 PCRs per plant line had to be performed to screen for all 5 sgRNAs. Successful amplification was verified by gel electrophoresis and PCR products purified and sent for Sanger sequencing. Sequencing chromatograms were used to perform the ICE analysis.

ICE analysis is shown for sgRNA F5, F7 and F11 in Figure 5-12. Hardly any editing efficiency was observed for F7. F5 showed two lines with ICE and KO score of around 90 percent and F11 displayed ICE and KO scores of over 90 percent for five lines. Amplicons from FucT1 could be purified, however the resulting chromatograms resulted in inconclusive ICE results, even upon repetition of the PCRs. Therefore no ICE and KO scores were obtained for sgRNA F2. The primer (FucT4) covers two cutting sites in F11 and F6. However, the cutting site of F6 was too close to the beginning of the initially used FucT4 reverse primer, so the site could not be identified during the T_1 analysis. The primer was redesigned for T_2, but T_1 decisions on which plants to breed further were based on the results for F5 and F11 (Figure 5-12).

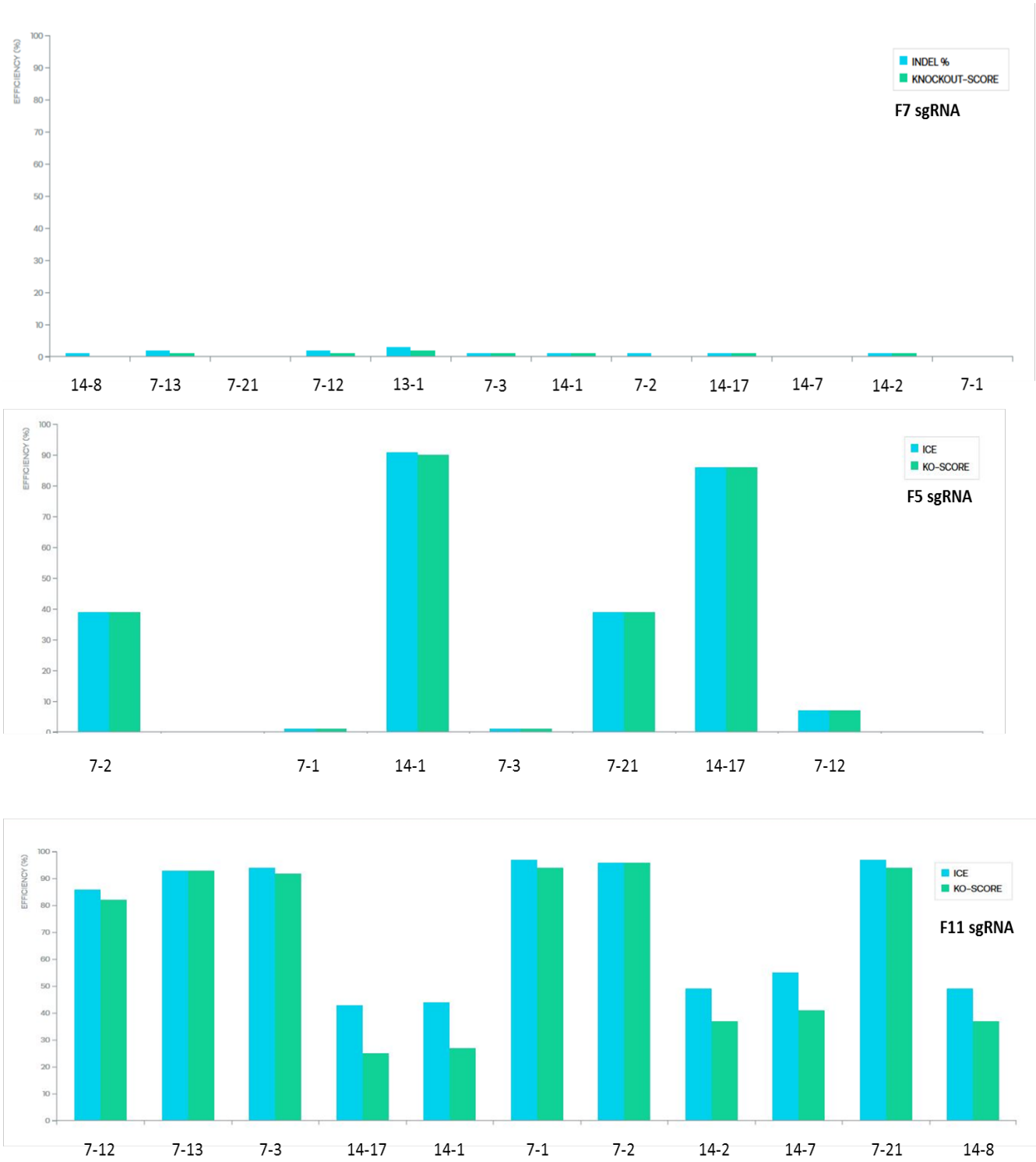

Figure 5-12: Results of ICE Analysis for selected T1 lines for sgRNAs F7 (top), F5 (middle) and F11 (bottom). ICE score is represented by blue bars and the KO score by green bars.

T_1 lines 14-1, 14-17 and 7-2, 7-21 were considered especially promising candidates for further breeding, as they showed high KO scores for one of the sgRNAs and medium KO scores for the other sgRNA.

5.4.6 T_2 lines reveal a high number of editing events

To generate the T_2 lines, the chosen T_1 lines were cross-fertilised and/or self-fertilised (Table 5-4). Seeds were grown directly on soil as it was assumed that all progeny of the chosen T_1 lines would contain the expression cassette. Plants were screened by ICE Analysis as described in 5.4.5. As parent lines only displayed minimal editing efficiency for sgRNA F7 and ICE failed for F2, these gRNA targets were excluded during the initial screening process.

Table 5-4: Parentage of T_2 putative ΔF lines

Label	Parent 1	Parent 2
A	14-1	7-13
B	14-1	7-21
C	14-7	7-21
D	14-17	7-21
E	14-1	7-2
F	14-1	14-17
T2 14-1	self	
T2 14-7	self	
T2 7-21	self	

For each T_2 plant line around 10 plants were screened. Occasionally, the guide RNA sequence could not be found in the amplified part of the DNA of the respective plant, thus no scores were assigned to the sample (for complete results see Appendix). For a few other samples, analysis failed, as the quality of the scores of the sample was considered too low. One repeat was attempted in such cases, however, this did not always result in usable chromatograms. Several plant lines exhibited low editing efficiency for both sgRNAs, whereas some showed high ICE scores that resulted in very low knockout scores (data see Appendix). Based on the obtained ICE results, a selection of

plants from three T_2 lines, which displayed the most favourable ICE and KO scores, were chosen for further analysis (Figure 5-13).

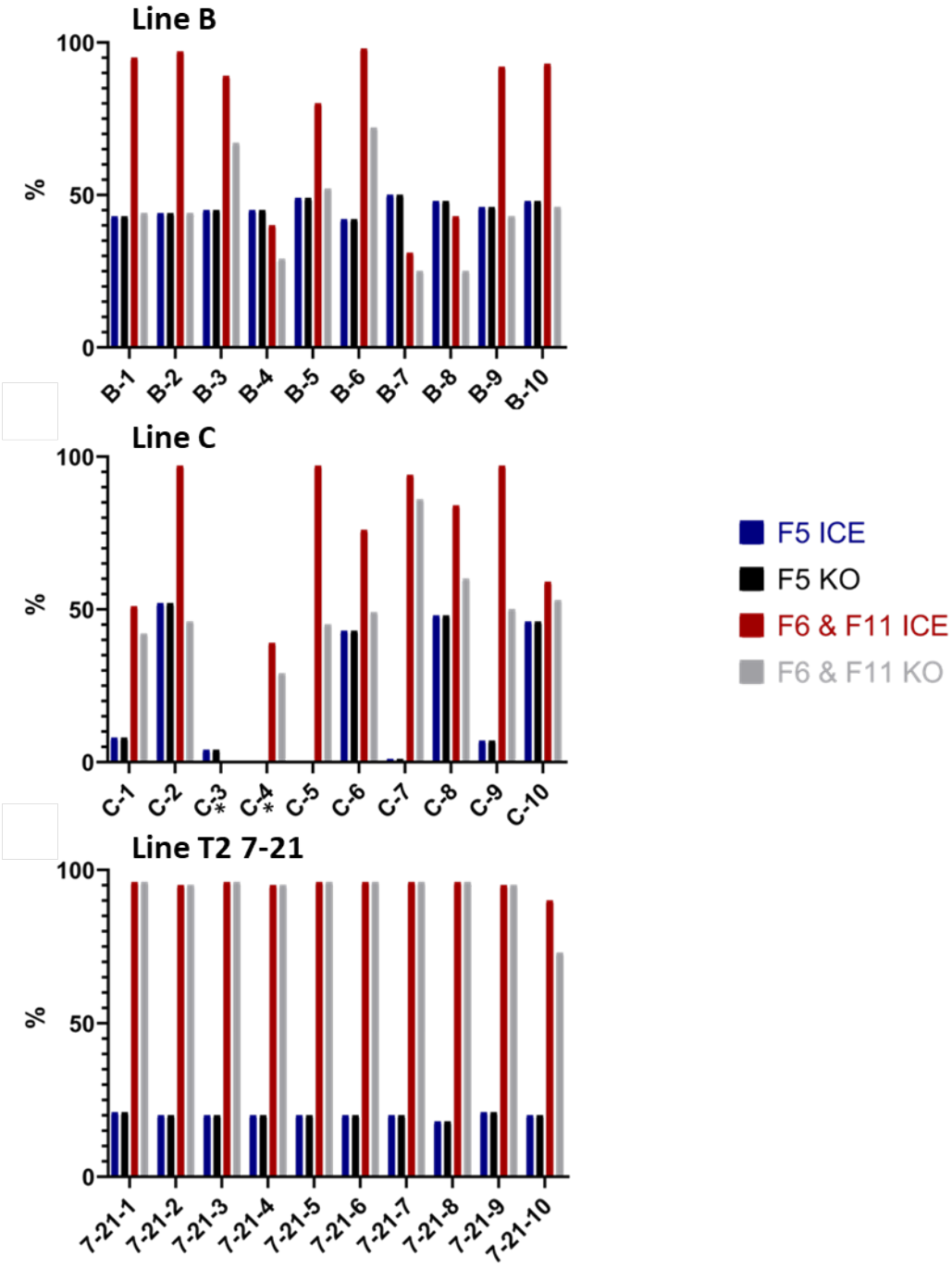

Figure 5-13: Results of ICE analysis for line B , line C and line T2 7-21 . ICE analysis was performed for sgRNA 5, 6 and 11.

**value missing due to failed sequencing*

Based on the rational outlined in Table 5-5 plants lines for further analysis were selected. For T_2 7-21 all plants showed almost the same ICE and KO scores for the three sgRNAs. Four were selected for further analysis at this stage. In this case 2 lines were chosen at random (T_2 7-21-4 and 7-21-7). It has to be noted that for ICE scores above 95% sequencing traces of plant lines often showed no presence of the original wild-type sequence.

Table 5-5: Putative knockout T_2 plant lines selected for further in-depth analysis

Line	**Reason for selection**
B-2	KO scores of 44% for F5 and F6&F11 97% ICE score for F6&F11
B-3	Second highest overall KO score for all the tgF B plants
B-6	Highest overall KO score out of all the tgF B plants
C-2	Highest KO scores for F5 and high ICE score for F6 and F11
C-7	Highest ICE score and KO score of the line for F6&F11
7-21-1	Highest overall KO score
7-21-4	Random
7-21-7	Random
7-21-10	Despite lowest KO scores, the only one of the 7-21 offspring that showed editing at F6 cutting site

For the selected lines screening for editing events of the F7 and F2 target site was performed. No editing could be observed for F7, which concurs with the data obtained for the T1 line. For F2, the primer spanning the region was redesigned, however, the sequencing results continued to be of low quality, thus ICE analysis could not be carried out.

5.4.7 Glycoanalysis reveals reduction in fucosylation

As several plants had ICE and/or KO scores of over 90%, absence or reduction of α(1,3)-fucosylation in the chosen plant lines was determined next. Due to the unreliability of the anti-α(1,3) fucose antibody, a different approach to estimating fucosylation was used. Glycoanalysis by mass spectrometry is very accurate and allows for quantification of the different glycoforms ((Grünwald-Gruber *et al.*, 2017). In order to perform precise glycoanalysis, one specific glycosylated protein had to be isolated from the plant. As antibodies are glycosylated and can be easily generated in *N. tabacum*, the bNAb VRC01 with reported yields around 100 mg/kg (Teh *et al.*, 2014) was chosen. Initial expression and purification tests were performed with 10-1074 HC, however, due to the limitation of possessing only one plant of each chosen T_2 line, an antibody with high yields, VRC01 (around 100 mg/kg), had to be used for expression.

To generate sufficient amounts of bNAb per plant, 8-10 leaves were infiltrated, harvested 6 dpi and frozen at -80 °C. Leaf tissue was disrupted using liquid nitrogen and pestle and mortar. Further purification steps were performed as explained in 2.1.4. An α-hIgG-κ western blot was performed to ensure the presence of fully assembled antibody (Figure 5-14). Purified VRC01 could only be isolated in sufficient quantities from lines T_2 7-21-1, 7-21-4, 7-21-7, 7-21-10, B6 and C7. Furthermore, VRC01 produced in wild-type *N. tabacum* cv. SR1 was also isolated, in order to compare glycosylation pattern and fucosylation frequency between putative knockout lines and the wild-type.

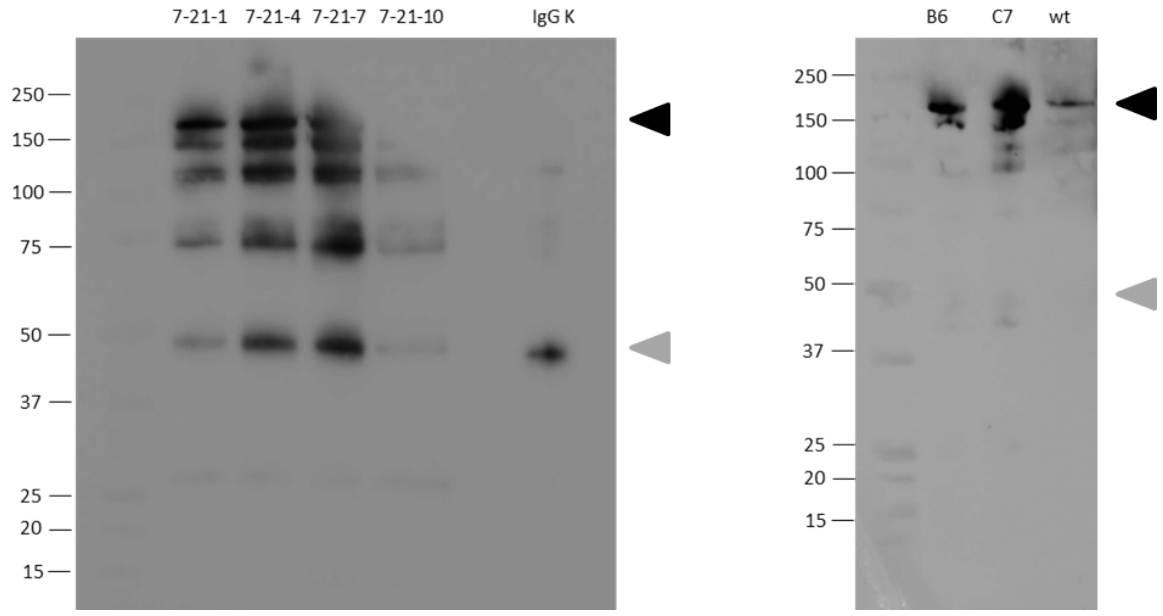

Figure 5-14: α-hIgG-κ western blot performed for VRC01 expressed in selected T_2 plant lines. 1 µg of protein was loaded onto each lane, except for the control of which 100 ng were loaded. . The fully assembled antibody is indicated by a black triangle. The heavy chain is indicated by a grey triangle. Several degradation products below 150 kDa are visible.

Glycoanalysis by mass spectometry was performed in the laboratory of Professor Friedrich Altmann at University of Natural Resources and Life Sciences Vienna under supervision of Dr Clemens Grünwald-Gruber. Samples were S-alkylated, digested overnight with trypsin and subsequently measured using a LC-MS (Q-TOF). The obtained spectra were analysed by manual glycopeptide search using DataAnalysis 4.0 (Bruker). For typical glycoforms found in plants and nomenclature, refer to the appendix.

Figure 5-15 displays spectra from the tryptic digest of VRC01; generated in *N. tabacum* wild-type (A) and in the putative knockout line T_2 7-21-1 (for all other spectra see Appendix). The highest glycan peak in each sample was used to adjust the intensity of the spectrum. For the wild-type produced VRC01, the majority of glycoforms contained XF, with GnGnXF being the dominating glycoform. The presence of GnGn could not be observed. Similarly, T_2 7-21-1 shows a peak for GnGnXF, though two more prominent peaks, which represent GnGn and GnGnX respectively, were also present. While this result indicates that editing events in T_2 7-21-1 have not translated in a complete knockout, an apparently significant knockdown of α(1,3)-fucosyltransferase was achieved,

as significant amounts of GnGn and GnGnX are present. Comparable results were observed for all other putative knockout lines. Initial spectra obtained of VRC01 produced in tgF B6 and C7 were suboptimal, due to low concentrations. The measurement was repeated with a higher amount of sample precipitated prior to performing the tryptic digest. Yet, signals of specific peaks were still of low intensity and of a high signal to noise ratio (SNR). Some glyco-peaks could be identified, however, results are not reliable, but are still presented (appendix) to show an overall trend of fucosylation reduction in the analysed 'knockout' plants.

As VRC01 is not only glycosylated in the Fc-region but also on the light chain in the Fab-region, a second digest of the samples with GluC (cleavage after E) was performed, as there were no cleavage sides for trypsin (cleavage after R/K) in the light chain. The samples measured with LC-MS (Q-TOF) (Figure 5-16). The spectra were again analysed by manual glycopeptide search using DataAnalysis 4.0 (Bruker). Spectra of the wild-type and putative knockout lines show much more similarities with regard to their glycoform profile. All of the wild-type glycoforms carry XF. In contrast, the putative knockout line shows a peak for GnGnX, however, no peak for GnGn could be observed.

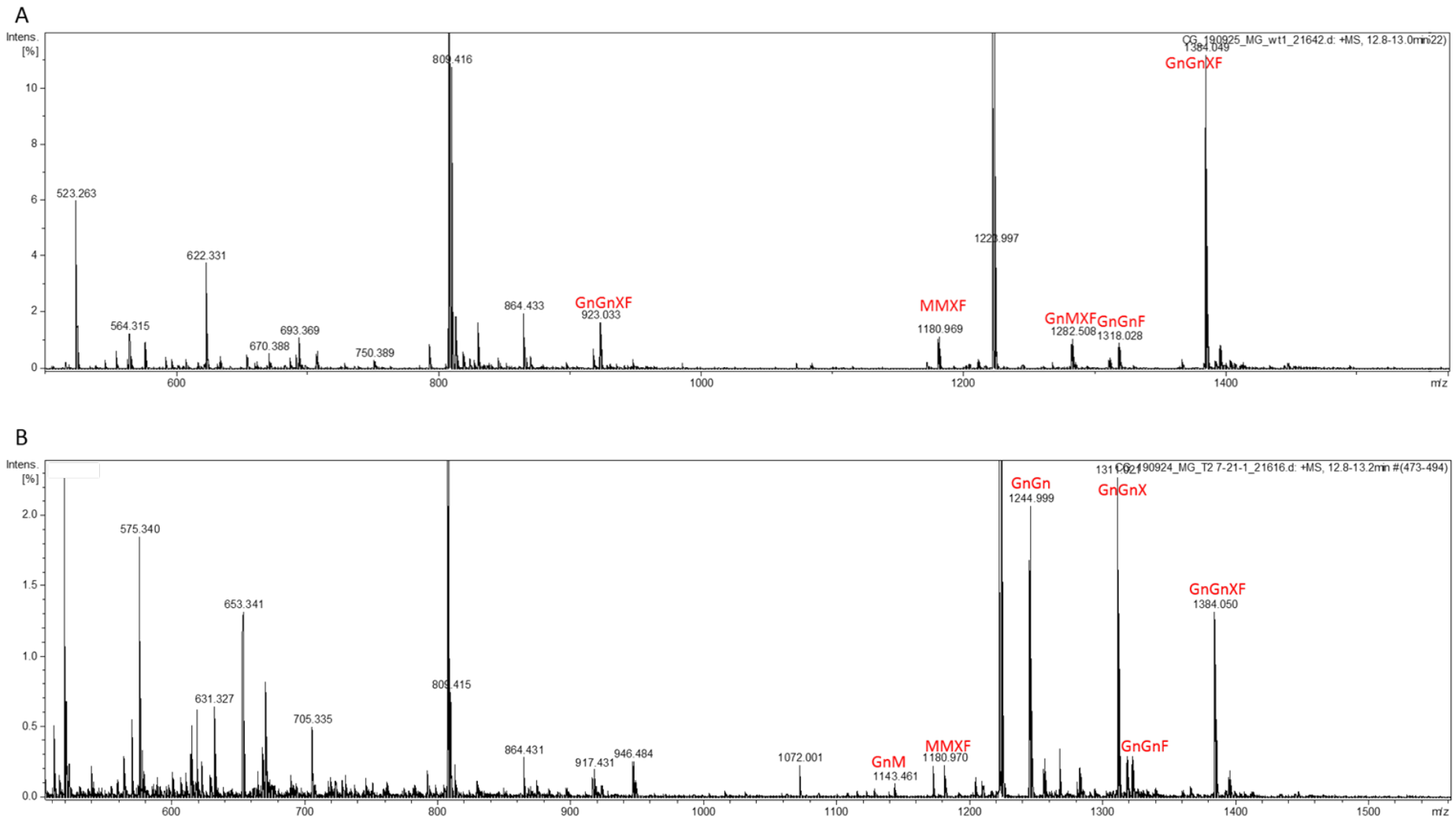

Figure 5-15: Spectrum for tryptic digest of VRC01 produced in N. tabacum SR1 wild-type (A) and the putative knockout line T2 7-21-1 (B). Peaks corresponding to specific glycoforms are labelled in red.

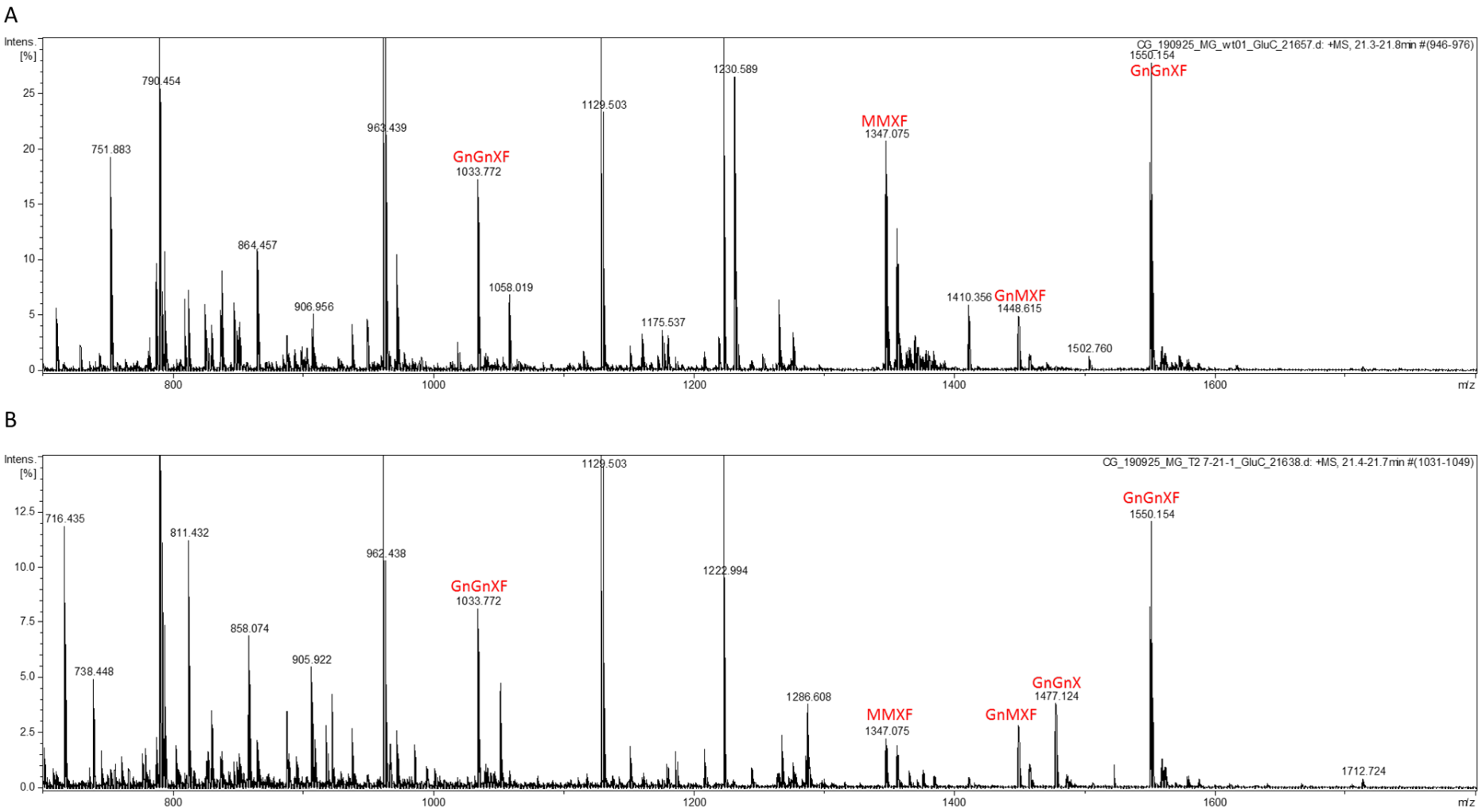

Figure 5-16: Spectrum for GluC digest of VRC01 produced in N. tabacum SR1 wild-type (A) and the putative knockout line T2 7-21-1 (B). Peaks corresponding to specific glycoforms are labelled in red.

In order to quantify the percentage of fucosylated or afucosylated glycoforms respectively, peak areas of EICs (extracted ion chromatogram) of the first four isotopic peaks were totalled, using Quant Analysis (Bruker) as software. Percentages were calculated for each individual glycoform and a sum of all fucosylated or afucoslyated glycoforms was calculated. The percentage of reduction in fucosylation for each putative knockout line in relation to the wild-type was determined (Figure 5-17). Reductions in fucosylation of 20 to 65 percent of the heavy chain glycan were obtained by expressing VRC01 in the putative knockout lines. The highest decrease of 65 percent was achieved with T_2 7-21-1. As observed in the spectra, the Fab-region is more heavily fucosylated compared to the Fc-region for all putative knockout lines. In accordance with the Fc-data, the highest reduction in fucosylation (about 15%) can be seen for T_2 7-21-1. For line B6 and C7 glycoforms with small peaks could not be identified for the Fab-glycan, due to the high signal-to-noise ratio. Therefore it was not possible to calculate a percentage for the Fab-glycan.

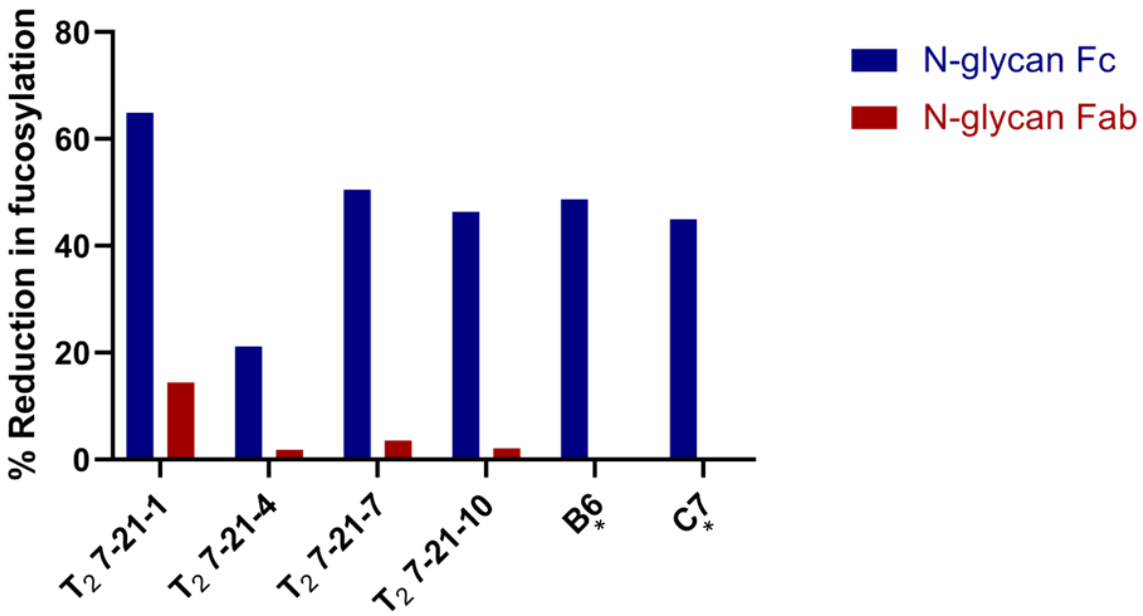

*Figure 5-17: Reduction in N-glycan fucosylation (given in percent) of VRC01 expressed in the putative knockout lines in relation to N-glycan fucosylation observed in the wild-type. The reduction is shown for the Fc-region (Fc) blue) and the Fab-region (Fab) (red) N-glycan respectively. *values for Fab glycan could not be determined.*

5.5 Discussion

A *FucT* knockdown *N. tabacum* cv. SR 1 line was generated, which showed significant reduction in α(1,3)-fucosylation compared to the wild-type parent line. While multiple plant lines exhibited a high number of editing events leading to frameshift mutations, at this stage of the project a complete ΔF knockout line was not obtained.

5.5.1 Impact of the choice of sgRNAs and multiplexing

The quality of sgRNAs is of paramount importance to achieve precise and fast knockouts using CRISPR/Cas9. Thus, the lack of a ΔF line at T_2 might be a consequence of the design and choice of sgRNAs. In this study, five mRNA sequences of *FucT* were retrieved from GenBank, aligned and analysed for similarities. As neither the genome nor *FucT* mRNA sequences of *N. tabacum* cv. SR1 are published, it was necessary to rely on sequences from other cultivars, that is four from cv. TN90 and one from cv. BY, therefore possible unidentified differences in the genomes might have hampered the design of highly efficient sgRNAs. However, the same mRNA sequences served as the basis for the sgRNA design to successfully knockout *FucT* in *N. tabacum* BY-2 cells (Hanania *et al.*, 2017; Mercx *et al.*, 2017).

Of the five retrieved mRNA sequences, two (*FucT* 4-5) differed significantly from the other three sequences (*FucT* 1-3), lacking 45 bp and 54 bp respectively, at the beginning of the gene and were considered putative pseudogenes. Even so, twelve sgRNAs were designed targeting sites in exon 1-3 of *FucT* 1-3 and/or *FucT* 4-5. All twelve sgRNAs were tested for their efficiency in inducing mutations, which yielded promising results. Two sgRNAs specific for *FucT* 1-3 or *FucT* 4-5, respectively, and one sgRNA recognising *FucT* 1-5 were chosen for stable plant transformations. These targeted sites in exon 1, 2 and 3 in order to induce frameshift mutations in various exons, thus theoretically leading to efficient disruption of the *FucT* genes. However, to obtain the ΔF *N. benthamiana* line, Jansing et *al.* (2019) mainly targeted exon 2 of *FucT* 1 and 2, plus one sgRNA targeting *FucT* 1-4. Mercx et *al.*

(2017) focused solely on exon 3 in BY-2 to obtain a knockout. Hence, the question arises whether mainly targeting one exon is more efficient than attempting to induce mutations in multiple exons. Then again, the successful knockout of *FucT* performed by Hanania et *al.* (2017) in BY-2 cells was carried out by targeting exons 1 to 3. Therefore, it seems implausible that targeting multiple exons would be disadvantageous for the establishment of a ΔF line.

In this study, the polycistronic tRNA-gRNA system (Xie, Minkenberg and Yang, 2015) was employed, as it simplifies effective delivery of multiple sgRNAs into the same cell, thus increasing the editing efficiency. Interestingly, however, the sgRNA multiplexing system appeared to negatively affect the efficacy of the individual sgRNAs. Gao *et al.*, (2015) obtained a reduced mutation efficiency of the individual sgRNAs in a duplex construct compared to individual delivery. The authors attributed this effect to competitive binding of both sgRNAs to a limited amount of available Cas9. Moreover, Xie et *al.* (2015) exposed that the mutation efficiency of a specific sgRNA changed significantly (from 76% to 24%) when positioned in the middle instead of the end of the multiplex construct. This was also found by Jansing et *al.* (2019); the same sgRNA exhibited significantly reduced efficiency (0-8% instead of 25-66%) when placed in the middle of the construct. The authors of both studies hypothesised that the presence or absence of the poly(U)tail, which is only attached to the last sgRNA in the polycistronic tRNA-gRNA (PTG) construct, is responsible for this change in mutation efficiency. A similar observation was made in this study; the highest mutation rate of all the screened sgRNAs in the transgenic line was obtained for F11, the sgRNA in the last position of the PTG construct. It has to be noted that the hypothesis of the poly (U) tail being responsible for this effect has not been proven for the CRISPR/Cas9 system. Recent findings demonstrated that the efficiency of sgRNAs was not linked to variability in length or absence of the poly (U) tail in HEK293T cells (Gao, Herrera-Carrillo and Berkhout, 2018). Another study showed that increased stability of sgRNAs could be achieved by introducing a 5'cap and 3'poly (A) tail, which in turn resulted in higher editing efficiency. However, no improvement was observed with just one of these modifications on

its own (Mu *et al.*, 2019). These studies refute the hypothesis of the impact of the poly (U) tail on sgRNA efficiency changes in a PTG system.

Another hypothesis is that these discrepancies in editing efficiency arise from tRNA processing. The first and last sgRNA are only flanked by one tRNA each, while sgRNAs in the middle are flanked by two, thus possibly slowing down the release of the sgRNA. This might result in decreased editing efficiency, especially if only limited amounts of Cas9 are available.

Better understanding of the phenomenon of sgRNA position-dependent cutting efficiencies would allow for optimisation of the PTG system, therefore further studies are necessary to decipher the underlying mechanism of reduction in sgRNA efficiency.

5.5.2 Impact of breeding

The residual α(1,3)-fucosyltransferase activitymight stem from incomplete editing of the *FucT* genes and therefore residual presence of the wild-type gene. In theory, the absence of the wild-type sequence was confirmed by ICE analysis; however, it is possible that sequencing peaks caused by the residual wild-type gene were not identified due to their low frequency. This issue could be resolved by further breeding, through removal of non-edited wild-type gene by genetic recombination and further editing events. In general, the speed of establishing a plant line with the desired traits using CRISPR/Cas9 varies greatly. Jansing et *al.* (2019) were able to obtain a *FucT* knockout line of *N. benthamiana* at T_2. Despite *N. tabacum* being from the same genus, the speed of mutation might differ due to the dissimilarities in their genome and the availability of the fully annotated *N. benthamiana* genome. In *N. tabacum* BY-2 cells *FucT* and *XylT* were knocked out by two independent research groups using different sgRNA targets. In this system both reported a complete knockout of the genes after one round of transformation (Hanania *et al.*, 2017; Mercx *et al.*, 2017). Irrespective of presumably almost identical genomes of *N. tabacum* cv. BY-2 and *N. tabacum* cv. SR1, a direct comparison of knockout efficiency cannot be made, as these studies performed gene editing in cells

rather than in plant tissue. CRISPR/Cas9 knockouts in *N. tabacum* plant tissue targeting other genes have been performed. A study by Gao et *al.* (2015) aimed to knockout phytoene desaturase (*PDS*) and PDR-type transporter (*PDR6*), to test the CRISPR/Cas9 system for its suitability in modifying the genome of *N. tabacum*. Indel rates of up to 87.5% were observed at T_0, however, further breeding was not performed. Another study aimed to generate a nicotine-free *N. tabacum* plant line by knocking out the berberine bridge enzyme-like (BBL) genes. Six isoforms were identified and one sgRNA was generated to target all of the isoforms. T_0 plant lines showed a reduction in nicotine content of 0-95%. In these lines all BBL genes, except for one were mutated. Further breeding to T_3 resulted in a plant line showing 99.7% reduction in nicotine content and mutations in all genes (Schachtsiek and Stehle, 2019). These studies not only highlight the variability in speed of generating a knockout line, but also underline that efficiency of CRISPR/Cas9 might differ between systems (e.g. cells vs plants), targets and species.

5.5.3 Impact of screening

A major difficulty during this project was the reliability of screening of the putative knockout lines, which was a contributing factor in the delay of obtaining a ΔF *N. tabacum* line. The determination of the cutting efficiency of the individual sgRNAs was performed using Indel Detection by Amplicon Analysis (IDAA). This screening method might be useful for small scale screening but unsuitable for screening of a high number of plants, as obtaining raw data from IDAA may take up to two weeks and interpretation of the results is not always straightforward. This was emphasised by the absence of the predicted wild-type peak for 2 out of 5 amplified regions of interest, which complicates the analysis of the data. Moreover, sequencing results and the distribution of peaks might be heavily influenced by not only the quality of the extracted DNA of the transformants but also by the quality of amplification of the region of interest. In retrospect, a sequencing approach followed by ICE analysis, as used in later stages of the project, would have been more appropriate to provide reliable results.

Given that IDAA was not suitable for rapid testing of transformants, initial screening was carried out by dot and western blot using an anti-α(1,3)-fucose antibody, as has been used in previous α(1,3)-fucosyltransferase knockout studies. To prevent non-specific binding to the *N. tabacum* plant leaf extract, the secondary anti-rabbit antibody was pre-absorbed, as described by Jansing et *al.* (2019). Nevertheless, this screening approach provided ambiguous results, especially for repeats of western blots performed with concentration-adjusted protein samples extracted from the same plants. While some discrepancies between dot and western blots might be expected, due to the lower sensitivity and specificity of dot blots (Villafañez, Gottifredi and Soria, 2019), inconsistencies of western blot repeats are unusual. A possible cross-reactivity with β(1,2)-xylose was suspected. The likelihood of such cross-reactivity is low, as each batch of antibodies is tested to validate the specificity, yet the obtained results were consistently unreliable.

A dot-blot published to exclude cross-reactivity (www.agrisera.com), showed a slight signal for a Xyl+/Fuc- control, but not for the Xyl-/Fuc- control, which was cautiously regarded to support the theory of cross-reactivity with β(1,2)-xylose. Yet, this screening approach was successfully used by several groups to screen for *FucT* knockout lines (Mercx *et al.*, 2017; Jansing *et al.*, 2019). Despite using the same primary antibody, Jansing et *al.* (2019) not only opted for high-salt TBS to reduce the background, but also used a secondary-AP conjugated antibody and colorimetric detection. Colorimetric detection is less sensitive than chemiluminescence, hence it is possible that cross-reactivity may not have been observed (https://www.bio-rad.com). Still, the authors reported no further reduction in signal intensity of completely homozygous T_2 knockout lines compared to partly heterozygous T_1 for *FucT* lines, which may indicate some degree of non-specific binding. Mercx *et al.* (2017) also made use of this screening approach with the same anti-fucose antiserum, but applied chemiluminescence as detection. Interestingly, the published western blots only show absence of fucosylation for BY-2 cells that were also devoid in xylosylation.

Another possibility of the failure of this screening approach, which might have been falsely interpreted as cross-reactivity, is potential changes in fucosylation at different growth stages of *N. tabacum*. A study has revealed that IgG produced in young tobacco leaves showed a higher percentage of high-mannose glycans and slightly reduced percentage of fucosylation compared to IgG produced in older leaves. However, no differences in fucosylation of endogenous proteins in leaves of different age were observed (Elbers *et al.*, 2001), suggesting that the age of the leaves used for fucosylation analysis of total crude extract protein is irrelevant. Yet, regardless of the basis for the observed ambiguity, the usage of the anti-α(1,3)-fucose antibody was an unreliable screening method for this project. This might have led to misidentifying highly edited plants as unedited, which have in turn been excluded from further breeding.

All further screening was performed on a genetic level by amplification of the target region and ICE analysis. As sgRNAs were designed for three different exons and two sets of *FucT* genes based on similarity, amplification of all targeted areas would have required four primer pairs to screen all five targets. SgRNA F7 resulted in a minimal ICE rate of around 3% at T_1, suggesting that no editing had occurred, as ICE scores of about 2% can be observed when analysing different amplification products of the same target region from wild-type *N. tabacum* (data not shown). Thus the FucTa primer pair was excluded as screening primer. PCR products obtained from the primer pair FucT1, which amplifies the region of the F2 cutting site, often led to inconclusive results of the ICE analysis. Despite being able to amplify and purify the region of interest in sufficient amounts, the analysis often failed. Therefore the two primer pairs FucT3 and FucT4, amplifying the regions of F5 and F6 plus F11, respectively, were chosen as screening primers. These primers flank cutting sites of either the gene and/or the putative pseudogene, therefore all *FucT* genes were included in the screening process. The highest mutation rates were observed for sgRNA F11, with an ICE and KO-score of up to 90% in T_1 and up to 97% in T_2. No wild-type sequence was present in T_2 lines. Mutations in the F6 region were observed at low levels for only a few plant lines. Despite having observed two T_1 lines

(14-1 and 14-17) with ICE and KO scores of about 90%, scores of only up to 50% could be observed for T_2 lines. This reduction in indels probably resulted from cross-fertilisation.

For a small set of selected T_2 plant lines the complete editing profile was investigated. This revealed that none of the nine plant lines showed any mutation events for F7, further underlining that this sgRNA is inactive. No ICE analysis for F2 could be performed, as sequencing repeatedly resulted in low quality, despite redesigning of the primer pair.

5.5.4 Glycoanalysis

Glycoanalysis by mass spectrometry of a mAb produced in a few chosen T_2 lines revealed that despite the high mutation rate, fucosylation was only reduced compared to the wild-type, with a maximum reduction of 65 percent. This result is similar to the report of bNAb 2G12 expressed in a putative ΔXF knockout line of *N. benthamiana* which still exhibited about 11 percent fucosylation, despite lacking signal in an α-(1,3)-fucose dot-blot and a significant mutation rate (Jansing *et al.*, 2019). Furthermore, about 50 percent of the N-glycans of the leaf proteome still contained α-(1,3)-fucose, highlighting that results from immunoblots and genetic data are merely indicative, rather than being able to accurately predict a complete knockout. The authors suspected that the controversy between genetic and MS analysis had arisen from the presence of somatic rather than germinal mutations of the fucosyltransferase gene, which might also be an explanation for the results in this thesis. The genetic data is based on the DNA of 2 leaf discs per transformant, therefore it is probable that results are slightly skewed due to somatic mutations, yet this approach has proven to be the most robust of the reasonably fast screening methods applied throughout this project.

Mass spectrometry not only revealed an incomplete knockout of *FucT*, but also displayed more fucosylation of the Fab-glycan, in this case located on the light chain, compared to the Fc-glycan of VRC01. This phenomenon was not only observed for bNAb expression here but also for another bNAb N6 expressed in the commonly used RNAi ΔXF *N. benthamiana* line (unpublished). Differences

in *N*-glycan profiles of Fab and Fc are not limited to mAbs generated in plants. Similar observations were made for an IgG isolated from myeloma serum. Despite the lack of fucosylation of the Fc-glycan, fucosylation of the Fab-glycan was reported (Mimura *et al.*, 2007). Additionally, studies indicate higher processing of Fab-glycans compared to Fc-glycans, demonstrated by a more homogenous, generally bi-antennary, core-fucosylated and sialylated glycan profile (Anumula, 2012; Castilho *et al.*, 2015). Interestingly, according to Anumula (2012), Fab-glycans show a lower percentage of fucosylation (around 80%) compared to Fc-glycans (95%), which is inconsistent with the findings presented here, showing similar percentages of fucosylation for the Fab and Fc-glycan of the wild-type generated bNAb. Regardless, these results suggest that the absence of fucosylation on the Fc-glycan of a mAb might not be sufficient for the verification of a complete *FucT* knockout. Therefore, in order to ensure inactivity of α(1,3) fucosyltransferase, it might be necessary to investigate fucosylation of both, the Fab- and Fc-glycan of a suitable mAb.

In conclusion, the generation of a *N. tabacum* cv. SR1 plant line with 65 percent reduction in fucosylation at T_2 was achieved. Further breeding may be required to obtain a complete knockout line of *N. tabacum*.

6 General discussion

There are currently around 38 million people living with HIV, about 25.5 million of them in sub-Saharan Africa (UNAIDS, 2019). Current treatments (anti-retroviral therapy, ART) cannot cure the infection but only control its progression. ART is also used for pre-exposure prophylaxis but requires good compliance and some side-effects have to be endured (Cihlar and Fordyce, 2016). Emergence of resistance to ART is increasing. Up to 26% of first-line ART initiators are infected with NNRTI-drug resistant viruses, thus the development of new therapeutics is of importance (Cihlar and Fordyce, 2016; World Health Organization (WHO), 2019). Broadly neutralising antibodies (bNAbs) offer a new perspective, especially when it comes to pre-exposure prophylaxis (Klein *et al.*, 2013; Caskey *et al.*, 2015). In clinical studies, different bNAbs have been well-tolerated and have had a half-life of up to 24 days in non-infected individuals (Caskey, Klein and Nussenzweig, 2016), which qualifies them for pre-exposure prophylaxis (Kubota *et al.*, 2009). Engineering of the Fc-region allows for improved effector functions by optimising glycosylation and prolonged half-life. Efforts are currently underway to prolong the natural half-life of bNAbs by introducing mutations into the Fc-region. This is to increase the binding affinity to the neonatal Fc receptor (FcRn), which has an important role in IgG recycling (Shields *et al.*, 2001; Petkova *et al.*, 2006; Zalevsky *et al.*, 2010).

6.1 Impact of bNAb with enhanced efficacy and their production in a plant expression system

Several pre-clinical studies have revealed the huge potential of combination bNAb therapy, but short half-lives would hamper the introduction of this new treatment. Therefore, pre-clinical and clinical trials have been or are being performed with various bNAbs that are carrying half-life extending mutations. The data is promising, showing up to 3.8 fold longer half-life in NHPs (Gautam *et al.*, 2018) and more than 4-fold in healthy human subjects (Gaudinski *et al.*, 2018). Yet all of the used bNAbs have been generated in mammalian cells. There is one report of a plant-produced bNAb

with a half-life extending mutation, which compared PGT121 to PGT121-YTE with regard to pharmacokinetics in macaques (Rosenberg *et al.*, 2019).

In the current study, a comprehensive characterisation of a plant-produced bNAb with a half-life prolonging mutation was performed for the first time. The improved pharmacokinetic parameters of the plant-produced 10-1074 YTE are in accordance with other reports (Dall'Acqua, Kiener and Wu, 2006; Robbie *et al.*, 2013; Rosenberg *et al.*, 2019) and reveal that the production of efficacious bNAbs is not limited to mammalian cells. Opening up the possibility of local production in low-income countries due to lower initial investment costs would not only simplify the supply chain but also be economically beneficial by the creation of new jobs (Ma *et al.*, 2013; Murad *et al.*, 2020).

Irrespective of the expression platform, improving half-life may reduce the treatment burden on countries, HIV-positive patients and high risk populations. While bNAbs with improved half-life may provide several benefits, the administration of bNAbs is less convenient when compared to conventional ART, which may impact patient acceptability. Studies evaluating the approval of bNAb therapy are necessary before the potential initiation of a change in treatment regimen. Regardless of patient preference, the application of bNAb therapy may be especially attractive for prevention of infection.

Prolonged half-life might provide a simplified approach to pre-exposure and post-exposure prophylaxis (PrEP and PEP). Current studies indicate that side-effects of bNAb treatment may be significantly lower than treatment with ART (Ledgerwood *et al.*, 2015; Schoofs *et al.*, 2017; Gaudinski *et al.*, 2018; Cohen *et al.*, 2019). Low adherence is often linked to the severity of side-effects that are experienced by patients (Zhang *et al.*, 2016; Iacob, Iacob and Jugulete, 2017), therefore, this effect is even more likely to be observed in uninfected high-risk populations taking PrEP. BNAb treatment offers a chance to better control PrEP and reduce the number of new infections. In 2018 six percent of new infections were among sex workers, with another 18 percent among clients of sex workers or people who have sex with other members of key populations (www.unaids.org). Thus by preventing

the infection of sex workers by prophylactic bNAb therapy, the transmission to clients would not occur and this would further impact the transmission to their sexual partners.

BNAbs can not only provide protection, but also result in reducing viral load immediately (Caskey *et al.*, 2015), which is important in MTCT. Aside from prolonged half-life, the higher affinity of 10-1074 YTE to FcRn resulted in improved transcytosis. The transport of IgG via FcRn is a vital mechanism for infants to obtain protective maternal IgGs *in utero* (Simister, 2003). With regard to HIV, enhanced placental transfer of bNAbs has the potential to lower or abolish the occurrence of vertical transmission, even in cases where the treatment of the expecting mother was delayed. Furthermore, several studies have revealed that infants of HIV-infected mothers often show lower levels of transplacental transfer of antibodies (Dangor *et al.*, 2017; Fouda *et al.*, 2018). Although this mechanism is not completely understood yet, bNAbs with improved affinity to FcRn might counteract this deficiency.

Enhancing IgG transcytosis could be important to help prevent MTCT, but there may also be additional benefits. Preliminary transcytosis experiments with Caco-2 cells, representing the intestinal epithelial barrier, displayed enhanced transfer of 10-1074 YTE compared to the other variants. MAbs generally have to be given intravenously, but this finding could potentially be exploited to design an alternative oral delivery route of mAbs. While other factors, like pH stability, have to be considered when using an oral delivery route, this is a first step towards simplifying delivery of mAbs.

The improvement of ADCC activation through the removal of core-fucose glycosylation may enhance the protection conferred by the bNAb and the disruption of cell to cell transmission. Even though most pre-clinical studies investigate the protective potential of bNAbs with regard to their half-life in the serum, several studies have shown that the protective ability of bNAbs decreases upon abrogation of effector functions (Hessell *et al.*, 2007, 2009; Bournazos *et al.*, 2014). So far, research has primarily employed effector function modulating mutations in the Fc-region of bNAbs

to study the relevance of effector functions in protection and not compared the impact of fucosylation (Hessell *et al.*, 2007, 2009; Bournazos *et al.*, 2014; Parsons *et al.*, 2019). One study showed that an afucosylated version of b12 resulted in improved binding to FcγRIIIa but did not provide superior *in vivo* protection in rhesus macaques (Moldt *et al.*, 2012).

The impact of FcγR-functions, particularly ADCC, on protection have to be evaluated for each individual bNAb, as studies have shown that FcγR functions seem to be necessary for maximum protection for some, but not all bNAbs. Challenge studies of pigtail macaques showed that PGT121 LALA (abrogation of effector functions) provided equivalent protection from cell-associated SHIV challenge when compared to the non-modified PGT121. Furthermore the study revealed that protection conferred by the non-modified PGT121 was not diminished in partially NK-cell depleted subjects when compared to animals without depletion, demonstrating that protection by PGT121 does not rely on effector functions (Parsons *et al.*, 2019). In contrast, Hessell *et al.* (2007 and 2009) demonstrated that the protective properties of the bNAb b12 were reduced when modified with the LALA mutation, for both – single high dose vaginal and repeated low dose vaginal challenges of rhesus macaques (Hessell *et al.*, 2007, 2009). A similar trend was shown for the bNAb 3BNC117. A mouse-human chimeric version of 3BNC117 with an FcγR-abolishing mutation showed less in vivo activity in mice, when compared to the IgG2a variant, the isotype that is generally superior in ADCC potency in mice when compared to IgG1. No significant difference between the two variants was observed in FcγR-deficient mice, underlining that enhanced activity of the bNAb is dependent on effector functions and not the complement system. Lastly, this study not only showed human versions of 3BNC117 with either a effector-function enhancing (GASDALIE) or abolishing (GLRL) mutation but also an improvement in protection when compared to the non-modified 3BNC117 (Bournazos *et al.*, 2014)..

With regard to the importance of ADCC for the treatment of established infection, there seems to be a correlation between slow disease progression and high ADCC activity of antibodies

(Baum *et al.*, 1996; Banks *et al.*, 2002; Gómez-Román *et al.*, 2005; Lambotte *et al.*, 2013; Madhavi *et al.*, 2017), suggesting that bNAbs with enhanced ADCC may be beneficial for virus control.

Introduction of the YTE mutation led to reduced ADCC activation when compared to the native plant-produced version. This reduction has been observed in other studies (Dall'Acqua, Kiener and Wu, 2006; Booth *et al.*, 2018) and has led to LS being preferred over YTE to enhance half-life (Gaudinski *et al.*, 2018, NCT03254277, NCT03538626, NCT03554408, NCT03721510). However, in our study, while the YTE mutation lowers ADCC, the impact was abrogated by ADCC enhancing effects resulting from fucose-removal.

Interestingly, the expression yields of the modified versions of a bNAb are rarely reported (Ko *et al.*, 2014; Gaudinski *et al.*, 2018; Cohen *et al.*, 2019; Rosenberg *et al.*, 2019). While yields may not be of high importance in initial stages of product identification, they have to be considered when trying to develop a product. In this study, initial quantification of expression showed similar expression of 10-1074 YTE and a substantial reduction for 10-1074 LS in comparison to the native version. Furthermore, downstream processing generally resulted in higher losses for 10-1074 YTE than for 10-1074 HC. This overall yield reduction for modified bNAbs expressed in plants has also been observed for VRC01 and 3BNC117, however, the reduction caused by the LS modification in these antibodies was not as substantial as for 10-1074 (personal communication Dr Audrey Teh). This data and observation is crucial to deciding which version of a bNAb is worth producing and taking forward to clinical trials. The LS version of 10-1074 might have proven to be more efficacious than the YTE version; however, the benefits of this improvement would not have outweighed the significantly lower yield. In general, reports about yields of either plant- or mammalian-produced modified bNAbs would be valuable information as it would give indications whether these mutations generally impact expression, or whether yield reduction is dependent on the individual bNAb or on the expression platform. Furthermore, details about purification processes would also be beneficial

to minimise loss. The almost 4-fold difference in purified protein yield of 10-1074 YTE compared to 10-1074 HC indicates that the purification process is suboptimal for this modified version.

6.2 Impact of a ΔF *N. tabacum* line

The generation of a *N. tabacum* line with significantly reduced or abolished fucosyltransferase activity would be an important advance as *N. tabacum* remains the most attractive solution for very large-scale production of mAbs and other glycoproteins. While transient expression in *N. benthamiana* is currently primarily employed for large-scale manufacturing (Goulet *et al.*, 2019), this system has the disadvantage of requiring vacuum infiltration, therefore also agrobacterium cultivation and disposal. These additional steps significantly increase the cost of facility construction and operations and might result in some limitations with regard to upscaling (Peters and Stoger, 2011; Q. Chen *et al.*, 2013). However, large-scale production of mAbs or other glycoproteins in *N. tabacum* was partially hampered by the unavailability of *N. tabacum* lines which provide more human-like glycosylation. Establishing of an appropriate glycoengineered *N. tabacum* plant line would result not only in improved efficacy of the product but also in simplifying regulatory approval (Ma *et al.*, 2015).

The partial *FucT* knockout line generated here allows for the production of a significant proportion of afucosylated mAbs. Further breeding and screening will be necessary to maximise the reduction in fucosylation, in order to ensure a homogenous and predictable glycan profile of a product.

In a separate project, a *XylT* knockout line is being generated, which will subsequently be crossed with a complete *FucT* knockout line to obtain a ΔXF *N. tabacum* line. Having stable plant lines that are lacking *FucT* and/or *XylT* activity will allow not only for further investigation of the specific impact of these two glycan moieties, but also to adjust the glycosylation profile of a product according to need.

An important aspect of this project was the use of CRISPR/Cas9, which was not only chosen due to its simplicity but also partly with the anticipation of the resulting plant line being regarded as non-GM (Sprink *et al.*, 2016). At the start of this project the European Union had not declared their stance on gene-edited plants by the CRISPR system, and as some other countries, like Argentina and Chile, ruled them to be non-GM, a similar decision was expected to be made by the EU. However, in 2018 the EU announced that gene-edited plants would be considered GM, thus treated under the same strict regulations (Callaway, 2018). While over a hundred institutions have petitioned to revoke this verdict (VIB, 2018), a reversal of this decision appears unlikely. However, the efforts of producing this ΔF plant line using CRISPR were not futile. In the EU this plant-line can be used in greenhouses for production, and in other countries (Canada, USA, Brazil, Argentina etc.) that regard gene-editing as non-GM, open-field cultivation would be possible (https://crispr-gene-editing-regs-tracker.geneticliteracyproject.org).

7 Conclusion and future work

In this project, it was demonstrated that the two versions of the broadly neutralising antibody 10-1074 produced in a glycoengineered *N. benthamiana* plant line exhibited equivalent neutralisation potency and improved *in vitro* ADCC activation compared to the mammalian counterpart. The introduction of the YTE mutation also led to significantly enhanced *in vitro* transcytosis and an average clearance reduction by 29 percent, which in turn resulted in prolonged half-life. Due to its favourable pharmacokinetic properties, improved transcytosis, and ADCC activation, 10-1074 YTE ΔXF may be an attractive candidate for inclusion in an efficacious antibody-cocktail. In anticipation of producing HIV bNAbs at very large scale in glycoengineered transgenic *N. tabacum*, a *N. tabacum* plant line at T_2 with 65 percent reduction in fucosylation has been generated using CRISPR/Cas9.

While this research presents an argument for the YTE version of 10-1074, further studies are certainly needed. Some limitations of the presented research need to be addressed in the future.

First of all, a yield comparison between the variant produced in CHO cells and plants may be necessary, in order to determine whether yield reduction upon introduction of the Fc-mutation is expression-system dependent or independent. Half-life studies were limited by the obtained animal licence, which did not allow for IV injection and blood sampling on the same day. While further transgenic mouse studies may not be needed, in any following *in vivo* studies it is essential to be able to determine serum levels shortly after the injection, to allow for proper evaluation of various pharmacokinetic parameters. Additionally, for future pre-clinical half-life studies it may be important to use an improved antibody purification protocol, e.g. to reduce aggregates in the final formulation and eliminate potential adverse effects caused by impurities. With regard to ADCC, repeats of the ADCC activity assay are needed in order to determine whether the higher potential for ADCC activation displayed by the plant-produced 10-1074 variants through the removal of the core-fucose translates into increased cytotoxicity. Once these limitations have been addressed, further studies have to be tailored to the intended application of a potential 10-1074 YTE containing bNAb cocktail.

Considering an application in MTCT, additional transcytosis studies with placental cells and/or *in vivo* transplacental transfer might be crucial to highlight the potential importance of modified bNAbs in prevention of MTCT. Moreover, other bNAbs have to be selected and their properties in antibody combinations have to be studied with regard to potency and interference or competition.

A decision of the manufacturing platform –transient or transgenic needs to be made and will be based on a number of issues including yield, product quality, cost, regulatory and public acceptance and others. Transient expression allowed for fast production of 10-1074 and its variants and facilitated determining the potential of each variant before developing a transgenic line, as demonstrated in this project. Yet, transgenic production of each bNAb component of the antibody-cocktail might prove more economical particularly if transferred to an LMIC (low-middle-income country) site. In order to provide glycoengineered bNAbs, the ΔF *N. tabacum* plant line would have to be developed further, which requires additional breeding and screening, as well as further

development if the ΔX trait is considered essential. In case Cas9 can be detected in the genome of the final plant line, backcrossing would also be necessary.

Moreover, it would be critical to optimise the conditions of production and purification for each bNAb, in order to significantly improve their yield. Whilst the native 10-1074 bNAb expressed at commercially acceptable levels, the yield of the YTE version was below a level that would be acceptable to move into large scale production. An increase in yield is imperative to offer the final product at comparatively low cost.

Only when these steps have been undertaken successfully will it be possible to proceed into clinical development, starting with pilot scale GMP manufacturing and pre-clinical toxicity studies, leading to human clinical trials.

8 Bibliography

Acqua, W. F. D. *et al.* (2002) 'Increasing the Affinity of a Human IgG1 for the Neonatal Fc Receptor: Biological Consequences', *The Journal of Immunology*, 169(9), pp. 5171–5180. doi: 10.4049/jimmunol.169.9.5171.

Anthony, C. *et al.* (2017) 'Cooperation between Strain-Specific and Broadly Neutralizing Responses Limited Viral Escape and Prolonged the Exposure of the Broadly Neutralizing Epitope', *Journal of Virology*, 91(18), pp. 1–16. doi: 10.1128/jvi.00828-17.

Anthony, R. M. and Ravetch, J. V (2010) 'A novel role for the IgG Fc glycan: the anti-inflammatory activity of sialylated IgG Fcs.', *Journal of clinical immunology*. Netherlands, 30 Suppl 1, pp. S9-14. doi: 10.1007/s10875-010-9405-6.

Anumula, K. R. (2012) 'Quantitative glycan pro fi ling of normal human plasma derived immunoglobulin and its fragments Fab and Fc', *Journal of Immunological Methods*. Elsevier B.V., 382(1–2), pp. 167–176. doi: 10.1016/j.jim.2012.05.022.

Armbruster, C. *et al.* (2004) 'Passive immunization with the anti-HIV-1 human monoclonal antibody (hMAb) 4E10 and the hMAb combination 4E10/2F5/2G12', *Journal of Antimicrobial Chemotherapy*, 54(5), pp. 915–920. doi: 10.1093/jac/dkh428.

Avery, L. B. *et al.* (2016) 'Utility of a human FcRn transgenic mouse model in drug discovery for early assessment and prediction of human pharmacokinetics of monoclonal antibodies', *mAbs*. Taylor & Francis, 8(6), pp. 1064–1078. doi: 10.1080/19420862.2016.1193660.

Banks, N. D. *et al.* (2002) 'Sustained antibody-dependent cell-mediated cytotoxicity (ADCC) in SIV-infected macaques correlates with delayed progression to AIDS.', *AIDS research and human retroviruses*. United States, 18(16), pp. 1197–1205. doi: 10.1089/08892220260387940.

Bansal, R., Dash, R. and Rathore, A. S. (2020) 'Impact of mAb Aggregation on Its Biological Activity:

Rituximab as a Case Study', *Journal of Pharmaceutical Sciences*, 109(9), pp. 2684–2698. doi: https://doi.org/10.1016/j.xphs.2020.05.015.

Bar-On, Y. *et al.* (2018) 'Safety and antiviral activity of combination HIV-1 broadly neutralizing antibodies in viremic individuals', *Nature medicine*. 2018/09/26, 24(11), pp. 1701–1707. doi: 10.1038/s41591-018-0186-4.

Bardor, M. *et al.* (2003) 'Immunoreactivity in mammals of two typical plant glyco-epitopes, core α(1,3)-fucose and core xylose', *Glycobiology*, 13(6), pp. 427–434. doi: 10.1093/glycob/cwg024.

Barre-Sinoussi, F. *et al.* (1983) 'Isolation of a T-lymphotropic retrovirus from a patient at risk for acquired immune deficiency syndrome (AIDS)', *Science*, 220(4599), pp. 868 LP – 871. doi: 10.1126/science.6189183.

Bas, M. *et al.* (2019) 'Fc Sialylation Prolongs Serum Half-Life of Therapeutic Antibodies', *The Journal of Immunology*, 202(5), pp. 1582–1594. doi: 10.4049/jimmunol.1800896.

Baum, L. L. *et al.* (1996) 'HIV-1 gp120-specific antibody-dependent cell-mediated cytotoxicity correlates with rate of disease progression.', *Journal of immunology (Baltimore, Md. : 1950)*. United States, 157(5), pp. 2168–2173.

Bencúr, P. *et al.* (2005) 'Arabidopsis thaliana β1,2-xylosyltransferase: An unusual glycosyltransferase with the potential to act at multiple stages of the plant N-glycosylation pathway', *Biochemical Journal*, 388(2), pp. 515–525. doi: 10.1042/BJ20042091.

Bencúrová, M. *et al.* (2004) 'Specificity of IgG and IgE antibodies against plant and insect glycoprotein glycans determined with artificial glycoforms of human transferrin', *Glycobiology*, 14(5), pp. 457–466. doi: 10.1093/glycob/cwh058.

Bern, M. *et al.* (2015) 'The role of albumin receptors in regulation of albumin homeostasis: Implications for drug delivery', *Journal of Controlled Release*. Elsevier B.V., 211, pp. 144–162. doi:

10.1016/j.jconrel.2015.06.006.

Bombarely, A. *et al.* (2012) 'A draft genome sequence of Nicotiana benthamiana to enhance molecular plant-microbe biology research', *Molecular Plant-Microbe Interactions*, 25(12), pp. 1523–1530. doi: 10.1094/MPMI-06-12-0148-TA.

Bonsignori, M. *et al.* (2016) 'Maturation Pathway from Germline to Broad HIV-1 Neutralizer of a CD4-Mimic Antibody', *Cell*. doi: 10.1016/j.cell.2016.02.022.

Booth, B. J. *et al.* (2018) 'Extending human IgG half-life using structure-guided design', *mAbs*. Taylor & Francis, 10(7), pp. 1098–1110. doi: 10.1080/19420862.2018.1490119.

Borrok, M. J. *et al.* (2015) 'PH-dependent binding engineering reveals an FcRn affinity threshold that governs IgG recycling', *Journal of Biological Chemistry*, 290(7), pp. 4282–4290. doi: 10.1074/jbc.M114.603712.

Bortesi, L. and Fischer, R. (2015) 'The CRISPR/Cas9 system for plant genome editing and beyond', *Biotechnology Advances*. Elsevier B.V., 33(1), pp. 41–52. doi: 10.1016/j.biotechadv.2014.12.006.

Bour, S., Geleziunas, R. and Wainberg, M. A. (1995) 'The human immunodeficiency virus type 1 (HIV-1) CD4 receptor and its central role in promotion of HIV-1 infection', *Microbiological Reviews*, 59(1), pp. 63–93. doi: 10.1128/mmbr.59.1.63-93.1995.

Bournazos, S. *et al.* (2014) 'Broadly Neutralizing Anti-HIV-1 Antibodies Require Fc Effector Functions for In Vivo Activity', *Cell*, 158(6), pp. 1243–1253. doi: 10.1016/j.cell.2014.08.023.

Bowles, E. J. *et al.* (2014) 'Comparison of neutralizing antibody responses elicited from highly diverse polyvalent heterotrimeric HIV-1 gp140 cocktail immunogens versus a monovalent counterpart in rhesus macaques', *PLoS ONE*, 9(12), pp. 1–29. doi: 10.1371/journal.pone.0114709.

Brambell, F. W. R. (1967) 'Transmission of iivimunity from mother to young and the catabolism of immunoglobulins', *Obstetrical and Gynecological Survey*, 22(4), pp. 574–577. doi: 10.1016/s0140-

6736(66)92190-8.

Bruel, T. *et al.* (2016) 'Elimination of HIV-1-infected cells by broadly neutralizing antibodies', *Nature Communications*, 7, pp. 1–12. doi: 10.1038/ncomms10844.

Burmeister, W. P. *et al.* (1994) 'Crystal structure at 2.2 Å resolution of the MHC-related neonatal Fc receptor', *Nature*. doi: 10.1038/372336a0.

Burton, D. R. *et al.* (1994) 'Efficient neutralization of primary isolates of HIV-1 by a recombinant human monoclonal antibody.', *Science (New York, N.Y.)*. United States, 266(5187), pp. 1024–1027. doi: 10.1126/science.7973652.

Buyel, J. F. (2019) 'Plant molecular farming – Integration and exploitation of side streams to achieve sustainable biomanufacturing', *Frontiers in Plant Science*, 9(January), pp. 1–17. doi: 10.3389/fpls.2018.01893.

Cabanes-Macheteau, M. *et al.* (1999) 'N-Glycosylation of a mouse IgG expressed in transgenic tobacco plants', *Glycobiology*, 9(4), pp. 365–372. doi: 10.1093/glycob/9.4.365.

Callaway, E. (2018) 'CRISPR plants now subject to tough GM laws in European Union', *Nature*, 560(7716), p. 16. doi: 10.1038/d41586-018-05814-6.

Cardozo, T. *et al.* (2007) 'Structural basis for coreceptor selectivity by the HIV type 1 V3 loop', *AIDS Research and Human Retroviruses*. doi: 10.1089/aid.2006.0130.

Caskey, M. *et al.* (2015) 'Viraemia suppressed in HIV-1-infected humans by broadly neutralizing antibody 3BNC117', *Nature*, 522(7557), pp. 487–491. doi: 10.1038/nature14411.

Caskey, M. *et al.* (2017) 'Antibody 10-1074 suppresses viremia in HIV-1-infected individuals', *Nature Medicine*, 23(2), pp. 185–191. doi: 10.1038/nm.4268.

Caskey, M., Klein, F. and Nussenzweig, M. C. (2016) 'Broadly neutralizing antibodies for HIV-1

prevention or immunotherapy', *New England Journal of Medicine*. doi: 10.1056/NEJMp1613362.

Castilho, A. *et al.* (2010) 'In Planta protein sialylation through overexpression of the respective mammalian pathway', *Journal of Biological Chemistry*, 285(21), pp. 15923–15930. doi: 10.1074/jbc.M109.088401.

Castilho, A. *et al.* (2011) 'N-Glycosylation engineering of plants for the biosynthesis of glycoproteins with bisected and branched complex N-glycans', *Glycobiology*, 21(6), pp. 813–823. doi: 10.1093/glycob/cwr009.

Castilho, A. *et al.* (2015) 'Processing of complex N-glycans in IgG Fc-region is affected by core fucosylation', (October), pp. 863–870.

Chaigne, B. and Watier, H. (2015) 'Monoclonal antibodies in excess: A simple way to avoid immunogenicity in patients?', *Journal of Allergy and Clinical Immunology*, 136(3), pp. 814–816. doi: 10.1016/j.jaci.2015.03.013.

Chan, D. C. *et al.* (1997) 'Core structure of gp41 from the HIV envelope glycoprotein', *Cell*, 89(2), pp. 263–273. doi: 10.1016/S0092-8674(00)80205-6.

Checkley, M. A. *et al.* (2010) 'The capsid-spacer peptide 1 Gag processing intermediate is a dominant-negative inhibitor of HIV-1 maturation', *Virology*. 2010/02/20, 400(1), pp. 137–144. doi: 10.1016/j.virol.2010.01.028.

Chen, B. *et al.* (2013) 'Dynamic imaging of genomic loci in living human cells by an optimized CRISPR/Cas system', *Cell*. Elsevier, 155(7), pp. 1479–1491. doi: 10.1016/j.cell.2013.12.001.

Chen, Q. *et al.* (2013) 'Agroinfiltration as an Effective and Scalable Strategy of Gene Delivery for Production of Pharmaceutical Proteins', *Advanced techniques in biology & medicine*, 1(1), p. 103. doi: 10.4172/atbm.1000103.

Chu, V. T. *et al.* (2015) 'Increasing the efficiency of homology-directed repair for CRISPR-Cas9-

induced precise gene editing in mammalian cells', *Nature Biotechnology*, 33(5), pp. 543–548. doi: 10.1038/nbt.3198.

Chuang, G.-Y. *et al.* (2019) 'Structural Survey of Broadly Neutralizing Antibodies Targeting the HIV-1 Env Trimer Delineates Epitope Categories and Characteristics of Recognition.', *Structure (London, England : 1993)*. United States, 27(1), pp. 196-206.e6. doi: 10.1016/j.str.2018.10.007.

Chung, C.-Y. *et al.* (2017) 'SnapShot: N-Glycosylation Processing Pathways across Kingdoms', *Cell*, 171(1), pp. 258-258.e1. doi: https://doi.org/10.1016/j.cell.2017.09.014.

Cihlar, T. and Fordyce, M. (2016) 'Current status and prospects of HIV treatment', *Current Opinion in Virology*. Elsevier B.V., 18, pp. 50–56. doi: 10.1016/j.coviro.2016.03.004.

Claeys, E. and Vermeire, K. (2019) 'The CD4 Receptor: An Indispensable Protein in T Cell Activation and A Promising Target for Immunosuppression', *Archives of Microbiology & Immunology*, 03(03), pp. 133–150. doi: 10.26502/ami.93650036.

De Cock, K. M. *et al.* (1993) 'Epidemiology and Transmission of HIV-2: Why There Is No HIV-2 Pandemic', *JAMA*, 270(17), pp. 2083–2086. doi: 10.1001/jama.1993.03510170073033.

Cohen, Y. Z. *et al.* (2019) 'Safety, pharmacokinetics, and immunogenicity of the combination of the broadly neutralizing anti-HIV-1 antibodies 3BNC117 and 10-1074 in healthy adults: A randomized, phase 1 study', *PLoS ONE*, 14(8), pp. 1–18. doi: 10.1371/journal.pone.0219142.

Coiras, M. *et al.* (2009) 'Understanding HIV-1 latency provides clues for the eradication of long-term reservoirs', *Nature Reviews Microbiology*. Nature Publishing Group, 7(11), pp. 798–812. doi: 10.1038/nrmicro2223.

Congy-Jolivet, N. *et al.* (2008) 'Fc{gamma}RIIIa Expression Is Not Increased on Natural Killer Cells Expressing the Fc{gamma}RIIIa-158V Allotype 10.1158/0008-5472.CAN-07-6523', *Cancer Research*.

Cooper, L. J. *et al.* (1994) 'Variable domain-identical antibodies exhibit IgG subclass-related

differences in affinity and kinetic constants as determined by surface plasmon resonance.', *Molecular immunology*. England, 31(8), pp. 577–584. doi: 10.1016/0161-5890(94)90165-1.

Cox, K. M. *et al.* (2006) 'Glycan optimization of a human monoclonal antibody in the aquatic plant Lemna minor', *Nature Biotechnology*, 24(12), pp. 1591–1597. doi: 10.1038/nbt1260.

Daëron, M. (1997) ' F c RECEPTOR BIOLOGY ', *Annual Review of Immunology*. doi: 10.1146/annurev.immunol.15.1.203.

Dahodwala, H. and Lee, K. H. (2019) 'The fickle CHO: a review of the causes, implications, and potential alleviation of the CHO cell line instability problem', *Current Opinion in Biotechnology*, 60, pp. 128–137. doi: https://doi.org/10.1016/j.copbio.2019.01.011.

Dall'Acqua, W. F., Kiener, P. A. and Wu, H. (2006) 'Properties of Human IgG1s engineered for enhanced binding to the neonatal Fc Receptor (FcRn)', *Journal of Biological Chemistry*, 281(33), pp. 23514–23524. doi: 10.1074/jbc.M604292200.

Dall'Ozzo, S. *et al.* (2004) 'Rituximab-dependent cytotoxicity by natural killer cells: Influence of FCGR3A polymorphism on the concentration-effect relationship', *Cancer Research*, 64(13), pp. 4664–4669. doi: 10.1158/0008-5472.CAN-03-2862.

Dangor, Z. *et al.* (2017) 'Vaccination of HIV-infected pregnant women: Implications for protection of their young infants', *Tropical Diseases, Travel Medicine and Vaccines*. Tropical Diseases, Travel Medicine and Vaccines, 3(1), pp. 1–8. doi: 10.1186/s40794-016-0044-7.

Dekkers, G. *et al.* (2017) 'Decoding the human immunoglobulin G-glycan repertoire reveals a spectrum of Fc-receptor- and complement-mediated-effector activities', *Frontiers in Immunology*. doi: 10.3389/fimmu.2017.00877.

Desikan, R., Raja, R. and Dixit, N. M. (2019) 'Early exposure to broadly neutralizing antibodies triggers a switch from progressive disease to lasting control of SHIV infection', *bioRxiv*, p. 548727. doi:

10.1101/548727.

Diamos, A. G. *et al.* (2020) 'High Level Production of Monoclonal Antibodies Using an Optimized Plant Expression System', *Frontiers in bioengineering and biotechnology*. Frontiers Media S.A., 7, p. 472. doi: 10.3389/fbioe.2019.00472.

DiCarlo, A. L. *et al.* (2014) '"Men usually say that HIV testing is for women": gender dynamics and perceptions of HIV testing in Lesotho', *Culture, Health and Sexuality*, 16(8), pp. 867–882. doi: 10.1080/13691058.2014.913812.

Diskin, R. *et al.* (2011) 'Increasing the potency and breadth of an HIV antibody by using structure-based rational design.', *Science (New York, N.Y.)*, 334(6060), pp. 1289–1293. doi: 10.1126/science.1213782.

Domachowske, J. B. *et al.* (2018) 'Safety, Tolerability and Pharmacokinetics of MEDI8897, an Extended Half-life Single-dose Respiratory Syncytial Virus Prefusion F-targeting Monoclonal Antibody Administered as a Single Dose to Healthy Preterm Infants', *The Pediatric infectious disease journal*, 37(9), pp. 886–892. doi: 10.1097/INF.0000000000001916.

Donini, M. *et al.* (2015) 'Antibody proteolysis: a common picture emerging from plants', *Bioengineered*, 6(5), pp. 299–302. doi: 10.1080/21655979.2015.1067740.

Doria-Rose, N. A. *et al.* (2009) 'Frequency and Phenotype of Human Immunodeficiency Virus Envelope-Specific B Cells from Patients with Broadly Cross-Neutralizing Antibodies', *Journal of Virology*, 83(1), pp. 188–199. doi: 10.1128/jvi.01583-08.

Doria-Rose, N. A. *et al.* (2017) 'Mapping Polyclonal HIV-1 Antibody Responses via Next-Generation Neutralization Fingerprinting.', *PLoS pathogens*, 13(1), p. e1006148. doi: 10.1371/journal.ppat.1006148.

Dumont, J. *et al.* (2016) 'Human cell lines for biopharmaceutical manufacturing: history, status, and

future perspectives', *Critical Reviews in Biotechnology*. doi: 10.3109/07388551.2015.1084266.

Edgeworth, M. J. *et al.* (2015) 'Global and Local Conformation of Human IgG Antibody Variants Rationalizes Loss of Thermodynamic Stability', *Angewandte Chemie - International Edition*, 54(50), pp. 15156–15159. doi: 10.1002/anie.201507223.

Eigenmann, M. J. *et al.* (2017) 'Quantification of IgG monoclonal antibody clearance in tissues', *mAbs*. doi: 10.1080/19420862.2017.1337619.

Einarsdottir, H. K. *et al.* (2013) 'Comparison of the Fc glycosylation of fetal and maternal immunoglobulin G', *Glycoconjugate Journal*. doi: 10.1007/s10719-012-9381-6.

Elbers, I. J. W. *et al.* (2001) 'Influence of growth conditions and developmental stage on N-glycan heterogeneity of transgenic immunoglobulin G and endogenous proteins in tobacco leaves', *Plant Physiology*, 126(3), pp. 1314–1322. doi: 10.1104/pp.126.3.1314.

Engler, C., Kandzia, R. and Marillonnet, S. (2008) 'A one pot, one step, precision cloning method with high throughput capability', *PLoS ONE*, 3(11). doi: 10.1371/journal.pone.0003647.

Falconer, D. J. *et al.* (2018) 'Antibody Fucosylation Lowers the FcγRIIIa/CD16a Affinity by Limiting the Conformations Sampled by the N162-Glycan', *ACS chemical biology*. 2018/07/27, 13(8), pp. 2179–2189. doi: 10.1021/acschembio.8b00342.

Fan, Y. Y. *et al.* (2016) 'Tissue expression profile of human neonatal Fc receptor (FcRn) in Tg32 transgenic mice', *mAbs*. doi: 10.1080/19420862.2016.1178436.

Fan, Y. Y. and Neubert, H. (2016) 'Quantitative Analysis of Human Neonatal Fc Receptor (FcRn) Tissue Expression in Transgenic Mice by Online Peptide Immuno-Affinity LC-HRMS', *Analytical Chemistry*. doi: 10.1021/acs.analchem.5b03900.

Fanales-Belasio, E. *et al.* (2010) 'HIV virology and pathogenetic mechanisms of infection: a brief overview', *Annali dell'Istituto superiore di sanita*, 46(1), p. 5—14. doi: 10.1590/s0021-

25712010000100002.

Feldmann, G. *et al.* (1972) 'Albumin synthesis by human liver cells: its morphological demonstration.', *Gastroenterology*, 63(6), pp. 1036–1048. doi: 10.1016/s0016-5085(19)33181-6.

Feng, Z. *et al.* (2014) 'Multigeneration analysis reveals the inheritance, specificity, and patterns of CRISPR/Cas-induced gene modifications in Arabidopsis', *Proceedings of the National Academy of Sciences of the United States of America*, 111(12), pp. 4632–4637. doi: 10.1073/pnas.1400822111.

Ferrara, C. *et al.* (2011) 'Unique carbohydrate-carbohydrate interactions are required for high affinity binding between FcγRIII and antibodies lacking core fucose', *Proceedings of the National Academy of Sciences of the United States of America*, 108(31), pp. 12669–12674. doi: 10.1073/pnas.1108455108.

Ferrer-Miralles, N. *et al.* (2009) 'Microbial factories for recombinant pharmaceuticals', *Microbial Cell Factories*, 8, pp. 1–8. doi: 10.1186/1475-2859-8-17.

Firan, M. *et al.* (2001) 'The MHC class I-related receptor, FcRn, plays an essential role in the maternofetal transfer of γ-globulin in humans', *International Immunology*. doi: 10.1093/intimm/13.8.993.

Fire, A. *et al.* (1998) 'Potent and specific genetic interference by double-stranded RNA in Caenorhabditis elegans.', *Nature*. England, 391(6669), pp. 806–811. doi: 10.1038/35888.

Fischer, R. and Emans, N. (2000) 'Molecular farming of pharmaceutical proteins', *Transgenic Research*. doi: 10.1023/A:1008975123362.

Folks, T. *et al.* (1986) 'Induction of HTLV-III/LAV from a nonvirus-producing T-cell line: Implications for latency', *Science*, 231(4738), pp. 600–602. doi: 10.1126/science.3003906.

Fouda, G. G. *et al.* (2018) 'The Impact of IgG Transplacental Transfer on Early Life Immunity', *ImmunoHorizons*, 2(1), pp. 14–25. doi: 10.4049/immunohorizons.1700057.

Frankel, A. D. and Young, J. A. (1998) 'HIV-1: fifteen proteins and an RNA.', *Annual review of biochemistry*. United States, 67, pp. 1–25. doi: 10.1146/annurev.biochem.67.1.1.

Fridman, W. H. (1991) 'Fc receptors and immunoglobulin binding factors', *FASEB Journal*. doi: 10.1096/fasebj.5.12.1916092.

Gao, J. *et al.* (2015) 'CRISPR/Cas9-mediated targeted mutagenesis in Nicotiana tabacum', *Plant Molecular Biology*, 87(1–2), pp. 99–110. doi: 10.1007/s11103-014-0263-0.

Gao, Z., Herrera-Carrillo, E. and Berkhout, B. (2018) 'Delineation of the Exact Transcription Termination Signal for Type 3 Polymerase III', *Molecular Therapy - Nucleic Acids*. Elsevier Ltd., 10(March), pp. 36–44. doi: 10.1016/j.omtn.2017.11.006.

Garabagi, F., McLean, M. D. and Hall, J. C. (2012) 'Transient and stable expression of antibodies in nicotiana species', *Methods in Molecular Biology*. doi: 10.1007/978-1-61779-974-7_23.

Garber, E. and Demarest, S. J. (2007) 'A broad range of Fab stabilities within a host of therapeutic IgGs', *Biochemical and Biophysical Research Communications*. Academic Press, 355(3), pp. 751–757. doi: 10.1016/J.BBRC.2007.02.042.

Garces, F. *et al.* (2014) 'Structural evolution of glycan recognition by a family of potent HIV antibodies', *Cell*. doi: 10.1016/j.cell.2014.09.009.

Gaudinski, M. R. *et al.* (2018) 'Safety and pharmacokinetics of the Fc-modified HIV-1 human monoclonal antibody VRC01LS: A Phase 1 open-label clinical trial in healthy adults', *PLOS Medicine*. Public Library of Science, 15(1), p. e1002493. doi: 10.1371/journal.pmed.1002493.

Gautam, R. *et al.* (2018) 'A single injection of crystallizable fragment domain-modified antibodies elicits durable protection from SHIV infection', *Nature Medicine*. Springer US, 24(5), pp. 610–616. doi: 10.1038/s41591-018-0001-2.

Gebregziabher, M. *et al.* (2018) 'Gender Disparities in Receipt of HIV Testing Results in Six Sub-

Saharan African Countries', *Health Equity*, 2(1), pp. 384–394. doi: 10.1089/heq.2018.0060.

Gelderblom, H. R., Ozel, M. and Pauli, G. (1989) 'Morphogenesis and morphology of HIV. Structure-function relations.', *Archives of virology*. Austria, 106(1–2), pp. 1–13. doi: 10.1007/bf01311033.

Georgiev, I. S. *et al.* (2013) 'Delineating antibody recognition in polyclonal sera from patterns of HIV-1 isolate neutralization', *Science*, 340(6133), pp. 751–756. doi: 10.1126/science.1233989.

German Advisory Committee Blood (Arbeitskreis Blut), S. 'Assessment of P. T. by B. (2016) 'Human Immunodeficiency Virus (HIV)', *Transfusion medicine and hemotherapy : offizielles Organ der Deutschen Gesellschaft fur Transfusionsmedizin und Immunhamatologie*. 2016/05/09. S. Karger GmbH, 43(3), pp. 203–222. doi: 10.1159/000445852.

Ghaderi, D. *et al.* (2012) 'Production platforms for biotherapeutic glycoproteins. Occurrence, impact, and challenges of non-human sialylation', *Biotechnology and Genetic Engineering Reviews*. doi: 10.5661/bger-28-147.

Gill, M. M. *et al.* (2016) 'Detectable viral load in late pregnancy among women in the Rwanda option B+ PMTCT program: Enrollment results from the Kabeho Study', *PLoS ONE*, 11(12), pp. 1–14. doi: 10.1371/journal.pone.0168671.

Gökengin, D. *et al.* (2016) 'HIV/AIDS: Trends in the Middle East and North Africa region', *International Journal of Infectious Diseases*, 44, pp. 66–73. doi: 10.1016/j.ijid.2015.11.008.

Gómez-Román, V. R. *et al.* (2005) ' Vaccine-Elicited Antibodies Mediate Antibody-Dependent Cellular Cytotoxicity Correlated with Significantly Reduced Acute Viremia in Rhesus Macaques Challenged with SIV mac251 ', *The Journal of Immunology*, 174(4), pp. 2185–2189. doi: 10.4049/jimmunol.174.4.2185.

Gómez Román, V. R., Murray, J. C. and Weiner, L. M. (2013) 'Antibody-Dependent Cellular Cytotoxicity (ADCC)', *Antibody Fc: Linking Adaptive and Innate Immunity*, pp. 1–27. doi:

10.1016/B978-0-12-394802-1.00001-7.

Gonda, M. A. *et al.* (1985) 'Sequence homology and morphologic similarity of HTLV-III and visna virus, a pathogenic lentivirus', *Science (New York, N.Y.)*, 227(4683), p. 173—177. doi: 10.1126/science.2981428.

Goo, L. *et al.* (2014) 'Early development of broadly neutralizing antibodies in HIV-1-infected infants', *Nature Medicine*. Nature Publishing Group, 20(6), pp. 655–658. doi: 10.1038/nm.3565.

Gottlieb, M. S. *et al.* (1981) 'Pneumocystis carinii Pneumonia and Mucosal Candidiasis in Previously Healthy Homosexual Men: Evidence of a New Acquired Cellular Immunodeficiency', *New England Journal of Medicine*. doi: 10.1056/NEJM198112103052401.

Goulet, M. C. *et al.* (2019) 'Production of biopharmaceuticals in Nicotiana benthamiana—axillary stem growth as a key determinant of total protein yield', *Frontiers in Plant Science*, 10(June). doi: 10.3389/fpls.2019.00735.

Greenwood, B. (2014) 'The contribution of vaccination to global health: Past, present and future', *Philosophical Transactions of the Royal Society B: Biological Sciences*, 369(1645). doi: 10.1098/rstb.2013.0433.

Griffin, M. P. *et al.* (2016) 'Safety, Tolerability, and Pharmacokinetics of MEDI8897, the Respiratory Syncytial Virus Prefusion F-Targeting Monoclonal Antibody with an Extended Half-Life, in Healthy Adults While RSV prevention exists in the form of a specific RSV immunoglobulin G (IgG', *Antimicrobial Agents and Chemotherapy*, 61(3), pp. e01714-16. doi: 10.1128/AAC.01714-16.

Grilo, A. L. and Mantalaris, A. (2019) 'The Increasingly Human and Profitable Monoclonal Antibody Market.', *Trends in biotechnology*. Elsevier Ltd, 37(1), pp. 9–16. doi: 10.1016/j.tibtech.2018.05.014.

Grobben, M., Stuart, R. AL and van Gils, M. J. (2019) 'The potential of engineered antibodies for HIV-1 therapy and cure', *Current Opinion in Virology*. Elsevier B.V., 38, pp. 70–80. doi:

10.1016/j.coviro.2019.07.007.

Grünwald-Gruber, C. *et al.* (2017) 'Determination of true ratios of different N-glycan structures in electrospray ionization mass spectrometry', *Analytical and Bioanalytical Chemistry*. Analytical and Bioanalytical Chemistry, 409(10), pp. 2519–2530. doi: 10.1007/s00216-017-0235-8.

Gupta, R. K. *et al.* (2018) 'HIV-1 drug resistance before initiation or re-initiation of first-line antiretroviral therapy in low-income and middle-income countries: a systematic review and meta-regression analysis', *The Lancet Infectious Diseases*. The Author(s). Published by Elsevier Ltd. This is an Open Access article under the CC BY 4.0 license, 18(3), pp. 346–355. doi: 10.1016/S1473-3099(17)30702-8.

Guyader, M. reille *et al.* (1987) 'Genome organization and transactivation of the human immunodeficiency virus type 2', *Nature*, 326(6114), pp. 662–669. doi: 10.1038/326662a0.

Ha, J. H. *et al.* (2019) 'Gendered relationship between HIV stigma and HIV testing among men and women in Mozambique: A cross-sectional study to inform a stigma reduction and male-targeted HIV testing intervention', *BMJ Open*, 9(10), pp. 1–10. doi: 10.1136/bmjopen-2019-029748.

Hanania, U. *et al.* (2017) 'Establishment of a tobacco BY2 cell line devoid of plant-specific xylose and fucose as a platform for the production of biotherapeutic proteins', *Plant Biotechnology Journal*, 15(9), pp. 1120–1129. doi: 10.1111/pbi.12702.

Harmoko, R. *et al.* (2016) 'N-glycan containing a core α1,3-fucose residue is required for basipetal auxin transport and gravitropic response in rice (Oryza sativa)', *The New phytologist*, 212(1), pp. 108–122. doi: 10.1111/nph.14031.

Hartman, T. L. and Buckheit, R. W. (2012) 'The Continuing Evolution of HIV-1 Therapy: Identification and Development of Novel Antiretroviral Agents Targeting Viral and Cellular Targets', *Molecular Biology International*, 2012, pp. 1–17. doi: 10.1155/2012/401965.

Havlir, D. and Gandhi, M. (2015) 'Implementation challenges for long-acting antivirals as treatment', *Current opinion in HIV and AIDS*, 10(4), pp. 282–289. doi: 10.1097/COH.0000000000000158.

Hehle, V. K. *et al.* (2011) 'Antibody degradation in tobacco plants: A predominantly apoplastic process', *BMC Biotechnology*, 11. doi: 10.1186/1472-6750-11-128.

Hehle, V. K. *et al.* (2015) 'Site-specific proteolytic degradation of IgG monoclonal antibodies expressed in tobacco plants', *Plant Biotechnology Journal*, 13(2), pp. 235–245. doi: 10.1111/pbi.12266.

Helenius, A. and Aebi, M. (2001) 'Intracellular functions of N-linked glycans.', *Science (New York, N.Y.)*. United States, 291(5512), pp. 2364–2369. doi: 10.1126/science.291.5512.2364.

Hernandez, I. *et al.* (2018) 'Pricing of Monoclonal Antibody Therapies: Higher If Used for Cancer?', *American Journal of Managed Care*, 24(2), pp. 109–112.

Hessell, A. J. *et al.* (2007) 'Fc receptor but not complement binding is important in antibody protection against HIV', *Nature*, 449(7158), pp. 101–104. doi: 10.1038/nature06106.

Hessell, A. J. *et al.* (2009) 'Effective, low-titer antibody protection against low-dose repeated mucosal SHIV challenge in macaques', *Nature Medicine*. Nature Publishing Group, 15(8), pp. 951–954. doi: 10.1038/nm.1974.

Hiatt, A., Cafferkey, R. and Bowdish, K. (1989) 'Production of antibodies in transgenic plants', *Nature*. doi: 10.1038/342076a0.

Hiatt, A. and Pauly, M. (2006) 'Monoclonal antibodies from plants: A new speed record', *Proceedings of the National Academy of Sciences of the United States of America*, 103(40), pp. 14645–14646. doi: 10.1073/pnas.0607089103.

Hogarth, P. M. and Pietersz, G. A. (2012) 'Fc receptor-targeted therapies for the treatment of inflammation, cancer and beyond', *Nature Reviews Drug Discovery*, 11(4), pp. 311–331. doi:

10.1038/nrd2909.

van der Hoorn, R. A. L. (2008) 'Plant Proteases: From Phenotypes to Molecular Mechanisms', *Annual Review of Plant Biology*, 59(1), pp. 191–223. doi: 10.1146/annurev.arplant.59.032607.092835.

Horner, H. *et al.* (2007) 'Intimate Cell Conjugate Formation and Exchange of Membrane Lipids Precede Apoptosis Induction in Target Cells during Antibody-Dependent, Granulocyte-Mediated Cytotoxicity', *The Journal of Immunology*. doi: 10.4049/jimmunol.179.1.337.

Horvath, P. and Barrangou, R. (2010) 'CRISPR/Cas, the immune system of Bacteria and Archaea', *Science*, 327(5962), pp. 167–170. doi: 10.1126/science.1179555.

Hossler, P., Khattak, S. and Li, Z. J. (2009) 'Optimal and consistent protein glycosylation in mammalian cell culture', *Glycobiology*, 19, pp. 936–949. doi: 10.1093/glycob/cwp079.

Houdebine, L. M. (2009) 'Production of pharmaceutical proteins by transgenic animals', *Comparative Immunology, Microbiology and Infectious Diseases*. doi: 10.1016/j.cimid.2007.11.005.

Hsu, P. D. *et al.* (2013) 'DNA targeting specificity of RNA-guided Cas9 nucleases', *Nature Biotechnology*, 31(9), pp. 827–832. doi: 10.1038/nbt.2647.

Huang, C. C. *et al.* (2007) 'Structures of the CCR5 N terminus and of a tyrosine-sulfated antibody with HIV-1 gp120 and CD4', *Science*. doi: 10.1126/science.1145373.

Huang, J. *et al.* (2016) 'Identification of a CD4-Binding-Site Antibody to HIV that Evolved Near-Pan Neutralization Breadth.', *Immunity*. United States, 45(5), pp. 1108–1121. doi: 10.1016/j.immuni.2016.10.027.

Hurtado, J. *et al.* (2020) 'In vitro and in vivo efficacy of anti-chikungunya virus monoclonal antibodies produced in wild-type and glycoengineered Nicotiana benthamiana plants', *Plant Biotechnology Journal*, 18(1), pp. 266–273. doi: 10.1111/pbi.13194.

Iacob, S. A., Iacob, D. G. and Jugulete, G. (2017) 'Improving the adherence to antiretroviral therapy, a difficult but essential task for a successful HIV treatment-clinical points of view and practical considerations', *Frontiers in Pharmacology*, 8(NOV). doi: 10.3389/fphar.2017.00831.

Igawa, T. *et al.* (2010) 'Reduced elimination of IgG antibodies by engineering the variable region', *Protein Engineering, Design and Selection*, 23(5), pp. 385–392. doi: 10.1093/protein/gzq009.

Jaganathan, D. *et al.* (2018) 'CRISPR for crop improvement: An update review', *Frontiers in Plant Science*, 9(July), pp. 1–17. doi: 10.3389/fpls.2018.00985.

Jansen, R. *et al.* (2002) 'Identification of genes that are associated with DNA repeats in prokaryotes', *Molecular Microbiology*. doi: 10.1046/j.1365-2958.2002.02839.x.

Jansing, J. *et al.* (2019) 'CRISPR/Cas9-mediated knockout of six glycosyltransferase genes in Nicotiana benthamiana for the production of recombinant proteins lacking β-1,2-xylose and core α-1,3-fucose', *Plant Biotechnology Journal*, 17(2), pp. 350–361. doi: 10.1111/pbi.12981.

Jaramillo, C. A. C. *et al.* (2017) 'Toward in vitro-to-in vivo translation of monoclonal antibody pharmacokinetics: Application of a neonatal Fc receptor-mediated transcytosis assay to understand the interplaying clearance mechanisms', *mAbs*. Taylor & Francis, 9(5), pp. 781–791. doi: 10.1080/19420862.2017.1320008.

Jensen, P. F. *et al.* (2017) 'A Two-pronged Binding Mechanism of IgG to the Neonatal Fc Receptor Controls Complex Stability and IgG Serum Half-life', *Molecular & Cellular Proteomics*, 16(3), pp. 451–456. doi: 10.1074/mcp.M116.064675.

Jiang, F. and Doudna, J. A. (2017) 'CRISPR–Cas9 Structures and Mechanisms', *Annual Review of Biophysics*. doi: 10.1146/annurev-biophys-062215-010822.

Jin, F. and Balthasar, J. P. (2005) 'Mechanisms of intravenous immunoglobulin action in immune thrombocytopenic purpura', *Human Immunology*, 66(4), pp. 403–410. doi:

10.1016/j.humimm.2005.01.029.

Jinek, M. *et al.* (2014a) 'Structures of Cas9 endonucleases reveal RNA-mediated conformational activation', *Science*. doi: 10.1126/science.1247997.

Jinek, M. *et al.* (2014b) 'Structures of Cas9 Endonucleases Reveal RNA-Mediated Conformational Activation', *Science*, 343(6176), pp. 1247997–1247997. doi: 10.1126/science.1247997.

Julien, J.-P. *et al.* (2013) 'Crystal Structure of a Soluble Cleaved HIV-1 Envelope Trimer', *Science*, 342(6165), pp. 1477 LP – 1483. doi: 10.1126/science.1245625.

Kamisugi, Y. *et al.* (2006) 'The mechanism of gene targeting in Physcomitrella patens: Homologous recombination, concatenation and multiple integration', *Nucleic Acids Research*, 34(21), pp. 6205–6214. doi: 10.1093/nar/gkl832.

Kaneko, Y., Nimmerjahn, F. and Ravetch, J. V. (2006) 'Anti-inflammatory activity of immunoglobulin G resulting from Fc sialylation', *Science*. doi: 10.1126/science.1129594.

Kang, C. *et al.* (2018) 'A novel therapeutic anti-HBV antibody with increased binding to human FcRn improves in vivo PK in mice and monkeys', *Protein and Cell*, 9(1), pp. 130–134. doi: 10.1007/s13238-017-0438-y.

Kelton, W. J. *et al.* (2016) 'Surveying the delivery methods of CRISPR/Cas9 for ex vivo mammalian cell engineering', *Chimia*, 70(6), pp. 439–442. doi: 10.2533/chimia.2016.439.

Kerwin, B. A. (2008) 'Polysorbates 20 and 80 Used in the Formulation of Protein Biotherapeutics: Structure and Degradation Pathways', *Journal of Pharmaceutical Sciences*. Elsevier, 97(8), pp. 2924–2935. doi: 10.1002/JPS.21190.

Kim, J. *et al.* (2018) 'Adherence to antiretroviral therapy and factors affecting low medication adherence among incident HIV-infected individuals during 2009-2016: A nationwide study', *Scientific Reports*. Springer US, 8(1), pp. 1–8. doi: 10.1038/s41598-018-21081-x.

Kiyoshi, M. *et al.* (2017) 'Glycosylation of IgG-Fc: A molecular perspective', *International Immunology*, 29(7), pp. 311–317. doi: 10.1093/intimm/dxx038.

Klasse, P. J. (2014) 'Neutralization of Virus Infectivity by Antibodies: Old Problems in New Perspectives', *Advances in Biology*, 2014, pp. 1–24. doi: 10.1155/2014/157895.

Klein, F. *et al.* (2013) 'Antibodies in HIV-1 vaccine development and therapy.', *Science (New York, N.Y.)*. United States, 341(6151), pp. 1199–1204. doi: 10.1126/science.1241144.

Ko, S. Y. *et al.* (2014) 'Enhanced neonatal Fc receptor function improves protection against primate SHIV infection', *Nature*. doi: 10.1038/nature13612.

Koene, H. R. *et al.* (1997) 'Fc gammaRIIIa-158V/F polymorphism influences the binding of IgG by natural killer cell Fc gammaRIIIa, independently of the Fc gammaRIIIa-48L/R/H phenotype.', *Blood*. United States, 90(3), pp. 1109–1114.

Kong, L. *et al.* (2013) 'Supersite of immune vulnerability on the glycosylated face of HIV-1 envelope glycoprotein gp120', *Nature Structural and Molecular Biology*. doi: 10.1038/nsmb.2594.

Koprivova, A. *et al.* (2004) 'Targeted knockouts of Physcomitrella lacking plant-specific immunogenic N-glycans', *Plant Biotechnology Journal*, 2(6), pp. 517–523. doi: 10.1111/j.1467-7652.2004.00100.x.

Kosaka, P. M. *et al.* (2017) 'Ultrasensitive detection of HIV-1 p24 antigen by a hybrid nanomechanical-optoplasmonic platform with potential for detecting HIV-1 at first week after infection', *PLoS ONE*, 12(2), pp. 1–13. doi: 10.1371/journal.pone.0171899.

Kräusslich, H. G. *et al.* (1995) 'The spacer peptide between human immunodeficiency virus capsid and nucleocapsid proteins is essential for ordered assembly and viral infectivity.', *Journal of virology*, 69(6), pp. 3407–3419. doi: 10.1128/JVI.69.6.3407-3419.1995.

Kubota, T. *et al.* (2009) 'Engineered therapeutic antibodies with improved effector functions', *Cancer Science*, 100(9), pp. 1566–1572. doi: 10.1111/j.1349-7006.2009.01222.x.

Kwong, P. D. *et al.* (2000) 'Structures of HIV-1 gp120 envelope glycoproteins from laboratory-adapted and primary isolates', *Structure*. doi: 10.1016/S0969-2126(00)00547-5.

Kwong, P. D., Mascola, J. R. and Nabel, G. J. (2013) 'Broadly neutralizing antibodies and the search for an HIV-1 vaccine: The end of the beginning', *Nature Reviews Immunology*. doi: 10.1038/nri3516.

Lai, H. *et al.* (2014) 'Structural and functional characterization of an anti-West Nile virus monoclonal antibody and its single-chain variant produced in glycoengineered plants', *Plant Biotechnology Journal*, 12(8), pp. 1098–1107. doi: 10.1111/pbi.12217.

Lambotte, O. *et al.* (2013) 'High Antibody-Dependent Cellular Cytotoxicity Responses Are Correlated with Strong CD8 T Cell Viral Suppressive Activity but Not with B57 Status in HIV-1 Elite Controllers', *PLoS ONE*, 8(9), pp. 1–5. doi: 10.1371/journal.pone.0074855.

Landais, E. and Moore, P. L. (2018) 'Development of broadly neutralizing antibodies in HIV-1 infected elite neutralizers', *Retrovirology*. BioMed Central, 15(1), pp. 1–14. doi: 10.1186/s12977-018-0443-0.

Latvala, S. *et al.* (2017) 'Distribution of FcRn Across Species and Tissues', *Journal of Histochemistry and Cytochemistry*. doi: 10.1369/0022155417705095.

Leach, J. L. *et al.* (1996) 'Isolation from human placenta of the IgG transporter, FcRn, and localization to the syncytiotrophoblast: implications for maternal-fetal antibody transport.', *Journal of immunology (Baltimore, Md. : 1950)*.

Ledgerwood, J. E. *et al.* (2015) 'Safety, pharmacokinetics and neutralization of the broadly neutralizing HIV-1 human monoclonal antibody VRC01 in healthy adults', *Clinical and Experimental Immunology*, 182(3), pp. 289–301. doi: 10.1111/cei.12692.

Lee, W. S. and Kent, S. J. (2018) 'Anti-HIV-1 antibody-dependent cellular cytotoxicity: Is there more to antibodies than neutralization?', *Current Opinion in HIV and AIDS*, 13(2), pp. 160–166. doi: 10.1097/COH.0000000000000439.

Lei, Y. *et al.* (2014) 'CRISPR-P: a web tool for synthetic single-guide RNA design of CRISPR-system in plants.', *Molecular plant*. England, pp. 1494–1496. doi: 10.1093/mp/ssu044.

Li, J. *et al.* (2016) 'Multiplexed, targeted gene editing in Nicotiana benthamiana for glyco-engineering and monoclonal antibody production', *Plant Biotechnology Journal*, 14(2), pp. 533–542. doi: 10.1111/pbi.12403.

Li, J. F. *et al.* (2013) 'Multiplex and homologous recombination-mediated genome editing in Arabidopsis and Nicotiana benthamiana using guide RNA and Cas9', *Nature Biotechnology*, 31(8), pp. 688–691. doi: 10.1038/nbt.2654.

Li, T. *et al.* (2017) 'Modulating IgG effector function by Fc glycan engineering', *Proceedings of the National Academy of Sciences of the United States of America*, 114(13), pp. 3485–3490. doi: 10.1073/pnas.1702173114.

Li, T. and Balthasar, J. P. (2018) 'FcRn expression in wildtype mice, transgenic mice, and in human tissues', *Biomolecules*, 8(4). doi: 10.3390/biom8040115.

Liang, Z. *et al.* (2014) 'Targeted mutagenesis in Zea mays using TALENs and the CRISPR/Cas system', *Journal of Genetics and Genomics*. doi: 10.1016/j.jgg.2013.12.001.

Liao, H.-X. *et al.* (2013) 'Co-evolution of a broadly neutralizing HIV-1 antibody and founder virus', *Nature*. 2013/04/03, 496(7446), pp. 469–476. doi: 10.1038/nature12053.

Liebminger, E. *et al.* (2009) 'Class I α-mannosidases are required for N-glycan processing and root development in Arabidopsis thaliana', *Plant Cell*, 21(12), pp. 3850–3867. doi: 10.1105/tpc.109.072363.

Liu, B., Saber, A. and Haisma, H. J. (2019) 'CRISPR/Cas9: a powerful tool for identification of new targets for cancer treatment', *Drug Discovery Today*. Elsevier Ltd, 24(4), pp. 955–970. doi: 10.1016/j.drudis.2019.02.011.

Lobo, E. D., Hansen, R. J. and Balthasar, J. P. (2004) 'Antibody pharmacokinetics and pharmacodynamics', *Journal of Pharmaceutical Sciences*, 93(11), pp. 2645–2668. doi: 10.1002/jps.20178.

Łojewska, E. *et al.* (2016) 'Extraction and purification methods in downstream processing of plant-based recombinant proteins', *Protein Expression and Purification*, 120, pp. 110–117. doi: 10.1016/j.pep.2015.12.018.

Lorenzo-Redondo, R. *et al.* (2016) 'Persistent HIV-1 replication maintains the tissue reservoir during therapy', *Nature*. Nature Publishing Group, 530(7588), pp. 51–56. doi: 10.1038/nature16933.

Lowder, L., Malzahn, A. and Qi, Y. (2016) 'Rapid evolution of manifold CRISPR systems for plant genome editing', *Frontiers in Plant Science*. doi: 10.3389/fpls.2016.01683.

Lu, J. *et al.* (2015) 'Structure of FcγRI in complex with Fc reveals the importance of glycan recognition for high-affinity IgG binding', *Proceedings of the National Academy of Sciences*, 112(3), pp. 833–838. doi: 10.1073/pnas.1418812112.

Luo, C. *et al.* (2017) 'Glycoengineering of pertuzumab and its impact on the pharmacokinetic/pharmacodynamic properties', *Scientific Reports*, 7(October 2016), pp. 1–10. doi: 10.1038/srep46347.

Ma, J. K. *et al.* (2015) 'Regulatory approval and a first-in-human phase I clinical trial of a monoclonal antibody produced in transgenic tobacco plants', *Plant Biotechnology Journal*, 13(8), pp. 1106–1120. doi: 10.1111/pbi.12416.

Ma, J. K. C. *et al.* (2013) 'Realising the value of plant molecular pharming to benefit the poor in developing countries and emerging economies', *Plant Biotechnology Journal*, 11(9), pp. 1029–1033. doi: 10.1111/pbi.12127.

Madhavi, V. *et al.* (2017) 'HIV-1 Env- and Vpu-Specific Antibody-Dependent Cellular Cytotoxicity

Responses Associated with Elite Control of HIV.', *Journal of virology*. United States, 91(18). doi: 10.1128/JVI.00700-17.

Mahaweni, N. M. *et al.* (2018) 'A comprehensive overview of FCGR3A gene variability by full-length gene sequencing including the identification of V158F polymorphism', *Scientific Reports*, 8(1), pp. 1–11. doi: 10.1038/s41598-018-34258-1.

Mahdi, M. *et al.* (2018) 'Inhibitory Effects of HIV-2 Vpx on Replication of HIV-1', *Journal of Virology*. Edited by F. Kirchhoff, 92(14), pp. e00554-18. doi: 10.1128/JVI.00554-18.

Makarova, K. S. *et al.* (2011) 'Evolution and classification of the CRISPR–Cas systems', *Nature Reviews Microbiology*, 9(6), pp. 467–477. doi: 10.1038/nrmicro2577.

Malek, A. *et al.* (1995) 'Transport of immunoglobulin G and its subclasses across the in vitro-perfused human placenta', *American Journal of Obstetrics and Gynecology*. doi: 10.1016/0002-9378(95)90336-4.

Malek, A., Sager, R. and Schneider, H. (1994) 'Maternal—Fetal Transport of Immunoglobulin G and Its Subclasses During the Third Trimester of Human Pregnancy', *American Journal of Reproductive Immunology*. doi: 10.1111/j.1600-0897.1994.tb00873.x.

Malek, A., Sager, R. and Schneider, H. (1998) 'Transport of proteins across the human placenta', *American Journal of Reproductive Immunology*. doi: 10.1111/j.1600-0897.1998.tb00064.x.

Marraffini, L. A. (2016) *The CRISPR-Cas system of Streptococcus pyogenes: function and applications*, *Streptococcus pyogenes: Basic Biology to Clinical Manifestations*.

Mascola, J. R. *et al.* (1996) 'Immunization with envelope subunit vaccine products elicits neutralizing antibodies against laboratory-adapted but not primary isolates of human immunodeficiency virus type 1. The National Institute of Allergy and Infectious Diseases AIDS Vaccine Evaluati', *The Journal of infectious diseases*. United States, 173(2), pp. 340–348. doi: 10.1093/infdis/173.2.340.

Masenyetse, L. J., Manda, S. O. M. and Mwambi, H. G. (2015) 'An assessment of adverse drug reactions among HIV positive patients receiving antiretroviral treatment in South Africa', *AIDS Research and Therapy*, 12(1), pp. 1–8. doi: 10.1186/s12981-015-0044-0.

Matsuo, K. and Atsumi, G. (2019) 'CRISPR/Cas9-mediated knockout of the RDR6 gene in Nicotiana benthamiana for efficient transient expression of recombinant proteins', *Planta*. Springer Berlin Heidelberg, 250(2), pp. 463–473. doi: 10.1007/s00425-019-03180-9.

May, K. *et al.* (2009) 'Antibody-dependent transplacental transfer of malaria blood-stage antigen using a human ex vivo placental perfusion model', *PLoS ONE*. doi: 10.1371/journal.pone.0007986.

Mbuagbaw, L. *et al.* (2018) 'Strategies to improve adherence to antiretroviral therapy and retention in care for people living with HIV in high-income countries: a protocol for an overview of systematic reviews', *BMJ open*, 8(9), p. e022982. doi: 10.1136/bmjopen-2018-022982.

McCoy, L. E. and Burton, D. R. (2017) 'Identification and specificity of broadly neutralizing antibodies against HIV', *Immunological Reviews*, 275(1), pp. 11–20. doi: 10.1111/imr.12484.

Mehandru, S. *et al.* (2007) 'Adjunctive Passive Immunotherapy in Human Immunodeficiency Virus Type 1-Infected Individuals Treated with Antiviral Therapy during Acute and Early Infection', *Journal of Virology*, 81(20), pp. 11016–11031. doi: 10.1128/jvi.01340-07.

Mercx, S. *et al.* (2017) 'Inactivation of the β(1,2)-xylosyltransferase and the α(1,3)-fucosyltransferase genes in Nicotiana tabacum BY-2 cells by a multiplex CRISPR/Cas9 strategy results in glycoproteins without plant-specific glycans', *Frontiers in Plant Science*, 8(March), pp. 1–11. doi: 10.3389/fpls.2017.00403.

Merk, A. and Subramaniam, S. (2013) 'HIV-1 envelope glycoprotein structure.', *Current opinion in structural biology*, 23(2), pp. 268–276. doi: 10.1016/j.sbi.2013.03.007.

Mills, E. J. *et al.* (2011) 'Life expectancy of persons receiving combination antiretroviral therapy in

low-income countries: A cohort analysis from Uganda', *Annals of Internal Medicine*, 155(4), pp. 209–217. doi: 10.7326/0003-4819-155-4-201108160-00358.

Mimura, Y. *et al.* (2007) 'Contrasting glycosylation profiles between Fab and Fc of a human IgG protein studied by electrospray ionization mass spectrometry', 326, pp. 116–126. doi: 10.1016/j.jim.2007.07.014.

Moldt, B. *et al.* (2012) 'A Nonfucosylated Variant of the anti-HIV-1 Monoclonal Antibody b12 Has Enhanced Fc RIIIa-Mediated Antiviral Activity In Vitro but Does Not Improve Protection against Mucosal SHIV Challenge in Macaques', *Journal of Virology*, 86(11), pp. 6189–6196. doi: 10.1128/jvi.00491-12.

Montero-Morales, L. and Steinkellner, H. (2018) 'Advanced plant-based glycan engineering', *Frontiers in Bioengineering and Biotechnology*, 9(JUN), pp. 1–8. doi: 10.3389/fbioe.2018.00081.

Moore, P. L. *et al.* (2013) 'Multiple Pathways of Escape from HIV Broadly Cross-Neutralizing V2-Dependent Antibodies', *Journal of Virology*, 87(9), pp. 4882–4894. doi: 10.1128/jvi.03424-12.

Moore, P. L., Williamson, C. and Morris, L. (2015) 'Virological features associated with the development of broadly neutralizing antibodies to HIV-1', *Trends in microbiology*. 2015/01/05, 23(4), pp. 204–211. doi: 10.1016/j.tim.2014.12.007.

Mor, T. S. (2015) 'Molecular pharming's foot in the FDA's door: Protalix's trailblazing story', *Biotechnology letters*. 2015/07/07, 37(11), pp. 2147–2150. doi: 10.1007/s10529-015-1908-z.

Morell, A. *et al.* (1973) 'Metabolic properties of human IgA subclasses.', *Clinical and Experimental Immunology*, 13(4), pp. 521–528.

Moreno-Mateos, M. A. *et al.* (2015) 'CRISPRscan: Designing highly efficient sgRNAs for CRISPR-Cas9 targeting in vivo', *Nature Methods*, 12(10), pp. 982–988. doi: 10.1038/nmeth.3543.

Morris, G. C. *et al.* (2014) 'MABGEL 1: first phase 1 trial of the anti-HIV-1 monoclonal antibodies 2F5,

4E10 and 2G12 as a vaginal microbicide.', *PloS one*. United States, 9(12), p. e116153. doi: 10.1371/journal.pone.0116153.

Mouquet, H. *et al.* (2012) 'Complex-type N-glycan recognition by potent broadly neutralizing HIV antibodies', *Proceedings of the National Academy of Sciences*, 109(47), pp. E3268–E3277. doi: 10.1073/pnas.1217207109.

Mu, W. *et al.* (2019) '5' capped and 3' polyA-tailed sgRNAs enhance the efficiency of CRISPR-Cas9 system', *Protein and Cell*, 10(3), pp. 223–228. doi: 10.1007/s13238-018-0552-5.

Muenchhoff, M. *et al.* (2016) 'Nonprogressing HIV-infected children share fundamental immunological features of nonpathogenic SIV infection', *Science Translational Medicine*. doi: 10.1126/scitranslmed.aag1048.

Murad, S. *et al.* (2020) 'Molecular Pharming for low and middle income countries', *Current Opinion in Biotechnology*. Elsevier Ltd, 61(November 2019), pp. 53–59. doi: 10.1016/j.copbio.2019.10.005.

De Muynck, B., Navarre, C. and Boutry, M. (2010) 'Production of antibodies in plants: Status after twenty years', *Plant Biotechnology Journal*, 8(5), pp. 529–563. doi: 10.1111/j.1467-7652.2009.00494.x.

Nandi, S. *et al.* (2016) 'Techno-economic analysis of a transient plant-based platform for monoclonal antibody production', *mAbs*. Taylor & Francis, 8(8), pp. 1456–1466. doi: 10.1080/19420862.2016.1227901.

Nekrasov, V. *et al.* (2013) 'Targeted mutagenesis in the model plant Nicotiana benthamiana using Cas9 RNA-guided endonuclease', *Nature Biotechnology*, 31(8), pp. 691–693. doi: 10.1038/nbt.2655.

Newell, M. L. (1998) 'Mechanisms and timing of mother-to-child transmission of HIV-1', *Aids*, 12(8), pp. 831–837. doi: 10.1097/00002030-199808000-00004.

Nichols, P. *et al.* (2015) 'Rational design of viscosity reducing mutants of a monoclonal antibody:

Hydrophobic versus electrostatic inter-molecular interactions', *mAbs*, 7(1), pp. 212–230. doi: 10.4161/19420862.2014.985504.

Nielsen, J. (2013) 'Production of biopharmaceutical proteins by yeast: Advances through metabolic engineering', *Bioengineered*. doi: 10.4161/bioe.22856.

Nimmerjahn, F. and Ravetch, J. V. (2008) 'Fcγ receptors as regulators of immune responses', *Nature Reviews Immunology*. doi: 10.1038/nri2206.

Nishimura, Y. *et al.* (2017) 'Early antibody therapy can induce long-lasting immunity to SHIV', *Nature*, 543(7646), pp. 559–563. doi: 10.1038/nature21435.

Nissim, A. and Chernajovsky, Y. (2008) 'Historical development of monoclonal antibody therapeutics', *Handbook of Experimental Pharmacology*. doi: 10.1007/978-3-540-73259-4-1.

Noguera-Julian, M. (2019) 'HIV drug resistance testing - The quest for Point-of-Care', *EBioMedicine*. 2019/12/03. Elsevier, 50, pp. 11–12. doi: 10.1016/j.ebiom.2019.11.040.

O'Connor, J. L. *et al.* (2016) 'A simple self-reported adherence tool as a predictor of viral rebound in people with viral suppression on antiretroviral therapy', *HIV Medicine*, 17(2), pp. 124–132. doi: 10.1111/hiv.12284.

Okazaki, A. *et al.* (2004) 'Fucose Depletion from Human IgG1 Oligosaccharide Enhances Binding Enthalpy and Association Rate between IgG1 and FcγRIIIa', *Journal of Molecular Biology*, 336(5), pp. 1239–1249. doi: 10.1016/j.jmb.2004.01.007.

Ovacik, M. and Lin, K. (2018) 'Tutorial on Monoclonal Antibody Pharmacokinetics and Its Considerations in Early Development', *Clinical and Translational Science*, 11(6), pp. 540–552. doi: 10.1111/cts.12567.

Owczarek, B., Gerszberg, A. and Hnatuszko-Konka, K. (2019) 'A Brief Reminder of Systems of Production and Chromatography-Based Recovery of Recombinant Protein Biopharmaceuticals',

BioMed Research International, 2019. doi: 10.1155/2019/4216060.

Palermo, G. *et al.* (2016) 'Striking plasticity of CRISPR-Cas9 and key role of non-target DNA, as revealed by molecular simulations', *ACS Central Science*. doi: 10.1021/acscentsci.6b00218.

Palermo, G. *et al.* (2019) 'Molecular Mechanism of Off-Target Effects in CRISPR-Cas9', *Biophysical Journal*, 116(3), p. 319a. doi: 10.1016/j.bpj.2018.11.1731.

Pancera, M. *et al.* (2010) 'Structure of HIV-1 gp120 with gp41-interactive region reveals layered envelope architecture and basis of conformational mobility', *Proceedings of the National Academy of Sciences of the United States of America*. doi: 10.1073/pnas.0911004107.

Pancera, M., Changela, A. and Kwong, P. D. (2017) 'How HIV-1 entry mechanism and broadly neutralizing antibodies guide structure-based vaccine design', *Current opinion in HIV and AIDS*, 12(3), pp. 229–240. doi: 10.1097/COH.0000000000000360.

Parsons, M. S. *et al.* (2019) 'Fc-dependent functions are redundant to efficacy of anti-HIV antibody PGT121 in macaques', *Journal of Clinical Investigation*, 129(1). doi: 10.1172/JCI122466.

Parsons, M. S., Chung, A. W. and Kent, S. J. (2018) 'Importance of Fc-mediated functions of anti-HIV-1 broadly neutralizing antibodies', *Retrovirology*. BioMed Central, 15(1), pp. 1–12. doi: 10.1186/s12977-018-0438-x.

Patel, P. *et al.* (2014) 'Estimating per-act HIV transmission risk: a systematic review.', *AIDS (London, England)*. England, 28(10), pp. 1509–1519. doi: 10.1097/QAD.0000000000000298.

Patel, P. H. and Preston, B. D. (1994) 'Marked infidelity of human immunodeficiency virus type 1 reverse transcriptase at RNA and DNA template ends', *Proceedings of the National Academy of Sciences of the United States of America*, 91(2), pp. 549–553. doi: 10.1073/pnas.91.2.549.

Pattison, R. J. and Amtmann, A. (2009) 'N-glycan production in the endoplasmic reticulum of plants.', *Trends in plant science*. England, 14(2), pp. 92–99. doi: 10.1016/j.tplants.2008.11.008.

Pau, A. K. and George, J. M. (2014) 'Antiretroviral therapy: Current drugs', *Infectious Disease Clinics of North America*, 28(3), pp. 371–402. doi: 10.1016/j.idc.2014.06.001.

Pejchal, R. *et al.* (2011) 'A potent and broad neutralizing antibody recognizes and penetrates the HIV glycan shield', *Science*. doi: 10.1126/science.1213256.

Peletier, L. A. and Gabrielsson, J. (2012) 'Dynamics of target-mediated drug disposition: Characteristic profiles and parameter identification', *Journal of Pharmacokinetics and Pharmacodynamics*, 39(5), pp. 429–451. doi: 10.1007/s10928-012-9260-6.

Pennings, P. S. (2013) 'HIV drug resistance: Problems and perspectives', *Infectious Disease Reports*, 5(SUPPL.1), pp. 21–25. doi: 10.4081/idr.2013.s1.e5.

Pereira, N. A. *et al.* (2018) 'The "less-is-more" in therapeutic antibodies: Afucosylated anti-cancer antibodies with enhanced antibody-dependent cellular cytotoxicity', *mAbs*. Taylor & Francis, 10(5), pp. 693–711. doi: 10.1080/19420862.2018.1466767.

Peschke, B. *et al.* (2017) 'Fc-Galactosylation of Human Immunoglobulin Gamma Isotypes Improves C1q Binding and Enhances Complement-Dependent Cytotoxicity', *Frontiers in immunology*. Frontiers Media S.A., 8, p. 646. doi: 10.3389/fimmu.2017.00646.

Peters, J. and Stoger, E. (2011) 'Transgenic crops for the production of recombinant vaccines and anti-microbial antibodies', *Human Vaccines*, 7(3), pp. 367–374. doi: 10.4161/hv.7.3.14303.

Petkova, S. B. *et al.* (2006) 'Enhanced half-life of genetically engineered human IgG1 antibodies in a humanized FcRn mouse model: potential application in humorally mediated autoimmune disease.', *International immunology*, 18(12), pp. 1759–69. doi: 10.1093/intimm/dxl110.

Pincetic, A. *et al.* (2014) 'Type I and type II Fc receptors regulate innate and adaptive immunity', *Nature immunology*, 15(8), pp. 707–716. doi: 10.1038/ni.2939.

Pinto, D. *et al.* (2019) 'Structural Basis for Broad HIV-1 Neutralization by the MPER-Specific Human

Broadly Neutralizing Antibody LN01', *Cell host & microbe*. 2019/10/22. Cell Press, 26(5), pp. 623-637.e8. doi: 10.1016/j.chom.2019.09.016.

Pogue, G. P. *et al.* (2010) 'Production of pharmaceutical-grade recombinant aprotinin and a monoclonal antibody product using plant-based transient expression systems', *Plant Biotechnology Journal*, 8(5), pp. 638–654. doi: 10.1111/j.1467-7652.2009.00495.x.

Prabakaran, P. *et al.* (2006) 'Structural Mimicry of CD4 by a Cross-reactive HIV-1 Neutralizing Antibody with CDR-H2 and H3 Containing Unique Motifs', *Journal of Molecular Biology*, 357(1), pp. 82–99. doi: https://doi.org/10.1016/j.jmb.2005.12.062.

Proetzel, G. and Roopenian, D. C. (2014) 'Humanized FcRn mouse models for evaluating pharmacokinetics of human IgG antibodies', *Methods*, 65(1), pp. 148–153. doi: 10.1016/j.ymeth.2013.07.005.

Promega (no date) 'ADCC Reporter Bioassay, Complete Kit (WIL2-S)'.

Pyzik, M. *et al.* (2017) 'Hepatic FcRn regulates albumin homeostasis and susceptibility to liver injury', *Proceedings of the National Academy of Sciences of the United States of America*. doi: 10.1073/pnas.1618291114.

Pyzik, M. *et al.* (2019) 'The neonatal Fc Receptor (FcRn): A misnomer?', *Frontiers in Immunology*, 10(JULY). doi: 10.3389/fimmu.2019.01540.

Qiu, X. *et al.* (2014) 'Reversion of advanced Ebola virus disease in nonhuman primates with ZMapp', *Nature*. 2014/08/29, 514(7520), pp. 47–53. doi: 10.1038/nature13777.

Quast, I. *et al.* (2015) 'Sialylation of IgG Fc domain impairs complement-dependent cytotoxicity.', *The Journal of clinical investigation*, 125(11), pp. 4160–4170. doi: 10.1172/JCI82695.

Raghavan, M. *et al.* (1995) 'Analysis of the pH Dependence of the Neonatal Fc Receptor/Immunoglobulin G Interaction Using Antibody and Receptor Variants', *Biochemistry*. doi:

10.1021/bi00045a005.

Ramirez, C. L. *et al.* (2012) 'Engineered zinc finger nickases induce homology-directed repair with reduced mutagenic effects', *Nucleic Acids Research*, 40(12), pp. 5560–5568. doi: 10.1093/nar/gks179.

Ran, F. A. *et al.* (2013) 'Genome engineering using the CRISPR-Cas9 system', *Nature Protocols*. doi: 10.1038/nprot.2013.143.

Ran, F. A. *et al.* (2015) 'In vivo genome editing using Staphylococcus aureus Cas9', *Nature*. 2015/04/01, 520(7546), pp. 186–191. doi: 10.1038/nature14299.

Rath, D. *et al.* (2015) 'The CRISPR-Cas immune system: Biology, mechanisms and applications', *Biochimie*. doi: 10.1016/j.biochi.2015.03.025.

Reading, S. A. and Dimmock, N. J. (2007) 'Neutralization of animal virus infectivity by antibody', *Archives of Virology*, 152(6), pp. 1047–1059. doi: 10.1007/s00705-006-0923-8.

Reh, L. *et al.* (2018) 'Phenotypic deficits in the HIV-1 envelope are associated with the maturation of a V2-directed broadly neutralizing antibody lineage', *PLoS Pathogens*, 14(1), pp. 1–27. doi: 10.1371/journal.ppat.1006825.

Ren, W. W. *et al.* (2020) 'Glycoengineering of HEK293 cells to produce high-mannose-type N-glycan structures', *Journal of Deaf Studies and Deaf Education*, 25(1), pp. 245–258. doi: 10.1093/jb/mvz032.

Rerks-Ngarm, S. *et al.* (2009) 'Vaccination with ALVAC and AIDSVAX to prevent HIV-1 infection in Thailand.', *The New England journal of medicine*. United States, 361(23), pp. 2209–2220. doi: 10.1056/NEJMoa0908492.

Reust, C. E. (2011) 'Common adverse effects of antiretroviral therapy for HIV disease', *American Family Physician*, 83(12), pp. 1443–1451.

Robbie, G. J. *et al.* (2013) 'A novel investigational Fc-modified humanized monoclonal antibody, motavizumab-YTE, has an extended half-life in healthy adults', *Antimicrobial Agents and Chemotherapy*, 57(12), pp. 6147–6153. doi: 10.1128/AAC.01285-13.

Rojo, F. P. *et al.* (2018) 'Crispr-cas systems: Ushering in the new genome editing era', *Bioengineered*. Taylor & Francis, 9(1), pp. 214–221. doi: 10.1080/21655979.2018.1470720.

Roopenian, D. C. and Akilesh, S. (2007) 'FcRn: The neonatal Fc receptor comes of age', *Nature Reviews Immunology*, 7(9), pp. 715–725. doi: 10.1038/nri2155.

Rosenberg, Y. *et al.* (2015) 'Pharmacokinetics and immunogenicity of broadly neutralizing HIV monoclonal antibodies in macaques', *PLoS ONE*, 10(3), pp. 1–15. doi: 10.1371/journal.pone.0120451.

Rosenberg, Y. J. *et al.* (2019) 'Introduction of the YTE mutation into the non-immunogenic HIV bnAb PGT121 induces anti-drug antibodies in macaques', *PLoS ONE*, 14(2), pp. 1–18. doi: 10.1371/journal.pone.0212649.

Ryman, J. T. and Meibohm, B. (2017) 'Pharmacokinetics of monoclonal antibodies', *CPT: Pharmacometrics and Systems Pharmacology*, 6(9), pp. 576–588. doi: 10.1002/psp4.12224.

Sabalza, M., Christou, P. and Capell, T. (2014) 'Recombinant plant-derived pharmaceutical proteins: current technical and economic bottlenecks', *Biotechnology Letters*. doi: 10.1007/s10529-014-1621-3.

Samuel Edward, K. *et al.* (2018) 'Factors Influencing Adherence to Antiretroviral Therapy among HIV Infected Patients in Nyamagana-Mwanza, Northern Tanzania: A Cross Sectional Study', *International Archives of Medical Microbiology*, 1(1). doi: 10.23937/iamm-2017/1710002.

Sander, J. D. and Joung, J. K. (2014) 'CRISPR-Cas systems for editing, regulating and targeting genomes', *Nature Biotechnology*. doi: 10.1038/nbt.2842.

Sanseviero, E. (2019) 'NK Cell-Fc Receptors Advance Tumor Immunotherapy', *Journal of Clinical Medicine*, 8(10), p. 1667. doi: 10.3390/jcm8101667.

Sather, D. N. *et al.* (2012) 'Broadly Neutralizing Antibodies Developed by an HIV-Positive Elite Neutralizer Exact a Replication Fitness Cost on the Contemporaneous Virus', *Journal of Virology*, 86(23), pp. 12676–12685. doi: 10.1128/jvi.01893-12.

Scanlan, C. N. *et al.* (2002) 'The Broadly Neutralizing Anti-Human Immunodeficiency Virus Type 1 Antibody 2G12 Recognizes a Cluster of 1->2 Mannose Residues on the Outer Face of gp120', *Journal of Virology*, 76(14), pp. 7306–7321. doi: 10.1128/jvi.76.14.7306-7321.2002.

Schachtsiek, J. and Stehle, F. (2019) 'Nicotine-free, nontransgenic tobacco (Nicotiana tabacum l.) edited by CRISPR-Cas9', *Plant Biotechnology Journal*, 17(12), pp. 2228–2230. doi: 10.1111/pbi.13193.

von Schaewen, A. *et al.* (1993) 'Isolation of a mutant Arabidopsis plant that lacks N-acetyl glucosaminyl transferase I and is unable to synthesize Golgi-modified complex N-linked glycans.', *Plant physiology*. United States, 102(4), pp. 1109–1118. doi: 10.1104/pp.102.4.1109.

Schiffner, T., Sattentau, Q. J. and Duncan, C. J. A. (2013) 'Cell-to-cell spread of HIV-1 and evasion of neutralizing antibodies', *Vaccine*. Elsevier Ltd, 31(49), pp. 5789–5797. doi: 10.1016/j.vaccine.2013.10.020.

Schillberg, S. *et al.* (2019) 'Critical Analysis of the Commercial Potential of Plants for the Production of Recombinant Proteins', *Frontiers in plant science*. Frontiers Media S.A., 10, p. 720. doi: 10.3389/fpls.2019.00720.

Schoberer, J. and Strasser, R. (2018) 'Plant glyco-biotechnology', *Seminars in Cell and Developmental Biology*. doi: 10.1016/j.semcdb.2017.07.005.

Schoch, A. *et al.* (2015) 'Charge-mediated influence of the antibody variable domain on FcRn-dependent pharmacokinetics', *Proceedings of the National Academy of Sciences*, 112(19), pp. 5997–

6002. doi: 10.1073/pnas.1408766112.

Schoofs, T. *et al.* (2017) 'Antibody 10-1074 suppresses viremia in HIV-1-infected individuals', *Nature Medicine*, 23(2), pp. 185–191. doi: 10.1038/nm.4268.

Shalem, O., Sanjana, N. E. and Zhang, F. (2015) 'High-throughput functional genomics using CRISPR-Cas9', *Nature Reviews Genetics*. doi: 10.1038/nrg3899.

Sharon, M. *et al.* (2003) 'Alternative conformations of HIV-1 V3 loops mimic β hairpins in chemokines, suggesting a mechanism for coreceptor selectivity', *Structure*. doi: 10.1016/S0969-2126(03)00011-X.

Shaw, G. M. and Hunter, E. (2012) 'HIV transmission', *Cold Spring Harbor Perspectives in Medicine*, 2(11), pp. 1–23. doi: 10.1101/cshperspect.a006965.

Shields, R. L. *et al.* (2001) 'High Resolution Mapping of the Binding Site on Human IgG1 for FcγRI, FcγRII, FcγRIII, and FcRn and Design of IgG1 Variants with Improved Binding to the FcγR', *Journal of Biological Chemistry*. doi: 10.1074/jbc.M009483200.

Shields, R. L. *et al.* (2002) 'Lack of fucose on human IgG1 N-linked oligosaccharide improves binding to human FcγRIII and antibody-dependent cellular toxicity', *Journal of Biological Chemistry*, 277(30), pp. 26733–26740. doi: 10.1074/jbc.M202069200.

Shingai, M. *et al.* (2013) 'Antibody-mediated immunotherapy of macaques chronically infected with SHIV suppresses viraemia', *Nature*. doi: 10.1038/nature12746.

Shioda, T., Levy, J. A. and Cheng-Mayer, C. (1992) 'Small amino acid changes in the V3 hypervariable region of gp120 can affect the T-cell-line and macrophage tropism of human immunodeficiency virus type 1', *Proceedings of the National Academy of Sciences of the United States of America*. doi: 10.1073/pnas.89.20.9434.

Shriner, D. *et al.* (2004) 'Pervasive genomic recombination of HIV-1 in vivo', *Genetics*, 167(4), pp.

1573–1583. doi: 10.1534/genetics.103.023382.

Shukla, A. A. *et al.* (2007) 'Downstream processing of monoclonal antibodies-Application of platform approaches', *Journal of Chromatography B: Analytical Technologies in the Biomedical and Life Sciences*, 848(1), pp. 28–39. doi: 10.1016/j.jchromb.2006.09.026.

Siemieniuk, R. A. *et al.* (2017) 'Antiretroviral therapy for pregnant women living with HIV or hepatitis B: A systematic review and meta-analysis', *BMJ Open*, 7(9), pp. 1–17. doi: 10.1136/bmjopen-2017-019022.

Simister, N. E. *et al.* (1996) 'An IgG-transporting Fc receptor expressed in the syncytiotrophoblast of human placenta', *European Journal of Immunology*. doi: 10.1002/eji.1830260718.

Simister, N. E. (2003) 'Placental transport of immunoglobulin G.', *Vaccine*. Netherlands, 21(24), pp. 3365–3369. doi: 10.1016/s0264-410x(03)00334-7.

Simister, N. E. and Rees, A. R. (1985) 'Isolation and characterization of an Fc receptor from neonatal rat small intestine', *European Journal of Immunology*. doi: 10.1002/eji.1830150718.

Singh, S. M. *et al.* (2017) 'Effect of Polysorbate 20 and Polysorbate 80 on the Higher-Order Structure of a Monoclonal Antibody and Its Fab and Fc Fragments Probed Using 2D Nuclear Magnetic Resonance Spectroscopy', *Journal of Pharmaceutical Sciences*. Elsevier, 106(12), pp. 3486–3498. doi: 10.1016/J.XPHS.2017.08.011.

Snijdewind, I. J. M. *et al.* (2018) 'Preconception use of cART by HIV-positive pregnant women increases the risk of infants being born small for gestational age', *PLoS ONE*, 13(1), pp. 1–18. doi: 10.1371/journal.pone.0191389.

Sok, D. *et al.* (2014) 'Promiscuous glycan site recognition by antibodies to the high-mannose patch of gp120 broadens neutralization of HIV', *Science Translational Medicine*. doi: 10.1126/scitranslmed.3008104.

Soto, M. J., Urbanowicz, B. R. and Hahn, M. G. (2019) 'Plant Fucosyltransferases and the Emerging Biological Importance of Fucosylated Plant Structures', *Critical Reviews in Plant Sciences*. Taylor & Francis, 38(4), pp. 327–338. doi: 10.1080/07352689.2019.1673968.

Sourrouille, C. *et al.* (2008) 'Down-regulated expression of plant-specific glycoepitopes in alfalfa', *Plant Biotechnology Journal*, 6(7), pp. 702–721. doi: 10.1111/j.1467-7652.2008.00353.x.

Spearman, M., Dionne, B. and Butler, M. (2011) 'The Role of Glycosylation in Therapeutic Antibodies', in *Cell Eng Vol 7 Antibody Expr Prod*, pp. 251–292. doi: 10.1007/978-94-007-1257-7_12.

Sprink, T. *et al.* (2016) 'Regulatory hurdles for genome editing: process- vs. product-based approaches in different regulatory contexts', *Plant Cell Reports*. Springer Berlin Heidelberg, 35(7), pp. 1493–1506. doi: 10.1007/s00299-016-1990-2.

Stadlmann, J. *et al.* (2008) 'Analysis of immunoglobulin glycosylation by LC-ESI-MS of glycopeptides and oligosaccharides.', *Proteomics*. Germany, 8(14), pp. 2858–2871. doi: 10.1002/pmic.200700968.

Stanley P, Taniguchi N, A. M. (2017) 'N-glycans', in *Essentials of Glycobiology*. doi: 10.1101/glycobiology.3e.009.

Stelter, S. *et al.* (2020) 'Engineering the interactions between a plant-produced HIV antibody and human Fc receptors', *Plant Biotechnology Journal*, 18(2), pp. 402–414. doi: 10.1111/pbi.13207.

Stiegler, G. *et al.* (2001) 'A potent cross-clade neutralizing human monoclonal antibody against a novel epitope on gp41 of human immunodeficiency virus type 1.', *AIDS research and human retroviruses*. United States, 17(18), pp. 1757–1765. doi: 10.1089/08892220152741450.

Strasser, R. *et al.* (1999) 'Molecular cloning and characterization of cDNA coding for beta1, 2N-acetylglucosaminyltransferase I (GlcNAc-TI) from Nicotiana tabacum.', *Glycobiology*. England, 9(8), pp. 779–785. doi: 10.1093/glycob/9.8.779.

Strasser, R. *et al.* (2004) 'Generation of Arabidopsis thaliana plants with complex N-glycans lacking

β1,2-linked xylose and core α1,3-linked fucose', *FEBS Letters*, 561(1–3), pp. 132–136. doi: 10.1016/S0014-5793(04)00150-4.

Strasser, R. *et al.* (2007) 'A unique β1,3-galactosyltransferase is indispensable for the biosynthesis of N-glycans containing Lewis a structures in Arabidopsis thaliana', *Plant Cell*, 19(7), pp. 2278–2292. doi: 10.1105/tpc.107.052985.

Strasser, R. *et al.* (2008) 'Generation of glyco-engineered Nicotiana benthamiana for the production of monoclonal antibodies with a homogeneous human-like N-glycan structure', *Plant Biotechnology Journal*, 6(4), pp. 392–402. doi: 10.1111/j.1467-7652.2008.00330.x.

Strasser, R. (2016) 'Plant protein glycosylation', *Glycobiology*, 26(9), pp. 926–939. doi: 10.1093/glycob/cww023.

Strasser, R., Altmann, F. and Steinkellner, H. (2014) 'Controlled glycosylation of plant-produced recombinant proteins', *Current Opinion in Biotechnology*. Elsevier Ltd, 30, pp. 95–100. doi: 10.1016/j.copbio.2014.06.008.

Subbaraman, H., Schanz, M. and Trkola, A. (2018) 'Broadly neutralizing antibodies: What is needed to move from a rare event in HIV-1 infection to vaccine efficacy?', *Retrovirology*. BioMed Central, 15(1), pp. 1–14. doi: 10.1186/s12977-018-0433-2.

Subedi, G. P. and Barb, A. W. (2015) 'The Structural Role of Antibody N-Glycosylation in Receptor Interactions', *Structure*. Cell Press, 23(9), pp. 1573–1583. doi: 10.1016/j.str.2015.06.015.

Surur, A. S. *et al.* (2020) 'Challenges and Opportunities for Drug Discovery in Developing Countries: The Example of Cutaneous Leishmaniasis', *ACS Medicinal Chemistry Letters*. American Chemical Society, 11(11), pp. 2058–2062. doi: 10.1021/acsmedchemlett.0c00446.

Tam, S. H. *et al.* (2013) 'Correlations between pharmacokinetics of IgG antibodies in primates vs. FcRn-transgenic mice reveal a rodent model with predictive capabilities', *mAbs*, 5(3), pp. 397–405.

doi: 10.4161/mabs.23836.

Taylor, S. *et al.* (2007) 'Stopping antiretroviral therapy', *AIDS (London, England)*, 21, pp. 1673–1682. doi: 10.1097/QAD.0b013e3281c61394.

Teasdale, C. A., Marais, B. J. and Abrams, E. J. (2011) 'HIV: prevention of mother-to-child transmission', *BMJ clinical evidence*, 2011(October 2009), pp. 1–33. doi: 10.1097/qad.0000000000000107.

Teh, A. Y. H. *et al.* (2014) 'Characterization of VRC01, a potent and broadly neutralizing anti-HIV mAb, produced in transiently and stably transformed tobacco', *Plant Biotechnology Journal*, 12(3), pp. 300–311. doi: 10.1111/pbi.12137.

Temming, A. R. *et al.* (2019) 'Human DC-SIGN and CD23 do not interact with human IgG', *Scientific Reports*, 9(1), p. 9995. doi: 10.1038/s41598-019-46484-2.

The Antiretroviral Therapy Cohort Collaboration (2008) 'Life expectancy of individuals on combination antiretroviral therapy in high-income countries: a collaborative analysis of 14 cohort studies', *The Lancet*, 372(9635), pp. 293–299. doi: 10.1016/S0140-6736(08)61113-7.

Thomann, M. *et al.* (2016) 'Fc-galactosylation modulates antibody-dependent cellular cytotoxicity of therapeutic antibodies', *Molecular Immunology*. doi: 10.1016/j.molimm.2016.03.002.

Tirumuru, N. *et al.* (2016) 'N6-methyladenosine of HIV-1 RNA regulates viral infection and HIV-1 Gag protein expression', *eLife*, 5(2016JULY), pp. 1–20. doi: 10.7554/eLife.15528.

Trkola, A. *et al.* (2005) 'Delay of HIV-1 rebound after cessation of antiretroviral therapy through passive transfer of human neutralizing antibodies', *Nature Medicine*, 11(6), pp. 615–622. doi: 10.1038/nm1244.

Tudor, D. and Bomsel, M. (2011) 'The broadly neutralizing HIV-1 IgG 2F5 elicits gp41-specific antibody-dependent cell cytotoxicity in a FcγRI-dependent manner', *AIDS*. doi:

10.1097/QAD.0b013e32834507bd.

Uchino, T. *et al.* (2017) 'Immunogenicity of protein aggregates of a monoclonal antibody generated by forced shaking stress with siliconized and nonsiliconized syringes in BALB/c mice', *Journal of Pharmacy and Pharmacology*, 69(10), pp. 1341–1351. doi: 10.1111/jphp.12765.

UNAIDS (2019) '2018 Global Hiv Statistics', *Unaids*, pp. 1–6.

Vaccaro, C. *et al.* (2006) 'Divergent activities of an engineered antibody in murine and human systems have implications for therapeutic antibodies', *Proceedings of the National Academy of Sciences of the United States of America*. doi: 10.1073/pnas.0606304103.

Valente, D. *et al.* (2020) 'Pharmacokinetics of novel Fc-engineered monoclonal and multispecific antibodies in cynomolgus monkeys and humanized FcRn transgenic mouse models', *mAbs*. Taylor & Francis, 12(1). doi: 10.1080/19420862.2020.1829337.

Vermeer, A. W. P. and Norde, W. (2000) 'The thermal stability of immunoglobulin: Unfolding and aggregation of a multi-domain protein', *Biophysical Journal*, 78(1), pp. 394–404. doi: 10.1016/S0006-3495(00)76602-1.

VIB (2018) 'Regulating genome edited organisms as GMOs has negative consequences for agriculture, society and economy', pp. 1–19. Available at: http://www.vib.be/en/news/Documents/Position paper on the ECJ ruling on CRISPR 12 Nov 2018.pdf.

Vidarsson, G. *et al.* (2006) 'FcRn: An IgG receptor on phagocytes with a novel role in phagocytosis', *Blood*. doi: 10.1182/blood-2006-05-024539.

Vidarsson, G., Dekkers, G. and Rispens, T. (2014) 'IgG subclasses and allotypes: From structure to effector functions', *Frontiers in Immunology*. doi: 10.3389/fimmu.2014.00520.

Villafañez, F., Gottifredi, V. and Soria, G. (2019) 'Development and optimization of a miniaturized

western blot-based screening platform to identify regulators of post-translational modifications', *High-Throughput*, 8(2), pp. 1–11. doi: 10.3390/ht8020015.

Vogelpoel, L. T. C. *et al.* (2015) 'Control of cytokine production by human Fc gamma receptors: Implications for pathogen defense and autoimmunity', *Frontiers in Immunology*. doi: 10.3389/fimmu.2015.00079.

Wälchli, R. *et al.* (2020) 'Accelerated Aggregation Studies of Monoclonal Antibodies: Considerations for Storage Stability', *Journal of Pharmaceutical Sciences*, 109(1), pp. 595–602. doi: https://doi.org/10.1016/j.xphs.2019.10.048.

Wallace, P. K., Howell, A. L. and Fanger, M. W. (1994) 'Role of Fcγ receptors in cancer and infectious disease', *Journal of Leukocyte Biology*, 55(6), pp. 816–826. doi: 10.1002/jlb.55.6.816.

Ward, A. B. and Wilson, I. A. (2015) 'Insights into the trimeric HIV-1 envelope glycoprotein structure', *Trends in Biochemical Sciences*. Elsevier Ltd, 40(2), pp. 101–107. doi: 10.1016/j.tibs.2014.12.006.

Ward, A. B. and Wilson, I. A. (2017) 'The HIV-1 envelope glycoprotein structure: nailing down a moving target', *Immunological Reviews*, 275(1), pp. 21–32. doi: 10.1111/imr.12507.

Watts, J. M. *et al.* (2009) 'Architecture and secondary structure of an entire HIV-1 RNA genome', *Nature*, 460(7256), pp. 711–716. doi: 10.1038/nature08237.

Wei, X. *et al.* (2003) 'Antibody neutralization and escape by {HIV-1}, Volume = {422}, Year = {2003}', *Nature*, 837(1988), pp. 307–312.

Weissenhorn, W. *et al.* (1997) 'Atomic structure of the ectodomain from HIV-1 gp41', *Nature*. doi: 10.1038/387426a0.

West, A. P. *et al.* (2014) 'Structural Insights on the Role of Antibodies in HIV-1 Vaccine and Therapy', *Cell*, 156(4), pp. 633–648. doi: https://doi.org/10.1016/j.cell.2014.01.052.

West, A. P. J. *et al.* (2012) 'Structural basis for germ-line gene usage of a potent class of antibodies targeting the CD4-binding site of HIV-1 gp120.', *Proceedings of the National Academy of Sciences of the United States of America*, 109(30), pp. E2083-90. doi: 10.1073/pnas.1208984109.

Westra, E. R., Buckling, A. and Fineran, P. C. (2014) 'CRISPR-Cas systems: Beyond adaptive immunity', *Nature Reviews Microbiology*. doi: 10.1038/nrmicro3241.

WHO (2017) *Global guidance on criteria and processes for validation of elimination of mother-to-child transmission of HIV and syphilis, second edition*.

Wieland, A. and Ahmed, R. (2019) 'Fc Receptors in Antimicrobial Protection.', *Current topics in microbiology and immunology*. Germany, 423, pp. 119–150. doi: 10.1007/82_2019_154.

Wildt, S. and Gerngross, T. U. (2005) 'The humanization of N-glycosylation pathways in yeast', *Nature Reviews Microbiology*. doi: 10.1038/nrmicro1087.

Wilken, L. and Nikolov, Z. (2012) 'Downstream Processing of Transgenic Plant Systems: Protein Recovery and Purification Strategies', in *Molecular Farming in Plants: Recent Advances and Future Prospects*, pp. 217–257. doi: 10.1007/978-94-007-2217-0_11.

Wines, B. D. *et al.* (2000) 'The IgG Fc Contains Distinct Fc Receptor (FcR) Binding Sites: The Leukocyte Receptors FcγRI and FcγRIIa Bind to a Region in the Fc Distinct from That Recognized by Neonatal FcR and Protein A', *The Journal of Immunology*, 164(10), pp. 5313–5318. doi: 10.4049/jimmunol.164.10.5313.

Wong, G. and Kobinger, G. P. (2015) 'Backs against the wall: novel and existing strategies used during the 2014-2015 Ebola virus outbreak', *Clinical microbiology reviews*. American Society for Microbiology, 28(3), pp. 593–601. doi: 10.1128/CMR.00014-15.

Woo, J. W. *et al.* (2015) 'DNA-free genome editing in plants with preassembled CRISPR-Cas9 ribonucleoproteins', *Nature Biotechnology*. doi: 10.1038/nbt.3389.

World Health Organization (WHO) (2019) *HIV Drug Resistance Report*. Available at: http://scholar.google.com/scholar?hl=en&btnG=Search&q=intitle:Who+hiv+drug+resistance+report+2012#5.

Wu, J. *et al.* (1997) 'A novel polymorphism of FcgammaRIIIa (CD16) alters receptor function and predisposes to autoimmune disease.', *Journal of Clinical Investigation*, 100(5), pp. 1059–1070. doi: 10.1172/JCI119616.

Wu, L. *et al.* (1996) 'CD4-induced interaction of primary HIV-1 gp120 glycoproteins with the chemokine receptor CCR-5', *Nature*, 384(6605), pp. 179–183. doi: 10.1038/384179a0.

Wu, S. J. *et al.* (2010) 'Structure-based engineering of a monoclonal antibody for improved solubility', *Protein Engineering, Design and Selection*, 23(8), pp. 643–651. doi: 10.1093/protein/gzq037.

Wu, X. *et al.* (2010) 'Rational Design of Envelope Identifies Broadly Neutralizing Human Monoclonal Antibodies to HIV-1', *Science*, 329(5993), pp. 856–861. doi: 10.1126/science.1187659.Rational.

Wu, X. *et al.* (2011) 'Focused evolution of HIV-1 neutralizing antibodies revealed by structures and deep sequencing', *Science*. doi: 10.1126/science.1207532.

Wyatt, R. *et al.* (1998) 'The antigenic structure of the HIV gp120 envelope glycoprotein', *Nature*. doi: 10.1038/31514.

Xie, K., Minkenberg, B. and Yang, Y. (2015) 'Boosting CRISPR/Cas9 multiplex editing capability with the endogenous tRNA-processing system', *Proceedings of the National Academy of Sciences of the United States of America*, 112(11), pp. 3570–3575. doi: 10.1073/pnas.1420294112.

Yang, Z. *et al.* (2015) 'Fast and sensitive detection of indels induced by precise gene targeting', *Nucleic Acids Research*, 43(9). doi: 10.1093/nar/gkv126.

Yin, B. jiao *et al.* (2011) 'Generation of glyco-engineered BY2 cell lines with decreased expression of

plant-specific glycoepitopes', *Protein and Cell*, 2(1), pp. 41–47. doi: 10.1007/s13238-011-1007-4.

Yogo, R. *et al.* (2019) 'The Fab portion of immunoglobulin G contributes to its binding to Fcγ receptor III', *Scientific Reports*. Springer US, 9(1), pp. 1–10. doi: 10.1038/s41598-019-48323-w.

Yoon, H. *et al.* (2015) 'CATNAP: A tool to compile, analyze and tally neutralizing antibody panels', *Nucleic Acids Research*, 43(W1), pp. W213–W219. doi: 10.1093/nar/gkv404.

Yoshida, M. *et al.* (2004) 'Human neonatal Fc receptor mediates transport of IgG into luminal secretions for delivery of antigens to mucosal dendritic cells', *Immunity*. doi: 10.1016/j.immuni.2004.05.007.

Yoshida, M. *et al.* (2006) 'Neonatal Fc receptor for IgG regulates mucosal immune responses to luminal bacteria', *Journal of Clinical Investigation*. doi: 10.1172/JCI27821.

Yu, L. and Guan, Y. (2014) 'Immunologic Basis for Long HCDR3s in Broadly Neutralizing Antibodies Against HIV-1', *Frontiers in immunology*. Frontiers Media S.A., 5, p. 250. doi: 10.3389/fimmu.2014.00250.

Yu, Q. H. *et al.* (2017) 'CRISPR/Cas9-induced Targeted Mutagenesis and Gene Replacement to Generate Long-shelf Life Tomato Lines', *Scientific Reports*. Springer US, 7(1), pp. 1–9. doi: 10.1038/s41598-017-12262-1.

Yu, X. Q. *et al.* (2017) 'Safety, tolerability, and pharmacokinetics of MEDI4893, an investigational, extended-half-life, anti-staphylococcus aureus alpha-toxin human monoclonal antibody, in healthy adults', *Antimicrobial Agents and Chemotherapy*. doi: 10.1128/AAC.01020-16.

Zalevsky, J. *et al.* (2010) 'Enhanced antibody half-life improves in vivo activity', *Nature Biotechnology*. Nature Publishing Group, 28(2), pp. 157–159. doi: 10.1038/nbt.1601.

Zetsche, B. *et al.* (2015) 'Cpf1 is a single RNA-guided endonuclease of a class 2 CRISPR-Cas system', *Cell*. 2015/09/25, 163(3), pp. 759–771. doi: 10.1016/j.cell.2015.09.038.

Zhang, L. *et al.* (2016) 'Side effects, adherence self-efficacy, and adherence to antiretroviral treatment: a mediation analysis in a Chinese sample.', *AIDS care*. England, 28(7), pp. 919–926. doi: 10.1080/09540121.2015.1124984.

Zhang, L. *et al.* (2019) 'An important role of l-fucose biosynthesis and protein fucosylation genes in Arabidopsis immunity', *New Phytologist*, 222(2), pp. 981–994. doi: 10.1111/nph.15639.

Zhang, X. (2018) 'Anti-retroviral drugs: current state and development in the next decade', *Acta Pharmaceutica Sinica B*. Elsevier B.V., 8(2), pp. 131–136. doi: 10.1016/j.apsb.2018.01.012.

Zhang, Y. *et al.* (2013) 'Processing-independent CRISPR RNAs limit natural transformation in Neisseria meningitidis', *Molecular cell*, 50(4), pp. 488–503. doi: 10.1016/j.molcel.2013.05.001.

Zhou, J. *et al.* (2015) 'Gene targeting by the TAL effector PthXo2 reveals cryptic resistance gene for bacterial blight of rice', *Plant Journal*, 82(4), pp. 632–643. doi: 10.1111/tpj.12838.

Zhou, T. *et al.* (2007) 'Structural definition of a conserved neutralization epitope on HIV-1 gp120', *Nature*. doi: 10.1038/nature05580.

Zhou, T. *et al.* (2010) 'Structural basis for broad and potent neutralization of HIV-1 by antibody VRC01', *Science*. doi: 10.1126/science.1192819.

Zhu, X. *et al.* (2001) 'MHC Class I-Related Neonatal Fc Receptor for IgG Is Functionally Expressed in Monocytes, Intestinal Macrophages, and Dendritic Cells', *The Journal of Immunology*. doi: 10.4049/jimmunol.166.5.3266.

Zischewski, J., Sack, M. and Fischer, R. (2016) 'Overcoming low yields of plant-made antibodies by a protein engineering approach', *Biotechnology Journal*, 11(1), pp. 107–116. doi: 10.1002/biot.201500255.

Zolla-Pazner, S. and Cardozo, T. (2010) 'Sequence-Variable Regions Provide a Paradigm for Vaccine Design', *Nat Rev Immunol*, 10(7), pp. 527–535. doi: 10.1038/nri2801.STRUCTURE.

9 Appendix

9.1 Buffers and Media

1 x PBS (pH 7.4)

g/L	
0.2	KH_2PO_4
1.15	Na_2HPO_4
8.0	NaCl
0.2	KCl

1 x TBS (pH 8.0)

g/L	
6	Trizma Base
8	NaCl

Plant Infiltration Buffer (pH 5.6)

g/L	
1.95	MES (2-(*N*-morpholino)ethanesulfonic acid)
2.03	$MgCl_2$

Western Transfer Buffer

g/L	
3	Trizma Base
14.4	Glycine
200 ml	Methanol

1x TAE

g/L	
4.84	Trizma Base
1.14	Glacial acetic acid
2 ml	0.5 M EDTA

Neutralisation buffer (pH 9)

g/L	
121	Trizma Base
pH adjusted to pH 9	HCl

Elution buffer (pH 2.7)

g/L	
7.51	Glycine
pH adjusted to pH 2.7	HCl

Binding Buffer (pH 7)

mL/L	
610	0.2 M Na_2HPO_4
390	0.2 M NaH_2PO_4

Luria-Bertani broth/agar (LB) (pH 7.0)

g/L	
5	Bacto-Yeast Extract
10	Bacto-Tryptone
10	NaCl
15	*Agar – only for LB Agar*

YM broth/agar (pH 7.0)

g/L	
0.4	Bacto-Yeast Extract
10	Mannitol
0.1	NaCl
0.2	$MgSO_4$
0.38	K_2HPO_4
15	*Agar – only for YM Agar*

9.2 Primers

Table 9-1: Primers used to synthesise the sgRNAs

Primer Name	Primer sequence (5'->3')
Primer F1	ATTGGCGCGCCAGAAATCTCAAAATTCCG
Primer R2RC	TTGTTAATTAATAATGCCAACTTTGTACA
Primer F1R	AAGATTTGAAGGTGTTGGGTCAATCACTACTTCGTCTCT
Primer F1F	GACCCAACACCTTCAAATCTTGTTTTAGAGCTAGAAATAGC
Primer F2R	ACAAGTGCAACTACTAGAGGCAATCACTACTTCGTCTCT
Primer F2F	GCCTCTAGTAGTTGCACTTGTGTTTTAGAGCTAGAAATAGC
Primer F3R	CTTTGGAGGTTGACCAAGACAATCACTACTTCGTCTCT
Primer F3F	GTCTTGGTCAACCTCCAAAGGTTTTAGAGCTAGAAATAGC
Primer F4R	TCGACACTCCTCACCAACCAATCACTACTTCGTCTCT
Primer F4F	GGTTGGTGAGGAGTGTCGAGTTTTAGAGCTAGAAATAGC
Primer F5R	TTGACCGAAGCACGCTAGCCAATCACTACTTCGTCTCT
Primer F5F	GGCTAGCGTGCTTCGGTCAAGTTTTAGAGCTAGAAATAGC
Primer F6R	CATTAGAATTCTCAAAAGCCAATCACTACTTCGTCTCT
Primer F6F	GGCTTTTGAGAATTCTAATGGTTTTAGAGCTAGAAATAGC
Primer F7R	CAAGAGTTGGCTTTTTCAGCAATCACTACTTCGTCTCT
Primer F7F	GCTGAAAAAGCCAACTCTTGGTTTTAGAGCTAGAAATAGC
Primer F8R	ACGGCGACGTTGAGGAGGTCCAATCACTACTTCGTCTCT
Primer F8F	GGACCTCCTCAACGTCGCCGTGTTTTAGAGCTAGAAATAGC
Primer F9R	AAGTAATGTTGTTCTCTGCAATCACTACTTCGTCTCT
Primer F9F	GCAGAGAACAACATTACTTGTTTTAGAGCTAGAAATAGC
Primer F10R	CTTGCAAGCTTTAGAAGCCCAATCACTACTTCGTCTCT
Primer F10F	GGGCTTCTAAAGCTTGCAAGGTTTTAGAGCTAGAAATAGC
Primer F11R	TGTTATGATGACAACTGCCAATCACTACTTCGTCTCT
Primer F11F	GGCAGTTGTCATCATAACAGTTTTAGAGCTAGAAATAGC
Primer F12R	AGTTTCCAAATTCCGATCACAATCACTACTTCGTCTCT
Primer F12F	GTGATCGGAATTTGGAAACTGTTTTAGAGCTAGAAATAGC

Table 9-2: Primers used for IDAA and ICE analysis. Numbered primers (1-4) amplify a region of the fucosyltransferase gene, lettered primers (a&c) amplify a region of the putative pseudogene. For the IDAA PCR forward primers were used with the overlap sequence to the FAM for primer (given in italics).

Primer Name	Primer sequence (5'->3')
FucT for 1	ATGGCAACAGTTATTCCAA
FucT rev 1	TCTTGGACTGACTCATTTTAC
FucT rev 1 new	GATTCTGTGGAGTATTCTAG
FucT for 2	CGACTGGACATGGCTGAA
FucT rev 2	TTCATGGCGGCGAAAAGG
FucT for 3	AAGTCTTGTGCCGTAGGA
FucT rev 3	AACATCATTACCGCACGACGA
FucT for 4/c	GTATGATATCATGGCTCCAG
FucT rev 4/c	TCTTTCAGTCTCTGGTAGC
FucT for a	ACGCACCCAATAAACAATGG
FucT rev a	GATTCTGTGGCTTATTCGAG

FAM for	Fam-*AGCTGACCGGCAGCAAAATTG*

9.3 Primary and secondary antibodies

Table 9-3: Antibodies and dilutions used for Western Blots and ELISAs

Dilution	Antibody	Primary/Secondary	Company
1:1000	Polyclonal anti-Human IgG (γ-chain specific)−Peroxidase antibody produced in goat	Primary	Sigma Aldrich, USA
1:1000	Polyclonal anti-Human Lambda Light Chains (Bound and Free)−Peroxidase antibody produced in goat	Primary	Sigma Aldrich, USA
1:1000	Polyclonal anti-Human Kappa Light Chains (Bound and Free)−Peroxidase antibody produced in goat	Primary	Sigma Aldrich, USA
1:1000	anti-Phaseolus vulgaris lectin developed in rabbit	Primary	Sigma Aldrich, USA
1:1000	Sheep anti-Rabbit Immunoglobulins-HRP	Secondary	The Binding Site, UK
1:5000	Polyclonal anti-α1,3-fucose antibody produced in rabbit	Primary	Agrisera, Sweden
1:1000	Polyclonal anti-Mouse IgM antibody produced in goat	Secondary	Sigma Aldrich,USA

9.4 Alignment of retrieved fucosyltransferase mRNA sequences

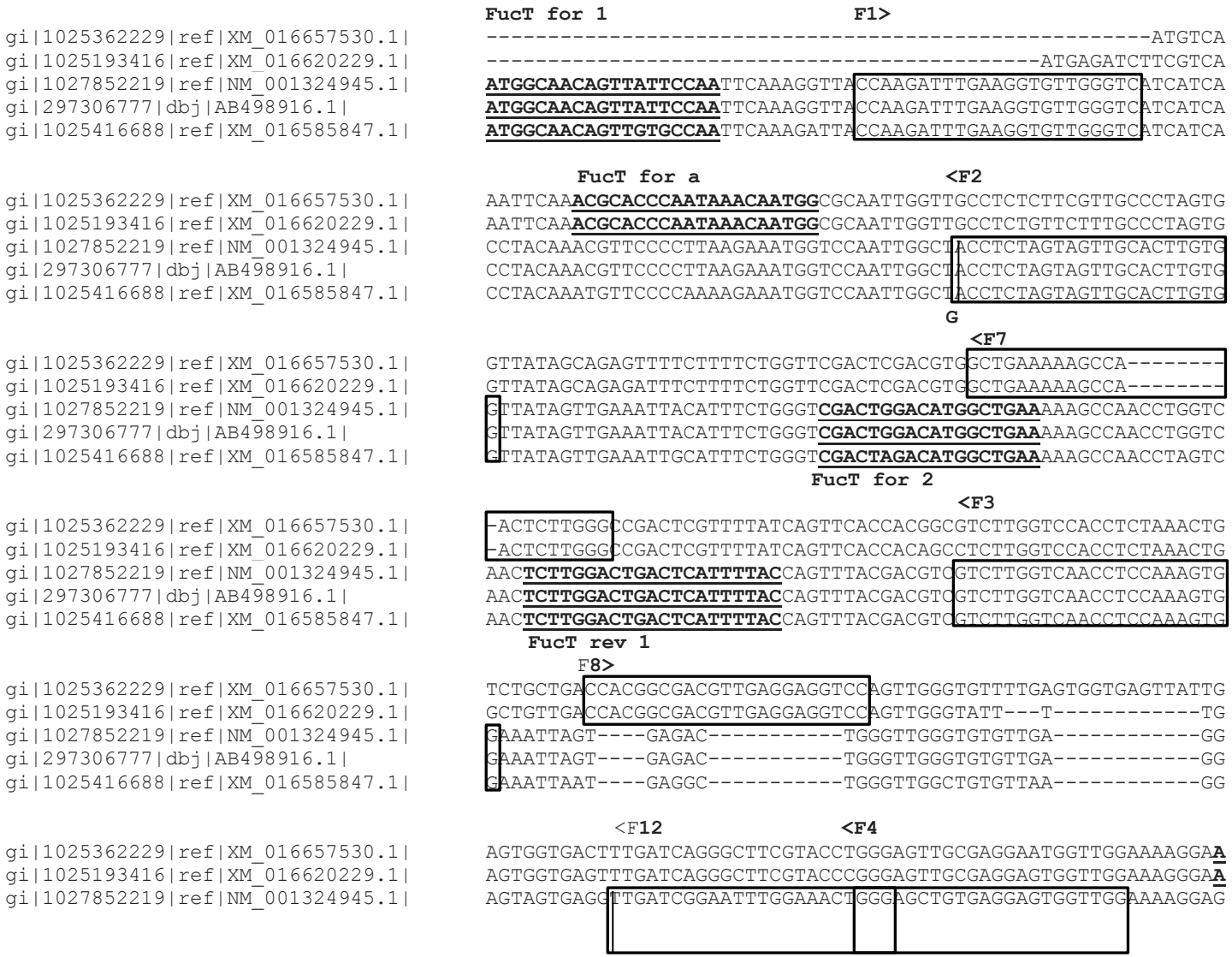

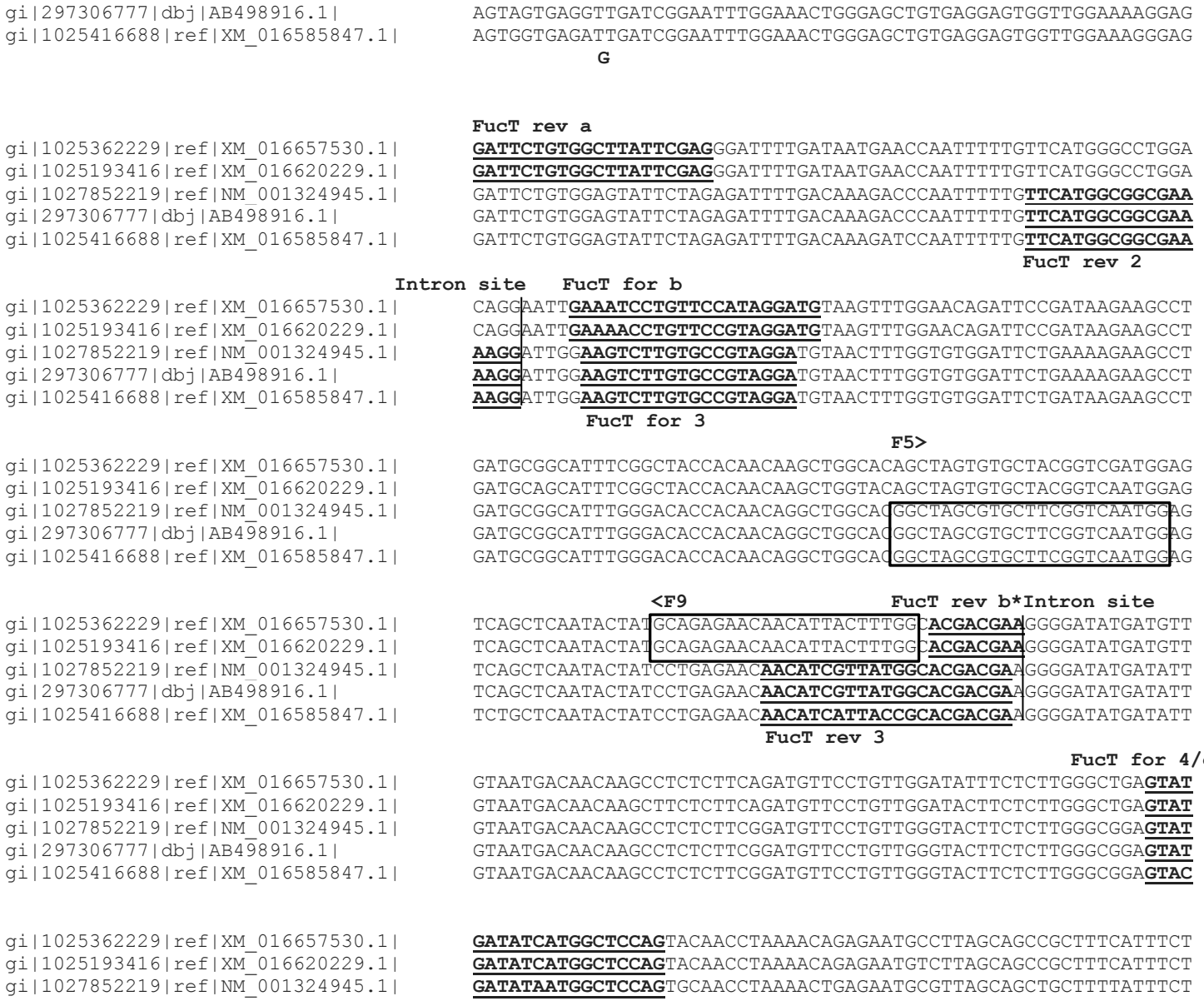
gi|297306777|dbj|AB498916.1| AGTAGTGAGGTTGATCGGAATTTGGAAACTGGGAGCTGTGAGGAGTGGTTGGAAAAGGAG
gi|1025416688|ref|XM_016585847.1| AGTGGTGAGATTGATCGGAATTTGGAAACTGGGAGCTGTGAGGAGTGGTTGGAAAGGGAG
G
FucT rev a
gi|1025362229|ref|XM_016657530.1| GATTCTGTGGCTTATTCGAGGGATTTTGATAATGAACCAATTTTTGTTCATGGGCCTGGA
gi|1025193416|ref|XM_016620229.1| GATTCTGTGGCTTATTCGAGGGATTTTGATAATGAACCAATTTTTGTTCATGGGCCTGGA
gi|1027852219|ref|NM_001324945.1| GATTCTGTGGAGTATTCTAGAGATTTTGACAAAGACCCAATTTTTGTTCATGGCGGCGAA
gi|297306777|dbj|AB498916.1| GATTCTGTGGAGTATTCTAGAGATTTTGACAAAGACCCAATTTTTGTTCATGGCGGCGAA
gi|1025416688|ref|XM_016585847.1| GATTCTGTGGAGTATTCTAGAGATTTTGACAAAGATCCAATTTTTGTTCATGGCGGCGAA
FucT rev 2
Intron site
FucT for b
gi|1025362229|ref|XM_016657530.1| CAGGAATTGAAATCCTGTTCCATAGGATGTAAGTTTGGAACAGATTCCGATAAGAAGCCT
gi|1025193416|ref|XM_016620229.1| CAGGAATTGAAAACCTGTTCCGTAGGATGTAAGTTTGGAACAGATTCCGATAAGAAGCCT
gi|1027852219|ref|NM_001324945.1| AAGGATTGGAAGTCTTGTGCCGTAGGATGTAACTTTGGTGTGGATTCTGAAAAGAAGCCT
gi|297306777|dbj|AB498916.1| AAGGATTGGAAGTCTTGTGCCGTAGGATGTAACTTTGGTGTGGATTCTGAAAAGAAGCCT
gi|1025416688|ref|XM_016585847.1| AAGGATTGGAAGTCTTGTGCCGTAGGATGTAACTTTGGTGTGGATTCTGATAAGAAGCCT
FucT for 3
F5>
gi|1025362229|ref|XM_016657530.1| GATGCGGCATTTCGGCTACCACAACAAGCTGGCACAGCTAGTGTGCTACGGTCGATGGAG
gi|1025193416|ref|XM_016620229.1| GATGCAGCATTTCGGCTACCACAACAAGCTGGTACAGCTAGTGTGCTACGGTCAATGGAG
gi|1027852219|ref|NM_001324945.1| GATGCGGCATTTGGGACACCACAACAGGCTGGCACGGCTAGCGTGCTTCGGTCAATGGAG
gi|297306777|dbj|AB498916.1| GATGCGGCATTTGGGACACCACAACAGGCTGGCACGGCTAGCGTGCTTCGGTCAATGGAG
gi|1025416688|ref|XM_016585847.1| GATGCGGCATTTGGGACACCACAACAGGCTGGCACGGCTAGCGTGCTTCGGTCAATGGAG
<F9
FucT rev b*Intron site
gi|1025362229|ref|XM_016657530.1| TCAGCTCAATACTATGCAGAGAACAACATTACTTTGGCACGACGAAGGGGATATGATGTT
gi|1025193416|ref|XM_016620229.1| TCAGCTCAATACTATGCAGAGAACAACATTACTTTGGCACGACGAAGGGGATATGATGTT
gi|1027852219|ref|NM_001324945.1| TCAGCTCAATACTATCCTGAGAACAACATCGTTATGGCACGACGAAGGGGATATGATATT
gi|297306777|dbj|AB498916.1| TCAGCTCAATACTATCCTGAGAACAACATCGTTATGGCACGACGAAGGGGATATGATATT
gi|1025416688|ref|XM_016585847.1| TCTGCTCAATACTATCCTGAGAACAACATCATTACCGCACGACGAAGGGGATATGATATT
FucT rev 3
FucT for 4/c
gi|1025362229|ref|XM_016657530.1| GTAATGACAACAAGCCTCTCTTCAGATGTTCCTGTTGGATATTTCTCTTGGGCTGAGTAT
gi|1025193416|ref|XM_016620229.1| GTAATGACAACAAGCTTCTCTTCAGATGTTCCTGTTGGATACTTCTCTTGGGCTGAGTAT
gi|1027852219|ref|NM_001324945.1| GTAATGACAACAAGCCTCTCTTCGGATGTTCCTGTTGGGTACTTCTCTTGGGCGGAGTAT
gi|297306777|dbj|AB498916.1| GTAATGACAACAAGCCTCTCTTCGGATGTTCCTGTTGGGTACTTCTCTTGGGCGGAGTAT
gi|1025416688|ref|XM_016585847.1| GTAATGACAACAAGCCTCTCTTCGGATGTTCCTGTTGGGTACTTCTCTTGGGCGGAGTAC
gi|1025362229|ref|XM_016657530.1| GATATCATGGCTCCAGTACAACCTAAAACAGAGAATGCCTTAGCAGCCGCTTTCATTTCT
gi|1025193416|ref|XM_016620229.1| GATATCATGGCTCCAGTACAACCTAAAACAGAGAATGTCTTAGCAGCCGCTTTCATTTCT
gi|1027852219|ref|NM_001324945.1| GATATAATGGCTCCAGTGCAACCTAAAACTGAGAATGCGTTAGCAGCTGCTTTTATTTCT

```
gi|297306777|dbj|AB498916.1|          GATATAATGGCTCCAGTGCAACCTAAAACTGAGAATGCGTTAGCAGCTGCTTTTATTTCT
gi|1025416688|ref|XM_016585847.1|     GATATAATGGCTCCAGTGCAACCTAAAACTGAGAATGCATTAGCAGCTGCTTTTATTTCT


                                                  F10>
gi|1025362229|ref|XM_016657530.1|     AATTGTGGTGCTCGCAACTTCCGCTTGCAAGCTTTAGAAGCCCTTGAAAGGGCAAATATC
gi|1025193416|ref|XM_016620229.1|     AATTGTGGTGCTCGCAATTTCCGCTTGCAAGCTTTAGAAGCCCTTGAAAGGGCAAATATC
gi|1027852219|ref|NM_001324945.1|     AATTGTGGTGCTCGCAACTTCCGGTTACAGGCTCTTGAAGTCCTTGAAAGGGCAAATATC
gi|297306777|dbj|AB498916.1|          AATTGTGGTGCTCGCAACTTCCGGTTACAGGCTCTTGAAGTCCTTGAAAGGGCAAATATC
gi|1025416688|ref|XM_016585847.1|     AATTGTGGTGCTCGCAACTTCCGGTTGCAGGCTCTTGAAGTCCTTGAAAGGGCAAATATC


                                          <F11
gi|1025362229|ref|XM_016657530.1|     AGAATTGATTCTTATGGCAGTTGTCATCATAACAGGGATGGAAGAGTTGACAAAGTGGAA
gi|1025193416|ref|XM_016620229.1|     AGAATTGATTCTTATGGCAGTTGTCATCATAACAGGGATGGAAGAGTTGACAAAGTGGAA
gi|1027852219|ref|NM_001324945.1|     AAGATTGATTCTTTTGGCAGTTGTCATCGTAACCGGGATGGAAATGTGGACAAAGTGGAA
gi|297306777|dbj|AB498916.1|          AAGATTGATTCTTTTGGCAGTTGTCATCGTAACCGGGATGGAAATGTGGACAAAGTGGAA
gi|1025416688|ref|XM_016585847.1|     AAGATTGATTCTTTTGGCAGTTGTCATCGTAACCGGGATGGAAATGTGGACAAAGTGGAA


                                                  <F6 (conserved motif)
gi|1025362229|ref|XM_016657530.1|     GCACTGAAGCGGTACAAGTTTAGCTTGGCTTTTGAGAATTCTAATGAGGAGGACTATGTA
gi|1025193416|ref|XM_016620229.1|     GCACTGAAGCGGTACAAGTTTAGCTTGGCTTTTGAGAATTCTAATGAGGAGGACTATGTA
gi|1027852219|ref|NM_001324945.1|     ACTCTCAAGCGCTATAAATTTAGCTTCGCTTTTGAGAATTCTAATGAGGAGGATTATGTC
gi|297306777|dbj|AB498916.1|          ACTCTCAAGCGCTATAAATTTAGCTTCGCTTTTGAGAATTCTAATGAGGAGGATTATGTC
gi|1025416688|ref|XM_016585847.1|     ACTCTCAAGCGCTACAAATTTAGCTTCGCTTTTGAGAATTCTAATGAGGAGGATTATGTC


                                    FucT rev 4/c          Putative intron site
gi|1025362229|ref|XM_016657530.1|     ACTGAAAAATTCTTTCAGTCTCTGGTAGCTGGATCAATCCCTGTGGTGGTTGGTGCTCCA
gi|1025193416|ref|XM_016620229.1|     ACTGAAAAATTCTTTCAGTCTCTGGTAGCTGGATCAATCCCTGTGGTGGTTGGTGCTCCA
gi|1027852219|ref|NM_001324945.1|     ACCGAAAAATTCTTCCAGTCTCTGGTAGCTGGATCAGTCCCTGTGGTGATTGGTGCTCCA
gi|297306777|dbj|AB498916.1|          ACCGAAAAATTCTTCCAGTCTCTGGTAGCTGGATCAGTCCCTGTGGTGATTGGTGCTCCA
gi|1025416688|ref|XM_016585847.1|     ACTGAAAAATTCTTCCAGTCCTTAGTAGCTGGATCAGTCCCCGTGGTGATTGGTGCTCCA


gi|1025362229|ref|XM_016657530.1|     AACATCCAAGACTTTGCTCCTTCTCCTAATTCAGTTTTACACATTAAAGAGATAAAAGAT
gi|1025193416|ref|XM_016620229.1|     AACATCCAAGACTTTGCTCCTTCTCCTAATTCAGTTTTACACATTAAAGAGATAAAAGAT
gi|1027852219|ref|NM_001324945.1|     AACATCCTAGACTTTGCTCCTTCTCCTAATTCACTTTTACACATTAAAGAGCTGAAAGAC
gi|297306777|dbj|AB498916.1|          AACATCCTAGACTTTGCTCCTTCTCCTAATTCACTTTTACACATTAAAGAGCTGAAAGAC
gi|1025416688|ref|XM_016585847.1|     AACATCCTAGATTTTGCTCCTTCTCCTAATTCACTTTTACACATTAAAGAGCTGAAAGAC


gi|1025362229|ref|XM_016657530.1|     GCTGAATCAATTGCCAATACCATGAAGTACCTTGCTCAAAACCCTATTGCATACAATGAG
gi|1025193416|ref|XM_016620229.1|     GCTGAATCAATCGCCAATACCATGAAGTACCTTGCTCAAAACCCTATTGCATACAATGAG
gi|1027852219|ref|NM_001324945.1|     GCTGCATCAGTTGCCGAGACTATGAAGTACCTTGCAGAAAATCCTAGTGCATATAATGAG
```

```
gi|297306777|dbj|AB498916.1|          GCTGCATCAGTTGCCGAGACTATGAAGTACCTTGCAGAAAATCCTAGTGCATATAATGAG
gi|1025416688|ref|XM_016585847.1|     GCTGCATCAGTTGCCAAGACTATGAAGTACCTTGCAGAAAATCCTAATGCATATAATGAG
```

9.5 IDAA and ICE results

Table 9-4: IDAA results for sgRNAs 7 and 8. The expected wild-type peak should show a band size of 320 bp. This peak size isn't present in any of the samples. Therefore, focus of the analysis were peaks with sizes that were present in all samples and the peaks close to these that were only present for CRISPR samples.

FucT a primer 320 bp

7-1	243.74	962	9598.0	246.35	787	6135.0				259.07	740	7901.0
7-2	243.72	587	5003.0	246.27	559	4308.0				259.02	607	6149.0
8-1	243.74	821	7131.0	246.27	747	5581.0	255.39	411	9149.0			
WT	243.3	7255	100947	246.19	6817	66600						

Table 9-5: IDAA results for sgRNAs 3,4 and 12. The expected wild-type peak was supposed to be around 271 bp. The actual one is at 269 bp (highlighted in blue).

FucT 2 primer 271 bp

Sample	Size	Height	Peak Area	Size	Height	Peak Area	Size	Height	Peak Area
WT	247.78	813	7811.0	269.01	8993	131810.0			
3-1	247.87	2855	29211.0	268.82	8982	84211.0	280.64	4664	41026.0
3-2				269.2	2795	24612.0	280.59	363	3178.0
4-1	248.21	2045	21371.0	268.9	9400	136987.0	280.74	4226	37216.0
4-2	247.57	1214	11164.0	269.03	9475	122438.0	280.73	3242	28513.0
12-1	248.16	523	4516.0	269.22	9155	108453.0	280.61	1955	16808.0
12-2	248.07	657	6362.0	269.12	9320	124071.0	280.72	4764	44842.0

Table 9-6: IDAA results for sgRNA 5. The expected wild-type peak is highlighted in green. Only the wild-type shows this peak, suggesting that sgRNA 5 has a cutting efficiency of a 100 percent.

FucT 3primer 187 bp

Sample	Size	Height	Peak Area	Size	Height	Peak Area	Size	Height	Peak Area	Size	Height	Peak Area
WT	174.15	8803	132761.0	181.08	758	14311.0	186.33	831	14858.0			
5-1	173.63	9391	83377.0							308.99	270	2676.0
5-2	173.63	9203	129949.0							308.96	271	2633.0

Table 9-7: IDAA results for sgRNAs 6, 10 and 11. The expected wild-type peak is not present in any of the samples. Therefore, focus of the analysis were peaks with sizes that were present in all samples (highlighted in orange) and the peaks close to these that were only present for CRISPR samples.

FucT 4 primer 295 bp

Sample	Size	Height	Peak Area	Size	Height	Peak Area	Size	Height	Peak Area	Size	Height	Peak Area	Size	Height	Peak Area	Size	Height	Peak Area
WT	144.57	4451	69315.0															
6-1	144.67	624	9748.0				180.9	101	1391.0	186.05	105	1411.0	252.43	323	4445.0	254.91	459	6882.0
6-2	144.57	307	4795.0										252.61	208	2741.0	254.97	321	4933.0
10-1	144.58	1642	25654.0													254.75	1058	16895.0
10-2	144.71	1530	24170.0	177.07	379	4691.0	178.11	443	6863.0				252.42	694	9136.0	254.77	1254	19476.0
11-1	144.67	532	8522.0										252.38	449	5956.0	254.84	805	12478.0
11-2	144.76	2823	45944.0										252.47	799	10500.0	254.76	1417	21729.0

Table 9-8: ICE results for the T2 generation

	F 6 & F 11		F 5	
Label	ICE	KO-Score	ICE	KO-Score
A-1	95	73		
A-2	82	60		
A-3	33	24		
A-4	94	68		
A-5	32	25		
A-6	51	44		
A-7	40	31		
A-8	45	34		
A-9	94	64	29	29
A-10				
B-1	95	44	43	43
B-2	97	44	44	44
B-3	89	67	45	45
B-4	40	29	45	45
B-5	80	52	49	49
B-6	98	72	42	42
B-7	31	25	50	50
B-8	43	25	48	48
B-9	92	43	46	46
B-10	93	46	48	48
C-1	51	42	8	8
C-2	97	46	52	52
C-3	91	89	4	4
C-4	39	29		
C-5	97	45	0	0
C-6	76	49	43	43
C-7	94	86	1	1
C-8	84	60	48	48
C-9	97	50	7	7
C-10	59	53	46	46
D-1	60	48	31	31
D-2	22	14		
D-3	26	18	38	38
D-4	26	19	41	41
D-5	24	17	46	46
D-6	90	67		
D-7	71	49	34	34
D-8	26	18	44	44
D-9	26	18	36	36
D-10	53	42	28	28
E-1			38	38
E-2	11	6	39	39

E-3	10	6	41	41
E-4	11	6	33	33
E-5	10	5	21	21
E-6	9	4	27	27
E-7	11	6	35	35
E-8	10	5	51	51
E-9	11	6	36	36
E-10	11	6		
F-1	92	0	21	21
F-2	92	1		
F-3	87	0	22	22
F-4	94	0	20	20
F-5	90	0	20	20
F-6	92	0	21	21
F-7	95	0	20	20
F-8			20	20
F-9				
F-10	93	0		
7-21-1	96	96	21	21
7-21-2	95	95	20	20
7-21-3	96	96	20	20
7-21-4	95	95	20	20
7-21-5	96	96	20	20
7-21-6	96	96	20	20
7-21-7	96	96	20	20
7-21-8	96	96	18	18
7-21-9	95	95	21	21
7-21-10	90	73	20	20
14-1-1			24	24
14-1-2			22	22
14-1-3			22	22
14-1-4	8	4	22	22
14-1-5	8	4	27	27
14-1-6	7	4	21	21
14-1-7			21	21
14-1-8	7	3	21	21
14-1-9	7	3	21	21
14-1-10			21	21
14-7-1	13	8	9	9
14-7-2	21	16	6	6
14-7-3	29	23	13	13
14-7-4	12	8	42	42
14-7-5	17	11		
14-7-6	92	74	53	53
14-7-7			16	16

14-7-8			0	0

9.6 Gels and Western Blots

9.6.1 SDS-PAGE with non-reduced and reduced samples

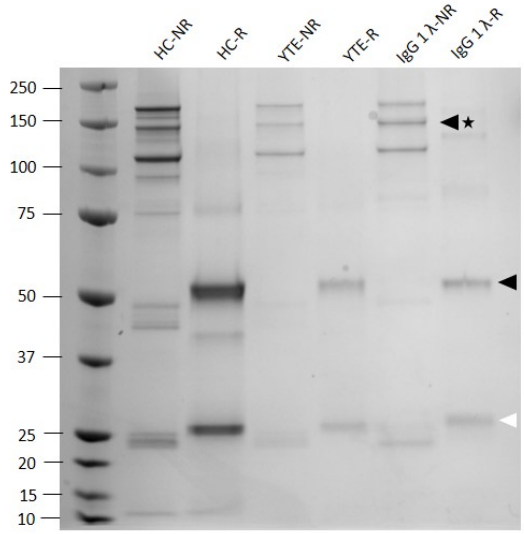

Figure 9-1: SDS PAGE for batch 1 with native 10-1074(HC), 10-1074 YTE (YTE) and an IgG λ control. The fully assembled antibody can be seen (black triangle with black star) in non-reduced (NR) samples (marked by black triangle with black star). The heavy chain is marked with a black triangle. The white arrow indicates the light chain

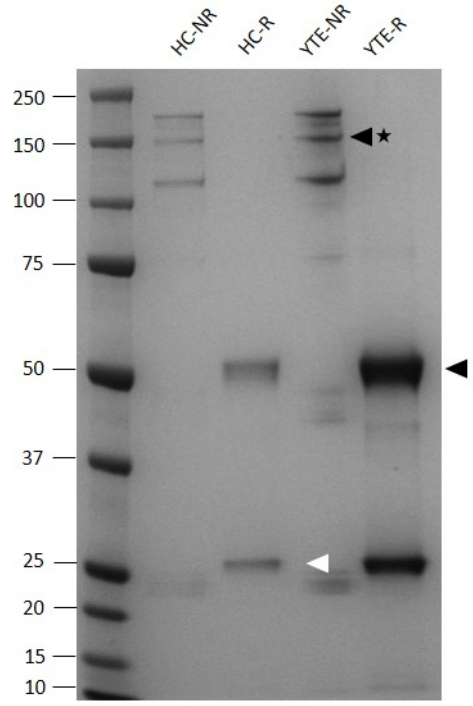

Figure 9-2: SDS PAGE from batch 2 with native 10-1074 (HC) and 10-1074 YTE (YTE). The fully assembled antibody can be seen (black triangle with black star) in non-reduced (NR) samples (marked by black triangle with black star). The heavy chain is marked with a black triangle. The white arrow indicates the light chain

9.6.2 Western Blots

- Anti-γ

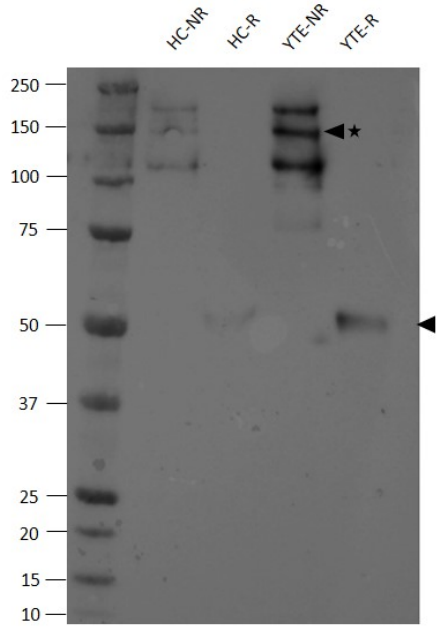

Figure 9-3: Anti-γ Western Blot performed for batch 2 to visualise the heavy chain. The fully assembled antibody can be seen (black triangle with black star) in non-reduced (NR) samples (marked by black triangle with black star). The heavy chain is marked with a black triangle.

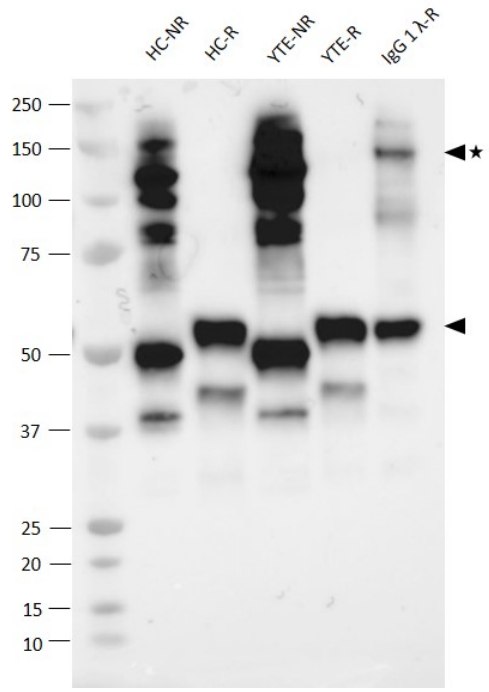

Figure 9-4: Anti-γ Western Blot performed for batch 3 to visualise the heavy chain. The fully assembled antibody can be seen (black triangle with black star) in non-reduced (NR) samples (marked by black triangle with black star). The heavy chain is marked with a black triangle.

- Anti-λ

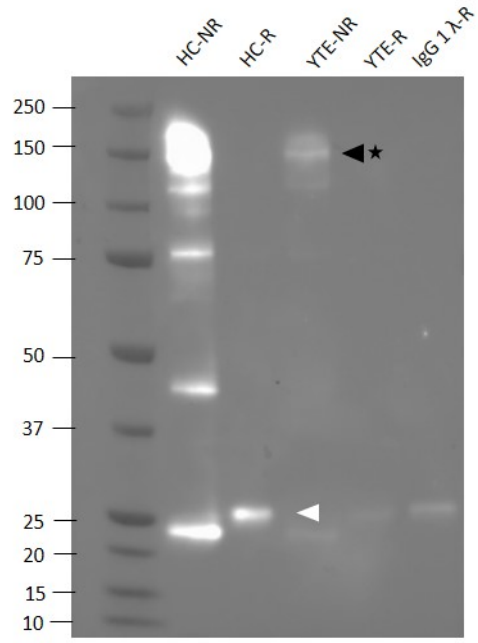

Figure 9-5: Anti-λ Western Blot of batch 1 to visualise the light chain. It verifies that the antibody is fully assembled (black triangle with black star).The white arrow indicates the light chain.

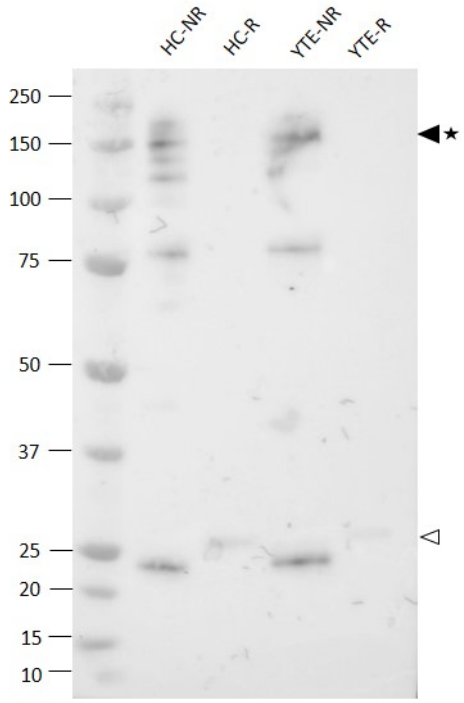

Figure 9-6: Anti-λ Western Blot of batch 3 to visualise the light chain. It verifies that the antibody is fully assembled (black triangle with black star).The white arrow indicates the light chain.

- Anti lectin

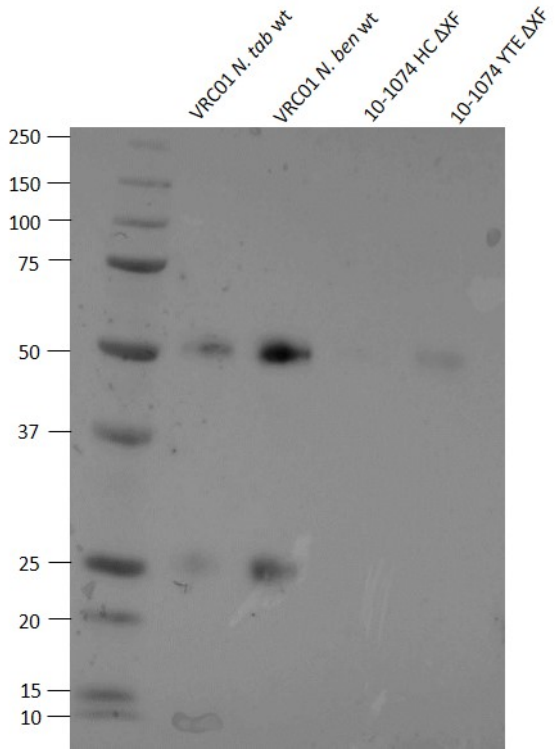

Figure 9-7: Anti-lectin Western Blot performed for batch 2. The two positive controls VRC01 produced in wild-type N. tabacum and N. benthamiana, respectively, display obvious bands at 50 kDa (heavy chain) and 25 kDa (light chain).

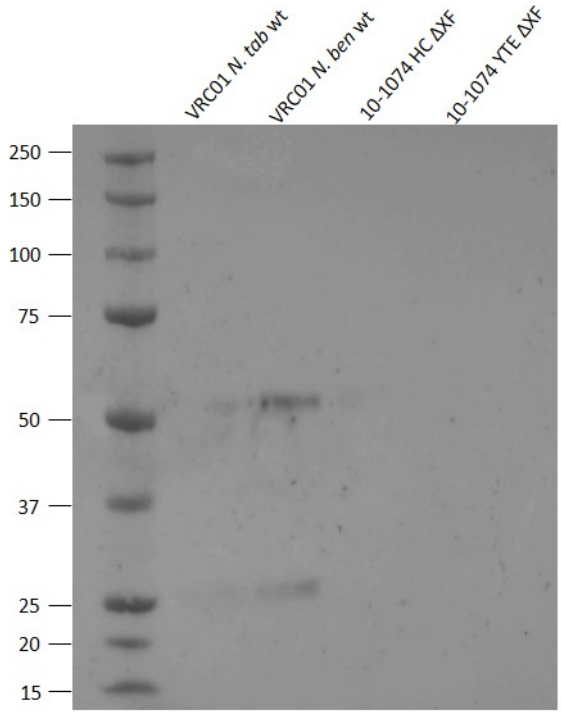

Figure 9-8: Anti-lectin Western Blot performed for batch 3. The two positive controls VRC01 produced in wild-type N. tabacum and N. benthamiana, respectively, display bands at 50 kDa (heavy chain) and 25 kDa (light chain).

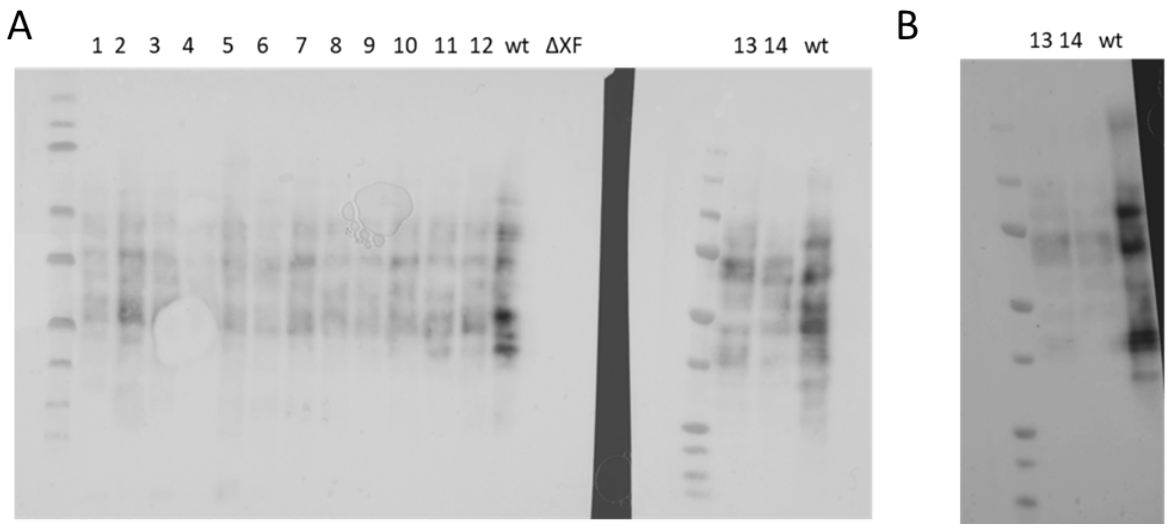

Figure 9-9: Repeats of anti-α(1,3)-fucose western blot for selected T_0 lines with samples adjusted to the same concentration. A) Repeat for all samples. B) Additional repeat for sample 13 and 14.

9.6.3 PNGase digest

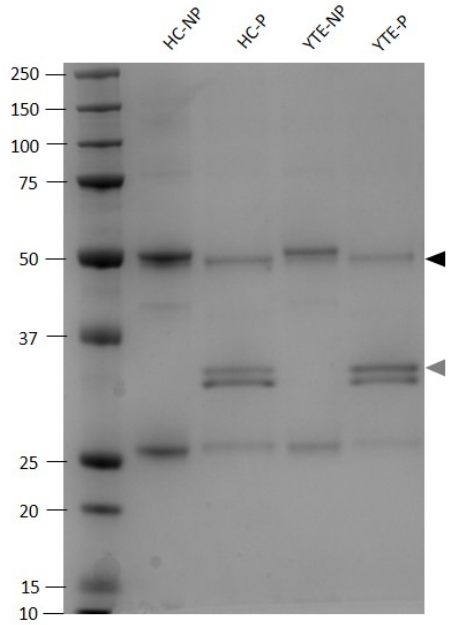

Figure 9-10: PNGase F digest (P) with non-digested control (NP) carried out for batch 1. A shift in band size (marked by black triangle) for the heavy chain can be observed for both plant-produced antibodies (HC, YTE) when digested with PNGase F, suggesting that no α1,3-fucose is present on the core GlcNAc. The band marked with the grey triangle is the enzyme (PNGase F) itself.

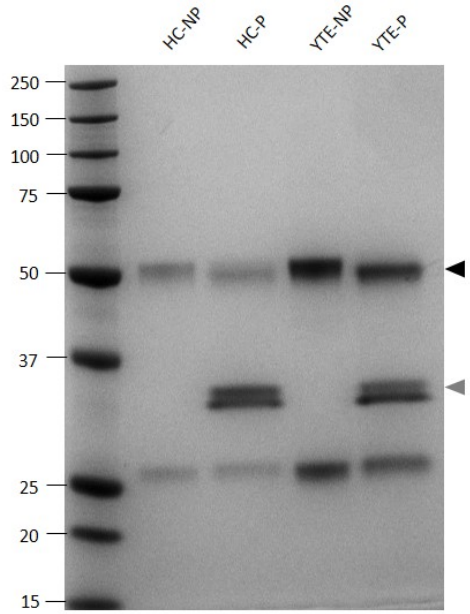

Figure 9-11: PNGase F digest (P) with non-digested control (NP) carried out for batch 2. A shift in band size (marked by black triangle) for the heavy chain can be observed for both plant-produced antibodies (HC, YTE) when digested with PNGase F, suggesting that no α1,3-fucose is present on the core GlcNAc. The band marked with the grey triangle is the enzyme (PNGase F) itself.

9.6.4 Transcytosis and pharmacokinetics

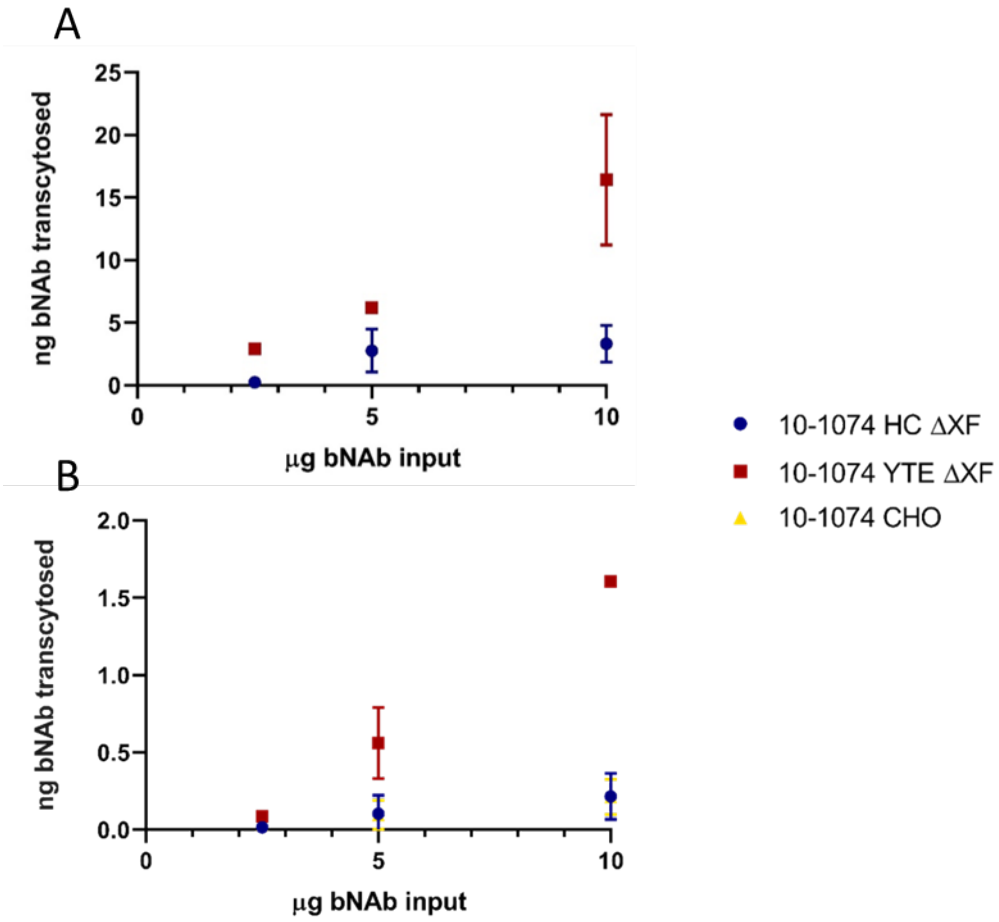

Figure 9-12: Repeats of transcytosis assays with hFcRn MDCK cells. A) Repeat for 10-1074 HC and 10-1074 YTE (n=2). B) Repeat for 10-1074 HC, 10-1074 YTE with a 10-1074 CHO control (yellow). Equivalent amounts of 10-1074 CHO compared to 10-1074 HC were transcytosed.

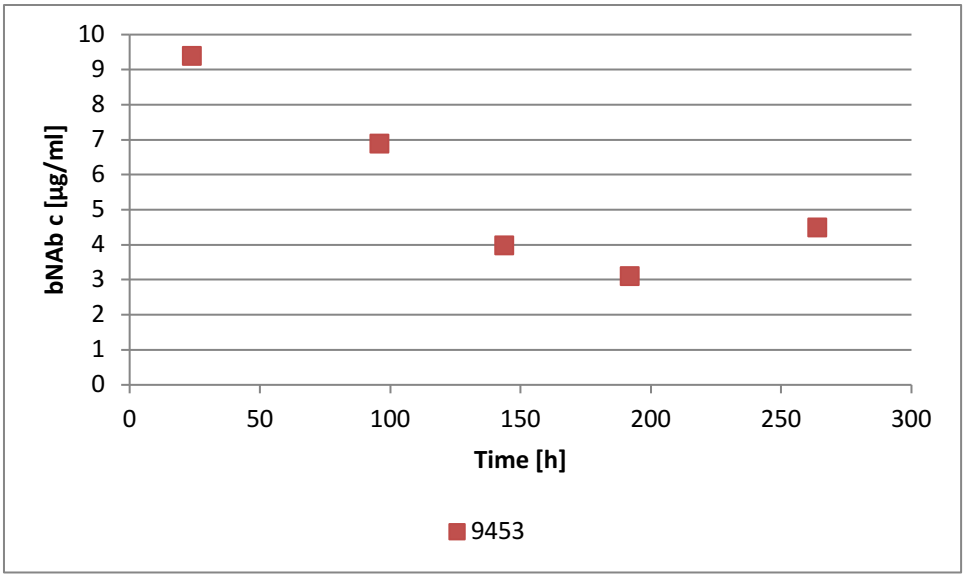

Figure 9-13: Pharmacokinetic profile of 10-1074 HC in mouse 9453

Table 9-9: Area under the curve given as mean for each study (including mouse 9453) and as total mean. Standard deviation (SD) and sample size (n) are given next to mean.

Study	10-1074 HC			10-1074 YTE			10-1074 CHO		
	Mean	**SD**	**n**	**Mean**	**SD**	**n**	**Mean**	**SD**	**n**
1	**64.5**	13.8	3	**120.4**	8.7	3			
2	**93.8**	26.9	5	**81.2**	6.9	4			
3	**104.4**	22.3	4	**134.4**	49.0	5			
4	**59.2**	2.1	2				**115.5**	32.6	3
total	***85.6***	*26.7*	*14*	***113.2***	*38.6*	*12*	***115.5***	*32.6*	*3*

9.6.5 Glycoanalysis

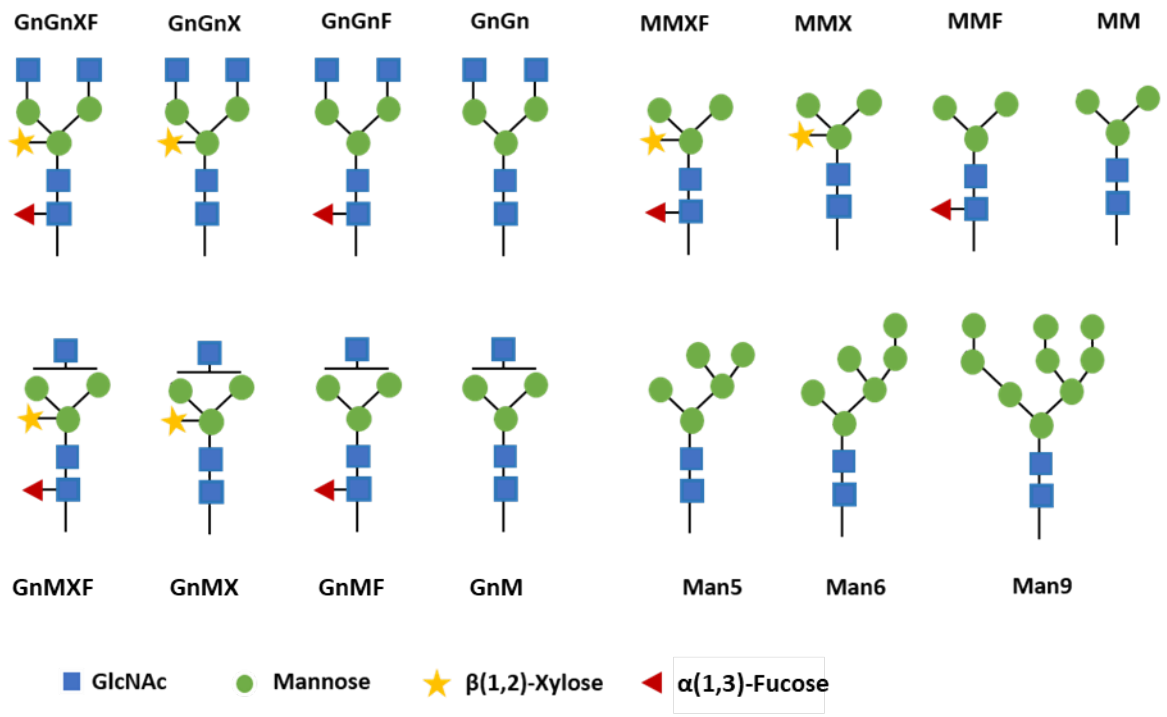

Figure 9-14: Typical glycoforms found in plants. High mannose structures are only represented by Man5, Man6 and Man9

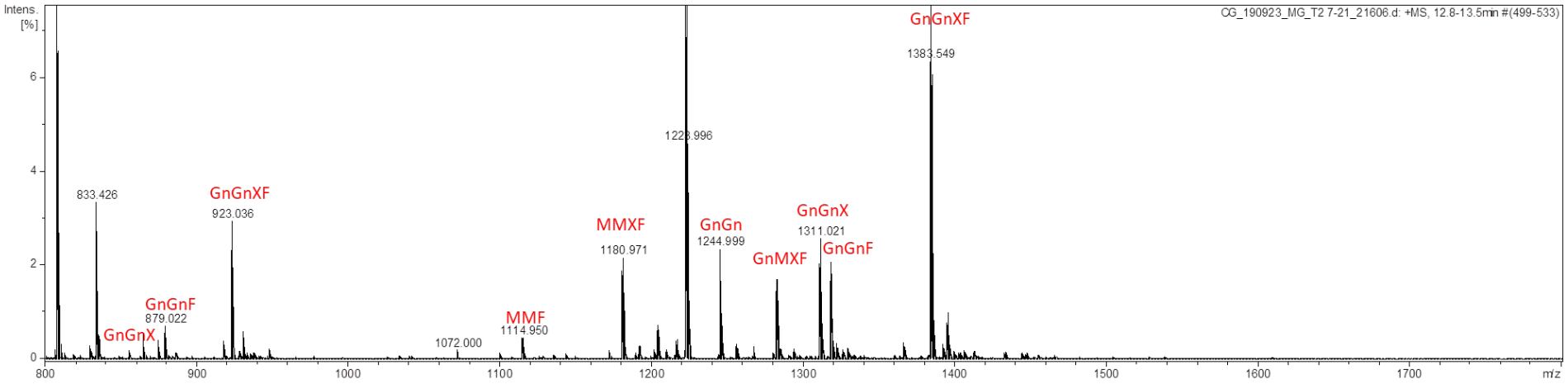

Figure 9-15: Spectrum for tryptic digest of VRC01 produced in the *N. tabacum* putative knockout line T2 7-21-4. Peaks corresponding to specific glycoforms are labelled in red.

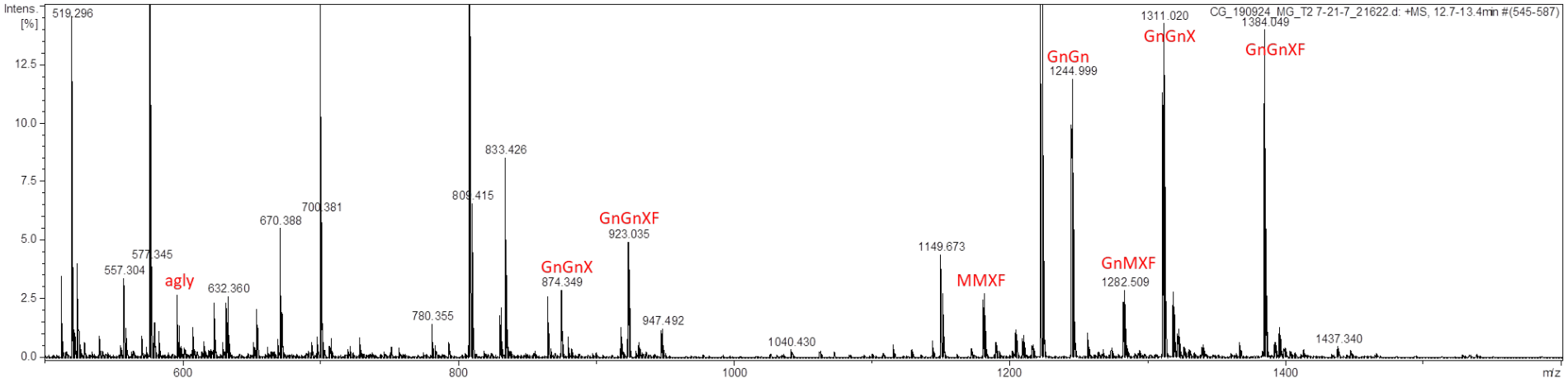

Figure 9-16: Spectrum for tryptic digest of VRC01 produced in the *N. tabacum* putative knockout line T2 7-21-7. Peaks corresponding to specific glycoforms are labelled in red.

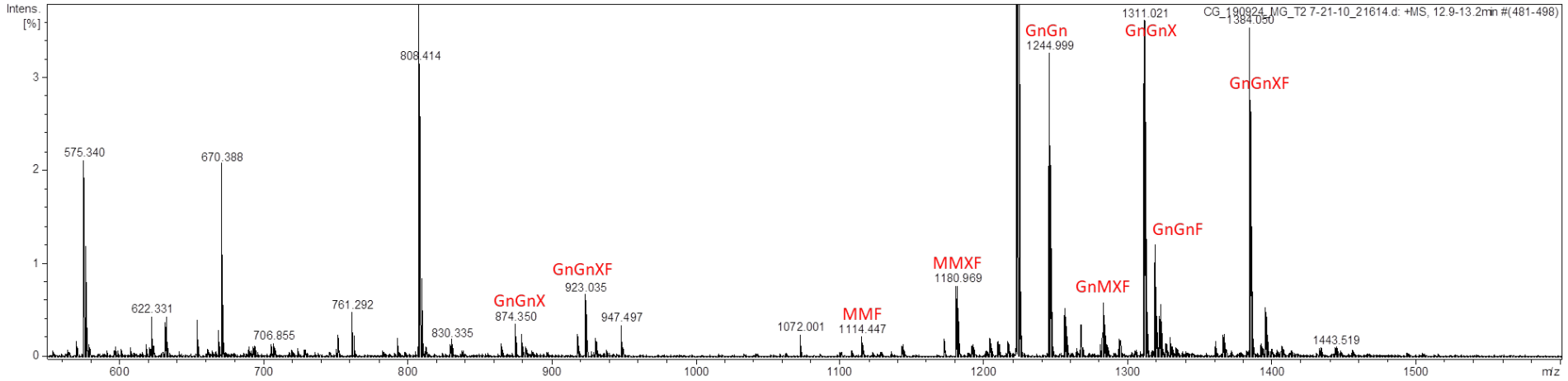

Figure 9-17: Spectrum for tryptic digest of VRC01 produced in the *N. tabacum* putative knockout line T2 7-21-10. Peaks corresponding to specific glycoforms are labelled in red.

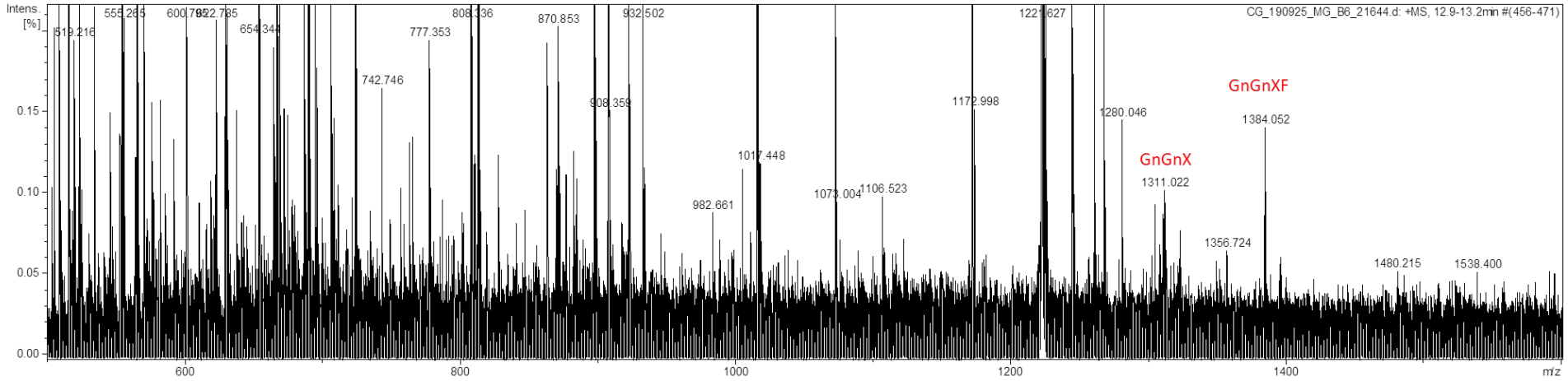

Figure 9-18: Spectrum for tryptic digest of VRC01 produced in the *N. tabacum* putative knockout line B6. Peaks corresponding to specific glycoforms are labelled in red.

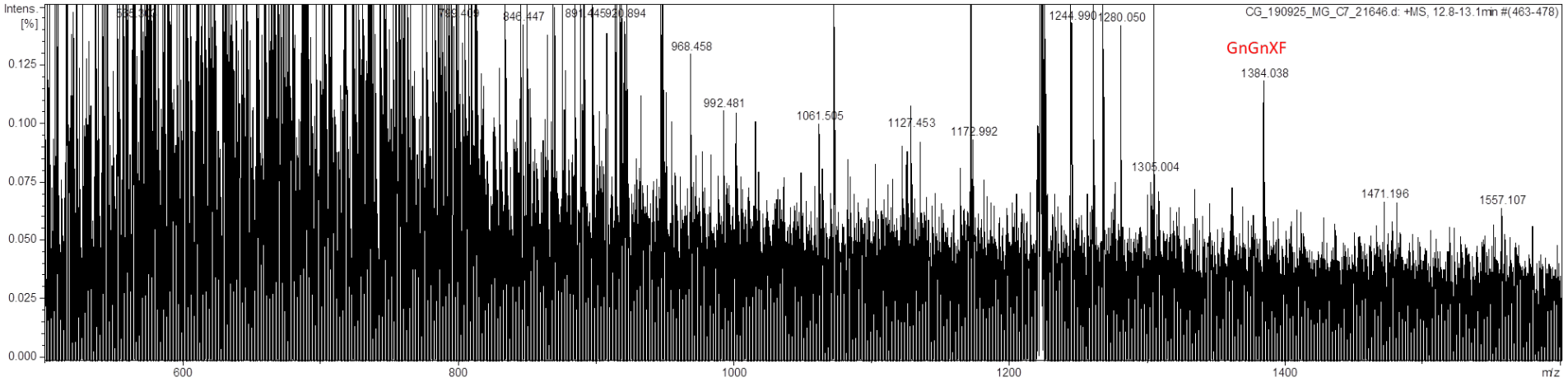

Figure 9-19: Spectrum for tryptic digest of VRC01 produced in the N. tabacum putative knockout line C7. Peaks corresponding to specific glycoforms are labelled in red.

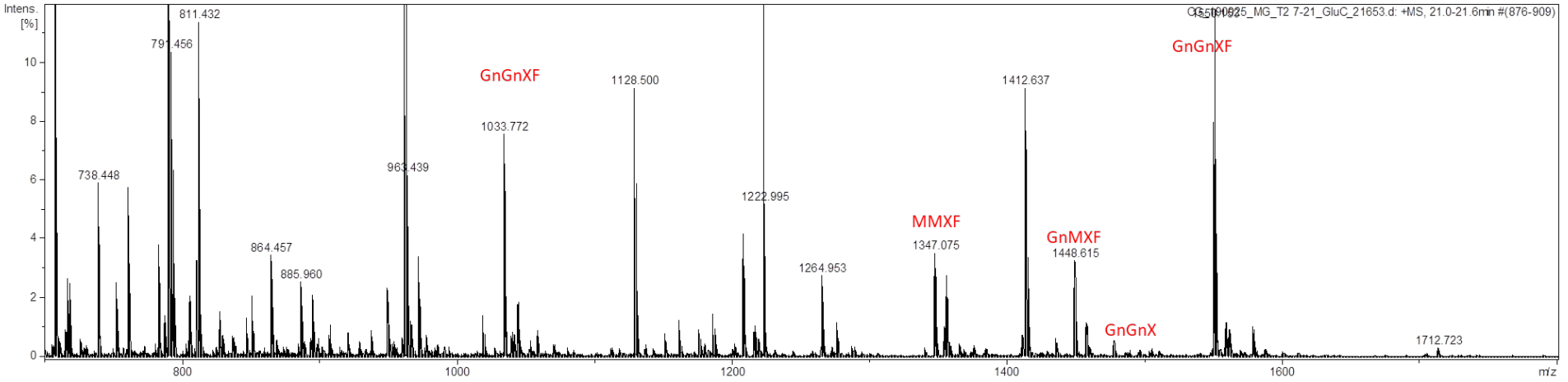

Figure 9-20: Spectrum for GluC digest of VRC01 produced in the *N. tabacum* putative knockout line T2 7-21-4. Peaks corresponding to specific glycoforms are labelled in red.

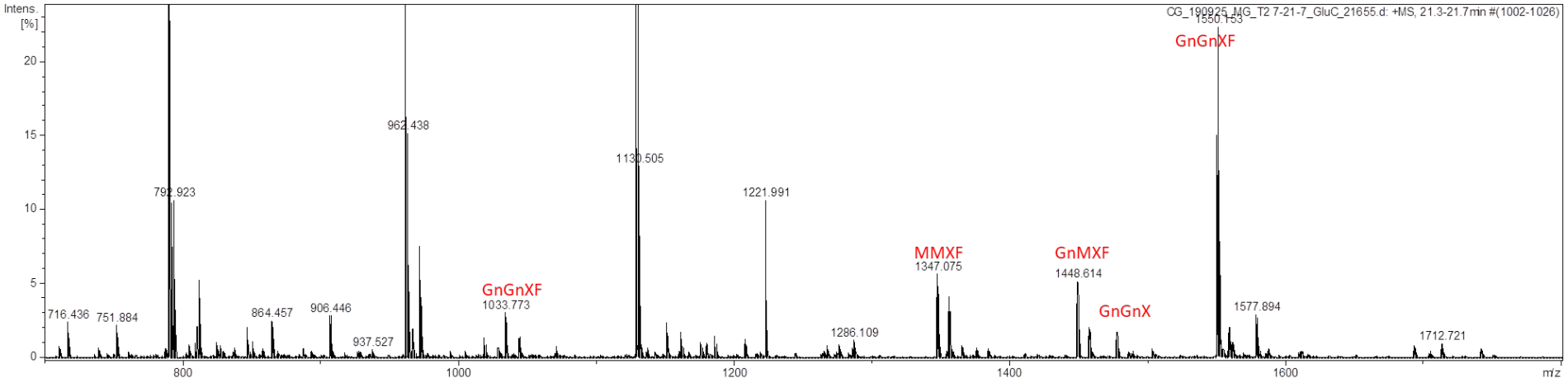

Figure 9-21: Spectrum for GluC digest of VRC01 produced in the *N. tabacum* putative knockout line T2 7-21-7. Peaks corresponding to specific glycoforms are labelled in red.

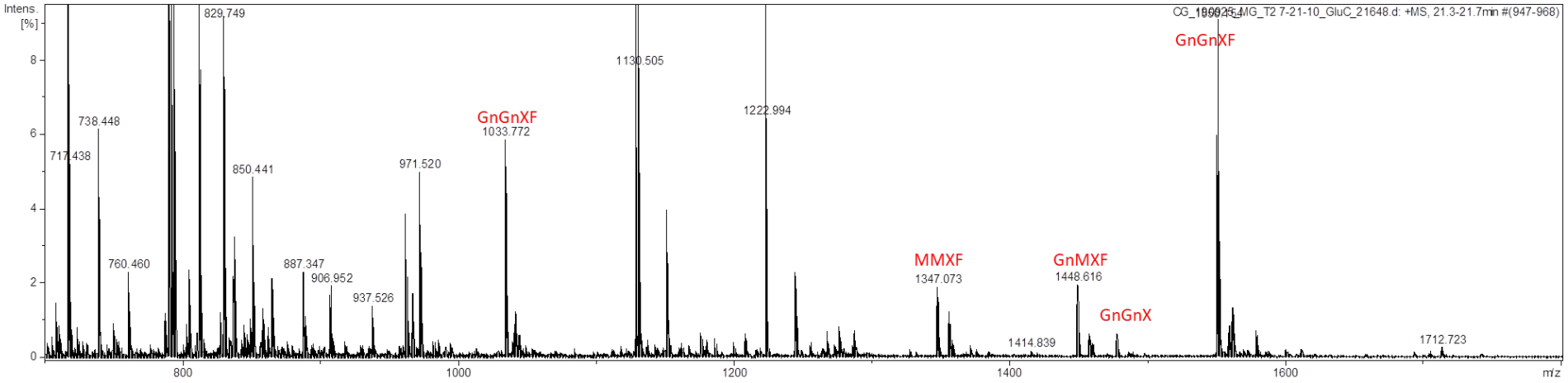

Figure 9-22: Spectrum for GluC digest of VRC01 produced in the *N. tabacum* putative knockout line T2 7-21-10. Peaks corresponding to specific glycoforms are labelled in red.